SCRUTINIZING MICROALGAE TO EXTRACT DYES FOR APPLICATIONS IN DYE-SENSITIZED SOLAR CELLS

Ph.D. Thesis

By

RAHUL CHAUHAN

DEPARTMENT OF BIOSCIENCES AND BIOMEDICAL ENGINEERING

INDIAN INSTITUTE OF TECHNOLOGY INDORE

JULY 2024

SCRUTINIZING MICROALGAE TO EXTRACT DYES FOR APPLICATIONS IN DYE-SENSITIZED SOLAR CELLS

A THESIS

Submitted in partial fulfillment of the

requirements for the award of the degree

of

DOCTOR OF PHILOSOPHY

by

RAHUL CHAUHAN

1901171006

DEPARTMENT OF BIOSCIENCES

AND BIOMEDICAL ENGINEERING

INDIAN INSTITUTE OF TECHNOLOGY INDORE

JULY 2024

INDIAN INSTITUTE OF TECHNOLOGY INDORE

I hereby certify that the work which is being presented in the thesis entitled **SCRUTINIZING MICRO ALGAE TO EXTRACT DYES FOR APPLICATIONS IN DYE SENSITIZED SOLAR CELLS** in the partial fulfilment of the requirements for the award of the degree of **DOCTOR OF PHILOSOPHY** and submitted in the **DEPARTMENT OF BIOSCIENCES AND BIOMEDICAL ENGINEERING, Indian Institute of Technology Indore**, is an authentic record of my work carried out during the period from July 2019 to July 2024 under the supervision of **Dr. Kiran Bala**, Professor, Department of Biosciences and Biomedical Engineering (BSBE), IIT Indore and **Dr. Parasharam M. Shirage**, Professor, Department of Metallurgical Engineering and Materials Science (MEMS), IIT Indore.

The matter presented in this thesis has not been submitted by me for the award of any other degree of this or any other institute.

Rahul 23/12/24

Signature of the student with date

RAHUL CHAUHAN

This is to certify that the above statement made by the candidate is correct to the best of our knowledge.

Kiran 23/12/24

Signature of Thesis Supervisor #1 with date

PROF. KIRAN BALA

23/12/24

Signature of Thesis Supervisor #2 with date

PROF. PARASHARAM M. SHIRAGE

RAHUL CHAUHAN has successfully given his Ph.D. Oral Examination held on 22/ 11/ 24.

Kiran 23/12/24

Signature of Thesis Supervisor #1 with date

PROF. KIRAN BALA

23/12/24

Signature of Thesis Supervisor #2 with date

PROF. PARASHARAM M. SHIRAGE

ACKNOWLEDGEMENTS

Completing this thesis has been an extraordinary journey, made possible by the unwavering support and contributions of many remarkable individuals. My heart overflows with profound gratitude for their boundless encouragement and invaluable assistance throughout this endeavor.

First and foremost, I wish to extend my deepest and most heartfelt thanks to my esteemed thesis supervisor Prof. Kiran Bala. Her boundless encouragement and steadfast support from the very beginning have been the cornerstone of this research. Her priceless and meticulous stimulation at every step of my Ph.D. journey has inspired me in countless ways, and I am forever indebted to her. I extend my profound appreciation to my esteemed co-supervisor Prof. Parasharam M. Shirage, whose insightful assistance and unwavering support have been active throughout this research journey. His dedication to making essential instruments available has been crucial to the triumphant completion of this thesis.

I am intensely grateful to the distinguished members of my research progress committee Prof. Devendra Deshmukh and Dr. Abhijeet Joshi. Their understanding comments and inspiration, coupled with their challenging questions, have significantly broadened my research perspectives. Their wisdom and guidance have been instrumental in shaping this work. Prof. Devendra Deshmukh, being a gem of IIT Indore; his righteousness and exemplary courage are worth admiring.

A devoted thank you goes to the Heads and all the esteemed faculty members of the Department of Biosciences and Biomedical Engineering. Their valuable backing has been a constant source of motivation, and I am deeply appreciative of their boost. I am deeply grateful to Prof. Ganti S. Murthy and Dr. Debayan Sarkar, whose unwavering encouragement and support in my curiosities and skill enhancement have been a constant source of inspiration throughout my PhD journey. Their positivity and belief in my work have significantly bolstered my confidence and motivation for my never-back down adapt. Additionally, I extend my gratitude to Sheetal Gupta, Ramanand Dadhich, Sumit Chorma, Kavita Singh, and Aditya Bhardwaj for their invaluable services towards my research. Their dedication and hard work behind the scenes have greatly facilitated this PhD. Along with them I also admire the nurturing nature of Dr. Anjan Chakraborty, Dr. Alestin Mawrie, Dr. Girish Chand Verma, Prof. Sharad Gupta, Prof. Santosh Kumar Vishvakarma, Prof. Pavan

Kumar Kankar, and Prof. Mirza S. Baig. I am also immensely thankful to the office staff of the department, whose efficient assistance in all official research matters has been vital.

Support from various institutions and facilities has been crucial to my research. I am grateful to the Sophisticated Instrumentation Center for providing access to essential instruments for measurements and sample analysis. I am deeply appreciative of the financial support from MHRD India and EPCO Bhopal. Their generous funding has been pivotal in advancing my research and enabling significant milestones. I am privileged to have had the companionship of my fellow lab mates Dr. Tonmoy, Dr. Bikash, Dr. Arjun, Ms. Palak, Ms. Smriti, Ms. Anshul, Mr. Dinesh, Ms. Konica, Ms. Diksha, Ms. Swagata, Mr. Vaibhav, Mr. Rudra, Mr. Ashish, and others equivalently. Special thanks to those who were always there to lend a helping hand and brighten my days with their presence, like Dr. Rajarshi (Departmental football envoy), Dr. Saumya, Dr. Amit, Dr. Gaurav, Dr. Monika, Ms Aarpita, Mr Vinay, Mr Kumod, Mr Rohan, Mr Akshay, Mr Yogesh, Mr Abhijeet, Mr Siddharth, Mr Mohan, Ms Shivani, and Mr Kanav. Special mention of support of my IIM Indore and other Indore buddies; you made me feel like a king in Indore.

I wanted to take a moment to extend my sincere thanks to each of the IT, IDO, Library, Sports, Housekeeping, Catering, and Medical Staff Teams for your exceptional efforts and dedication. Your hard work, expertise, and collaboration have truly made a significant impact on our projects. From ensuring smooth operations to tackling complex challenges, your contributions are deeply valued and appreciated. I want to thank all my Animal welfare family, Chanakya family, Athletics family, Football family, Intern family, and Gymkhana family for keeping me evolving mentally and physically.

A special note of gratitude goes to my dear B. Tech, Master's, and Ph.D. juniors and friends who have been my pillars of strength. Their encouragement and unwavering support have been a constant source of motivation, especially during challenging times. Above all, my deepest appreciation goes to my family and my ancestors' blessings. Their patience, understanding, and staunch belief in me have been my guiding light. Their love and support have been my anchor, and I am eternally grateful for their presence in my life.

This journey has been a collective effort, and I am deeply thankful to everyone who has contributed to it in any way. This thesis stands as a testament to their incredible support, and I am forever obliged to them.

This thesis is dedicated to my

Dharti Mata,

Bharat Mata, and

Janani Mata

माता भूमिः पुत्रोऽहं पृथिव्याः।

Atharva Veda, Prithvi Sukta, Shlok no. 12

With the auspicious wishes of

(Surya Devata, Dadhyangatharvana Rishi)

तच्चक्षुर्देवहितम्पुरस्ताच्छुक्रमुच्चरत् । पश्येम शरदः शतञ्जीवेम शरदः शतँ शृणुयाम शरदः शतम्प्र ब्रवाम शरदः शतमदीनाः स्याम शरदः शतम्भूयश्च शरदः शतात् ॥

यजुर्वेद 36,24

(That light divine, blissful to the divinities, pure and wide awake since eternity, may we continue to see for a full hundred years, live under its benign eye for a hundred years, hear for a hundred years, speak and celebrate for a hundred years, and be fit and fine in a state of freedom and independence for a hundred years, and even more!)

SYNOPSIS

1. Introduction

Dye-sensitized solar cells (DSSCs) have emerged as a promising technology within the realm of photovoltaic energy conversion, predominantly relying on inorganic dyes to excite electrons for energy harvesting. Inorganic dyes, such as ruthenium polypyridyl complexes, have demonstrated impressive conversion efficiencies reaching approximately 11% [1]. However, the production of these dyes involves complex and costly processes and raises significant environmental concerns due to the potential release of heavy metals. This has spurred interest in identifying alternative dyes that are both cost-effective and environmentally benign. Despite the potential of natural dyes, their efficiency in DSSCs has been relatively low. For instance, natural dyes that are *Chlorophyll* (*Chl*) centric have achieved maximum efficiencies of around 2.5%, while those having carotenoid and phycobilin have reached about 1% or less [2].

Natural organic dyes present a viable alternative, offering a greener and more sustainable approach to light harvesting. These dyes, derived from natural sources such as plants and algae, are generally biodegradable and non-toxic, making them an attractive option for eco-friendly solar cells. Among these, microalgae-based dyes hold particular promise due to their specific absorbance, transmittance, and reflectance properties, which are influenced by the pigments they contain. The primary pigments in microalgae include chlorophylls and carotenoids. *Chls* in microalgae, specifically *Chl a* and *b*, absorb light in the narrow red and broader blue-violet regions and reflect green light, which gives the cells their characteristic green color. Carotenoids, on the other hand, absorb light in the blue region and extend into the green and yellow regions. They also have a secondary absorption peak in the green region, helping to absorb excess light energy and protect the cells from photo-oxidative damage by transferring absorbed energy to *Chl*. The production and accumulation

of these pigments are influenced by factors such as light intensity, nutrient availability, temperature, and environmental stresses [3].

Various methods for extracting pigments from algae exist, including supercritical extraction, laser techniques, and hydrodynamic cavitation. Among these, the electric field method offers reduced extraction time but requires significant energy and infrastructure investment. Consequently, researchers often prefer the classic solvent extraction method due to its lower operational costs despite being less efficient and solvent intensive [4]. The efficacy of these extraction methods depends on factors such as solvent purity, water content, and the resolution properties of spectrophotometers used in the process. The extracted dyes must be evaluated for their light-harvesting pigments and spectral absorption efficiency using various green solvents like acetone, ethanol, and methanol. There has been always a curiosity about the presence of various functional groups to enhance attachment to the semiconducting layer and improve electron-donating capability.

Combining methods of extraction can improve extraction efficiency as the choice of solvent, extraction parameters, and target dye nature are essentially considered. Given the high costs associated with extraction processes in small lab-scale environments, alternatives like solar heaters for large-scale extraction have been proposed too, to create additional value-added products in bioreactor systems while generating electricity. Stability studies have been conducted to understand the degradation rates of these dyes and how frequently they need replenishment. Temperatures higher than 60 °C - 80 °C are generally not recommended for microalgal pigment extraction due to potential degradation. Microalgal pigments are sensitive to high temperatures, which can lead to changes in color, loss of fluorescence, and reduced pigment concentration [5]. The emission spectra of dyes, influenced by their electronic structure and environmental factors, also play a critical role. Several strategies to enhance the stability of algal dyes at elevated temperatures have been employed, such as using thermally stable dyes, co-sensitizing with stable synthetic dyes, encapsulating dyes within protective matrices, and optimizing electrolytes.

All these findings could make DSSCs more cost-effective and sustainable by reducing infrastructure and energy investments while enhancing the stability and efficiency of large-scale applications of natural dyes in solar cells.

The following objectives were designed to achieve the needed output of the thesis:

Major Objective:

To explore the potential fabrication of natural, efficient, and stable dye-sensitized solar cells using augmented dyes derived from microalgae.

Minor Objectives:

i. Screening of microalgal species and different solvents for dye extraction.
ii. Assessing the influence of various properties and extraction systems on selected dyes.
iii. Integration of selected dyes as photo harvesters in natural dye-sensitized solar cells (DSSCs).
iv. Estimating gaps in extraction optimization and storage through specific pigments of selected dyes.
v. Evaluating compound formations following degradation and accretion due to extraction and storage.

2. Summary of the results

The above-mentioned objectives were achieved by the following scheme of experiments shown in Figure 1.

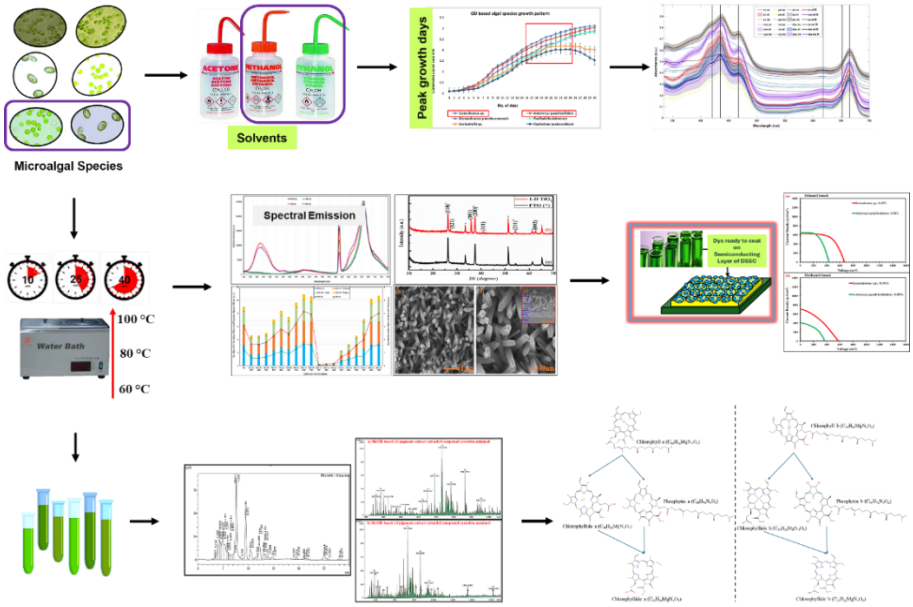

Figure 1: Schematic overview of the experimental approach for screening algal species and further dye characterization for DSSC fabrication.

Chapter 2: Screening of Microalgal Species and different Solvents for Dye Extraction

Starting with the first objective, six microalgal species namely *Scenedesmus sp., Coelastrella sp., Pediludiela daitoensis, Coelastrum proboscideum, Asterarcys quadricellulare,* and *Desmodesmus pseudocommunis* which were isolated from nearby regions of Indore (Madhya Pradesh, Bharat) were considered for photo harvesting properties present in their dyes. UV–Vis spectroscopic analysis and dye characterization confirmed the photosensitizing nature of the extracted microalgal dyes. Their scanned spectra showed absorption peaks corresponding to *Chl a* (435 nm, 665 nm), *Chl b* (467 nm, 652 nm), and carotenoids (450-470 nm). Other peaks at 421 nm and 435 nm likely corresponded to Pheophytin (*Phytin) a* and *b*. Solvent extraction efficiency analysis using three solvents (acetone, ethanol, methanol) was evaluated using MATLAB. Acetone showed ineffective results, while ethanol and methanol demonstrated varying extraction

capabilities. Ethanol consistently performed well across different dye species, with methanol showing effectiveness only at higher concentrations. Ethanol at 80% concentration was identified as the optimal solvent condition for further extraction studies. Methanol exhibited higher baselines and peak shifts, indicating dilution effects, but performed well at 90% or higher. Here, *Pediludiela daitoensis* was not considered suitable for further testing due to lower efficiency. Further, species selection under optimal extraction conditions was done by assessing extraction efficiency over different growth periods (15^{th} to 30^{th} day) for the remaining five species, with the 20^{th} day showing the highest efficiency due to stable pigment extraction before degradation phases set in. Here, a comparison between cold and hot solvent extraction methods was also done which favored hot extraction methods due to higher pigment yield. Methanol showed comparable results to ethanol but with limited efficiency at lower concentrations. Then, electrochemical analysis by cyclic voltammetry assessed electron transfer capabilities and energy levels (HOMO and LUMO) of selected extracted dyes of *Scenedesmus sp*. and *Asterarcys quadricellulare,* which exhibited quasi-reversible behavior, and also correlated electrochemical band gap data with optical band gap data. The data was further checked for support from Fourier Transform Infrared (FTIR) spectroscopy for functional group analysis in the extracted dyes that can bind better to the semiconducting surface of solar cells. It confirmed the presence of strong peaks for hydroxyl groups (3350–3250 cm^{-1}), alkanes (2850–2960 cm^{-1}), alkenes (1640–1680 cm^{-1}), and other characteristic bonds of chlorin structures. Also, the dyes were studied for degradation under varying temperatures and light intensities (10,000 lx) highlighting differences in dye stability between solvents particularly in *Chl* terms. *Scenedesmus sp.* (*sc*) dye showed better stability in methanol (*mt*), while *Asterarcys quadricellulare* (*as*) dye was more stable in ethanol (*et*).

Chapter 3: Influence of varying Extraction Parameters on Dye Properties and Stability

For the second objective, reflectance spectroscopy was done where *Scenedesmus sp.* dye in aqueous ethanol showed the least reflectance, indicating higher absorption. The reflectance of *as et* overlapped with *sc mt* in the red and blue regions but not in the green due to less carotenoid extraction by methanol. It was followed by photoelectron energy spectroscopy where *sc et* required the least energy for electron excitation. Energy order further was *as et* ≈ *sc mt* > *as mt*. Next in fluorescence spectroscopy order of intensity was *as mt* > *sc et* > *sc mt* > *as et*. Peaks at 675 nm are higher for *sc et* than *as et*. Methanol dyes showed a slight delay in emission at 676 nm, extending to 678 nm for *as mt*. These dyes were also analyzed for extraction methods combination efficiency via UV–Vis Spectroscopy where *as mt* with heating and sonication, had the best performance at 25 min. *as et* effective with intensified heating or sonication, 1.5 to 2-fold increase at 70-80% concentration. *sc et* effective at 80%, better with sonication. Sonication was effective at 80% concentration, with extraction rates 1.5-fold higher than the control. *sc mt* showed high extraction at 70% and 80% with heating, and better performance with sonication. *as et* showed efficient extraction at 80%, with minimal effect with sonication. *sc et* effective at 80% with heating and sonication, best at 40 min sonication [7]. The stability of dyes ranged from 36 to 80 hours, longer for dyes extracted with sonication. Heating-extracted dyes were less stable due to degradation and lower pigment amounts. Overall longer sonication duration extracted more pigments, providing better stability.

Chapter 4: Integration of Dyes in Natural Dye-Sensitized Solar Cells (DSSCs)

In achieving the tasks of the third objective, Photoanodes were prepared first by developing a semiconducting layer on glass with the

pure embedding of the utilized material, here TiO_2 was used. synthesized 1-dimensional TiO_2 arrays on Fluorine-doped Tin Oxide (FTO) substrates using the hydrothermal method aligned vertically and randomly as nanorods whose purity was checked by X-Ray diffraction analysis (XRD) peaks at 2θ values which were 26.27°, 27.21°, 35.87°, 37.48°, 41.04°, 54.19°, 62.66° that corresponded to rutile TiO_2 phases. Identified (hkl) planes were (110), (121), (101), (200), (111), (211), (002). The crystallinity matched rutile TiO_2 with JCPDS data (21–1276) and no extra peaks/humps indicated pure phase 1-D TiO_2 nanorods. Also, the top FE-SEM view showed square-shaped top facets, consistent with tetragonal crystal growth. The cross-sectional view shows the vertical orientation of nanorods, length ~1.8 ± 0.2 μm, average diameter ~90 ± 5 nm at the bottom and 85 ± 5 nm at the top increasing surface area and charge transfer ability. Further, UV–visible absorbance spectra show a strong absorption edge at ~420 nm, corresponding to a rutile TiO_2 bandgap. The energy band gap (*Eg*) of 1-D TiO_2 nanorods was calculated as 2.97 eV using a Tauc plot. After that, the fabricated solar cell with the dyes was tested for current-voltage (J-V) measurement where the maximum power conversion efficiency **(**PCE) out of all tested DSSCs with selected dyes was 0.25% with the composition of Glass/ FTO/ compact-TiO_2/ 1-D TiO_2 nanorods/ *sc* (*et*) dye/ I^- /I_3^- electrolyte/ carbon counter electrode [8].

Chapter 5: Optimization and Storage in coordination with different Pigmental Analysis

The fourth objective of estimating gaps in extraction optimization and storage through specific pigments of selected dyes a high-performance liquid-chromatography (HPLC) based Chromatogram analysis was done with the selected dyes. Here it was observed that *sc et* at 421 nm, 435 nm, and 467 nm had *Pheophorbide a (Phide a)* peak peaking on the 20th day, followed by the 15th and 25th days. Carotenoid peaks were significant at 421 nm on the 25th day, and *Chlorophyllide a* (*Chlide)*

and derivatives were prominent at 435 nm, higher on the 25th day. *Chl a* reduction converts to *Chlide a* and *Phide a* over time, with significant *Phide a* derivatives due to *mt* oxidation. *as et* showed *Pheophytin (Phytin)* formation is indicative of magnesium ion loss. Carotenoids were higher compared to *sc.* By the 25th day, *β-carotene* (*B-car*), *Chlide b*, and *Phytin b* are prevalent. *sc mt* and *as mt* had higher *Chl a* stability, with significant presence of *Chlide a* and *Chlide b*. *Phide* peaks higher at 421 nm and 435 nm. Carotenoids consistency at 421 nm and 435 nm. The *mt* preserves magnesium ions and minimizes degradation while *et* yields higher but more degraded products. The dyes were also evaluated for their stability during storage via chromatograms. When samples from *sc* and *as* were stored at room temperature in darkness for 10 to 30 days, notable pigment degradation occurred. *Chl a* and *Phide a* derivatives significantly reduced, with *Chl* being less stable than other pigments, indicating weakened bonding from high-temperature *et* extraction. At 652nm, *Chl a* converted to *Phide a* derivatives due to hydroxide in *mt*. *Chlides* remained relatively stable, partially reducing and converting to *Phides*. In *as* dye, *Chl a, Chl b, Phytin b,* and *B-car* were mostly constant, while *Phide a* derivatives and *Chlides* decreased. *Chl a* and *Chl b* reductions increased *Chlide a and Chlide b* derivatives. *B-car* was extinct by day 10, and by day 30, *Chl a* and *Phytins* were considerably reduced. *Phide a* and *Chlide a* derivatives showed significant peak strength reduction throughout.

Chapter 6: Exploring the stability of extracted Dye Component Compounds

For the last objective, which is evaluating compound formations following degradation and accretion due to extraction and storage analysis by LC – Mass Spectrometry (LC-MS) was done. Spectrum analysis via chromatograms facilitated the selection of the range, viewing of compound spectra, smoothening the spectrum data,

applying a smart formula, selecting adducts, locating isotopic peaks, and deconvoluting for best possible structural calculations of the resulting compounds from pigmental degradation happening in the samples. Before analyzing the samples, a *B-car* standard powder analysis was done where a significant peak at m/z 325, indicated a stable breakdown product in *et* whereas multiple significant peaks at m/z 325 (100% intensity), 403, 301, and 279 (at varying intensities), indicated diverse compound formations in *mt* purely due to solvent as there is no extraction involved there. The compound spectra analysis of the *sc et* extracted at 80 °C over the 15^{th}, 20^{th}, and 25^{th} day, more significant peaks at m/z 325 and 987 were consistently observed. On the 20^{th} day, *Chl a* production peaked, followed by a reduction or conversion to other carotenoids. The peak at 325 increased over time, indicating *Chl* breakdown and conversion. At 100 °C extraction, the peak at m/z 987 reduced, and new peaks appeared at 961 and 941-943, with an intensity halt at 67% and a notable peak at 543. In *as et,* similar patterns to *sc* dye were observed. At 80 °C, heavier intermediary compounds were formed compared to 100 °C. For *sc mt* at 80 °C, peaks were observed at m/z 543, 523, 691, and 653. After 10 days, peaks at 543 and 523 disappeared, stabilizing at 453 and 867. At 60 °C, peaks at 691, 543, and 785 remained stable with minor erosion over time. For *as mt*, at 60 °C for 25 and 40 minutes, peaks were densely packed between m/z 650-800. The 100% intensity peak shifted from 783 to 691 after 25 minutes, with decreasing peak heights indicating degradation cum stabilization. Further, these samples had the major peak shifted from m/z 691 to 453, indicating an almost 250 m/z decline in mass. Finally, various possible compounds were created using these observed patterns of degradation with all the samples present close pigmental compounds.

3. Conclusions

The study showed how these microalgal dyes interact with light and their spectral characteristics across the electromagnetic spectrum as these dyes cover the visible, UV, and near-infrared spectra, unlike many plant-derived dyes, and have all the benefits related to the production of microalgae utilizing wastewater [9].

The cold solvent (acetone) method is insufficient for completely extracting less polar pigments like *Chl a* and some carotenoids. Experimental data indicates that methanol and ethanol, via a hot solvent extraction method, provide better extraction results. Research on developing microalgal dyes with broad spectral responses and better electron-donating capabilities is showing promise with *Scenedesmus sp.* and *Asterarcys quadricellulare* dyes in around 80% ethanol and performed best on the 20^{th} day, followed by the 15^{th} and 25^{th} days. These dyes have confirmed the presence of desired functional groups aiding attachment to the semiconductor layer. These dyes remained relatively stable at 10,000 lx and might survive long diffused light durations for a few days. Further research is needed to enhance dye stability with appropriate eco-friendly additives. Ethanol is the best green solvent for extraction via hot solvent extraction, but lower temperatures need to be identified to avoid early dye degradation.

Scenedesmus sp. dye in ethanol performed best in the visible region, requiring the least energy for photoelectron excitation in comparison to other combinations. DSSC performance is influenced by extraction procedures and solvent choices, impacting the photoactive layers' structural and morphological characteristics. The extraction method hence affects photosensitizer quality in terms of light absorption, and charge transfer processes.

An extraction temperature of 60 °C is promising for dye extraction but risks rapid degradation. Sonication for 40 minutes at 80% ethanol extracted 105% more dye for *Asterarcys quadricellulare* and 106% more for *Scenedesmus sp.* dye, with stability of almost 80 hours. Current research has identified dyes that can be extracted well at lower

temperatures and exhibit enhanced stability too for DSSC development. Future advancements in biomaterials discipline and fabrication systems could lead to more efficient, temperature-tolerant DSSCs using natural dyes.

The current research replaced hazardous synthetic dyes with microalgal-based photo harvesters, enhancing DSSC's easy disposal after utilization. Using carbon as a counter electrode has further reduced costs by avoiding expensive metals like platinum but has significantly impacted efficiency too. J-V analysis showed a DSSC configuration comprising *sc* dye in *et* achieved the highest PCE of 0.25% which needs to be improved further by more dye and some other component optimization like electrolyte.

Overall elevated temperatures above 60 °C are not favourable for maintaining *Chl* stability and prolonged efficiency. *Chl a* is less stable than *Chl b*, degrading more quickly and overall *Chl* remains stable at low extraction temperatures, with *Chl* degradation leading to color changes. Derived compounds like *Chlides* maintain structural integrity and energy extraction efficiency when incorporated into DSSCs, making them suitable for moderate temperature conditions. Improved extraction processes and thermal encapsulation techniques can enhance the efficiency and stability of natural dyes, making them viable for large-scale DSSC applications. Overall, it needs to be further developed that microalgal cells can also be used for energy production by replicating photosynthesis-based electron movement without the need for dye extraction in the future of this research.

4. References:

1. Shalini, S., Balasundaraprabhu, R., Kumar, T. S., Prabavathy, N., Senthilarasu, S., & Prasanna, S. (2016). Status and outlook of sensitizers/dyes used in dye sensitized solar cells (DSSC): A

Review. International Journal of Energy Research, 40(10), 1303–1320. https://doi.org/10.1002/er.3538

2. Lai, W. H., Su, Y. H., Teoh, L. G., & Hon, M. H. (2008). Commercial and natural dyes as photosensitizers for a water-based dye-sensitized solar cell loaded with gold nanoparticles. Journal of Photochemistry and Photobiology A: Chemistry, 195(2–3), 307–313. https://doi.org/10.1016/j.jphotochem.2007.10.018
3. Zhao, S., Blum, J. A., Ma, F., Wang, Y., Borejsza-Wysocka, E., Ma, F., Cheng, L., & Li, P. (2022b). Anthocyanin accumulation provides protection against high light stress while reducing photosynthesis in Apple leaves. International Journal of Molecular Sciences, 23(20), 12616. https://doi.org/10.3390/ijms232012616
4. Zhang, Q.-W., Lin, L.-G., & Ye, W.-C. (2018). Techniques for extraction and isolation of natural products: A comprehensive review. Chinese Medicine, 13(1). https://doi.org/10.1186/s13020-018-0177-x
5. Sun, H., Wang, Y., He, Y., Liu, B., Mou, H., Chen, F., & Yang, S. (2023). Microalgae-derived pigments for the food industry. Marine Drugs, 21(2), 82. https://doi.org/10.3390/md21020082
6. Chauhan, R., Shirage, P. M., & Bala, K. (2023). Unravelling the spectral enigma with enhanced extraction of algal dyes: A sustainable energy tactic. Journal of Photochemistry and Photobiology A: Chemistry, 444, 115006. https://doi.org/10.1016/j.jphotochem.2023.115006
7. Chauhan, R., Shirage, P. M., & Bala, K. (2024). Delving into judiciously extracted inexpensive micro-algal dyes for DSSCs: Spectral decipherment and time-oriented extraction systems. Sustainable Energy Technologies and Assessments, 64, 103746. https://doi.org/10.1016/j.seta.2024.103746
8. Chauhan, R., Srivastava, A., Shirage, P. M., & Bala, K. (2024). Innovating dye-sensitized solar cells through novel microalgal and cyanobacterial species extricated dyes: A sustainable tack for material scarce Earth. Solar Energy, 270, 112369. https://doi.org/10.1016/j.solener.2024.112369

9. Chauhan, R. (2022). Scanning prevalent technologies to promote scalable devising of DSSCs: An emphasis on dye component precisely with a shift to ambient algal dyes. Inorganic Chemistry Communications, 139, 109368. https://doi.org/10.1016/j.inoche.2022.109368

LIST OF PUBLICATIONS

1. Chauhan, R. (2022). Scanning prevalent technologies to promote scalable devising of DSSCs: An emphasis on dye component precisely with a shift to ambient algal dyes. *Inorganic Chemistry Communications*, 139, 109368. https://doi.org/10.1016/j.inoche.2022.109368 {I.F. – 4.4}

2. Chauhan, R., Shirage, P. M., & Bala, K. (2023). Unravelling the spectral enigma with enhanced extraction of algal dyes: A sustainable energy tactic. Journal of Photochemistry and Photobiology A: Chemistry, 444, 115006. https://doi.org/10.1016/j.jphotochem.2023.115006 {I.F. – 4.1}

3. Chauhan, R., Shirage, P. M., & Bala, K. (2024). Delving into judiciously extracted inexpensive micro-algal dyes for DSSCs: Spectral decipherment and time-oriented extraction systems. Sustainable Energy Technologies and Assessments, 64, 103746. https://doi.org/10.1016/j.seta.2024.103746 {I.F. – 7.1}

4. Chauhan, R., Srivastava, A., Shirage, P. M., & Bala, K. (2024). Innovating dye-sensitized solar cells through novel microalgal and cyanobacterial species extricated dyes: A sustainable tack for material scarce Earth. Solar Energy, 270, 112369. https://doi.org/10.1016/j.solener.2024.112369 {I.F. – 6.0}

5. Rahul Chauhan (2024). Optimising Microalgal Dyes Extraction Design for Stable DSSCs: Chromatographic Insights on Bio-Deterioration and Longevity (Accepted - Analytica Chimica Acta)

6. Rahul Chauhan (2024). Analysing hot solvent extracted microalgal dyes via mass spectrometry: identifying accretion and fragmentation for enhanced stability (Manuscript under revision- Algal Research)

TABLE OF CONTENTS

LIST OF FIGURES

LIST OF TABLES

NOMENCLATURE

Abbreviation	Full Form
(5c)	2-cyano-3-(4-(9-(dimethylamino) dibenzo [b, h] [1,6] naphthyridin-2-yl) phenyl) acrylic acid
(D–A–π–A)	donor-acceptor–π bridge–acceptor' type zinc porphyrin sensitizers
$[Co(phen)_3]^{3+/2+}$	Tris (1, 10-phenanthroline) cobalt (II)/ (III)
2nd type	4-(Bis- {4- [5-(2, 2-dicyano-vinyl)-thiophene-2-yl]-phenyl}-amino)-4-phenylpyridine
5c	D-π-A organic dyes bearing fused dibenzo [b, h] [1,6] naphthyridine as the conjugate dπ-bridge
80% R + 20% G	80% Red beetroot (*Beta vulgaris*) + 20% Green spinach (*Spinacia oleracea*)
Alkoxysilyl	anchor dye ADEKA-1 and carboxyl-anchor organic dye LEG4
ac	acetone
as	*Asterarcys quadricellulare*
Asta	Astaxanthin
Au NP	gold nanoparticles
Au therm	gold CE prepared by deposition of $HAuCl_4$ (5 mM in 2-Propanol) using one layer of adhesive tape, followed by sinterization in air atmosphere using four ways with a different temperature for different time
B-car	β-carotene
BHJ	Bulk-heterojunction
Black mulberry fruit juice	*Morus nigra*
BPY	2, 2'-bipyridine
BrGNP	Edge-selectively Halogenated Bromine Graphene nanoplatelets
C	Carbon
C10	20 ml red dye+80 ml yellow dye (20% red+80%

(Combination 10)	yellow)
C4 (Combination 4)	40% red (red spinach (*A. dubius*)) + 60% yellow (turmeric (*C. longa*)) anthocyanin and chlorophyll
CB 1 H	Carbon black single coating layer with heat treatment
CB 3 H	Carbon black triple coating layer with heat treatment
CCI	composite conductive inks
CdTe	Cadmium telluride
CE	counter electrode
Chl a	Chlorophyll a
Chl b	Chlorophyll b
Chlide a	Chlorophyllide a
Chlide a der	Chlorophyllide a derivative
Chlide b	Chlorophyllide b
CIGS	Copper indium gallium selenide
CNT	candle nip technique
coe	*Coelastrella sp.*
co	*Coelastrum proboscideum*
Co (bpy) 3]$^{2+/3+}$	Tris (2, 2'-bipyridine) cobalt (II)/ (III)
Cu (tmby) 2	- bis-(4, 4', 6, 6'-tetramethyl-2, 2'-bipyridine) copper
CV	cyclic voltammetry
des	*Desmodesmus pseudocommunis*
Diadino	Diadinoxanthin
DSSC	dye-sensitized solar cell
D-TNW	dual TiO_2 nanowires
E_g	energy gap
EMPL	Eidgenössische Materialprüfungs- und Forschungsanstalt
et	ethanol
ETL	Electron Transport Layer
ETM	Electron Transport Material

eV	electron Volt
Fe_2O_3	Ferric Oxide
FLG	few layers of graphene
FRET	Förster (fluorescence) Resonance Energy Transfer
FTIR	Fourier Transform Infrared Spectroscopy
FTO	fluorine-doped tin oxide
Fuco	Fucoxanthin
GaAs	gallium arsenide
GNP	Graphene nanoplatelets
H_2PO_3	Phosphoric acid
H_2PtCl_6	Chloroplatinic acid
HOMO	Highest Occupied Molecular Orbital
HTL	Hole Transport Layer
HTM	Hole Transport Materials
I^-/I_3^-	iodide/triiodide redox electrolyte
IGNP	Edge-selectively Halogenated Iodine Graphene nanoplatelets
ITO	indium–tin oxide
LUMO	Lowest Unoccupied Molecular Orbital
Lut	Lutein
Lv	*Leucanthemum vulgare*
MC	mercurochrome
mt	methanol
N719	([RuL2 (NCS) 2(TBA) 2], where L =1172, 20-bipyridyl-4, 40-dicarboxylic acid
Nb_2O_5	Niobium pentoxide
NCP	neocuproine hydrate
NiO	Nickel Oxide
NP	nanoparticles
NZT-40	Ni- Zn doped TiO_2 (99% TiO_2, 0.4% Ni and 0.6% Zn)
PAM	pulse amplitude modulated
PBT- 2	N719 + two flat fused aromatic hydrocarbons

	fused rings
pe	*Pediludiela daitoensis*
PEDOT	poly (3,4-ethylenedioxythiophene)
PEDOT: PSS	Poly (3, 4-ethylenedioxythiophene)-poly(styrenesulfonate)
PEG	Polyethylene glycol
PEN	polyethylene naphthalate
PET	polyethylene terephthalate
Phide a	Pheophorbide a
Phide a der	Pheophorbide a der
Phide b	Pheophorbide b
Phytin a	Pheophytin a
Phytin b	Pheophytin b
PIW	*Pterocarpus indicus willd*
p-n junction	an interface or a boundary between two semiconductor material types, namely the p-type (positive) and the n-type (negative), inside a semiconductor
Poly (AMPS-IA-F-Cl-Br-An)	liquid electrolyte adsorbed into poly (2-acrylamide-2-methylpropane sulfonic acid/ itaconic acid) hydrogel and its doped derivatives.
PProDOT	Poly 3, 4-propylenedioxythiophenes
Pt	platinum
PV	Photovoltaic
PVDF	Poly (vinylidenefluoride)
SA1	(2-Cyano-3-(4-nitrophenyl)-N-phenylacrylamide)
sc	*Scenedesmus sp.*
Si	Silicon
SiO_2	Silicon dioxide
SO_3H	Sulfonic acid
$SrTiO_3$	Strontium titanate
S-TNW	Single TiO_2 nanowires
TBA	tetrabutylammonium

TBAPF6	0.1 M tetrabutylammonium perchlorate (TBAP) in Tetrahydrofuran
TBP	4-tert-butylpyridine
TCO	Transparent Conductive Oxide
TH-2F	one of the three (D–A–π–A) with a benzothiadiazole (BTD) unit bearing two fluorine as the auxiliary acceptor and thiophene as the π bridge.
TiO_2	Titanium dioxide
Type 2 electrolyte	solvent- acetonitrile with the addition of some amount of KI and iodine
Viola	Violaxanthin
W-NO_2	2-methoxy-4, 6-bis (4-(4-nitrostyryl) phenyl) nicotinonitrile Y123 + CDA in 4-TB: acetonitrile = 0.1 mM Y123 and 5 mM chenodeoxycholic acid in solution of 4-tert-butanol: acetonitrile (1:1 v/v)
Zea	Zeaxanthin
Zn_2SnO_4	Zinc stannate
ZnO	Zinc oxide

CHAPTER 1

Introduction

CHAPTER 1

Introduction

1.1. Background information

The sun is the replenishing source of most of the energy on and under the earth's surface and the primary source of all light and heat energy continuously reaching the earth. While confronted by the energy demands of the soaring population and the economic value of energy, the energy extraction of already stored and instantaneous conversion of daily entering energy of the sun in a suitable form without much environmental damage becomes a tenacious task for humankind. Upon realizing the already sky-high emission levels, with the most significant chunk coming from non-renewable fossil fuels, the only choice is to employ only renewable energy sources.

Efficiency improvements in renewable energy sources can lower the emitted carbon levels [www.iea.org]. Still, the future of energy generation is being determined by socio-political scenarios [Beretta, 2007]. In the prevailing setup, one of the best options is exhibited by direct electricity-yielding solar PV cells providing enough sustainable energy access to all to maintain a decent living standard besides environmental stature. Other renewable energy systems, like hydrogen fuel [Eaves & Eaves, 2004; Shinnar, 2003], tidal, and bioenergy, are available, but without much better green traits. They possess the potential to be an equivalent alternative with better efficiency and low-grade technology requirements. Still, they are in pursuit of efficient light and fast rechargeable batteries for stockpiling [Eaves & Eaves, 2004]. The continuous decline in distributed solar PV costs and slashed electricity prices [www.pvwatts.nrel.gov] has a bright history of the average supply rate of solar PV from 1990 to 2017 of 37.0% [www.iea.org/statistics] in the renewable category. It stands quite better than 23.4% of wind and almost four times biogas and hence promises to succeed in global electricity enhancement [www.iea.org/reports] undeniably.

Silicon cells are the most commercially available solar PV cells with better efficiency than other materials but are less environmentally friendly than other thinner solar alternatives. One of these thinner solar cell-type alternatives is DSSCs, first fabricated in 1991 by Professor Gratzel [O'Regan & Grätzel, 1991] and his team, that is compact, lightweight, and have economic gains while reducing environmental hazards. Many researchers have gathered information later to suggest better fabricating ideas that make it commercially attractive with increased efficiency. Out of all the components, the component dye in these solar cells comes with many different options: synthetic or natural dye, inorganic (metallic), or organic dye. Since non-natural dyes come with an environmental cost, natural dyes were ultimately preferred and studied to accommodate in DSSC. A recent review by Baby et al. has gathered previous research and explains in terms of methods used for extraction, dye volume, pH level, fabrication temperature, solvents involved, and coating techniques that need to be monitored and that can be adjusted to the desired parameters [Baby et al., 2021]. A revolution is required in DSSC using natural dye to address environmental concerns that were previously unresolved in the renewable energy field.

Shalini and their team (2015) discussed DSSC operation with natural dye/pigments and combination with other components in tabular form, emphasizing improvement scopes [Shalini et al., 2015]. Their review could only briefly focus on four sensitizer pigments, namely *Chls*, Flavonoids, Anthocyanins, and Carotenoids, but it needed detailed specifications. Another review from Jamalullail et al. in 2017 focused only on the role of plant pigments in a solar cell while drawing attention to betalain pigment extract from purple wild Sicilian prickly pear dye, declaring it better than *Chl* and anthocyanin [Jamalullail et al., 2017]. Richhariya et al. have reviewed simple extraction and application of natural dyes, mostly from plant parts, for DSSC application to replace the chemical synthesis process of expensive non-natural dyes [Richhariya et al., 2017]. The review by Kumara et al.

[Kumara et al., 2017] provided insight into the practices to increase the performance of pigments in DSSC and their limitation, along with the comparison of the cost of synthetic dye-based and natural dye-based DSSC. Nahar mentioned [Nahar, 2021] in his review the importance of the chromophore group in natural pigments that perform the sensitizing job in DSSC and that it is the most substantial component. Also, natural dye should be preferred because organic dye shows deleterious effects and can be a health concern. Bist and Chatterjee's review [Bist & Chatterjee, 2021] highlighted that combining variable dyes for light harvesting, electrolyte types, semiconductors variety, solvent types, effects, and CE modification do not develop positively enhanced efficiency alone.

1.2. PV Technology

1.2.1. General Solar Cell Working Principle

When sunlight strikes a solar cell, its semiconductor material absorbs the light. This solar radiation (photons) typically hits the p-n junction through a thin n-type semiconductor. The photons generate electron-hole pairs when their energy is sufficient. This disrupts the junction's thermal equilibrium. Free electrons in the depletion region move to the n-type side, while holes move to the p-type side. Once electrons reach the n-type side, they cannot cross back due to the junction's barrier potential. Similarly, the holes cannot cross back to the n-type side, preventing electron recombination. This results in a higher electron density on the n-type side and a higher hole concentration on the p-type side, causing the p-n junction to act like a tiny battery. This process creates a voltage known as photovoltage. When this junction is connected to a small load, a current flows through it, known as photocurrent.

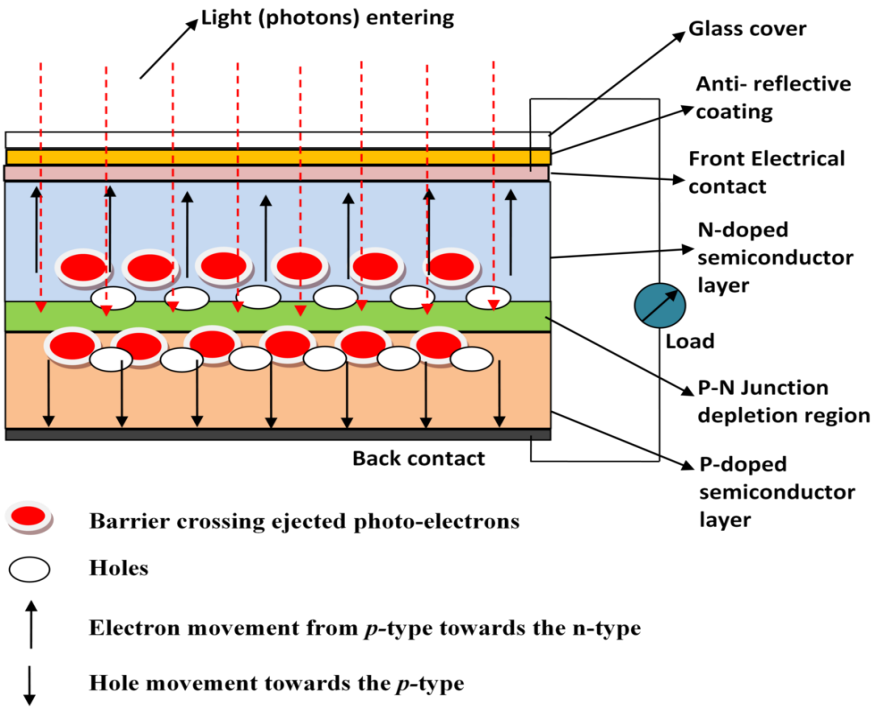

Figure 1.1. Structural overview of the operational mechanism in basic solar cells.

The working principle of solar cells is illustrated in **Figure 1.1**. Silicon-based single-junction solar cells have an efficiency of about 20%. Using various semiconductors and multiple p-n junctions, multi-junction cells improve efficiency by capturing different energy bands at each intersection. Sodium hypochlorite is an anti-reflective texturation coating [Basu et al., 2010]. The Shockley-Queisser limit for single-junction cells is around 30% because they only absorb photons within a specific frequency range, with the rest passing through [Neville, 1995]. Solar panels connect cells in series and parallel to achieve higher voltage.

1.2.2. Recent PV technology in the market

Another central area of research in the solar industry is BHJ organic or polymer solar cells. These cells have an active layer composed of a fullerene acceptor and a conjugated polymer donor. Excitons are generated and diffuse to the donor/acceptor interface, dissociating and enabling charge carrier transport (**Figure 1.2.**). Perovskite solar cells

are another crucial contemporary type structurally similar to DSSCs. Their device architecture involves various ETL and HTL materials, which facilitate the collection of electrons and holes through transparent electrodes. The perovskite absorber is solution-deposited on top of the HTL, followed by the ETL deposition (**Figure 1.3.**).

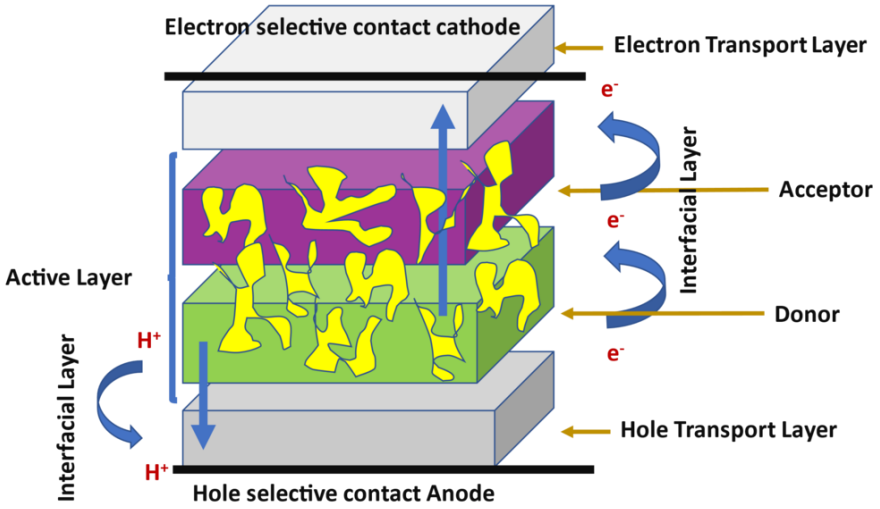

Figure 1.2. Schematic illustration of an organic solar cell in charge extraction mode.

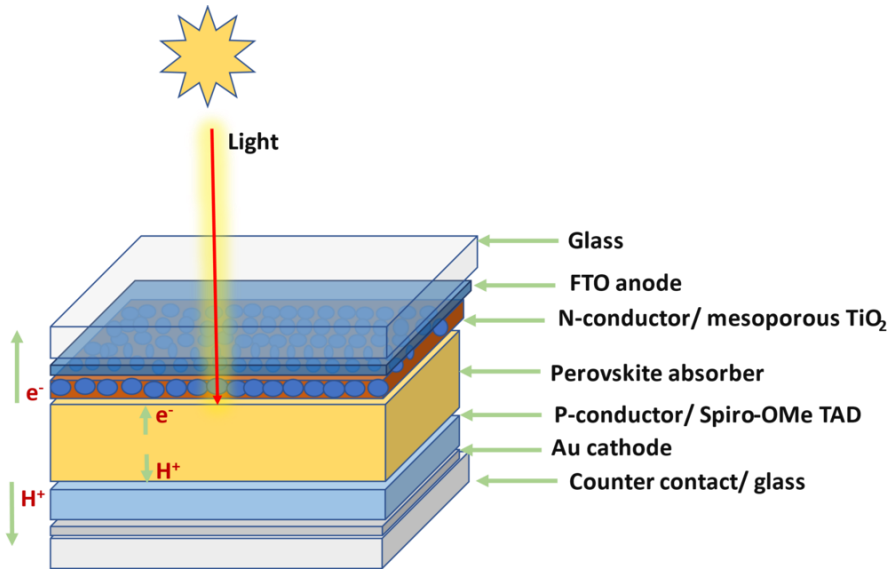

Figure 1.3. A simplified display of 3rd generation cells - Perovskite solar cell.

1.2.3. Impacts of Materials in Solar Cell Designing

The better cost-efficient substrates for cell design are more transparent polymers like PET and PEN, when compared to metal sheets of stainless steel and titanium, with better-insulating properties and no metallic impurities [Galagan, 2018]. Flexible polymer substrate has low contamination but slightly roughness compared to glass substrate sheets, in addition to high-temperature processing compatibility and high optical transparency [Brown, 2014]. The Swiss Federal Laboratories for Materials Science and Technology EMPL Switzerland has reported 20.4 % efficiency with flexible polymer foil, confirmed by German FhG- ISE Freiburg [Galagan, 2018; Garner et al., 2014]. After selection in bandgap terms, CdTe (~1.5 *eV*) [Williams et al., 2014] and CIGS (approx. 1.0–1.12 *eV*) [Ramanujam & Singh, 2017] films are deposited by techniques like closed space sublimation [Alamri, 2003] to achieve a high growth rate with more grain size. The reported efficiency of CdTe is 16.4% on flexible glass substrate [Mahabaduge et al., 2015], 13.8% on polymer foil, and 10.9 % on steel [Kranz et al., 2013]. A flexible *a*-Si cell layer is deposited onto the plastic substrate by a transfer method [Rath, 2010] or by direct deposition with the efficiency of PEN and PET at 6.2% and 5.9% [Rath, 2010].

In conventional cells, the absorptivity is related to the thickness of the cell. Changing thickness without disturbing solar cell absorption (like that for GaAs cells, which are less than 100 nm) is the main part of the comforts that steer the study toward ultrathin solar cells.

1.2.4. Important criterion for materials in solar cells

The semiconductors used in solar cells must have a bandgap in the range of 1*eV* to 1.8 *eV* for better efficiency. The semiconducting materials must have high optical absorption to absorb a large number

of photons in a small area. Materials embedded in the structure must have high electrical conductivity to avoid charge losses. Also, the abundant availability of raw materials in nature makes up for the low cost of the solar cell.

1.2.5. Global scenario and Costing

Sophisticated processing, use of non-abundant materials, and harmful waste release pressurized the need to develop cells with less toxic materials to avoid expenditure in health care [Stamford & Azapagic, 2018]. DSSCs have been an ideal alternative in this scenario, but efficiency is less for large-scale installations [Parisi et al., 2011].

A regular silicon cell has silicon as an originator of photoelectrons and electric field supply for current generation by charge separation. In contrast, DSSCs have charge transportation work assigned to most of the semiconductor parts, whereas excited electrons are made available by adsorbed dyes with photo-sensitizing ability. The E_g between the valence and conduction band is responsible for free electrons. Searching for cheaper and less costly process material with the required energy gap is the main task for commercializing. Multiple E_g values for more wavelength ranges generate more free electrons in a multi-junction structure. The maximum bandgap layer should be at the top, followed by lower bandgap layers. There are two options for research within DSSCs: one with some inorganic materials and the other with complete organic components, ultimately pulling down the cost. The dyes used can be organic and inorganic, of which organic and particularly natural ones are far cheaper. The chemical dyes used in ruthenium have shown the highest light conversion efficiency at 14.7%. An all-natural dye with natural and other organic components is promising and stands at an efficiency of around 3% [Maiaugree et al., 2015], but it still needs to be explored more for equivalent efficiency with all-natural components. This review later details using natural dyes extracted from algae and other microorganisms for photosensitizing applications.

1.3. DSSC

DSSC is a thin film under research evolving in the PV category. The principle of operation as described by researchers of DSSC can be summarized with four necessary elements, which are assembled for designing a DSSC in the following pattern:

1.3.1. Photo Electrode

The first is a transparent substrate glass negative electrode with either fluorine (FTO) or indium (ITO) doping in tin oxide. The glass substrate comprises soda-lime coated with a layer of any mentioned TCO [Kawashima et al., 2004] on one side. Over this side, which is conducting, a thin layer of mesoporous oxide or nano-structured wide-band-gap oxide with porosity of 50-60% (primarily achievable by TiO_2) is developed by various techniques to achieve higher uniformity in that layer [Zaki et al., 2011]. Other than TiO_2, the different semiconductor examples of metal oxides are ZnO, SiO_2, Zn_2SnO_4, $SrTiO_3$, and Nb_2O_5. In the past, photo electrodes of solar cells were prepared from heavy semiconducting materials like Si or GaAs, which have photo-corrosion [Weng et al., 2019] drawback with light exposure. Still, with TiO_2 coating [Didden et al., 2015], ZnO photo corrosion chances are less. Another drawback is the light conversion efficiency because of the sensitizing element's weak adsorption on the surface [Chang et al., 2012] of the electrode due to limited area or due to the roughness factor of the photoelectrode [Joshi et al., 2011]. Recently, nano-structuring has brought productive upgrades in electrical, chemical, and optical properties [Zhang & Cao, 2011; Aly, 2017]. Also, one dye molecule covers a greater area at its optical cross-section, but adsorption on a nano-structured layer or nano-morphological patterns of semiconducting materials take less surface area of the semiconducting layer [Aly, 2017; Yu & Chen, 2008]. These structures provide an upraised roughness factor with increased surface area for dye adsorption, and higher PV efficiency is possible with the

same elements as the non-nano-structured photo-electrode [Aly, 2017; Yu & Chen, 2008].

1.3.2. Photosensitizing Material

The second is a mono-molecular layer of a charge-transferring or photo-sensitizing dye covalently attached over the semiconducting mesoporous oxide layer's surface. The dye helps in the peak absorption of the incident light to enhance the production of photon-energized electrons. DSSCs in the past had transition metal coordinated compounds like ruthenium polypyridyl complexes for sensitizing as they possess efficient visible band absorption and metal-to-ligand charge transfer, with longer electron excitation life [Pashaei & Shahroosvand, 2020]. However, the high cost of production and health effects [www.lenntech.com] call for safe, natural dyes. Dye, the critical factor for photon energy absorption, should possess the required photophysical and electrochemical properties [Ghann et al., 2017]. The essential properties include luminosity, capable of injecting electrons into the semiconductor layer upon excitation, whose absorption spectra cover ultraviolet, visible, and near-infrared regions [Ghosh et al., 2018]. They can resist oxidation and reduction without degradation [Xue et al., 2012]. The HOMO of the dye, *i.e.,* the molecular orbital of the dye molecule, which is filled, should have a position that is distanced from the mesoporous oxide conduction band surface [Hagberg et al., 2007]. This mesoporous oxide conduction band surface should have a potential slightly lower than the potential of the LUMO (molecular orbital which is unfilled) of the dye [Hagberg et al., 2007]. The hydrophobic nature of the dye minimizes the chances of forming a direct connection between the electrolyte and water-induced deformity in the dye utilizing the surface of mesoporous oxide [Desta et al., 2017]. Hence, this is essential for the longevity and stability of the dye. Also, the use of co-absorbents helps in achieving stability [Cisneros et al., 2016] and better adsorption, like cheno deoxycholic acid (CDA) [Salvatori et al., 2013]. Stability is also achieved using anchoring groups of phosphonic acid or carboxylic acid [Zhang &

Cole, 2015]. These anchoring groups can be added in the middle of the dye and mesoporous oxide to reduce the dye molecule's non-uniform collection on the mesoporous oxide surface. They further limit the recombination between electrolytes and electrons on the mesoporous oxide surface [Wiberg et al., 2009]. Together with the dye layer, the electrode is called the photoanode.

1.3.3. Electrolyte

Third, is an electrolyte of heavy halogenic ions (such as iodide/ triiodide couple I^- /I_3^- or bromide/ dibromide Br^- /Br^{2-}), and in some devices, thiocyanate based SCN^- /SCN^{2-} or selenium cyanate based $SeCN^-$/ $SeCN^{2-}$ and bipyridine cobalt complexes Co (II)/ Co (III) whose fast oxidation and reduction are must for the recovery of dye [Nakade et al., 2005]. It can be outlined as a solution containing reducing and oxidizing forms and comprising solvents and additives with ionic liquids and cations. The electrolyte should possess properties like a non-corrosive nature, conductivity enhancer, electrochemically and thermally stable, and fast diffusion of charge carriers [Wu et al., 2015]. An electrolyte's absorption spectra should not overlap with that of a dye. Its redox couple should effectively regenerate the oxidized dye [Daeneke et al., 2012] while developing good contact between the counter and the anode. Also, an electrolyte possessing a redox mediator prepared using an organic solvent is vital as a deciding parameter of dye regeneration [Yun et al., 2017]. The ionic liquids electrolytes have a higher leakage factor. The volatility of the organic solvents can be avoided in sealed cells by some long-term light soaking tests and by using various types of solid materials to replace conventional liquid electrolytes [Iftikhar et al., 2019; Pujiarti et al., 2014]. The use of other ionic liquids or ionic solids or the use of organic-HTM can be of significant aid. Polymer gel electrolytes, being highly thermally stable and better conductive, can be a better option [Cheng et al., 2017].

1.3.4. Counter Electrode (CE)

It is one more glass substrate plate with a layer of any of the TCO prepared separately, over which a thin layer coating of the catalyst [Guo et al., 2015] mainly using Pt [Guo et al., 2015] or C [Aftabuzzaman & Kim, 2018] is prepared. This CE regenerates the electrolytic element's ions and acts as a cathode. Pt is the most efficient because of compatible facile I^- /I_3^- redox kinetics and higher light reflection [Guo et al., 2015]. But Pt, being costly, is replaced by C as in carbon wrapped or its nanotubes form, which gives almost equivalent efficiency to Pt [Aftabuzzaman & Kim, 2018; Gnanasekar et al., 2019]. Other conducting polymers have potential, too, like stainless steel with a polyaniline layer that is cheaply produced by electro-chemical polymerization [Qin et al., 2010]. Alternatively, cobalt sulfide (Co_xS_y) [Huo et al., 2015], nickel sulfide (NiS) [Song et al., 2014, Yang et al., 2014], cobalt and nickel selenides, e.g. ($Co_{0.50}Ni_{0.50}Se$) [Jiang et al., 2019] Cobalt- Nickel or Iron-Selenium alloys, or silver nanoparticles (AgNPs) [Yue et al., 2016] can be used too. Preparation of the electrodes requires various techniques such as chemical vapor deposition [Lee & Hyun, 2016], sputtering, electro-deposition [Jiang et al., 2019], and others. An essential objective of a potential catalyst is to complete the process by reducing redox couple on the CE surface by electron acceptance through the ionic transport material that is transported back to the cell in electron circulation. Also, a reflection of the unabsorbed light by the CE helps in better utilization of the light by photoanode. The main desirable properties in a CE [Song et al., 2014; Yang et al., 2014] are high conductivity, efficient catalytic activity, porous for maximum surface area, corrosion resistance, and stability.

1.4. Operational Mechanism

DSSCs operate in four phases:

1. Incoming photons pass through the transparent TCO layer on a glass substrate along with the semiconducting mesoporous oxide layer and get absorbed by photosensitizing moiety. As wavelength absorption on dye is correlated with photon energy, these photosensitizing molecules transfer their absorbed energy to their electrons to excite them from a

non-energy absorbed state (S to S^*) to the photon energy absorbed state. The electron emission occurs from the dye molecule as (S^* to S^+).

2. Then, the excited electron with a concise life moves into the conduction band of nano-structured broad bandgap oxide present at a level below the energy-absorbed state of the dye. The oxidation of dye takes place here with the removal of an electron.

3. The excited electrons travel inside semiconducting mesoporous oxide layer nanoparticles and disseminate towards the TCO of the photoanode, from where electrons travel towards CE by the attached circuit.

4. Further, at this CE side, the electrons from the I_3^- state reduce to the I^- state and reduce the dye to its unexcited state. Here, to again oxidize I to the I_3^- state, electrons must be accepted, or current must be collected from the I^- ion redox mediator.

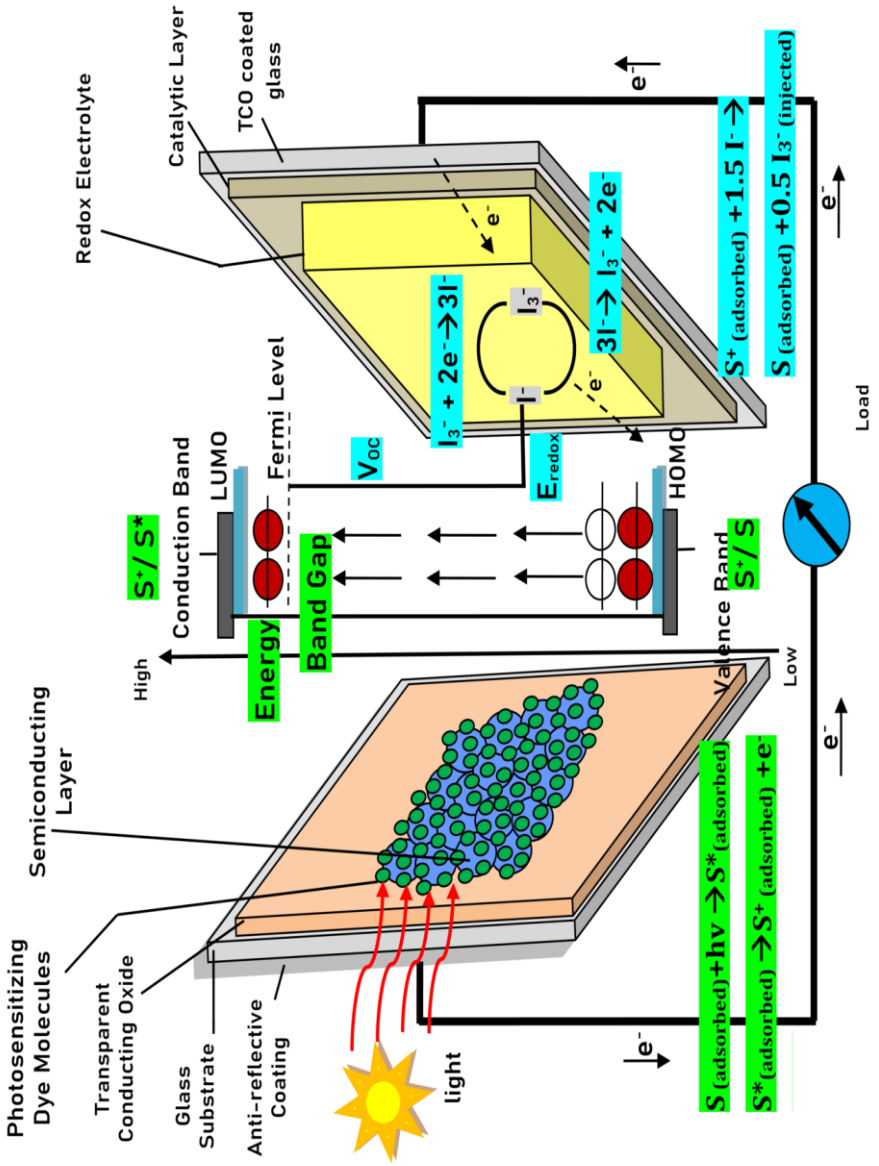

Figure 1.4. Structural components and working mechanism of DSSC.

As shown in **Figure 1.4.**, the basic idea kept here is a wider separation of the process of light absorption from that of charge collection in combination with sensitizers.

1.4.1. Time duration for photon absorption and electron movement

In electron injection, the LUMO electrons of the excited dye molecule (S^*) move within femtoseconds (~10−15 fs) [Kumar et al., 2016] to the mesoporous semiconducting oxide layer. Then, the semiconducting layer's Fermi level shifts to the conduction band for *n*-type and *p*-type

towards the valence band. The oxidized or ionized dye molecule stays as (S^+), and within milliseconds (10^{-3} s) [Nanostructured Solar Cells, 2017], the electrons pass through the semiconducting nanolayer to the conducting substrate. Electrons from this substrate reach the catalytic CE, passing through an external circuit load. The electrons recombine with the ionized dye molecule in 10^{-4} to 10^{-6} s [Tractz et al., 2018]. During the transfer process, the movement of photoelectrons in the TiO_2 conduction band tries to prevent electron recombination by two concurrently occurring competing recombination reactions. Moreover, it was confirmed that the electron transfer rate between the excited dye molecules into the TiO_2 conduction band is in femtoseconds [Asbury et al., 2001]. However, the oxidized dye is reduced in 10^{-8} s, which shows that the reduction of dye molecules is at a double rate compared to recombination with photoelectrons [Marchini et al., 2020]. A blocking layer can be developed over the oxide of the electrode material to reduce the recombination loss in semiconductors by using ZnO or insulating materials such as Calcium carbonate and Barium carbonate. Back electron transfer on the FTO surface is ceased to some extent by TiO_2 by giving a larger contact surface area between TiO_2/FTO (and TiO_2/ITO) for faster electron transfer.

1.4.2. Recombination Affinity

Recombination of charge carriers may occur and scale down the current generated in two ways, *i.e.*, directly with the oxidized form of dye or indirectly with the I^{3-} in the electrolyte, as primarily reviewed in studies. The excited electrons move toward the semiconductor's conduction band by creating inter-facial bonds and get deposited at the anode. The holes reside on the dye molecule, meanwhile, due to the broader separation of HOMO from LUMO of the dye.

1.4.3. Sensitizer Dye

The dye-sensitizing molecule is a light absorber and electron dispenser. An ideal dye or sensitizer must possess the following properties:

1. A broader absorbance spectrum to generate a higher photocurrent.

2. Should have the anchoring groups for attachment on the semiconducting layer to help dye LUMO transfer electrons to the semiconducting conduction band.
3. For electron injection, the HOMO potential of the dye should be more favorable than the redox level. In contrast, the LUMO should be less positive than the semiconducting layer conduction band.
4. Dye should have the least aggregation on the semiconducting layer surface.

Suppose the dye energy gap (HOMO - LUMO energy difference) is equivalent to photon energy. In that case, the photon will be dye absorbed and hence excite an electron to move from the HOMO position to that of the LUMO position [Velusamy et al., 2005]. For adequate electron excitement, one needs HOMO to exist in the semiconductor bandgap level and the level for LUMO to be well inside the conduction band. The injection time has yet to be discovered, but different calculations are available as electron injection efficiency manipulates PV efficiency [Koops et al., 2009]. The energy conversion efficiency of the DSSCs depends upon standardizing these discussed points combined with dye response to photons. The need for a high surface area of semiconductor film helps maximum dye adsorption, implying better photon absorption due to enhanced optical density. Calculations can be made for the potential difference voltage V_{OC} of the open circuit between the anode and cathode to determine the difference between electrolyte anion energy and the conduction band energy at its lower limit.

1.4.4. Performance evaluation

The DSSCs efficiency can be calculated with these specific measurements:

1.4.4.1. Short circuit current density (J_{SC}) generated with the unit as ($mAcm^{-2}$), which involves the following equation for calculating: [163]

$$J_{SC} = \int q.IPCE(\lambda) \cdot \Phi(\lambda) d\lambda \quad (1)$$

$$J_{SC} = \int q.LHE(\lambda) \cdot \varphi(\lambda) \cdot \eta(\lambda) \Phi(\lambda) d\lambda \quad (2)$$

Where q denotes the charge of electron/ proton (Coulombs, C),

$\phi(\lambda)$ denotes the incident photon intensity/ flux on the cell surface at a certain wavelength (J/(m^{2}s)

IPCE denotes the current efficiency generated for incident photons (in percentage)

η denotes the overall efficiency of the cell (in percentage)

φ denotes the quantum yield (from 0 to 1)

LHE denotes the efficiency for light-harvesting, *i.e.*, the fraction of light intensity absorbed by the dye (in percentage) at a certain wavelength can be equated as [Mihi et al., 2006; Mihi & Míguez, 2005]

$$LHE = \frac{I_A}{I_O} = A \quad (3)$$

Where A is absorptance (absorption factor) which gives the ratio of the absorbed to the incident radiant power,

I_A denotes the intensity of light absorbed (W/m^2) and

I_0 denotes the intensity of light incident on cell (W/m^2).

By comparing the absorptance of a photonic nanocrystalline layer of mesoporous oxide-based DSSC (LHE_{pc}) at some wavelength to that of the standard DSSC ($LHE_{Standard}$), the enhancement of the photo-current efficiency $\Delta J_{SC} / J_{SC}$ can be estimated according to the following expression:

$$\frac{\Delta J_{SC}}{J_{SC}} = \frac{\int (LHE_{pc}(\lambda)\varphi(\lambda)d(\lambda) - \int LHE_{standard}(\lambda)\varphi(\lambda)d(\lambda))}{LHE_{standard}(\lambda)\varphi(\lambda)d(\lambda)} \quad (4)$$

1.4.4.2. Efficiency for incident photons-to-current conversion ratio (IPCE) for monochromatic light, *i.e.*, percentage IPCE also called the Quantum efficiency of the solar device. It has an evaluation type as percentage EQE (External Quantum Efficiency), which assists in calculating the total light generated electrons each second inside the external circuit divided by the total photons reaching the cell surface each second. But not all surface-reaching photons excite as they get

reflected or lose their energy in transmission and only those getting absorbed determine what is known as IQE (Internal Quantum Efficiency) [Hagfeldt et al., 2018].

Note: Lower IQE means the solar cell is inefficient in utilizing photons

$$IPCE\ (\lambda) = \frac{electron\ released\ (\lambda)}{incident\ photons\ (\lambda)} = \frac{Photocurrent\ density}{Wavelength\ Photon\ Flux}$$

$$IPCE\ (\lambda) = \frac{J_{SC}(\lambda)}{q \cdot \Phi(\lambda)} = \frac{hc \cdot J_{SC}\ (\lambda)}{q \cdot \lambda \cdot P_{inc}\ (\lambda)} \qquad (5)$$

Where J_{SC} - short-circuit current density at a certain wavelength λ (Acm^{-2}),

Φ - Photon flux at some wavelength λ ($J/(m^2s)$)

P_{inc} - the intensity of photons at some wavelength λ (W/m^2),

q - Charge carried by a single proton/ electron (Coulombs, C)

Along with Planck constant and light speed h and c

$$IPCE = LHE \cdot \varphi_{inj} \cdot \varphi_{reg} \cdot \eta_{coll} \qquad (6)$$

φ_{inj} - quantum yield for electron injection from the excited sensitized molecules of dye to the mesoporous oxide's conduction band

φ_{reg} - dye regeneration quantum yield

η_{coll} - efficiency for collection of electron/ proton charge

A Halogen lamp (mostly Xenon) attached to a monochromator is used to measure IPCE. Calibrated photo-diode measures incident photon intensity within the range of dye absorption threshold and at regular wavelength intervals after the current attains stability. Additional biased light is put on for measurements to verify that IPCE at an applicable intensity of light is valid. The charge-collection efficiency increasing with an increase in light intensity or decrease with electrolyte mass transport constraints proves that the IPCE depends on the intensity of light.

The Internal Quantum Efficiency (considering only absorbed photons) is afflicted by resistances created in series connection and internally generated. The other resistances are further created by recombination affinity, quality of back contact material, and surface states. External

efficiency accounts for other additional factors, namely reflection and external loss of photons. Overall efficiency (observed efficiency) is reasonable when it is measured while accounting for all the losses and practical factors. However, if you know the incident light intensity, and reflected light intensity, and you know measured reflectance along with observed efficiency, then you can find out internal efficiency (will be higher than measured efficiency).

When the quantum efficiency is evaluated internally, then the total amount of photogenerated current (I_{ph}) can be expressed by

$$I_{ph} = q \int \Phi(\lambda)(1 - R(\lambda))IQE(\lambda)d\lambda \qquad (7)$$

Where $\Phi(\lambda)$ - photon flux at wavelength λ incident on the cell (J/ (m^2s)),

$R(\lambda)$ - coefficient of reflection at the surface top (expressed as a complex no.),

This is integrated over all wavelengths (λ in nm) of light absorbed by the solar cell.

The spectral response or Responsivity (denoted by R_λ in Ampere/Watt (A/W) unit) gives the ratio of the solar cell-generated current under monochromatic light radiation of a specific wavelength to that of the spectral radiation flux or irradiance (in W/ m^2). It estimated that with specific units of light intensity, how much electricity can the device generate and the equation for spectral response if expressed with the quantum efficiency term relating irradiance and number of photons, will be as follows: [Markvart & Castañer, 2013]

$$R_\lambda = \frac{q\lambda}{hc} QE\ (\lambda) = 0.808 \cdot \lambda \cdot QE\ (\lambda) \qquad (8)$$

Where λ is taken in micrometers (μm),

And if QE_λ is to be calculated from responsivity (R_λ) in A/W, then it is expressed by the following: [Hagfeldt et al., 2013]

$$QE_\lambda = \frac{N_e}{N_v} = \frac{\Phi_\xi}{\Phi_o} = \frac{R_\lambda}{\lambda} \times \frac{hc}{q} = \frac{R_\lambda}{\lambda} \times (1240W \cdot nm/A) \qquad (9)$$

Where N_e = no. of electrons generated

N_v = no. of photons absorbed

Φ_ξ = optical power absorbed in the depletion layer (watts)

Φ_o = optical power incidentally (watts)

λ = wavelength (nm)

q = the charge on electron/ proton

Here, it has been assumed that every depletion layer absorbed photon produces a practicable electron-hole pair, but it also considers that not all photons get absorbed. The type of quantum efficiency values used to find out internal or external spectral response.

1.4.4.3. Open circuit Normalized Photo voltage (Voc)

It measures the semiconducting layer conduction band energy potential and the electrolyte's redox potential. It is known by first measuring the energy of the semiconducting material's highest electron-filled orbital (Fermi level) [Hagfeldt et al., 2018] while the material resides at absolute zero temperature. The highest electron-filled orbital when experiencing an illumination (or under increased temperature), moves electrons to higher energy states and the Nernst potential calculation gives the redox couple in the electrolyte. The Nernst potential is that considered point of energy when there is no net (overall) transfer of a particular ion from either side. A Fermi level helps in the analysis of solids for thermal and electrical properties. A Fermi Sea is built at absolute zero where electrons pack into the lowest available energy states, and the surface of the sea is marked by the Fermi level. For a *p*-type semiconductor, the more positive (more holes) mean lesser work and a lower Fermi level. Fermi's energy constant for each solid is also the maximum kinetic energy an electron can attain at 0 K. Here an electron band called the valence band is formed by the combination of energy orbitals in the lower energy state, whereas the band formed by the combination of energy orbitals with higher energy is the

conduction band. The energy gap present between the two bands of conduction and valence implies that there is more energy requirement for the flow of electrons from the valence band to the available orbital sites of the conduction band with wider bandgaps. The Fermi level situated between the two bands changes as the solids are warmed, and more electrons are provided to the solid or taken out.

The exhibited open-circuit photovoltage (V_{OC}) [Elumalai & Uddin, 2016] is always comparatively less than the existing potential gap between the lower boundary of the conduction band and the potential of the redox couple. V_{OC} is generally different for different photosensitizers and fluctuates in nature for various available pathways of charge recombination, and rate and mode of electron transfer. Designing or choosing competent sensitizing elements for a device requires upgrading the functioning proficiency and relational changes of the reaction rates with systematic analysis of the working mechanism.

1.5. Advantages and Disadvantages of DSSC

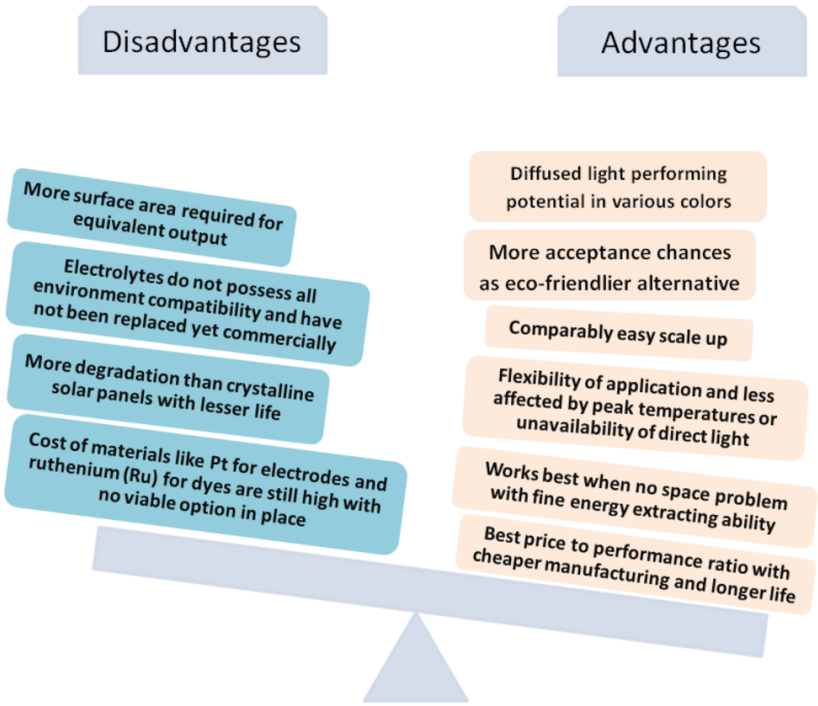

Figure 1.5. Advantages and Disadvantages balance of DSSCs.

DSSC is comparably easy to scale up with more acceptance chances as an eco-friendly alternative. The flexibility of the application is less affected by peak temperatures or the unavailability of direct light. They work best when there are no space problems with fine energy-extracting ability while generating lesser toxic waste. They have the best price-to-performance ratio with cheaper manufacturing and longer life. Hence, light on pocket power. It has diffused light-performing potential in various colors. In DSSCs, more degradation occurs compared to crystalline solar panels, which have lesser life and require more surface area for equivalent output. The cost of materials like Pt for electrodes and ruthenium for dyes is still high, with no sustainable option. Electrolytes do not possess all environmental compatibility and have yet to be replaced commercially. All advantages and disadvantages of the DSSC are briefly described in **Figure 1.5.**

1.6. Current status and Efficiency evaluation

These DSSC devices are called Inorganic, Organic, Excitonic [Gregg, 2003] or Hybrid [Arkan & Izadyar, 2017] Solar Cells. So, they are classified based on the generation of excitonic pair and nano-interface charge separation [Gregg, 2003; Wang et al., 2011]. DSSCs, realized, have utilized inorganic dyes and mostly complexes of Ru, which are non-abundant and have higher efficiency. However, further research with natural and organic compounds displayed tolerable resulting efficiency.

1.6.1. Electrolytic Efficiency evaluation

The characteristics of the suitable electrolyte can be summarized as being stable electrochemically, non-volatile, inflammable, conductive for ions, temperature range scope, and compatibility with electrolyte materials with lower cost but without compromising the environment. For efficiency improvement, the material for hole transportation or different electrolytes of various types has been used as mediators.

Electrolytes like liquid electrolytes, a polymeric electrolyte [Duan et al., 2015], either conjugated hole conducting or ion-conducting, and solid-state electrolytes were used.

The electrolyte in the liquid phase has either organic solvent to play leading roles in forming counter ions based on their stability, viscosity, Lewis' basicity value, and elevated dielectric constant [Wu et al., 2007]. The other option is ionic liquids (IL), also used alternatively for benefits like high conductivity, minimal vapor pressure, and less flammable nature [Bella et al., 2015].

Few studied organic solvents are γ-butyrolactone, 3-methoxypropionitrile (MPN), acetonitrile (ACN), methoxyacetonitrile (MAN), valeronitrile (VAN), ethylene carbonate (EC), γ-butyrolactone (GBL), N-methylpyrrolidone (NMP), and propylene carbonate (PC) which have shown better results in properties mentioned above. Other than solvents, the option of a co-absorbent reduces photoelectron recombining ability and positively affects the position of the conduction band's edge, further reducing the aggregation of dye [Manthou et al., 2015]. Alongside these, the inclusions of a few additives for electric potential enhancement, like guanidinium thiocyanate and N-methylbenzimidazole, help [Yu et al., 2010].

Oxidized dyes, after charge transportation, are reduced back by electron acceptance from liquid electrolytes. Still, the electron injection rate from the dye into the mesoporous layer is observed at around 10ps [Virkki et al., 2018]. It is not a match for liquid electrolytes if the speed of hole transportation to the opposite electrode is compared. There has not been a significant improvement in almost three decades of efficiency, with a mere increase of around 2.5% with various electrolyte replacements [Juozapavicius et al., 2012].

There is a need for electrode material and electrolyte development, which are desirable combinations, to achieve a wider potential window. The following advancements or the recent relevant breakthroughs for this can be reviewed:

a) Cell voltages increase via novel electrolytes or new solution-modified electrolytes.

b) High-density packed and effective specific surface area possessing electrodes of porous C increasing particular capacitance.
c) Formulate each element for interactive effect on each other's efficiency.
d) Organic electrolytes with more significant operational potential and lower toxicity

The other major problem we still need is the high commercial production cost due to the non-stability of electrolytes for longer duration and at higher temperatures. Electrolytes must deal with sealing issues like corrosion and leakage after enclosing or ionic loss of electrolytes efficiency using ionic liquids [Scendo & Uznanska, 2011]. Electrolytes also suffer from drawbacks like restricted dye regeneration because the slower rate of ions movement and their highly viscous nature hinders further. A concentrated electrolyte is generally preferred to handle high viscosity, and experimental combinations of additives have been shown to enhance efficiency [Ren et al., 2018]. Other substitutional methods and designs for a combination, like adding dyes in solvents of electrolytes, have been reported for solvent's vapor pressure reduction by dye [Heo et al., 2013; Puspitasari et al., 2017]. This dye addition is also manipulated, such as when the mesoporous oxide interface position is adjusted [Puspitasari et al., 2017].

It is reported that the addition of the derivative of the pyridine ring on the surface of TiO_2 boosts the density of electrons with a shift in band edge [Yin et al., 2007]. This affects the recombination rate of the charge transfer and enhances voltage but also shows reduced current density. Further, various combinations of different derivatives of Guanidinium, Alkyl Carboxylic Acids, or Phosphonic Acids and changes of polarity for recombination rate have been studied too for voltage enhancement [Idigoras et al., 2014].

Solidification of electrolytes to develop quasi-solid-state electrolytes [Jin et al., 2016] with minimal vapor pressure within the mesoporous oxide layer has been shown by polymerizing electrolytic ion's redox

couple and its oligo cum monomers [Li et al., 2015]. This approach has been further evaluated regarding efficiency with SiO_2 nanoparticles [Li et al., 2015; Caimi et al., 2018]. A comparison of solidified electrolytes with that of liquid-state has shown no significant impact on stability, lifetime, and efficiency when tested with polymerized polyvinyl butyral as the thin film [Chen et al., 2013].

1.6.2. Dyes and Electrolyte Efficiency Relation

DSSC lifespan surviving dye regeneration and degradation dependent and is marked by the turn-over number *N* [Saeed et al., 2018], which is calculated as:

$N = [k_r/k_d]$ Electrolytic ion (10)

Here, k_r denotes the electron flow rate from electrolyte ions to dye molecules.

k_d denotes dye degradation rate with oxidation

An Australian company, Great Cell Solar Limited, previously known as Dyesol, has evaluated the turnover number and reported around 10^7, approaching 10^8 (100 million), for an estimated efficient life span of at least two decades. Performance loss was not significant with time and accelerated temperature variation, nor was higher temperature variation outdoors and indoors when tested for stability.

The PV Laboratory at the Institute of Micro Technique, Switzerland, on energy conversion characterization confirmed that the derivatives of porphyrin dye, when assimilated in a combination of an artificially developed sensitizing dye of zinc porphyrin with a Y123 co-sensitizing organic dye, resulted in a record-high conversion efficiency of 12.3% with a double pyridine ring containing Cobalt electrolyte [Yella et al., 2011].

1.7. Current Status of Dyes

DSSCs developed in 1993 with Ru complex dye had an efficiency of 9.6 % and could reach 10 % until 1997 at NREL. The functional groups present in the sensitizer perform the adsorption job onto semiconducting layer surfaces like phosphonate, carboxylic acid, or

boronic acid group by providing stability till some temperature and time.

Low-temperature sintered DSSCs have shown better stability with enhanced charge collection efficiency (η_{coll}) and photoconversion (η). Also, multilayering of photoelectrode with the topmost layer based only on TiO_2-Ru (II) complex has achieved an even higher η_{coll} (74%), presenting a η of around 8.75% [Kunzmann et al., 2018] and stabilities of 600 h. Experimental studies were evaluated for light-harvesting by molecules of inorganic dyes with CE of positive Copper Oxide nanorods and various electroactive polymers [Alami et al., 2019]. A detailed summary of recent innovations of some dyes with different combinations of cell type, anode, cathode, and electrolyte is mentioned in **Table 1.1**.

Table 1.1. Recent DSSCs with different combinations of cell types, anode materials, cathode materials, and various electrolytes with dyes.

Cell type	**Dye**	**Photoanode/ photocathode**	***FF***	***η* (%**	**REFERENCES**
Solid-state *p*-type	Pb6	Solution-processed NiO-dye-ZnO (NiO/FTO)	45 (%)	0.135	Xu et al., 2019
Liquid *n-type*	N719	TiO_2/ FTO	0.45	3.23	Nemala et al., 2018

Liquid type	*n*-	N719 ([RuL2(NCS)2(TBA)2]	D-TNW/FTO	72.85(%)	2.36	Liu et al., 2018
Liquid type	*n*-	N719 ([RuL2(NCS)2(TBA)2]	S-TNW/FTO	72.05(%)	5.30	Liu et al., 2018
Liquid type	*n*-	N719	TiO_2/FTO	0.80	9.22	Ahmad et al., 2010
Liquid type	*n*-	N719	TiO_2 nanotubes/ FTO	83.145 (%)	10.241	Sun et al., 2016
Liquid type	*n*-	*Chl*	Nanocrystalline TiO_2 anatase/ ITO	28.648 (%)	0.0194	Puspitasari et al., 2017
Liquid type	*n*-	Turmeric-*Chl*	Nanocrystalline TiO_2 anatase/ ITO	25.529 (%)	0.0158	Puspitasari et al., 2017
Liquid type	*n*-	*Chl*-Turmeric-Mangosteen	Nanocrystalline TiO_2 anatase/ ITO	35.635 (%)	0.0566	Puspitasari et al., 2017
Organic dye		IQ4	TiO_2/	0.688	7.79	Yang et

		FTO			al., 2014
Organic dye	YA421	TiO_2/ FTO	0.712	9.00	Yang et al., 2014
Organic dye	YA422	TiO_2/ FTO	0.689	9.22	Yang et al., 2014
Organic dye	IQ4	TiO_2/ FTO	0.666	7.57	Yang et al., 2014
Organic dye DSSC	YA421	TiO_2/ FTO	0.712	8.84	Yang et al., 2014
Organic dye DSSC	YA422	TiO_2/ FTO	0.693	9.60	Yang et al., 2014
Organic dye	DN216	ZnO/ FTO	60(%)	3.84	Ruess et al., 2018
Organic dye	DN216	ZnO/ FTO	72(%)	3.85	Ruess et al., 2018
Organic dye	DN216	ZnO/ FTO	67(%)	3.70	Ruess et al., 2018
Organic dye	DN216	ZnO/ FTO	62(%)	3.56	Ruess et al., 2018
Organic dye	DN216	ZnO/ FTO	70(%)	3.42	Ruess et al., 2018
Liquid DSSC	N719	TiO_2/ FTO	0.722	8.29	Wu et al., 2016
Co-sensitized cell	ADEKA-1 and LEG4	TiO_2/ FTO	0.748	11.2	Kakiage et al., 2015

Co-sensitized cell	ADEKA-1 and LEG4	TiO_2/ FTO	0.771	14.3	Kakiage et al., 2015
Organic dye	Z907	TiO_2/ FTO	0.72	7.21	Liu et al., 2017
Organic dye	Y123	TiO_2/ FTO	0.74	8.81	Liu et al., 2017
Organic dye	JK-306	TiO_2/ FTO	71.6(%)	10.03	Jeon et al., 2015
Organic dye	JK-306	TiO_2/ FTO	71.3(%)	10.31	Jeon et al., 2015
Mixed one layer Pigment combination	*Chl* and anthocyanin volumetric proportion of 1:1	TiO_2/ FTO	0.73	0.85	Hosseinpanahi et al., 2019
Two distinct layer Pigment combination	*Chl* and anthocyanin volumetric proportion of 1:1	TiO_2/ FTO	0.74	0.74	Hosseinpanahi et al., 2019
Wine Daisy flower petals	Anthocyanin (Lv)	TiO_2/ ITO	0.2622	0.792	Ferreira et al., 2020
Wine Daisy flower petals	Anthocyanin (Lv)	TiO_2/ ITO	0.2659	0.878	Ferreira et al., 2020

Ru (II) complexes bearing diamine-based bidentate ligands	Ru (II) 8A	TiO_2/ FTO	0.68	2.25	Dayan et al., 2020
Co-additive CDA	N719 + 7.5 m M CDA	TiO_2/ FTO	0.76	7.00	Kumar et al., 2020
Co-additive CDA	RhB + 10 m M CDA	TiO_2/ FTO	0.69	1.75	Kumar et al., 2020
Co-additive CDA	D149 + 10 m M CDA	TiO_2/ FTO	0.69	7.72	Kumar et al., 2020
TiO_2/ ZnO Blocking Layer	N719	TiO_2 NP/TiO_2/ ZnO/ FTO	59(%)	7.1	Zatirostami, 2020
2-cyanoacetanilide based organic dyes co-sensitization	Ru (II) complex HD-2 with SA1	TiO_2/ FTO	57.84(%)	8.02	Elmorsy et al., 2020
Catecholpyrano-5,7,3′,4′-tetrahydroxy flavylium pyranoflavylium salts	Pyrano-anthocyanin	TiO_2/ FTO	0.53	1.15	Pinto et al., 2019

Natural liquid dye extract 12-hour immersion	PIW Leaf *Chl*	TiO_2/ITO	0.406345	0.023209	Diantoro et al., 2019
Screen printing 0.25cm^2	D35	TiO_2 NP/ FTO	72(%)	5.48	Raïssi et al., 2020
Digital printing 0.25cm^2	D35	TiO_2 NP/ FTO	75(%)	7.40	Raïssi et al., 2020
(D–A–π–A) type zinc porphyrin sensitizers	TH-2F	TiO_2/ FTO	63.92(%)	6.98	Jie et al., 2020
D-π-A organic dyes based on π-bridge of dibenzo [b, h] [1,6] naphthyridine	N719 (5c+ CDA)	TiO_2/ FTO	0.74	5.02	Arslan et al., 2019
Nickel Zinc Co-doped TiO_2 blocking layer	MC	NZT-40/ FTO	0.459	0.76	Bramhankar et al., 2020

Thiophenyl bridged triarylamine-donor based dyes in *p*-DSSC with pyridine anchoring groups	2nd type	NiO/FTO	36(%)	0.060	Marri et al., 2019
2-methoxy-4,6-bis(4-(4-nitrostyryl) phenyl) nicotinonitrile as co sensitizing dye	N719+W-NO_2	TiO_2/FTO	71.11(%)	2.60	B. et al., 2019
Gel polymer electrolyte-based DSSCs	Black mulberry fruit juice	TiO_2/FTO	0.488		Önen et al., 2019
Molecular engineered metal-free organic sensitizers (polycyclic benzenoid hydrocarbon donor)	PBT–2	TiO_2	70.16(%)	7.54	Zhang et al., 2020

Molecular engineered metal-free organic sensitizers (polycyclic benzenoid hydrocarbon donor)	PBT–2 + 2 mM CDA	TiO_2	66.42(%)	7.45	Zhang et al., 2020
Combination of natural red and green dyes	80% R + 20% G	TiO_2/FTO	0.55	0.99	Bashar et al., 2019
Gold CE	Y123 + CDA in 4-TB: acetonitrile	TiO_2/FTO	0.52	4.3	Gullace et al., 2020
Pulsed laser ablation (PLA) prepared nanostructured gold CE	Y123 + CDA in 4-TB: acetonitrile	TiO_2/FTO	0.57	4.9	Gullace et al., 2020
Combination of natural dyes	C4 = 40% R + 60% Y	TiO_2/FTO	0.481	1.267	Kabir et al., 2019
Natural dyes combination with $TiCl_4$-treated FTO	C4 = 40% R + 60% Y	TiO_2/FTO (without water effect)	0.541	1.572	Kabir et al., 2019

Natural dyes combination with $TiCl_4$-treated FTO	C10=20% R+80%Y	TiO_2/ FTO (with water effect)	0.541	1.171	Kabir et al., 2019

The DSSCs mentioned in **Table 1.1**. prove that there is no specific pattern for achieving high efficiency. Different combinations of dye work for other materials, and the presence of functional groups and their absorption range mostly play a decisive role. In the CE part, C as graphene or when nanostructured like nanotubes is more efficient than even simple Pt and C. Similarly, polymers of PVDF and PEDOT also seem promising enough as CE. In the case of electrolytes, Iodine-based electrolytes are very common, but cobalt-based and copper-based electrolytes also show good efficiency. The most important one is photoanodes and dyes in DSSCs and their combinations, which gave the following conclusions for the entries in the above table. Solid-state electrolytes containing p-type semiconducting material are not efficient so far. In n-type solar cells, the most compatible and successful ones have been TiO_2 (with or without nano-structuring) and N719 combinations, with their efficiency generally reaching 9%. TiO_2 has performed equally well with organic dyes but cannot do so with natural *Chl* or other natural extracts. Even ZnO has performed exceptionally well with organic dyes, which were not observed in the case of inorganic dyes. Further techniques of co-sensitization have helped DSSCs reach efficiency values between 11-13% with inorganic/ organic dyes on TiO_2. Mixing natural dyes has helped increase efficiency but could not cross the 1% efficiency barrier. They are using methods like adding co-additives to raise efficiency in the case of TiO_2 and ZnO. The Inclusion of other methods like molecular engineering of sensitizers, modifications with anchoring groups, and other printing techniques led to significantly efficient solar cells.

No guaranteed modification can work for all as different dyes may have different suitability of electrodes and electrolytes. Dye molecule composition includes long alkyl chains acting as hydrophobic groups or a short chain with opposite hydrophilic polarity with pH deciding its adsorption on semiconductor surface [Kroeze et al., 2006; da Silva & Freeman, 2019]. The nature of the chemical substituents of a dye, such as organic or inorganic, size, shape, type, and range of intramolecular charge transfer [Qin et al., 2019], and solution environment susceptibility [Habib et al., 2015] are the other essential influencers of the cell performance. In some studies, dye-based devices perform better than basic silicon-based ones with various electrolytes, photoelectrodes, and photosensitizer replacements [Hamed et al., 2017]. More and more experiments are being conducted chiefly with inorganic complexes of ruthenium, mordant dyes, and sensitizers like quantum dots or perovskite layers [Shalini et al., 2016].

1.7.1. Inorganic and Organic Dyes

The stable and scaled-up inorganic dyes in the market are Ru-polypyridyl-complex sensitizers with chemical composition as cis-dithiocyanato bis (4,4'-dicarboxy-2,2'-bipyridine) ruthenium (II) [Liska et al., 1988] (usually named N3 or N719, Z907, etc.). Whereas organic dyes are alkyl-functionalized carbazole dyes like 1,2-dimethyl-3-n-propylimidazolium iodide (LiI), 4-tert-butylpyridine (TBP) [Boschloo et al., 2006] in ACN and Y123 dyes. Both dyes have shown efficiencies of around 8%, without compromising stability, and demonstrated negligible performance loss after almost 2000 hours at 50 °C under constant UV filtered light below 420 nm at AM 1.5 G irradiation.

Transient absorption spectroscopy measurement has confirmed that oligothiophene moiety [Hara et al., 2005] present in organic dyes delays degradation by hole delocalization, leading to cations of dye remaining stabilized [Hara et al., 2005; Katoh et al., 2009] after photoexcitation. Performance was further checked in white light, not just UV-visible light circumstances, and at a high temperature of

around 80 °C. A gradual performance loss was observed without any dye molecule dissolution or degradation. The well-researched reason for the performance of dye lies in the kinetics of electron transportation and is controlled by the measure of electron diffusion [He et al., 2008].

$$L = \sqrt{D \cdot \tau} \quad (11)$$

Here, D is the coefficient of electron diffusion, and τ is the excited electron lifespan. The inorganic metallic dyes of the Ruthenium complex showed a higher value of τ than that of organic ones, implying smooth recombining of charges between electrolytic ions and electrons of the semiconducting layer. More analysis was done for hydrophobic steric effects for the presence and absence of alkyl chains for better electron lifespan.

1.7.2. Dye aggregation

Dye aggregation is affected by all the defined states of hydrophilicity, hydrophobicity, and organic nature and their interaction within their molecules [Zhang & Cole, 2017; Pal, 1965]. Also, the homogenous arrangement after adsorption on the semiconducting element interface is a subject of lateral distribution, instead of longitudinal to avoid dye aggregation one over another. The layering of different dyes can neutralize electron movement, and dye molecule interactions when bound very near to each other on a semiconducting layer may enhance or degrade charge transfer. Dye aggregation within the solution and over solid support has solvatochromic shifts bimodally, which are classified into bathochromic or hypsochromic shifts [Ravi Kumar et al., 2016]. These shifts are detected in UV/vis absorption spectral analysis and are well explained by the theory of molecular excitons.

1.7.3. Recent Developments

The recent innovation involves the addition of energy relay dyes (ERD) to the electrolyte, which makes it cogent to supply energy to the dye by helping to absorb for more range of solar spectrum and forward to sensitizer dye [US20100307571A1, 2010]. When mixed, their

efficiency on the excitement is measured in terms of Transfer Efficiency [US20100307571A1, 2010; Margulis et al., 2013]. The displayed molar absorption coefficient at 700nm is high for the dye 4-(dicyanomethylene)-2-methyl-6-(4-dimethylaminostyryl)-4H-pyran (DCM) when mixed with zinc pthalocyanine [Mattioli et al., 2012]. Energy relay dye PTCDI (perylene-3, 4, 9, 10-tetracar-boxylic diimide derivative) with zinc pthalocyanine organic dyeTT1 (dinitrilotetrabenzo [c, h, m, r] tetraazacycloeicosinator-(22)-N29, N30, N31, N32 zinc (II) derivative) [Takekuma et al., 2018] was reported with an optical window of 400–590 nm as DCM grabbed photons between 400-550nm. The increase in photo-current density is attributed to FRET from relay dye.

Co-sensitization has the drawback of adsorption of dyes on mesoporous oxide surfaces only, whereas it is not the case with ERDs. Multiple ERDs, with wavelength range perfecting spectrum, on insertion, transfer energy to the main sensitizing dye surface. Reportedly used dyes are Rhodamine B and DCM, when inserted in a nanocrystalline porous layer, demonstrating the more significant movement of electrons [Takekuma et al., 2018]. As the following equation shows, the ERDs containing DSSCs have one extra energy transfer stride to mark ERD's role in efficiency.

$$EQE_{ERD} = \eta_{AB,ERD} \cdot IQE \cdot ETE \qquad (12)$$

Here, EQE_{ERD} – External Quantum Efficiency enhanced by ERD use.

$\eta_{AB,\ ERD}$ – spectrum fraction of absorbed light within a layer of mesoporous oxide

IQE – Internal Quantum Efficiency

ETE - Excitation transfer efficiency average or sensitizing dye transferred energy probability average from ERD.

DCM is physisorbed due to electrostatic forces or steric reasons on to the TiO_2, enhancing dye loading inside the TiO_2 film. At higher

concentrations of ERD, the estimated $\eta_{AB,\ ERD}$ is shown to be 52% higher than the measured $\eta_{AB,\ ERD}$ of 32-39% with few chances of DCM concentration reduction inside the film's tiny pores because of aggregation. Reports of the problem faced by inaccurate estimation are caused by non-determination of $\eta_{AB,\ ERD}$ due to measurement inaccuracy of dye concentration. In chloroform electrolyte filling action, there is evaporation loss and scattering of photons by a porous semiconducting layer. These anomalies are solved by designing a quantified experiment and choosing solvents for electrolytes with higher boiling points [Shah et al., 2017]. The rate of FRET, which depends on the separation distance between ERD and the leading dye, must be higher than the decay rate of ERDs under radiation and in the absence [Hardin et al., 2011].

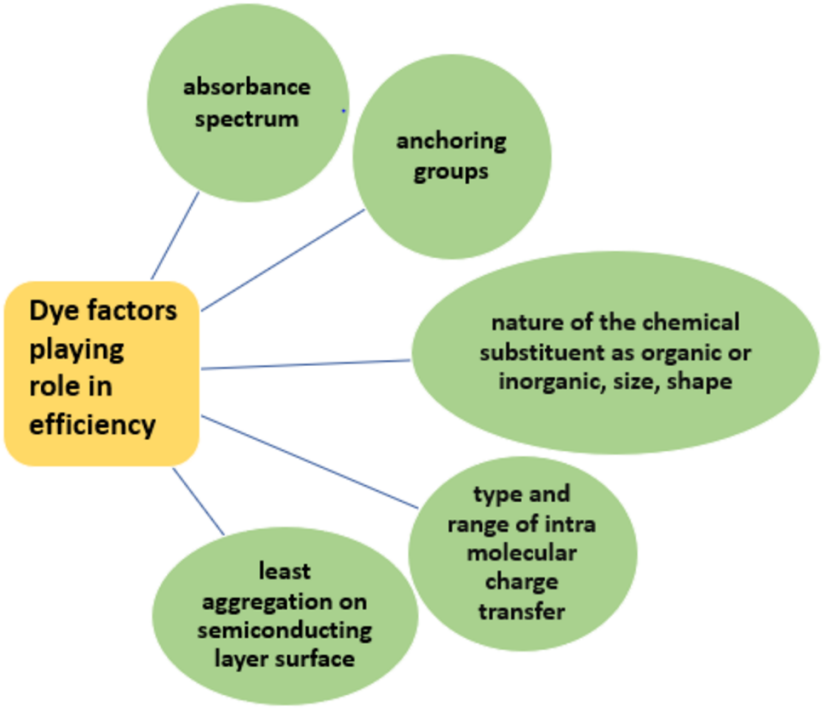

Figure 1.6. Representation of Dye factors playing a role in the efficiency

1.8. Natural Algal Dyes

Natural dye extraction technologies and basic solvent extraction methods are explored using various plant parts and micro single or multicellular species. These extractions generally use solvents like acetone, methanol, and ethanol, sometimes combined with distilled water or acids like acetic or hydrochloric acid. Pigment extraction from algae and bacteria often involves green extraction techniques or methods requiring fewer organic solvents. The methods depend on the specific pigment and its solubility. Key extraction parameters include time, method, and storage conditions. Dyes can be separated into specific pigments or mixed for efficiency and are checked for extraction efficiency through pigment concentration or absorption spectra. The dye is then applied to the photoanode or tested with techniques like spin coating and may be co-sensitized with synthetic or natural dyes, maintaining pH and temperature. Stability is assessed over time while attached to a semiconducting layer.

Natural algal pigments fall into three categories: *Chls*, carotenoids, and phycobilins. *Chls* and carotenoids are water-insoluble, while phycobilins are water-soluble. Microalgae, a key source of photosynthetic pigments for PVs, offer advantages over higher plants such as no land requirement, high biomass yield, higher pigment concentration per gram of dry biomass, and lower production costs. Both marine and freshwater macroalgae and microalgae produce pigments like *Chls* and carotenoids, which absorb visible light. Light-driven charge separation identifies electron-exciting carotenoids in the reaction center, particularly *B-Car*, *Zea*, Neoxanthin, *Lut*, and *Viola*. Pigment-based combinations of DSSCs and their efficiency parameters are detailed in Table 2.

B-Car concentration of 7.4µg/mL showed maximum power at 1.8µW/cm^2, with a calculated FF value of 0.303 and an efficiency of 0.022 % due to less fluorescence decay [Nurachman et al., 2015]. All photosynthetic organisms have carotenoids for photoprotection. In natural organic solar cells (OSCs), carotenoids, namely, *Fuco*, *B-Car*, and lycopene together with the electron-acceptor fullerene derivative

[6,6]-phenyl-C61-butyric acid methyl ester (PCBM) act as electron-donor molecules. Lycopene readily forms aggregates with high carrier motion of up to 2.1×10^{-2} $cm^2/(Vs)$ through spin coating, but *Fuco* and *B-car* form amorphous films with values of (8.1 and 1.8) $\times 10^{-5}$ $cm^2/(V\ s)$. Lycopene with PCBM was augmented for charge transport and film morphology in a 1:1 blending ratio which helped in attaining efficiency improvements in lycopene-based OSCs [Wang et al., 2013].

1.8.1. Bacterial Pigments in DSSC

Other than algae, Bacterial-based pigments have been tested, such as Bacteriochlorophyll (*BChl*), Bacterial photosynthetic membrane vesicles (chromatophores), xanthophyll carotenoids, and lycopene carotenoids. Along with the other components such as pigment-protein complexes (PPC) like reaction center (RC) proteins, RC PS- I and light-harvesting complexes such as LH2, LH4, LHCII, and Bacteriorhodopsin (BR) proteins were also checked. Specialized thylakoid membranes are photosynthesis chambers, while a photosystem (PS) is the basic unit. Photosystems, including PSI and PSII, utilize the electrons naturally via the Z-scheme. Photosystems are multi-subunit trans-membrane pigment-protein complexes encompassing antenna subunits (membrane proteins except cyanobacterial phycobilisomes), a reaction center, and accessory stabilized subunits. The redox potential of PSI acceptors is more negative; hence, we can use semiconductor substrates with wider band gaps. Antenna pigments absorb photons, and electrons move to the reaction center, where charge separation occurs. *Chl a* derivative is mostly (methyl 3-carboxy-3-devinyl-pyro-pheophorobidea) of which the most efficient is methyl trans-32-carboxy-pyropheophorbide [Wang et al., 2005]. Other than *chl a* and *b*, many *chl c* (*chl c1, chl c2, chl c3*, and others) exist. They absorb extended wavelengths, also known as *chl d* and *chl f*. In contrast, *chl d* can roughly replace all *Chl* functions in oxygenic photosynthesis, while *chl f* is the red-shifted *Chl*. The scale of unsaturation inside the macrocyclic ring separates bacteriochlorophylls from *Chls*. Also, the phycobilisomes containing

phycobiliproteins function like antennae complexes and have spectra in the green, yellow, and red regions [Musazade et al., 2018].

Photosynthetic purple sulfur bacteria have a type II RC with a central domain comprising the *H-, L-*, and *M*-polypeptides. Fabricating electrodes with it helps, as they are the tiniest to execute light-induced charge separation, and generally, the extraction is simpler than photosystem complexes of oxygenic organisms. The particular pair of bacteriochlorophylls is specified as P870 due to its longwave absorption maximum, spanning nearly 10 nm [Janfaza et al., 2013]. The redox potential of this special pair is E° (P870+/P870) ~=+ 0.45 V. DSSC's η and J_{SC} increases together with firm attachment and by increasing the number of carboxyl/hydroxyl groups. The faster electron injection, proteins/carotenoid hybrid dyes induced absorbance range, increased conjugated π-bonds (n > 13), and the integration of chromatophores give unidirectional electron flow here. *RC*-sensitized DSSCs have more improved optoelectronic properties than LHCs (LH2). Antioxidants encumber the degradation of pigmented photoanodes and solid-state redox, improving device stability. Bilayer dye photoanode structure also lowers recombination as protein complexes (Light-Harvesting Complex 2(*LH2*), Bacteriorhodopsin (BR), and Reaction Center (RC)) and *Chl a* derivative combined with carotenoids displayed better η. Also, a lower value of HOMO-to-LUMO bandgaps (< 2.46 eV) enhanced HOMO-electron excitation. Xanthophyll carotenoids with polysaccharides co-adsorbents expand bonding onto TiO_2 nanoparticles for heightened charge carrier transport [Fu et al., 2014].

A 10% conjugated spacer addition has been done in carotenoids with records of conjugated double bonds, n = 9-13, namely neurosporene, lycopene, spheroidene, and spirilloxanthin to neutralize the dye radical cation and to stop the reverse electron transfer. They have shown 4.0% efficiency for spirilloxanthin (n = 13), usually 3.1% with no carotenoid [Maddah et al., 2020]. When Bacterial Chromatophores from *Rhodospirillum rubrum* were used instead of organic light-harvesting dye in association with biological electrolytes of quinone [Q] and

cytochrome *c*, it had eight times higher efficiency using near-IR photons (till 880 nm) compared to white light. Also, incorporating electrolytes in the liquid phase, which freely percolate through the TiO_2 matrix, decreased η as in the combination of TiO_2 with cytochrome c, Q0, or Q0+ cytochrome *c* combined due to opening recombination centers at the pores. It is shown that light-harvesting takes place in the presence of chromatophores, as this TiO_2+ chromatophores+ Q0+ cytochrome *c* system performs much more efficiently than the individual. TiO_2+ chromatophores +Q0+ cytochrome *c* system performed comparatively better than other controls after an 890 nm bandpass filter was set up with the LH1 complex of Rubrum chromatophores, whose absorbance maximum is at 880 nm [Woronowicz et al., 2012]. RC photoelectric conversion was better than *LH*s as *RC*-sensitized DSSC reached 0.57% η, whereas, with *LH2*, only 0.49% was achieved at the optimal concentration of 46.8 µg *Bchl* ml^{-1} *LH2*. Also, species matter as energy transfer efficiency of *LH2* in *Rhodobacter sphaeroides* was more efficient than that of *LH2* and *LH4* in *R. palustris* [Magis et al., 2011]. Absorbance decay assays have shown high photostability of bacterial carotenoids. *Hymenobacter sp.* (red) and *Chryseobacterium sp.* (yellow) carotenoid pigments where the yellow pigment may correspond to lutein and zeaxanthin, and the red pigment may be oxidized lycopene, zeaxanthin, and lutein with a carbonyl group [Órdenes-Aenishanslins et al., 2016]. These pigments arise by incorporating oxygen in any of the *C-C* double bonds by oxidation of the OH group in the chemical structure of carotenoids, forming red/orange keto-carotenoids such as astaxanthin and canthaxanthin. The solar cell sensitized with the yellow pigment presents an efficiency of 0.0323%, and the red pigment showed an efficiency of 0.0332% [Órdenes-Aenishanslins et al., 2016]. Two *Halobacterium salinarum* cytoplasmic natural biomolecules, BR and bacterioruberin sensitizers, were immobilized, and a mixture of these biomolecules was also made. The mixture showed the highest overall energy conversion efficiency of 0.16% [Molaeirad et al., 2014]. Individually photoactive protein BR with acetamide-based gel

electrolyte has shown four times higher quasi-Fermi level and electron lifetime than the triiodide-based liquid electrolyte, and η of 0.49% is more than twice. Also, J_{SC} and V_{OC} increased with DNA and contaminant-free BR, showing that BR, compared with other natural photoactive protein systems, has 13 times higher efficiency [Chellamuthu et al., 2016]. The combination of LH protein bacteriorhodopsin with TiO_2 nanoparticles was tested, and η of 0.35% was observed.

Orange-Xanthophylls pigment extracted from *Hymenobacter sp*. UV11 collected in Antarctica were tested in the presence and the absence of a slimy substance co-adsorbent (α-1, 4-glucan polysaccharide produced by UV11). The one with a slimy substance gave η improvement of 0.03%, signifying the importance of using co-adsorbents as co-adjuvants in the manufacturing with bacterial dyes, which is even better than the mix of dyes or the one in the purest form [Montagni et al., 2018].

1.8.2. Natural Algal Pigments for DSSC in the contemporary research

The effect of the duration of immersion in dye and the dying temperature was demonstrated in the DSSCs sensitized with the extracts of parsley, *Spinach oleracea*, and green algae, showing that increased dying temperature from 30 °C to 60 °C and then deteriorations on further growth. In contrast, the immersion time remained good until 12 hours and saturated afterward. However, green algae had a unique drying effect, which showed decreased η at 0.1% post-drying the dye compared to pre-drying [Taya et al., 2013].

Leucine and Lysine tagged to heterologously expressed LHC4 from *Chlamydomonas reinhardtii,* with proper orientation and immobilization on plasma-treated thin-film graphene electrodes, obtained a photocurrent density of 40.30μA/cm^2 through liquid electrolytes with a charge transfer facilitating phosphonated viologen. This created the chance that vital energy transfer processes should be

searched for synthetic interfacing materials with biological components [Ortiz-Torres et al., 2020].

Naturally occurring pigments, β-carboline alkaloids (βCs), and the red protein R-phycoerythrin (R-PE) on evaluation have shown that R-PE has quite a high stability with η at 0.11 %, compared to other recombinant proteins, which lack stability at η = 0.30 %. On the other hand, the use of βCs as an additive reduces the overall conversion efficiency of the R-PE-based DSSCs. These cells were assessed to back the hypothesis that these alkaloids would be hindering the incident of UV-B/ UV-A radiation for the stability of the primary pigment. The conformational structure of the proteins of dye was evaluated at a *pH* of 2.0, and it resulted in around 30 % reduced η, implying that R-PE protein works best in its native form with the highest absorption coefficient, best coloration, and smallest size reaching η up to 0.110%. The cost and time taking purified extracts reduce η compared to raw extracts [Yañuk et al., 2020]. Natural pigments obtained from microalga *Scenedesmus obliquus*, mostly *Chl*, with pure carminic acid (CA) from a cochineal scale insect, papaya peel extract when tested as sensitizers for sensitizing individually and in the co-sensitized mode. An efficiency of 0.064% was obtained by the algae individually, whereas a combination of all three extracts achieved 0.36%, which was even more than the other two individual extracts. Using *Chl* in separate combinations with PA or CA presents little photogeneration but high recombination resistances (R_{rec}) [Orona-Navar et al., 2020].

Cyanobacteria PSI possesses 127 cofactors in its monomer of core complex with 12 subunits each. It contains 96 *Chl* molecules, 22 carotenoid molecules, two phylloquinones, 3 iron-sulfur protein Fe4-S4 clusters, and 4 lipids, giving an efficiency of almost 1, which is difficult for artificial devices to achieve [Kargul et al., 2012]. A remodeling of PSI of thermophilic cyanobacteria on quinone-monolayer-modified electrodes, with dichloroindophenol (DCIP)/ ascorbate as a sacrificial electron donor, was done. One more PSI was

developed too, which was electropolymerized with thioaniline functionalized Pt nanoclusters (NC) to yield a bis-aniline crosslinked PSI/Pt NC composite for the generation of photocurrents with the same dichlorophenol indophenol (DCPIP)/ascorbate as a donor [Yehezkeli et al., 2013].

An algae antenna, *i.e.*, phycobilisome coupled with Chlorin e6 (a *Chl a* derivative and has a similar absorption spectrum with ~ 390 nm and ~ 663 nm peaks), on ZnO nanowires and TiO_2 showed expansion in absorption range and improved conversion efficiency and was higher than the standalone ZnO combined sensitization of phycobilisome and chlorine6 [Yu et al., 2008].

A combined PSI/PSII on electrodes displayed directional photocurrents, which avoided needing an electron donor of DCIP/ ascorbate and instead utilized an electrolyte water donor to remove P680 (Photosystem II primary donor). PSI has been stabilized by surfactant peptides using Co (II/III) as an electron transfer mediator and obtained the best J_{SC} of 362 mA cm^{-2} and η of 0.08% in a PSI-TiO_2 solar cell. A red algal PSI associated with LHC-I coupled with TiO_2 and α-Fe_2O_3 as bio photoanodes using electrolyte (I_2/I_3) has also achieved the best J_{SC} 56.9 mA cm^{-2} and η of 0.17% for PSI LHC-I/ α-Fe_2O_3 solar cell [Ocakoglu et al., 2014].

Anchoring groups like -COOH, -H_2PO_3, -SO_3H, *etc*., are used by the dye to bind. The standard anchoring group is a carboxylic acid (-COOH), which reacts with surface hydroxyl groups to develop chemical bonds. Adsorption of PSI and LHC-II on the TiO_2 electrode is facilitated by the many carboxyl residues of aspartic or glutamic acid with binding modes as covalent, carboxylate, and hydrogen bonds in the protein sequences of PSI or LHC-II. Increased TiO_2 layer thickness gives considerably higher absorbance, reaching 4.7–6.0 mg *Chl* cm^{-2}. The absorbance of LHC-II is increased by the scattering layer addition.

The antenna system of *A. platensis* (cyanobacteria) PSI comprises many *Chl* and carotene molecules, which perform excitation energy

transfer to an electron transfer chain (ETC). This transfer facilitates reducing plastocyanin or cytochrome *c*6 to soluble ferredoxin. This further in P700 (special *Chl* pair) enhances the energy level of a single electron in the photochemical reaction center. There is a high energy transfer efficiency from *Chl b* to *Chl a* for the LHC-II trimer, and its aggregate is in spinach. However, the transfer efficiency of carotenoid to *Chl a* remains constant at around 70%. Therefore, PSI trimers disassemble monomers in some detergent solutions and are less stable than LHC-II trimers. PSI-Solar Cell, after optimization, got enhanced to J_{SC} of 1.31 mA cm-2 and η of 0.47%, whereas LHCII- Solar Cell stands even higher at 1.51 mA cm^{-2} and 0.52% and can improve or vary by changing the redox couples [Yu et al., 2015]. The stability of PSI crystals is for years under multiple light-induced photovoltage cycles while promoting its orientation in films. Hopefully, with cheaper and faster processing, PSI-hybrid electrodes can be a significant performer.

Phycocyanin, a blue protein, has high molar absorption coefficients at 620 nm and was extracted from *Spirulina sp.* It mostly reaches an electric potential E_v = -0.76V upon excitation, confirming the possibility of electron transfer reactions to the semiconductor TiO_2, which has an E_v value of 0.53 V. This, in turn, predicts the regenerated oxidized dye from I^- / I^{3-} redox couple has E_v value of 0.35V. Under electrolyte concentration conditions, the dye loss due to the protein denaturalization is very low. Although the absorbance decreases significantly at high temperatures, extinction coefficients are still high enough for use in the cells. On analyzing suitable redox potentials in the aqueous solution phase, it was found that phycocyanin has a value of 1.96 V for the potential difference between the ground state, *S0*, and that of the first electronic excited state, *S1*, which is vibrationally relaxed. [Enciso et al., 2013]

Antarctic algal red dyes of different concentrations were calculated for phycoerythrin at 6×10^{-7} M from *Iridaea obovata* and *Plocamium hookeri* and 12×10^{-7} M for *Delesseria lancifolia*. *Plocamium hookeri*

was five times higher than others in phycocyanin concentration. Moreover, *Chl a* concentration was 2×10^{-5} M for *Iridaea* and *Delesseria* and 0.76×10^{-5} for *Plocamiun*. The redox behavior of the dye was evaluated by cyclic voltametric measurements using gold screen printed electrodes. CV was completed at 0.1 Vs^{-1} potential scan rates, and the oxidation peak was detected at 1.1 *V*. This peak is accredited to the redox processes that come from the mixture of pigments mainly from phycocyanin and phycoerythrin in the algae, apart from *Chl a*. The reported redox potential value for *Chl a* is 0.9 *V* and was obtained low because larger amounts of *Chl a* decrease the measured parameters. In *Delesseria lancifolia*, which has higher amounts of phycoerythrin, the *Chl a* did not behave so. *Delesseria lancifolia* has a higher concentration of phycoerythtin, which shows an overall measured efficiency of 0.045% compared to the other two at approx. 0.02% due to the low coverage of the TiO_2 by the protein molecules. In *Delesseria lancifolia* the value of R_{recom} is nearly 400 times higher than $R_{trans,}$ whereas in the other two, it was 150 times higher only when measured with impedance spectroscopy [Enciso & Cerdá, 2016].

Spectral shifts were created via films formed with Coumarin 1 and Solvent Orange 63 in tetrahydrofuran (THF) and encapsulated in polydimethylsiloxane (PDMS) silicone elastomer matrix, respectively which converts UV light to blue light and green light to red light. *Dunaliella* has high CO_2 uptake properties, and further, this strain does not produce high amounts of *B-car* in contrast to other strains and with this technology can grow denser algae cell cultures. Airlift photobioreactor (ALB) grown *Dunaliella salina* (strain CCAP 19-30), when coated with the wavelength shifting films, has increased in optical density by 36.9 % for UV to blue and by 18.8 % for green to red when compared with an uncoated one [Burak et al., 2019].

Green seaweed *Sargassum myriocystum's* extracted pigments, using a solvent system of *mt* and *et*, indicated the presence of *Chls*, carotenoids, and flavonoids in phytochemical analysis. A higher yield

was obtained with heating than without heating from both solvent methods when a rotary evaporator was employed while recycling back the alcohol in the process [Renita & Davuluri, 2015]. Nutrient-stressed freshwater microalga *Haematococcus pluvialis* (orophyceae) when cultured in a modified WC (Wilkins-Chalgren) medium and harvested in the non-motile asexual stage to obtain a crude extract which was primarily purified (PP). The comparison between PP and a pure *Asta* (a secondary carotenoid) standard (*as*) showed PP has a higher efficiency of 0.1% than 0.036 % of *as*, mostly due to a wider range of absorption and embedded diffusion in the mesoporous TiO_2 layer. *Asta* which has absorption maxima at 477 nm (a range not covered by *Chls*) has no role as photosynthetic pigment and is synthesized outside the chloroplast. As soon as stress conditions arise, these microalgae generate astaxanthin in higher amounts compared to *Chl* and *B-car* and accumulate up to 3.0% of astaxanthin by dry weight. Unlike *B-car*, which lacks oxygen in its structure and lacks anchoring groups, *Asta*, is a type of xanthophyll (carotenes oxygenated derivatives), that possesses hydroxyl groups in their structures which help in TiO_2 film assembly [Orona-Navar et al., 2017].

Accessory pigments in red and blue-green algae are Phycobilisomes (composed of phycobiliproteins) which form 40-60% of the total soluble protein in cells and are an alternative to *Chl a* with an absorption range of 500-660 nm. Their major types are the red-colored phycoerythrins (PEs), blue-colored phycocyanins (PCs), and allophycocyanins (APCs) with a prefix of the letter of algal origin like *Cyano* for cyanophycean [Gantt, 1980]. They have shown enough capability in DSSC for sensitization along with water as an electrolyte citing their solubility.

Wastewater utilization for algal growth and pigment extraction is also tested in two models of 10 μm nanoparticular TiO_2 electrode and 20 μm long vertically oriented nanotube arrays of TiO_2 film, concluding that nanoparticular electrode works more efficiently in comparison to nanotubular one. It is hypothesized that the nanotubular electrode's

back-illumination design results in lots of optical absorption by a CE and electrolyte and less absorption by the dye in one dimension, whereas nanoparticular electrodes have the front-illumination design. DSSC using microalgal photosynthetic pigments is extra competent and less expensive than those fabricated using other natural dyes as isolation of PS-I from species like *Thermo-Synechococcus elongates* is much more expensive than the microalgal pigment extraction. It is noted that bacterial culture, PS-I stabilization, and extraction methods are tough and time-consuming. The reported efficiency of ~ 0.08% using PS-I, was even lower than the expected results. It was also considered that these microalgae grown on domestic wastewater were hired to lessen pollutants in wastewater besides photocurrent generation [Mohammadpour et al., 2014].

Analogs of two natural porphyrins: *Chl* and hemoglobin, are Phthalocyanines (*Ptcs*) which are robust and intensely colored macrocycles (blue pigments) with high chemical, thermal, and light stability developed by synthetic strategies. *Ptcs* have shown concentrated absorption in the red/near-infrared (NIR) region due to 18 delocalized photoelectrons with the anchoring group appended to the macrocycle ring. *Ptcs* are different for their intense Soret- and Q-band. Extinction coefficients as high as 300,000 $M^{-1}cm^{-1}$ are achieved by Q-band along with high fluorescence quantum yields. *Ptcs* can be termed as Red/NIR sensitizers as they absorb in the 600–800 nm region, which is the utmost photon-rich range. The performance of *Ptc*-based devices has gone beyond 6% due to their rational structural design [Urbani et al., 2019].

Marine seaweed (*Sargassum wightii*) extracts possessing *c*-type *Chl*, such as *c1* and *c2*, other than *Chl a*, *Chl b*, carotenoids, and fucoxanthin have terminal carboxyl groups connected to the porphyrin macrocycle. These were embedded on a ZnO photoanode-based DSSC displaying three absorption peaks. The stability test disclosed consistency in the photoelectric conversion with a η of 0.07% for a 600 s light period [Anand & Suresh, 2015].

Phytoplankton-like diatoms are optimized for light absorption through evolution and developed frustules (3-dimensional nanostructured porous silica skeleton), which found use in DSSCs without any complex processing. They were dispersed throughout the regioregular poly 3-hexylthiophene (P3HT) and fullerene derivative PCBM active layer, and it was found that one can accomplish the same power conversion efficiencies as standard thickness cells while using 36 % thinner active layers. This was important in proving that frustules act as a scattering center and textures the silver back contact, causing increase in the optical path length inside devices. This also does not make DSSCs depend on too expensive fabrication methods for large-scale production. These nanostructures can be converted or employed as an electrode or diode [McMillon-Brown et al., 2017]. The *Nitzschia palea* diatom frustules of amorphous silica when coated with TiO_2 by metabolic incorporation can be used for the construction of titanium nanotubes by two-stage cultivation in *f/2* (half of Guillard and Ryther produced medium in 1962) medium and could replace titanium employed nanostructured surface doping for energy production. They have shown almost double power efficiency of 9.45 % and can be further utilized live too with the added benefit of lipid extraction, which was not tested earlier with *Pinnularia sp*. and *Coscinodiscus wailesii* [Gautam et al., 2016].

Less toxic alginate gel entrapment of live algae as semi-dry biofilm was prepared and used within a bio-PV device. This generated a power of 0.289 mWm^{-2}, which was 18 % more than the conventional suspension culture device, along with oxygen production and CO_2 reduction. Here, the biofilm's species were Chorophyte *Chlorella,* Cyanobacterial *Spirulina,* and *Synechococcus* sp. on anodes of ITO coating. Their power output ranging to 3.13×10^{-4} Wm^{-2} was enhanced by 119 % with reduced graphene oxide (*r*GO) introduction in place of ITO while using 2-hydroxy-1, 4-naphthoquinone as redox shuttle. It was more powerful than the thylakoid membranes of *Cyanobacterium arthrospira*, which stand at 1.12×10^{-4} W m^{-2} using

ITO-PET anode. When compared to synthetic polymers, naturally present carboxylic groups exist in alginate alone, which are evenly distributed in the polymer chain providing better contact with the algal cells and ITO. Alginate beads of *Anabaena variabilis* of 0.2% efficiency were reported, too, whereas *Chlorella vulgaris* displayed 9.40 % and 14.1 % of charge extraction to transfer efficiency. A PAM (Pulse amplitude modulation) fluorometer was used to measure the yield of fluorescence to develop knowledge of photochemical efficiency and dissipated heat [Ng et al., 2017].

Enteromorpha intestinalis (*Ulva intestinalis Linnaeus*), a green alga used for co-pigmentation from a raw ethanolic extract with anthocyanin extract of red cabbage used for DSSCs with and without the adjustment of pH, particularly at pH = 1, 5.4, and 8. It is known that anthocyanins have a greater capacity to be adsorbed onto TiO_2 surfaces in comparison with *Chls*. The co-sensitization led to a broad absorption band (350 – 750 nm) due to the band of *Chl* joining with anthocyanins, but the efficiency remained low in comparison to only algae-based DSSC. It proved that cocktails and pigments are dependent on pH value, too, as they influence the peptization process. Also, the co-pigmentation in the basic medium enhanced vegetal pigment efficiency [Dumbrava et al., 2016].

Freshwater filamentous green algae *Cladophora sp.* dye extracts of *Chls* and xanthophylls (interconverting derivatives, namely *Viola*, antheraxanthin, and *Zea*) in the mixed case showed synergistic activity with 1.5-to-2-fold higher performance compared to any individual dye. Xanthophylls dissipate extra energy via reversible conformational structural changes through the xanthophyll cycle for photoprotection, increasing the effective electron lifetime on mixing while reducing electron recombination. Without this quenching effect, *Chl* dye alone with η of 0.055% showed a reduction in retention when storage temperatures were increased above 27ºC, indicating a high photosensitivity shortcoming [Lim et al., 2015]. The concept of a normal "mixed drink color sensitizer" rather than metal complex

sensitizers for color was developed as a message to those researchers who have chipped away at increasing the efficiency of DSSC [Johari et al., 2017].

The microbial fuel cell system (MFC) has been tested with multiple, highly photosynthetic algal species, including *Chlorella Vulgaris*, *Nannochloropsis*, and *Spirulina*. Electric power output relatively was highest for *Nannochloropsis* at a higher absorption rate of 286 cm^{-1} (absorption frequency A) with a value of 35 mW while *Chlorella* displayed 30.2 mW at 123 cm^{-1} and *Spirulina* at 142 A showed 31 mW [Fleury, 2017]. Electrochemical Techniques like CV and electrochemical impedance spectroscopy (EIS) were used to study pH (7.5 or 8.5) factors and fatty acids like heptadecanoic acid (HA). These techniques were used to measure co-adsorbent's influence on the efficiency of DSSCs, which were used with 0.04 % efficient phycocyanin. Optimized dipping along with mixing *Chl* with phycocyanin improves protein adsorption, whereas HA affects solution viscosity or avoids hydrophobic interactions to prevent protein agglomeration [Enciso et al., 2016].

Spirulina, due to its phycobiliprotein, has an 18 % solar energy utilization efficiency and 43 % photosynthetic efficiency, which are three times that of advanced plants. The living spirulina DSSC was prepared, which had approximately~ 70μA photocurrent, which could rise by 100μA with the addition of carbohydrates such as glucose and sucrose. A maximum power density of 63 mW/m^{-2} is achieved here through sucrose, as it improves the activity of hexokinase (significant in cyanobacterial photosynthesis). Phycobiliprotein composite with squaraine dye is efficient in UV-Vis's light absorption, and its TiO_2 film emits fluorescently. A slight decrease was observed when the light was removed due to the slight loss of spirulina whereas, with the addition of 3.8 g sucrose in the anode chamber, the photocurrent of the spirulina bio solar cell was increased 389 μA [Wang et al., 2014]. Tests done on red (genus *Laurencia obtusa*) seaweed extract of phycoerythrin pigment in a water-based dye solution with different

temperatures, solvents, and pH revealed that an acidic *pH* of 3 of this solution at 35 ^{o}C showed the highest η of 0.52%. J_{SC} and V_{OC} of 1.26 mA/cm^2 and 0.66V were achieved along with it. The J_{SC} of the concentrated dye solution sensitized cell was almost 29 % lower when matched to that of the cell sensitized with the original Millipore water dye solution and similarly had half the efficiency. It was noticed here that a concentrated dye solution could not enhance the cell's electrical parameters, as theoretically predicted earlier [Rapsomanikis et al., 2016].

The brown algae *Undaria pinnatifida* of Venice Lagoon area was used in setting up an eco-protocol that is easy and fast for *Chl c* extraction. The weak interaction of ester and keto carbonyl groups within *Chl a* hinders efficient adsorption on the hydrophilic oxide surface, making *Chl c* get critical here. *Chl c1* and *Chl c2* possess a terminal carboxyl group connected to the porphyrin macrocycle through a conjugated double bond that binds strongly to TiO_2 and records an efficiency of 0.36 %. To avoid the effects of stacked sandwich-type H- aggregate of *Chl* π-aggregation or a side-by-side J-aggregate soaking time should be increased, and the use of concentrated solutions should be done. Research is ongoing for the use of fatty acid with a long alkyl chain or structurally rigid to inhibit this accumulation while enhancing the ratio between *Chl c* and *Chl a* while having increased recovery of *Chl c* (79 μg g^{-1} here) [Armeli et al., 2016]. Oxidized forms of both *Chl c1* and *c2* isolated from brown seaweed *Undaria pinnatifida* showed an efficiency of around 2.5 %, comparatively lesser than 3.4 % of *c1* and 4.6 % of *c2*. The order was hypothesized by the resultant elevated electron densities in *c2* than in *c1* and the presence of a more extended conjugated chain, along with vinyl carboxyl group configurations, to form a hydrogen bond [Wang et al., 2007].

Table 1.2. Recent significant Bacterial and Algal-based DSSCs with different combinations of cell types, anode materials, cathode materials, and various electrolytes with dyes.

Dye/ Pigment	**Specification**	**Important component**	**Highlighted parameter**	**η (%**	**REFERENCES**
B-Car (7.4µg/mL)			FF - 0.303	0.022	Nurachman et al., 2015
Lycopene		PCBM	Charge Carrier motion - 2.1×10^{-2} $cm^2/(Vs)$		Wang et al., 2013
Spirilloxanthin	Carotenoids			4.0	
Bacterial Chromatophores	*Rhodospirillum rubrum*		absorbance maximum is at 880 nm		Woronowicz et al., 2012
Bacteriorhodopsin and bacteriorubein mix	*Halobacterium salinarum*			0.16	Molaeirad et al., 2014
red protein R-phycoerythri	Stable dye			0.11	Yañuk et al., 2020

n (R-PE)

Chl extract	*Scenedesmus obliquus*			0.064	Orona-Navar et al., 2020
Asta (type of xanthophyll)	*Haematococcus pluvialis*		Pigment possesses hydroxyl groups gives stability	0.036	Orona-Navar et al., 2017
c-type *Chl*, as *c1* and *c2*	*Sargassum wightii*	ZnO photoanode	carboxyl groups connected to the porphyrin macrocycle	0.07	Anand & Suresh 2015
Diatom frustules	*Nitzschia palea*	Ti nanotubes	Power efficiency – 9.45%		Gautam et al., 2016
Chlorella, Spirulina and *Synechococcus* sp.	Biofilm species-Chorophyte and Cyanobacteria	rGO ITO	Power - 3.13×10^{-4} Wm^{-2}		Ng et al., 2017

raw ethanolic extract with anthocyanin extract	*Enteromorpha intestinalis*	TiO_2	pH 8 more efficient		Dumbrava et al., 2016
Phycobiliprotein	*Spirulina*	carbohydrates addition	63 mW/m^{-2}		Lim et al., 2015
extract of phycoerythrin	*Laurencia obtusa*		*pH* of 3 at 35 ºC	0.52	Rapsomanikis et al., 2016
Chl c	*Undaria pinnatifida*		Oxidized forms of *Chl c1* and *c2*	2.5 %	Wang et al., 2007

1.9. Current progress in Natural DSSC

DSSC concepts are attracting purchasers by recognizing new techniques for commercial application while maximizing efficiency. Various experiments in the past with natural dyes have helped in understanding the influence of dye, and particular parts of plant selection, like that of leaves and fruits, have been the most efficient. Selection is based on the availability of the plant part, and that's why the omnipresent algae can be a good alternative, even better than plants. The stability of pigments also needs to be compared for selection like xanthophyll being more stable than other pigments. The use of additives or performance enhancers along with natural dyes also enhances the stability of the dyes in the cells and aids the current density. Due to their favorable properties, many experiments are

carried out to discover valuable additives that can bond with the DSSC parts to develop better solar-based products.

Photocurrent visualization and stability testing are now done using imaging techniques and cell mapping to better analyze and mark effects in DSSC [Macht et al., 2002]. Electrolyte efficiency is also a point of focus as stopping I_3^- reduction has increased internal resistance and is a signal of degradation as FTIR confirms that no reverse iodate formation occurs [Pazoki et al., 2017]. FTIR also confirms the hydroxyl group stretch mode that water possesses; tertbutyl pyridine (TBP) acts as a weak base due to increased water concentration in acetonitrile-containing electrolyte after 84 days [Pazoki et al., 2017]. So, working on this can increase the lifetime of the dye and cell as well.

There has been the revelation that when acetonitrile or water solvent electrolytes were mapped for photocurrent with Z907 dye on the electrodes, the electrons were able to flow everywhere except filling holes of dye which created photocurrent loss proving interdependency of TBP and water [Scott et al., 2008; Risbridger et al., 2012]. The interaction of dye molecules with water has been studied; water adsorbing over the semiconducting layer confirms the hindering action toward electron recombination in the electrolyte [Leandri et al., 2014]. This is supported by excited-state calculation for a squaraine dye which is based on extensive time-dependent density functional theory (TDDFT) [Pugliese et al., 2014]. It highlighted that intensive solvent re-organization around the carboxylic group of dye, which is bound to the mesoporous oxide layer, is the reason for the transition from the bridged-bidentate configuration to the monodentate adsorption configuration. MPN and ACN-like solvents that lack hydrogen bonding are highly soluble with a large dielectric constant in comparison to many inorganic and organic salt solutions and additives and enhance the efficiency of electron injection as observed through transient absorption spectroscopy (TAS) [Katoh et al., 2007].

Combining water with organic solvents has grabbed attention in the past, but FF along with η and V_{OC} was lower for MPN compared to ACN [Zhu et al., 2012]. ACN had lower water content in comparison to MPN, leaving only J_{SC} with conflicting results [Zhu et al., 2012; Hui et al., 2007]. The liquid electrolyte composition such as 1M 1-propyl-3-methylimidazolium iodide, 0.15M iodine crystals, and 0.1M guanidinium thiocyanate with water supplementation has shown better V_{OC} and J_{SC} for organic solvents but with reduced FF values, but these results get contradicted when Z907 is replaced by N3 [Hui et al., 2007].

The electron transportation and recombination measurements jointly manifested that the charge-collection efficiency increased cooperatively with charge-injection efficiency [Schlichthörl et al., 1999]. This was due to the TiO_2 conduction band's lower energy level shift upon water addition, ultimately leading to improved J_{SC} values. This action was rationalized if the recombination decrease was considered by a factor of 4–5 initially before analysis. Also, there is an enhanced dark exchange current due to the increased number of dark electrons with the availability of water [Lu et al., 2011]. If water replaces organic solvents, it will have eco advantages and will be safe too. It can be versatile, too, as in released water-ethanol mixture effluents from the industry and labs where their separation is uneconomical [Avetta et al., 2013]. So, the reuse can be proposed in aqueous DSSCs.

Aqueous electrolytes, when added with specifically selected additives (nitrogen-containing heterocyclic compounds), have shown remarkable improvements by consequently adsorbing on the TiO_2 surface better [Saito et al., 2004]. These aqueous electrolytes, with additives, block the reaction between I3- ions, giving a positive shift to the redox mediator's electrochemical potential value. But this affects already attached dye molecules and hence reduces J_{SC} values [Le Bahers et al., 2010].

1.9.1. Present Focus in DSSC

Specific technologies need to be incorporated that avoid maximum water contamination and use the least water during the whole manufacturing process. The entire operational life needs to be taken into consideration or propose components that adjust with a partial or full aqueous environment which guarantees many advantages. Before 1991 when aprotic solvents did not exist as an option in the electrolyte, the photoelectrochemical cells were developed with the idea of the complete aqueous state in electrolyte [Desilvestro et al., 1985], and even the Grätzel team in 1988 proposed a sensitization by RuL34 for those aqueous cells along with a novel Br-based redox couple [Vlachopoulos et al., 1988]. That regenerative dye cell showed one of the highest efficiencies of 12 % of that time with a little more than 1 sun incident light of 470nm wavelength. Noticing the climate destruction organic solvents do, their complete replacement by water has again been thought of since 2010 [Leandri et al., 2014; Hui et al., 2007]. Methods like using hydrophobic dye (like TG6) or inserting 1% Triton X-100 surfactant to evade phase separation can be efficient in the water-electrolyte [Le Bahers et al., 2010]. A high 1-Propyl-3-methylimidazolium iodide (PMII) based supramolecular ionic liquid gel can act as both a surfactant and a source of more water-soluble iodide. Water has not shown any performance loss till 40 % volume and shown a significant reduction only after 1000h at 35 °C when the volume of water is increased to 80% [Zhu et al., 2012; Hui et al., 2007]. Natural algal dye utilizing aqueous DSSCs can be made possible by optimized designing with live cells, and novel additives focused on crucial work of stability. Algal dyes must make their way to get more emphasis than other natural (plant-based or flower-based) dyes which are also abundant in nature but must be given more inputs. They require comparatively more water and nutrients along with structural soil requirements in comparison to algae. Their pigment yield to requirements ratio is significantly low. One of the other most

important things that must be taken care is of the poor adsorption of natural dyes on the semiconducting layers and subsequent rapid degradation. They need to be protected by reducing their oxidative degradation and factors causing it as well as creating new combinations of solvents or materials for their effective adsorption.

1.10. Research gaps and motivation

Sensitizers obtained from nature are easily accessible and non-harmful, but with not even half the efficiency, they still convert around 1-2 %. This scope for performance improvement can be researched with unexplored algal species with a different wavelength combination and optimizing those wavelengths absorbing pigments for better activity. Natural algal pigments, especially macro forms of brown and red algae, possess the capability of producing better efficiencies with their *Chl* pigment varieties, but the degradation in the *Chl* in DSSCs must be monitored. It is noticed that the type of solvent used for separation and existing pH, or the one adjusted of the dye has some effect on the stability and life span of dye, which in turn influences DSSCs performance. Existing information on new natural pigments for DSSCs should focus on their structure, their linking via anchoring groups and conjugation, extraction bio-information, dye band gaps, and photoelectrochemical performance of bio-sensitized cells.

With this literature review, the information on the need to switch to live bacterial or algal cells while working on the dyes extracted from them is supplied. Low efficiency is a big factor with these cells, but cheapness and device integration can be very helpful too at the same time. Optimization of dye fabrication with all the right conditions can result in the emergence of these DSSCs as a technology for industrial application. Also, natural DSSCs need to be developed along the lines of synthetic dye cells and with their technology of preparation like laser drilling and thermochromism and identify the right desired field of application too. Involving these live algal DSSCs for multi-purpose

functions and developing interdisciplinary solutions with their application will be taking nature and technology ahead together.

1.11. Relevance of the Research

The relevance of this research lies in addressing a few of these key aspects in the field of DSSCs that have significant implications for sustainability, efficiency, and practical large-scale application.

- Exploration of Algal Dyes
- Enhancing Efficiency and Stability of Dyes
- Integration of Novel Additives
- Addressing Environmental and Safety Concerns
- Advanced Analytical Techniques
- Optimizing Extraction and Storage
- Innovative Use of Natural Resources
- Sustainable Production Processes: Proposing the use of wastewater and minimizing contamination during manufacturing aligns with global sustainability goals and promotes the development of eco-friendly DSSCs.
- Addressing Low Efficiency Issues
- Interdisciplinary approach and applications

1.12. Research Objective

To explore the potential fabrication of natural, efficient, and stable dye-sensitized solar cells using augmented dyes derived from microalgae.

<u>Minor Objectives:</u>

vi. Screening of microalgal species and different solvents for dye extraction.

vii. Assessing the influence of various properties and extraction systems on selected dyes.

viii. Integration of selected dyes as photo harvesters in natural dye-sensitized solar cells (DSSCs).

ix. Estimating gaps in extraction optimization and storage through specific pigments of selected dyes.

x. Evaluating compound formations following degradation and accretion due to extraction and storage.

CHAPTER 2

Screening of Microalgal Species and Solvents for Dye Extraction

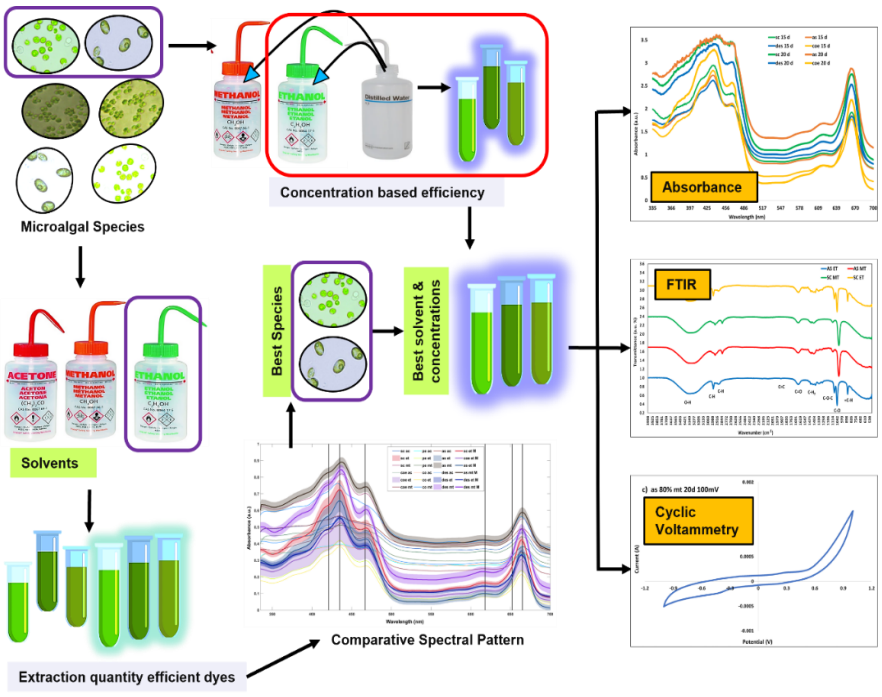

CHAPTER 2

Screening of Microalgal Species and Solvents for Dye Extraction

2.1. Introduction

The dye-sensitized photovoltaic technology uses primarily inorganic and fairly organic dye, to excite electrons for energy harvesting. In dye-sensitized solar cells (DSSCs), dyes such as that of transition compounds like ruthenium polypyridyl complexes are admirable, as the conversion efficiencies reached about 11%. But its production undertakes a complex and costly process while creating the problem of undesirable heavy metals exposure to the environmental resources. Alternatively, using organic natural dyes in solar cells as a sensitizer is a greener and inexpensive light harvesting approach with adequate efficiency and low stability. These pigment-compounded dyes which are assumed to be environmentally friendly because of their biodegrading capacity and non-toxic nature, exist in algae other than plants.

Natural dyes from microalgae have specific absorbance, transmittance, and reflectance based on the combined property of all colored pigments in them. These dyes possess few major pigments; the most commonly identified are *Chls*, Phycobiliproteins, and Carotenoids. *Chls* of microalgae (*Chl a* and *b*) absorb light typically in the narrow red and broader blue-violet regions and reflect green light making cells appear green. Carotenoids peak in the blue region and extend into the green and yellow regions along with an additional second absorption peak in the green region, to absorb excess light energy and protect from photo-oxidative damage or by transferring absorbed energy to *Chl*. Phycobiliproteins (PBPs) in microalgal habitats fix carbon due to the three subunits assembly of phycocyanin (PC), phycoerythrin (PE), and allophycocyanin (APC). In various works concerning natural dyes, 2.5% is the maximum efficiency achieved via the *Chl* family but for

the carotenoid family or the phycobilin family, the maximum reported efficiency has remained around 1% or less [Chauhan, 2022]. The oxidized variants of *Chl c1* and *c2*, obtained from *Undaria pinnatifida*, a type of brown seaweed, exhibited an efficiency of approximately 2.5%, which is comparatively lower than the 3.4% efficiency of c1 and the 4.6% efficiency of c2. However, in the case of microalgae, the efficiency has not surpassed even 0.5% [Chauhan, 2022].

Chls are located within specialized structures called chloroplasts, where they play a critical role in absorbing light and initiating the conversion of light energy into chemical energy. The biosynthesis of *Chls* in algae involves a series of enzymatic reactions. The initial steps of *Chl* synthesis occur in the cytoplasm of algal cells, where certain molecules are synthesized and then transported into the chloroplasts. Within the chloroplasts, these molecules undergo further enzymatic reactions, ultimately leading to the formation of *Chl* pigments. Carotenoids, on the other hand, are synthesized via a separate biosynthetic pathway. These pigments are produced in various parts of the algal cell, including the chloroplasts and other cellular compartments. Carotenoids serve important functions in algae, such as light absorption, photoprotection, and as precursors for the synthesis of other compounds. The production and accumulation of pigments in algae are influenced by several factors, including light intensity, nutrient availability, temperature, and environmental stresses. For example, different light conditions can trigger the synthesis of specific pigments, enabling algae to adapt to varying light wavelengths and intensities. Nutrient availability, particularly nitrogen, and iron, can also affect pigment production in algae. Furthermore, some environmental stresses, such as high light, low temperature, or nutrient limitation, can lead to changes in pigment composition and content as a part of the algal stress response. These changes in pigmentation can help algae adapt and survive under unfavorable conditions.

The two major absorption maxima *(λ_{max})* in *Chl* with increasing water content/ polarity of the solvent incline to shift to longer wavelengths.

The shift of λ_{max} in the blue region is more than that in the red, particularly for *Chl b* than for *Chl a*. The specific λ_{max} is highest in pure solvent compared to the water-saturated solvent of diethyl ether, acetone, and methanol [Lichtenthaler, 1987]. With dilution, the absorption also gets broader while also decreasing for older or light-exposed solutions. Different authors have given several equations for different solvents and different extracts of pigments for quantitative pigment determination but the drawback remains of non-unique pigment values and one obtained in one solvent does not fits well with another solvent. The inconsistencies are even larger for the ratio of *Chl* a/b as in the popular equations specified by Arnon [Arnon, 1949] for 80% acetone which was built on the specific absorption coefficients of Mackinney [Mackinney, 1941].

Many research papers have tried to modify the equations but the variances in the wavelength positions of the maxima in the red region and the comparative absorption of *Chls* and carotenoids remain different in different solvents. These differences remain due to the purity of the solvents primarily non-accuracy of water content or organic material as well as the resolution properties of the spectrophotometer.

Further to evaluate from the profile of the spectrum and understand whether one has taken an unblemished pigment/ dye solution, the complete absorption spectrum of the purified pigment/ dye extract solution in the visible range is necessary. As it displays deviations of up to 25% in the amounts of *Chl b* and the total carotenoid, plus in the ratio of *Chl a/b* [Lichtenthaler, 1987].

Various methods of pigment extraction exist and the more eco-friendlier techniques are that of supercritical extraction, laser technique, and hydrodynamic cavitation [Tzima et al., 2023; Tourlouki et al., 2020, Waghmare et al., 2019]. In terms of the reduced time of extraction electric field method has an edge over others. But all these methods require a high amount of energy and high investment in infrastructure. Considering these obstructions researchers have always preferred to classic solvent extraction method over others. Though this

method is less efficient and requires a high amount of solvents nevertheless comparatively this is inexpensive in operation and infrastructure requirements.

This paper explores the spectral profiles of dyes extracted from six lab-available indigenous species of microalgae in different solvents and with minimally aqueous concentrations. The extracted dyes were evaluated for light-harvesting pigments with spectral absorption efficiency by using various types of solvents like acetone, ethanol, and methanol along with proportional dilution by deionized (DI) water. From the experiments, the link between the solvent used and the effectiveness of the DSSCs to absorb added sunlight after adsorption is evaluated. These dyes were further investigated to know about the presence of various functional groups present for better attachment on the semiconducting layer and better electron-donating capability. Due to a costly extraction process in a small lab-scale environment, this extraction can be done with solar heaters on a large scale and create other value-added products in the bioreactor system while generating electricity. The stability studies aid to understand their degradation rate and how frequently they need to be replenished.

2.2. Experimental Section

2.2.1. Materials and Reagents

Solvents procured were of Sigma-Aldrich Co. LLC with American Chemical Society (ACS) standards, with test specifications as Acetone, ≥99.5% pure, Ethanol, ≥99.8% pure, and Methanol, ≥99.8% pure.

The dilution of the following solvents was done by the addition of DI water as per the requirements of the experiments (predominantly 80% solvent) and a baseline was set with these as per the type of measurements involved. The overall reagents were in several concentrations 100%, 90%, 80%, 70%, and 55%.

2.2.2. Growth and culture conditions of microalgae

Six different indigenous lab-available strains of freshwater microalgae cultured axenically were used namely *Scenedesmus sp., Coelastrella sp., Pediludiela daitoensis, Coelastrum proboscideum, Asterarcys quadricellulare, and Desmodesmus pseudocommunis*. These species were grown in a basic BG-11 medium at a pH of 7.2 - 7.4 which was maintained using diluted acid (HCl) or base (NaOH).

The seed cultures for all six species that were grown in the Erlenmeyer flasks for 10 days were subcultured from these cultures axenically. Then similar experimental cultures flasks were inoculated with an original cell density of 0.1 at 680 nm and the readings of growth were taken every 24 h and were grown till the 30th day. The cultures were maintained in the culture room at a temperature of 27 ± 5 °C with 12 hours of light photoperiod followed by 12 hours of dark period. During the light period, at an appropriate distance from the cultures, the light intensity of 3000 lux was maintained using white fluorescent lamps to sustain the proper growth of the cultures in 250ml Erlenmeyer flasks [Stanier et al., 1971]. After harvesting on the 0^{th}, 5^{th}, 10^{th}, 15^{th}, 20^{th}, 25^{th}, and 30^{th} day, the algal extracted dyes were analyzed for absorbance spectra, main pigment points, and other characterizations as per requirement.

2.2.3. Dye Synthesis and Methodology

2.2.3.1. Dye extraction

Six different species containing flasks were sampled for dye extraction on the respective interval of 5 days with acetone, ethanol, and methanol separately. Three different concentrations of acetone, ethanol, and methanol were taken at 80%, 90%, and 100%.

2.2.3.2. Extraction techniques

The solvent acetone and methanol used modified cold solvent extraction [UNESCO, 1966; Strickland & Parsons, 1968; Lichtenthaler & Wellburn, 1983] while ethanol used the modified hot solvent extraction method. In the case of cold extraction, a known volume of

the microalgal culture of a particular species was centrifuged, and the residue was mixed with one particular concentration of acetone/ methanol, sonicated in the Ultrasonic Sonicator Bath for 15 minutes, and incubated overnight at 2 - 6 °C using a refrigerator. The solution is again centrifuged and the supernatant is collected.

In the hot solvent method, the microalgal residue is mixed with the same concentration of ethanol and heated in a Sub Aqua Pro SAP 26 Grant Instrument's boiling water bath for 5 minutes. The solution is similarly centrifuged, and the supernatant is collected [Pápista et al., 2002]. The *Chl* and carotenoid contents in the pooled supernatant extract were estimated spectrophotometrically. The dyes extracted from all six species in all three concentrations of the three solvents were characterized by UV-Vis spectral scans from 335nm to 700nm to visualize the absorption pattern of the dyes. This pattern was analyzed thoroughly on the 0^{th} and 5^{th} day using MATLAB plotting and further shortlisting of species was done using MATLAB algorithm. UV-Vis spectral scans were done for all five shortlisted species in the selected solvent in solvent-optimized concentration. *Chl* readings were also taken for both *Chl* a and b with 95% ethanol on all the interval days as per the formula modified by Lichtenthaler, 1987. Also, four types of dilutions were made 55%, 70%, 80%, and 90% in the top-performing solvent to extract dyes of two top-performing species.

2.3. Characterization

All obtained dye absorbances were measured through a UV–Vis absorption spectrum scan logged on the DR-6000 HACH spectrophotometer in the range of 300 to 800 nm. The scans were taken in near UV range to understand the effect of UV range absorption in early dye degradation and losing its efficiency [Baran et al., 2008].

The ANALAB Ultrasonic Sonicator Bath frequency was preset at 33 ± 3 KHz for 15 minutes.

The onset oxidation and reduction potential were analyzed on an AUTOLAB PGSTAT302N Electro Chemical workstation operating at a current range of 250 mA and having a −10 to 10 V potential range with a 3-electrode arrangement. The redox scan was recorded using a 500ml Borosil glass beaker with Ag/AgCl as the reference electrode, glassy carbon as the counter electrode, and dye either dried or solvent evaporated as the working electrode) and 1M KOH of pH 14 was used as an electrolyte.

2.4. Result and Discussion

The extended light-shaded portion of a particular color denotes the standard deviation of all the readings taken. The dark thick line denotes the mean (M) of all the obtained scanned readings which qualified as the best dyes in the respective solvent. The light thinner lines are of the dyes which were not efficient enough as per the algorithm set in MATLAB. All the color-denoting indicators are rightly mentioned in the legends of the figure. The stacked plots run in increasing order of the days (d) from bottom to top.

2.4.1. UV- Vis spectroscopy

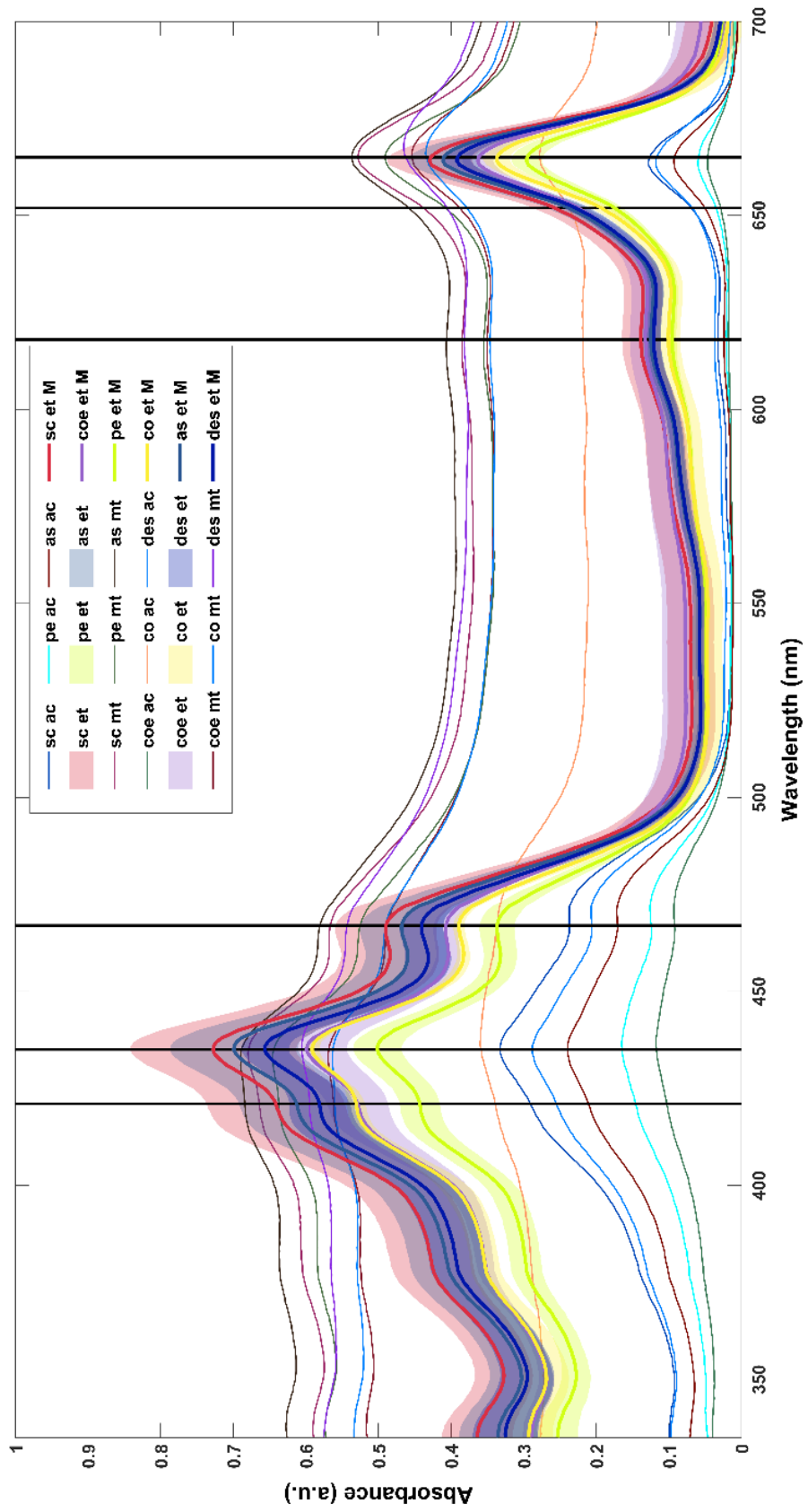
Absorbance (a.u.)
Wavelength (nm)
sc ac
sc et
sc mt
coe ac
coe et
coe mt
pe ac
pe et
pe mt
co ac
co et
co mt
as ac
as et
as mt
des ac
des et
des mt
sc et M
coe et M
pe et M
co et M
as et M
des et M

a. 80% solvent

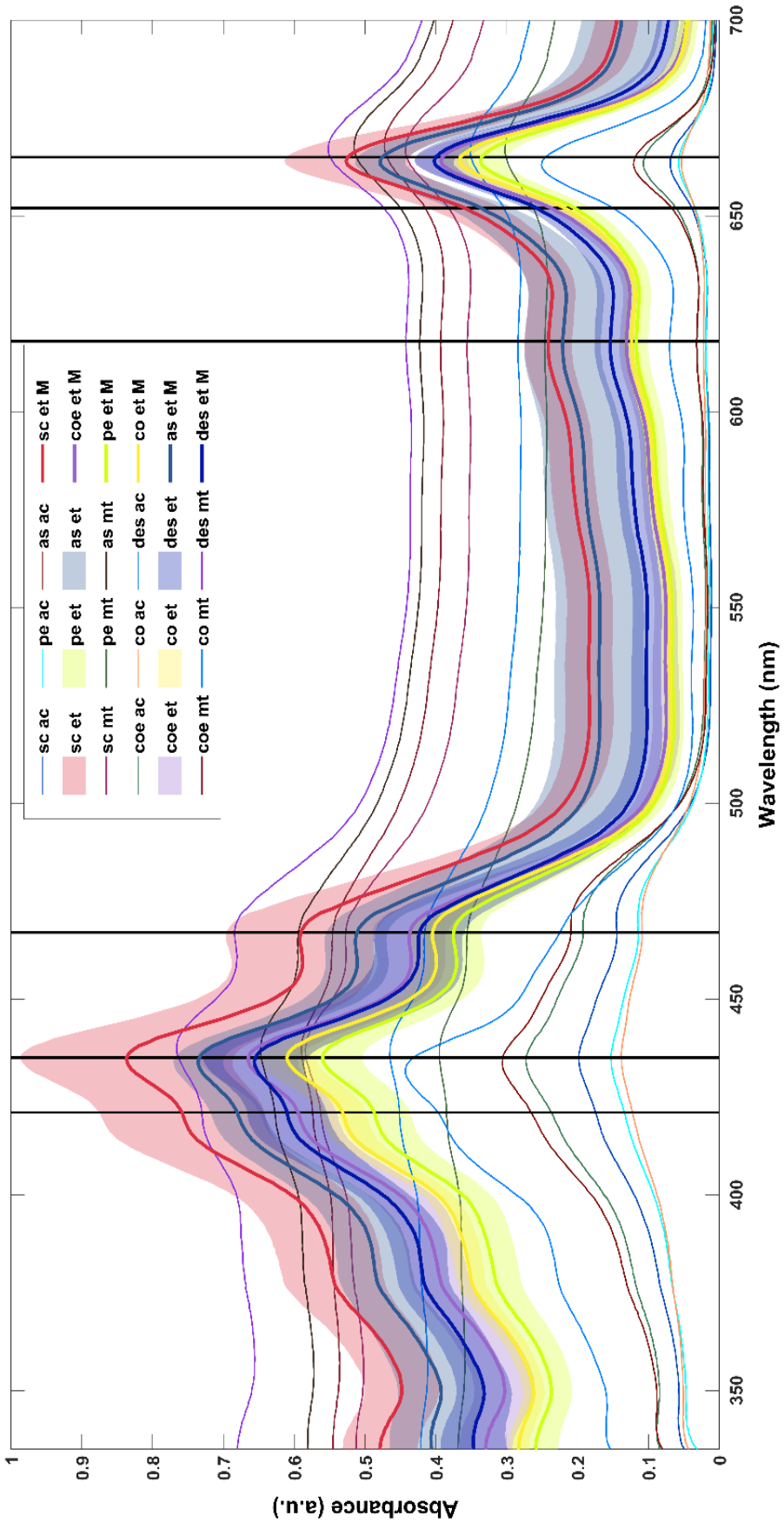
Absorbance (a.u.)
Wavelength (nm)
sc ac
sc et
sc mt
coe ac
coe et
coe mt
pe ac
pe et
pe mt
as ac
as et
as mt
des ac
des et
des mt
sc et M
coe et M
pe et M
co et M
as et M
des et M
co ac
co et
co mt

b. 90% solvent

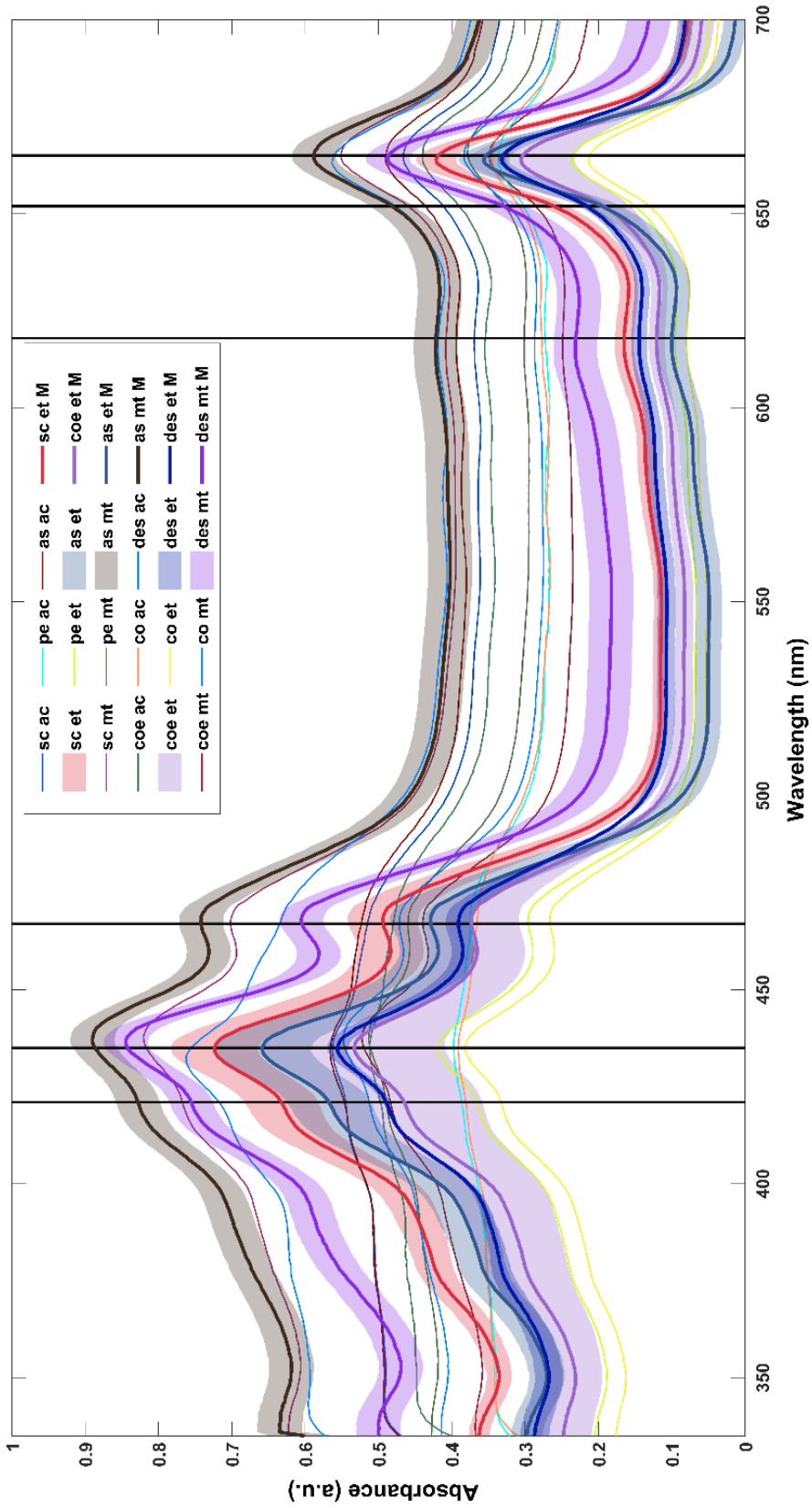

c. 100% solvent

Figure 2.1. Visible absorption spectra of different species (6 in no.) with different solvents (3 in no.) and methods of extraction (hot solvent extraction using ethanol and cold solvent extraction using methanol and acetone) in the concentration of a. 80% b. 90% and c. 100% solvent with a comparison of solvents extraction efficiency on 5th day of microalgal growth beside sorting of species in order of more dye (pigments) producing microalgae.

The UV–Vis spectroscopic analysis was done as the dyes are photosensitizing in nature, and the subsequently obtained spectral scans are shown in **Figure 2.1.** The scanned dyes spectra were marked with some peak markings to identify pigments. These markings are the averaged absolute wavelength value of the peaks that coincided closely with the particular region. The dyes were compared with the literature absorption peak values of particular pigments listed in Table 2.1.

Table 2.1. Overview of various identified pigments and their peak absorbance wavelength values in particular solvent concentrations.

Identified Pigment	**Solvent & Concentration (%)**	**Peak Absorbance Wavelength (nm)**	**References**
Luteol	et 100	447	Zscheile et al., 1942
B-car	et 100	453	Isler et al., 1956
Myxoxantho phyll	ac 100	478	Hertzberg & Liaaen-Jensen, 1969
Chl c1	ac 90	443	Jeffrey, 1972
Chl c2	ac 90	444	
Diadino	ac 100	448	Johansen et al., 1974
Dinoxanthin	ac 100	442	
Chl a	ac 90	664	Jeffrey & Humphrey,

Chl b	ac 90	647	1975
Chl c	ac 90	630	
Chl a	et 100	430, 662	
Chl a	et 100	432	Lichtenthaler, 1987
Chl b	et 100	464	
Phytin a	et 100	417	
Phytin b	et 100	437	
Viola	et 100	437	Acemoglu et al., 1988
Chl a	et 100	665	Rowan, 1989
Chl b	et 100	649	
Fuco	ac 100	443	Haugan & Liaaen-
Chl a	ac 90	430	Jensen, 1989
Chl b	ac 90	460	
Chl c1	ac 90	442	
Chl a	mt 100	665	Porra et al., 1989
Chl b	mt 100	652	
9'-Z-	et 100	437	Baumeler et al., 1994
Neoxanthin			
Chl d	mt 100	696	Miyashita et al., 1997
Chl c	et 100	629	Ritchie, 2006
Chl d	et 100	696	
Chl c	mt 100	632	
Chl d	ac 90	691	
C-	Water	620	Eriksen, 2008
Phycocyanin			

In all the scanned dyes, irrespective of solvents, *Chl a* display two absorbance peaks (λ_{max}) at 435 nm and 665 nm, whereas *Chl b* exhibit peaks at 467 nm and 652 nm, respectively. These values were well enough to be in decent arrangement with formerly reviewed data in **Table 2.1.** It is also seen in **Figure 2.1.** that other visualized peaks can be that of carotenoids, particularly *B-car* because of a spread broad peak in the region of 450 nm to 470 nm, which very well represents *B-*

car's λ_{max} value of 450 nm as per previous publications. Other non-sharp peaks are probably like that of pheophytin a at 421 nm and pheophytin b at 435 nm. 618 nm can be a mix of both c-Phycocyanin and *Chl* a minor peak.

The scan was also taken slightly in the UV region to check for the influence of this absorption on the degradation process as the dyes that intensively absorb UV light may damagingly influence the production of hydroxyl radicals whose creation causes early degradation [Baran et al., 2008]. The dye extraction efficiency by the three solvents was analyzed using MATLAB software version - 9.14.0.2206163 (R2023a) and a particular algorithm was set up to shortlist the top-performing species and top-performing solvents. In the algorithm, the baseline of the extraction scan was appropriately normalized by adjustment to the average of equivalent lowest value at wavelength points of 700nm and 520nm. A total of 5 readings were taken for each type of extraction and then the values of standard deviation were plotted for all the same species extracted dyes values in the same solvent with the use of MATLAB plotting tool. Similarly, this is performed for all the remaining five species in all three solvents. The standard deviations were plotted in the form of light-shaded color throughout the scan range. The mean scan line of the best-performing six dyes scans is denoted by the M and the legend of thick dark colors, and the mean of other different dyes which were not in the top six was plotted by thinner (half-thick) scan lines without any display of their deviation region. Now algorithm decides the best-performing solvent in extracting a particular dye by the display of its spectral scan and all the species are obtained in a decreasing order of efficient extraction considering all the parameters. The evaluation is based on subtracting the lowest value in the mean of the scan from the highest value of that scan for that particular dye. Similarly, this is performed for all the other dyes too. These obtained values are compared in all the mean scans and the values are sorted.

It can be understood from **Figure 2.1**. that the spectrophotometric values of the three solvents almost form different baselines and consistent fluctuations are visible. First of all, acetone demonstrates good absorption peaks at relevant places for the five dyes. The best of the five dyes is that of species of *Scenedesmus sp. and Desmodesmus pseudocommunis*. Dye from *Coelastrum proboscideum* was not able to follow the baseline and has a far higher deviation than others also it is not showing peaks at applicable points and has broader peaks which are signs of low extraction.

With ethanol, all dyes demonstrate a good peak and the best being observed for the species in the order of *Scenedesmus sp.> Asterarcys quadricellulare > Desmodesmus pseudocommunis > Coelastrella sp.> Coelastrum proboscideum > Pediludiela daitoensis.* In the case of methanol, the normalized baseline of the six dyes was significantly higher due to the property of methanol whereas the absorption peaks were not that elevated enough to be making a mark of efficient extraction and a lot of shift can be seen in the peaks which are in line with the dilution effects of methanol. For methanol, we have to consider the peaks in the red region predominantly for sorting as the peaks in the blue region are not good for comparison and *Scenedesmus sp.* was the better executor.

Also, as per the figure plotted for 100% and 90% solvents values following the same algorithm, it was seen that they follow similar trends. In the 100% solvent category, the best performances were achieved by four dyes in ethanol of *Scenedesmus sp., Coelastrella sp., Asterarcys quadricellulare, and Desmodesmus pseudocommunis* species and two dyes in methanol of *Asterarcys quadricellulare, and Desmodesmus pseudocommunis* species. For the solvent concentration of 90%, all six dyes in ethanol performed good extraction in the order of *Scenedesmus sp. > Asterarcys quadricellulare > Coelastrella sp > Desmodesmus pseudocommunis > Coelastrum proboscideum > Pediludiela daitoensis.* Significant fluctuations in baseline were visible in methanol in all the concentrations of solvents.

Acetone was not able to generate high enough values of peaks showcasing lower extraction capability hence cold solvent extraction method was phased out for further testing. Methanol being an alcohol like ethanol is only used further with the hot solvent extraction method but it is to be acknowledged that it has a different boiling point than ethanol and that can create significant versatile values and create comparable extraction. The dyes which were not significantly obtained were of the species of *Pediludiela daitoensis* followed by *Coelastrum proboscideum* irrespective of solvents. Hence, *Pediludiela daitoensis* was also removed from further tests for shortlisting more sharply. The dye extraction was previously done on the 0^{th} day as well and the results were very supportive of the data of extraction on the 5^{th} day of growth. 100% Methanol works best for all species but with the dilution of methanol, it rapidly loses efficiency after 90%. Also, it has too much variation in its baselines in all concentrations. Acetone was ineffective at all concentrations except around 90% concentration and slight fluctuations in the baseline. Ethanol at all concentrations is most effective and with decreasing concentration it shows peak reduction and shifts but still maintains consistency till 80% concentration making it a better option to be used at lower concentrations and getting significant extraction of pigments soluble in water as well.

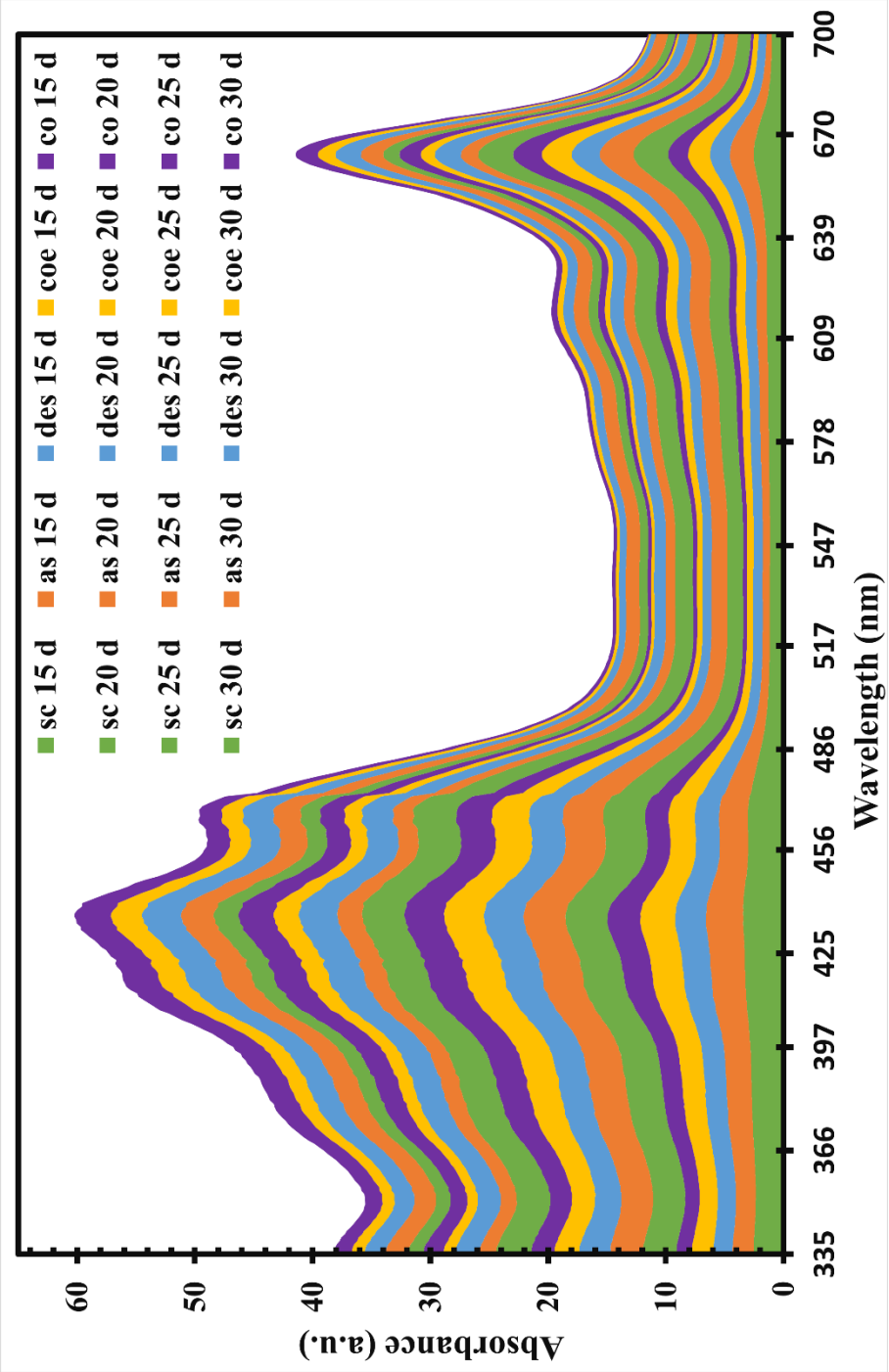

Figure 2.2. Stacked plot of absorption spectra of extracted dyes from five algal species from 15-30 days of growth in ethanol at 80% concentration using the hot solvent method.

Now, considering ethanol and its concentration of 80% as the solvent of choice further extraction of dyes is carried out on the 15th, 20th, 25th,

and 30th day with five qualified species of *Scenedesmus sp., Asterarcys quadricellulare, Desmodesmus pseudocommunis, Coelastrella sp. and Coelastrum proboscideum*. The days of extraction are displayed in **Figure 2.2.** from bottom to top which means 1st color is for the 15th day, 2nd repeat is for the 20th day, 3rd repeat is for the 25th day, and 4th repeat is for the 30th day toward the top. The best performance phase of days was found to be between the 15th and 20th day as by the 25th day the pigments (particularly *Chl*) tend to degrade down and growth also runs in the stationary phase with not much value addition to the efficiency of pigments. It is known from growth profile data that *Scenedesmus sp., and Asterarcys quadricellulare,* are fast-growing species encompassing more no. no. of cells when compared to the *Coelastrella sp. and Desmodesmus pseudocommunis.* But these two species along with *Scenedesmus sp.* remain in a longer stationary phase in comparison to other remaining species making them competent still in terms of stable dye for extraction. *Coelastrum proboscideum* does not achieve significant extraction efficiency on any of the four days to outnumber the other four species. The 20th day of extraction can be the most profitable day of extraction followed by the 15th day with the use of species *Scenedesmus sp.* and *Asterarcys quadricellulare.*

The best-performing species were also cross-verified for their *Chl* and carotenoid profile as per the spectroscopic formulas in literature to support their growth efficiency as well. The results of the *Chl* data also proved that *Asterarcys quadricellulare* and *Scenedesmus sp.* were the best species comparatively followed by *Desmodesmus pseudocommunis* on the 15th and 20th day.

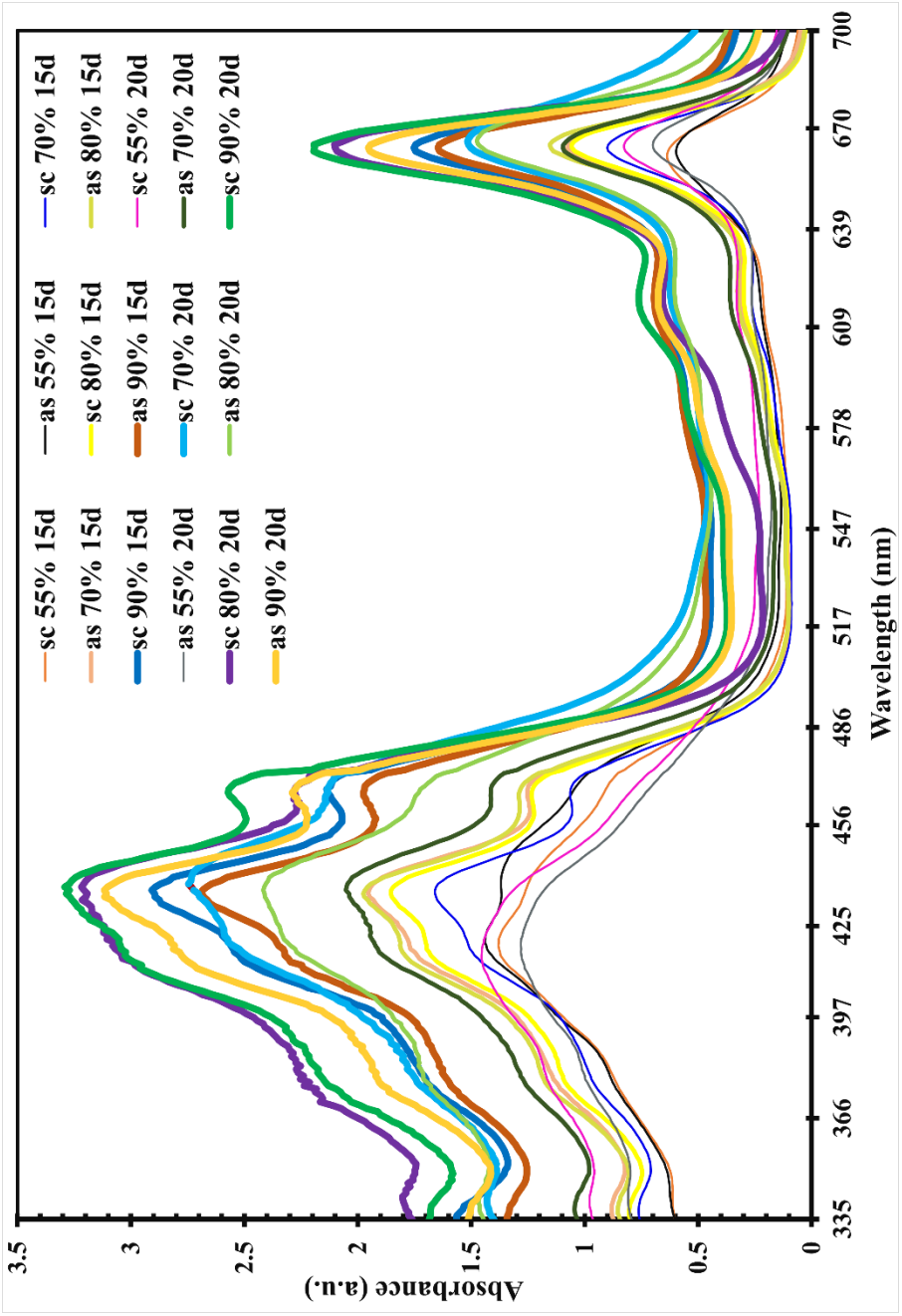

Figure 2.3. The ethanol-water solvent effect on the normalized plot of averaged visible absorption spectra, (55%, 70%, 80%, and 90%) with ethanol on the 15th and 20th days for two species using the hot solvent method.

Further when the two species were selected for dye generation with the solvent of ethanol primarily. The task of reducing the cost of extraction of dyes by simple water or (even waste water) along with adding

water-soluble pigments to the mixture of extraction. The water-diluted ethanol was compared in different concentrations and their capability to extract efficient dyes in the lowest possible concentrations was checked out as envisioned in **Figure 2.3.** The efficiencies were categorized into three categories based on the extraction i.e., low, medium, and high. The legends and scan line are the thickest for highly efficient, medium thick for average extraction, and least thin for low-performing dyes. The dyes were extracted with four concentrations of ethanol (55%, 70%, 80%, and 90%) for the species of *Asterarcys quadricellulare* and *Scenedesmus sp.*

Scenedesmus sp. at concentrations of more than 70% was quite effectively extracted of its pigments via the hot solvent method on the 20^{th} day but shows only at 90% concentration on the 15^{th} day. Whereas *Asterarcys quadricellulare* extracts only at 90% concentration on both the 15^{th} and 20^{th} day. Also, it is seen that concentrations on or below 70% do not extract enough for *Scenedesmus sp.* on the 15^{th} day whereas on the 20^{th} day, it is seen at 55% concentration. *Asterarcys quadricellulare* perform consistently well for both days till 70% concentration. It was observed that the *Scenedesmus sp.* is most efficient in extraction at 70-90% concentration of ethanol in comparison to others on the 20th day. The dye from *Asterarcys quadricellulare* was seen with reduced efficiency of *Chl b* extraction at the concentration below 80% while *Scenedesmus sp.* show a similar impact below 70%. The dilution of ethanol significantly reduces the efficiency of extraction of ethanol around or below 55% as major peak shifts were seen as well as peaks marking lower values with significant broadness. As per the authors Louda and Monghkonsri's comparison in 2006, the Spectrophotometric evaluation of pigments, particularly *Chls* was almost equally acceptable when compared with the high-performance liquid chromatography (HPLC) results. It is less expensive and faster than HPLC analyses. Also, UV–Vis spectroscopy displayed a rise in light absorbance in the UV section, which possibly

favors efficiency in solar cells but simultaneously has a probability to degrade early in natural light having UV content.

The dyes from species of *Scenedesmus sp.,* and *Asterarcys quadricellulare* were further tested with the hot solvent extraction method using methanol too and the results were better and comparable to ethanol. But the solvent of methanol does not work well with concentration reductions below 90%.

2.4.2. FT-IR spectroscopy

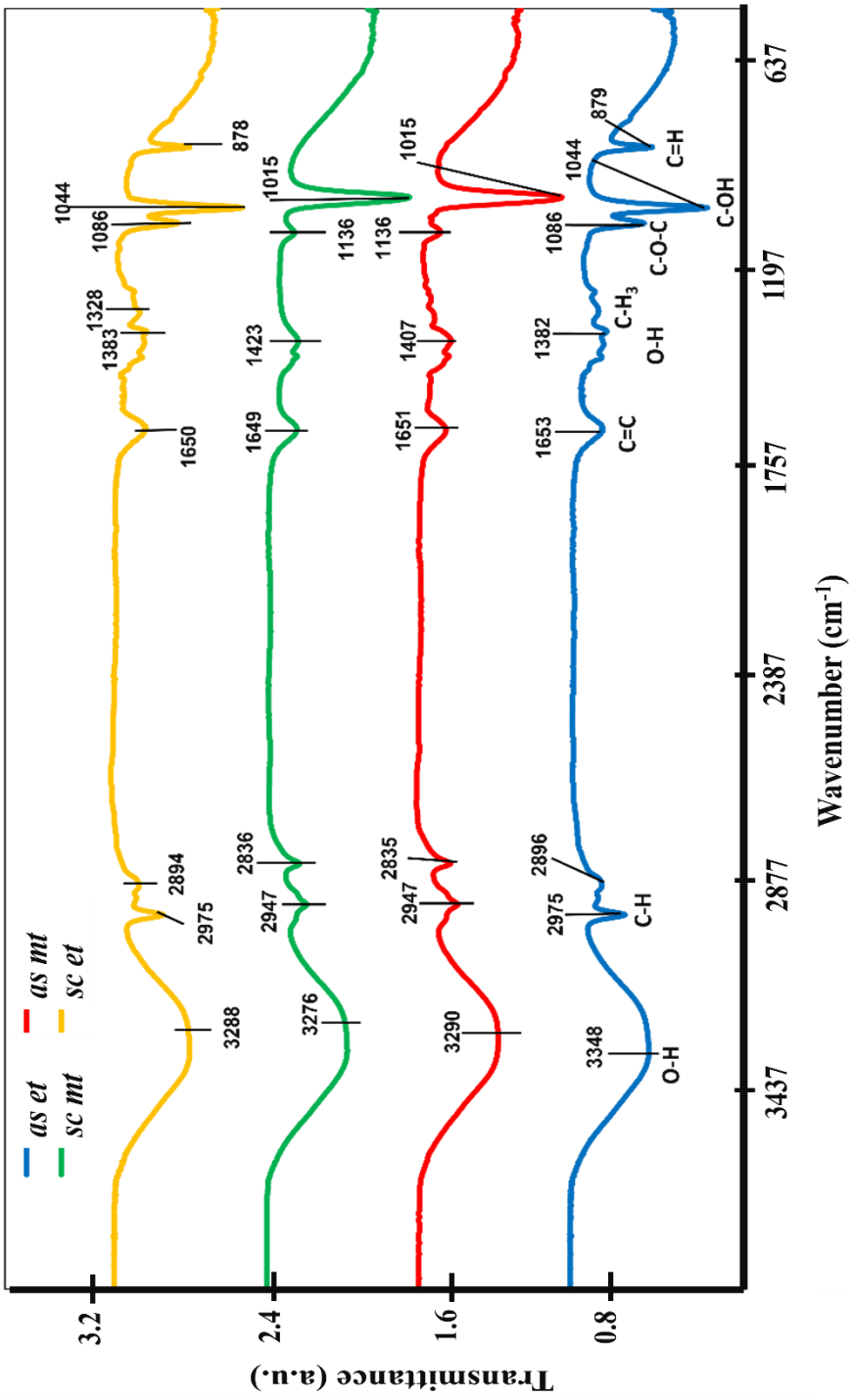

Figure 2.4. FTIR of two liquid dyes in different solvents (90% methanol & 80% ethanol) for finding out functional groups' efficiency in light absorption.

The Fourier Transform Infrared (FTIR) spectral study was carried out using Bruker Optik Alpha T- ATR - FTIR Spectrometer to categorize the major functional groups existing in the extracted dyes. FTIR

spectrum represented in **Figure 2.4.** shows distinct peaks. It is seen that all four dyes broadly and strongly peak in the region 3350-3250 cm^{-1} which makes it a probable hydroxyl group that can be of alcohols or phenols. The two ethanol-based dyes show C-H stretching vibrations that represent alkanes that peaks between 2850-2960 cm^{-1} (medium to strong). The intensity and position of the peaks can vary depending on the alkane's structure and neighboring functional groups. The two methanol-based dyes also show these peaks but at little different positions due to the C-H (sp^3) asymmetrical stretching vibration from alkanes. C=C stretching vibrations peaks between 1640-1680 cm^{-1} confirm the presence of the alkenes group. The peak shown at 1407 and 1423 cm^{-1} is allocated to the -OH in-plane distortion as of the alcohol group. The transmittance peak at 1382 and 1383 cm^{-1} presents the $-CH_3$ bending vibration. The peaks seen at 1086 cm^{-1} and 1136 cm^{-1} are assigned to the C-O-C stretching vibrations from the aliphatic and conjugated ester and ether functional group. Peaks between 1000-1350 can also be associated with the stretching vibrations of the C-N bond in the chlorin structure. The piercing and robust transmittance peak at 1044 and 1015 cm^{-1} represents the C-OH stretching vibration from the primary alcohol group. The ethanol-based dyes demonstrate a high-pitched absorption peak at 878 and 879 cm^{-1} corresponding to the C=H in-plane deformation from the four pyrrole ring structure.

2.4.3. Degradation Study

Besides, the various electrochemical and absorbance properties of dyes temperature and light intensity also affect the efficiency of DSSCs before the semiconducting layers are coated with dyes. The dyes which are most stable at high temperatures and light intensity are a suitable choice for researchers and industries for manufacturing. From the experiment that has been conducted, most of the dye in solvent-water solution extracted at a temperature of 100 °C is not so stable. The 10

ml of dyes were stored in glass vials and were observed for UV-visible spectra at an interval of 2 hours were observed for 16 hours in the presence of the light of 10, 000 lux (equivalent to ambient daylight) provided continuously and artificially with an LED lamp. Here **Figure 2.5.a.** shows the comparison of dyes from these two species when prepared in 80% ethanol and **Figure 2.5.b.** in 90% methanol for both.

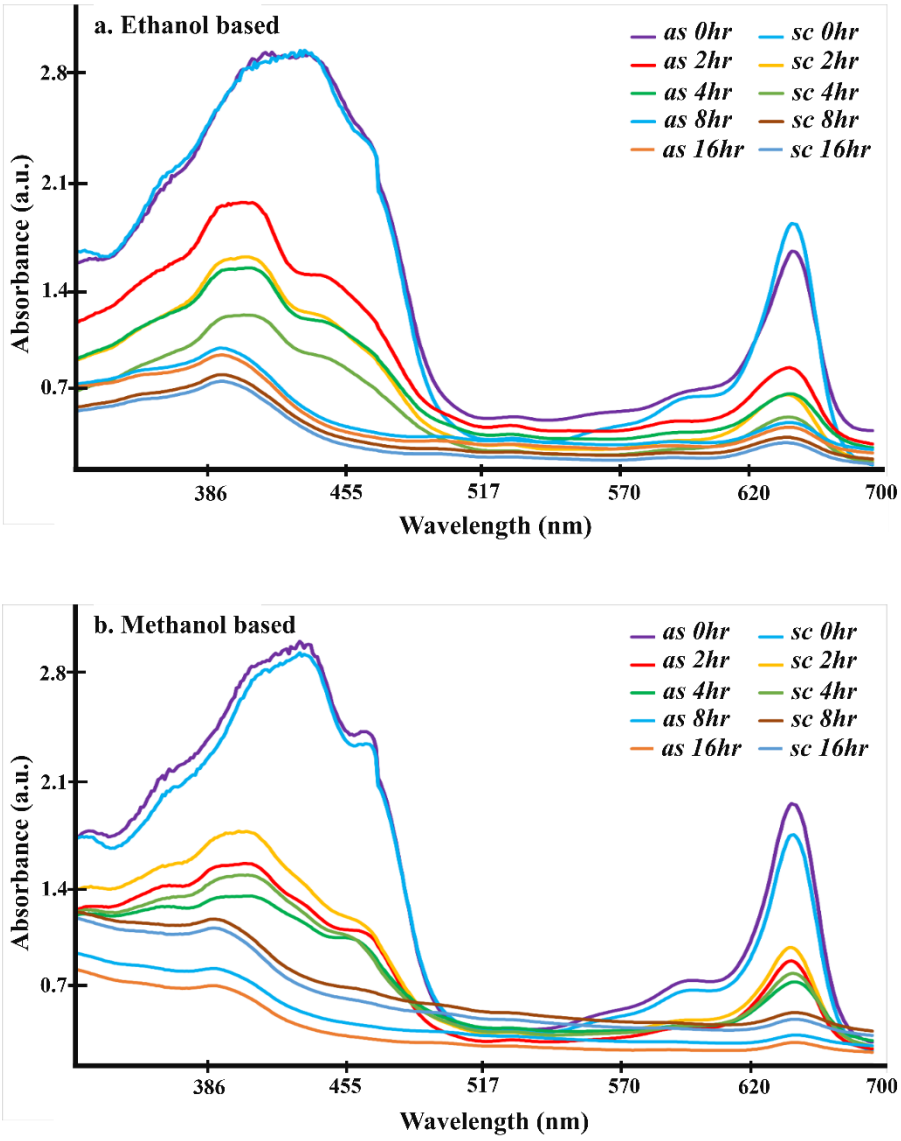

Figure 2.5. Absorption spectra for the stability of dyes (2 in no.) from species namely *Scenedesmus* and *Asterarcys* at 10,000 lux (ambient daylight) for 16 hours in a. ethanol and b. methanol.

Figure 2.5. shows that *Scenedesmus sp.* dye is comparatively less stable than *Asterarcys quadricellulare* dye in ethanol solvent whereas *Scenedesmus sp.* dye seems to be more stable in methanol. It can be seen that the pigment *Chl a* has reduced drastically along with other accessory pigments meant for photoprotection. The stability of these two dyes can remain close enough to these values or may change upon adsorption to the semiconducting layer and based on the hydroxyl group attachment and detachment type. Also, it is well established that pigments can be stored for longer periods in an organic solvent devoid of water compared to an aqueous solution.

The decolorization and photocatalytic degradation efficiency are also good parameters, which can be calculated as in Eq. 5 and can be inferred from the stability scan values at specific wavelengths.

$$Efficiency\ (\%) = C_0 - C_eC_0 \times 100$$

where the variables C_0 and C_e represent the dye's initial and final concentrations, respectively i.e., before and after photo-irradiation.

2.5. Conclusions

The widely used method to extract pigments by 80% acetone is not good enough to entirely extract the less polar pigments like *Chl a* and some of the carotenoids as realized. Hence, the best extraction as shown in experimental data is possible with methanol and ethanol via the particular hot solvent extraction method. Research on the development of dyes for a broad spectral response and better electron-donating capability has been done continuously and these microalgal-based dyes show a promising potential for use in DSSCs as per those constraints. Dyes in ethanol of *Scenedesmus sp.* and *Asterarcys quadricellulare* performed the best among all the six species on the 20^{th} day followed by the 15^{th} day and 25^{th} day. The optimized cost-effective concentration with unreduced efficiency is 80% and similarly, in methanol, it is a 90% concentration with the same hot

solvent method that performs equivalently well for both species. Based on the electron-donating capability of these *Asterarcys quadricellulare* outperforms *Scenedesmus sp.* slightly in both solvents.

The FTIR spectroscopy showed a decent presence of desired functional groups that can be helpful in attachment to the semiconductive layer. Dye from *Scenedesmus sp*. and *Asterarcys quadricellulare* remained relatively stable at 10000 lux and may have a chance to survive in long diffused light durations at least for a few days. Further parameters have to be researched and the stability of these dyes should be enhanced by some stabilizing chemical additions.

Ethanol remains the best and most green solvent for extraction by the simple classic method of hot solvent extraction, but lower temperatures need to be identified for better stable extraction and to avoid early degradation of dyes. Their absorption spectra cover the major part of the visible region while elongating into the UV and near-infrared range. This is a unique situation since many natural dyes from plants in comparison to algae lack this spectral coverage property. Also, these algal cells can be used as it is for energy production without dye extraction by replicating photosynthesis and harnessing electricity. As per the conclusions drawn from this chapter, the idea of new approaches in testing various natural dye sensitizers based on algae for enhanced DSSCs performance and stability will be further evaluated in the upcoming chapter. The forthcoming study will focus on different extraction protocols, such as heating and sonication for extraction of dyes, followed by analyzing their optical properties like reflectance and photo-electron energy scans.

CHAPTER 3

Influence of varying Extraction Parameters on Dye Properties and Stability

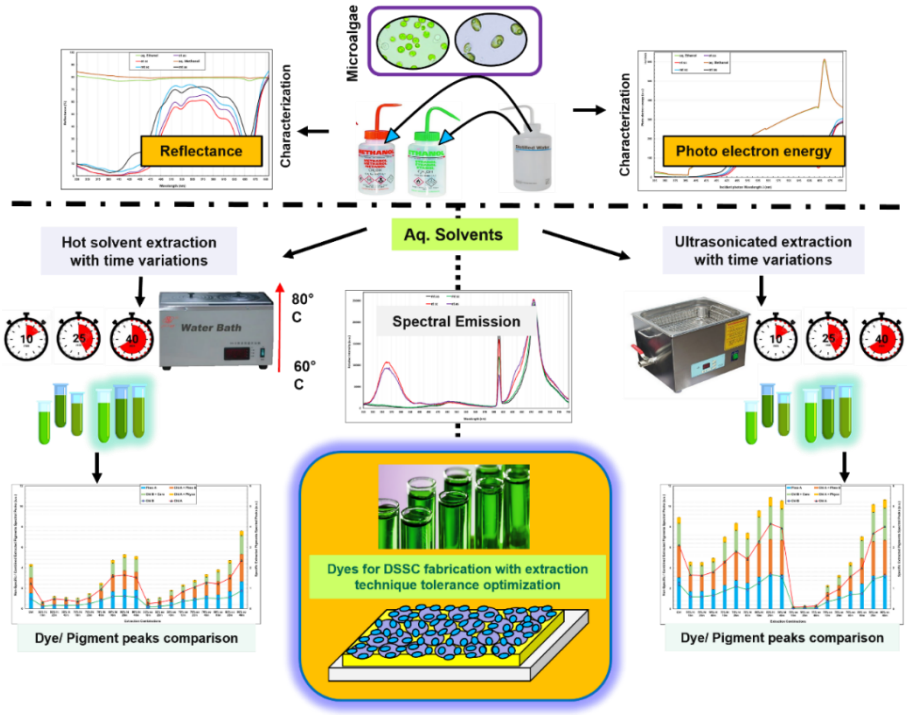

CHAPTER 3

Influence of varying Extraction Parameters on Dye Properties and Stability

3.1. Introduction

Algal dyes as potential sensitizers for dye-sensitized solar cells (DSSCs) due to their abundant availability, environmentally friendly nature, and low-cost production are concerned by the temperature of utilization, which varies with specific dye and cell configuration [Chauhan, 2022]. Elevated temperatures accelerate dye degradation processes, leading to reduced dye adsorption and decreased cell performance. They are more susceptible compared to synthetic dyes due to their complex weakly bonded chemical composition and sensitivity to environmental factors [Talaei et al., 2022]. To enhance the stability of algal dyes in DSSCs at elevated temperatures, several strategies have been employed as choosing algal dyes with high thermal stability, or combining algal dyes with other stable synthetic dyes through co-sensitization or encapsulating algal dyes within protective matrices or incorporating them into polymer films or electrolyte optimization [Lamnatou & Chemisana 2023; Kabir et al., 2019].

Other efficiency losses can be due to the reflectance properties of dyes. Individual pigments in dyes interact with each other, leading to modifications in their absorption and reflectance properties. These interactions can result in shifts in the spectral characteristics and overall reflectance behavior of the extracted dyes [Groeneveld et al., 2023].

Another major factor of dyes is their emission spectra which are influenced by the electronic structure and energy levels of the dye/ pigment. Moreover, the emission spectra of dyes can be influenced by factors such as solvent polarity, pH, temperature, and the presence of other molecules [Gáspár et al., 2008].

Solvent polarity decides on solvent extraction techniques primarily involving sonication and heating methods and can enhance the efficiency and effectiveness of solvent extraction processes. Sonication, aka ultrasonication, involves the use of high-frequency sound waves to agitate a liquid sample creating tiny bubbles that undergo rapid expansion and contraction, which generates localized pressure changes and intense mechanical forces. Sonication enhances the contact between the solvent and the target dye. Whereas heating increases molecular motion by increasing the kinetic energy of molecules, leading to more frequent collisions and enhanced diffusion rates [Constantino-Robles et al., 2022].

When combined, sonication and heating can synergistically improve the extraction efficiency of algal pigments but need to be performed in dim light or under nitrogen to prevent degradation [Liu et al., 2022; Mittal et al., 2017]. This combined approach is particularly useful for economic challenges or when time is a limiting factor. Here, the choice of solvent, extraction parameters including sonication power and duration, heating temperature, etc., and the nature of the target dye should be well thought out. The technique of heating temperatures higher than 60 °C is generally not recommended for algal pigment extraction due to the potential for pigment degradation and other undesirable effects. Algal pigments, particularly *Chl*s, carotenoids, and phycobiliproteins, are sensitive to high temperatures [Steephen et al., 2023]. Prolonged exposure to temperatures above 60 °C can lead to the degradation of these pigments, resulting in changes in color, loss of fluorescence, and reduced pigment concentration [Pez Jaeschke et al., 2021; Pagels et al., 2021]. The operation at higher temperatures requires more energy input, which can add to the overall cost of the extraction process. Maintaining temperatures below 60 °C is generally considered a safe practice to minimize pigment degradation and maximize extracted dye variety.

This paper investigates the role of techniques like sonication and heating for extraction and their combination in achieving higher or desired extraction efficiency. Further, these techniques are cross-

verified with reflectance and emission values for the same and conclude on better stable dyes providing species and solvents. This paper will be a solution to the use of expensive extraction processes through a lab-scale setting, as the heating-based extraction can be carried out with light-covered solar heaters on a large scale and can be used for creating additional value-added products in the bioreactor system just instead of DSSCs technique alone while producing electricity. The identified optimum durations of heating and sonication will save on infrastructure and energy investments and will help to develop inexpensive large-scale DSSCs [Gondi et al., 2022; V. et al., 2021].

3.2. Experimental Section

3.2.1. Materials and Reagents

The solvents were from Sigma-Aldrich Co. LLC. Ethanol (C_2H_6O) and Methanol (CH_4O) both ≥99.8% pure. For experimental purposes, these solvents were diluted with deionized (DI) water to achieve concentrations of 80%, 70%, and 55%.

3.2.2. Growth and culture settings of microalgae

The two axenic cultures of freshwater microalgae: *Asterarcys quadricellulare* and *Scenedesmus sp.* [Chauhan et al., 2023; Chauhan et al., 2024] were cultivated in a basic BG-11 medium, maintaining a pH range of 7.2 to 7.4 through the use of diluted base (NaOH) or acid (HCl). Seed cultures of both species were cultivated for 10 days in Erlenmeyer flasks and subsequently, sub-cultured axenically and were used to inoculate with an initial cell density of 0.1 at 680 nm, and growth readings were recorded every 24 hours, continuing for 30 days. These cultures were housed in a designated culture room with a constant temperature of 27 ± 5°C and followed a light photoperiod of 12 hours. To ensure optimal growth, white, fluorescent lamps were

positioned at an appropriate distance, providing a light intensity of 3000 lux [Stanier et al., 1971].

3.2.3. Dye Extraction and Methodology

3.2.3.1. Dye extraction

On the 20th day, dye extraction was performed from two separate sets of 250 ml Erlenmeyer flasks containing different species using ethanol and methanol individually. We used three different concentrations for both methanol and ethanol as mentioned.

3.2.3.2. Extraction techniques

In the first extraction method, a known volume of the microalgal culture of a specific species was subjected to centrifugation, and the resulting residue was blended with 55%, 70%, or 80% ethanol or methanol. This mixture was then sonicated with the help of an Ultrasonic Sonicator Bath for durations of 10, 25, and 40 minutes, followed by heating for 5 minutes in a boiling water bath. The solution was subsequently centrifuged again, and the supernatant was collected. In the second case hot solvent method was individually carried out, and the microalgal residue was mixed with the same concentrations of ethanol or methanol and heated in a boiling water bath for the same durations as above. Afterward, the solution underwent centrifugation, and the resulting supernatant was collected [Pápista et al., 2002; Henriques et al., 1970].

3.2.4. Characterization

The UV–vis absorption spectra of all acquired dyes were recorded using the DR-6000 HACH spectrophotometer to measure their absorptions. Reflectances as well as photo-electron energy rates for respective wavelengths were measured through a Perkin Elmer Victor Nivo Multimode Plate reader in the range of 300 to 800 nm.

The ANALAB Ultrasonic Sonicator Bath was configured to operate at a fixed frequency of 33 ± 3 KHz for durations of 10, 25, and 40 minutes.

3.3. Result and Discussion

3.3.1. UV- vis Reflectance spectroscopy

These two species were decided based on some tests for dye-making with ethanol as the chosen solvent primarily and consequently with methanol as per greener solvent comparison and based on the UV-visible data [Chauhan et al., 2023; Chauhan et al., 2024]. The objective was to lower the extraction expenses for dyes by incorporating a straightforward water addition, or even wastewater, while also introducing water-soluble pigments into the extraction mixture. To achieve this, experiments were conducted using the hot solvent extraction method with methanol on dyes obtained from *as* and *sc* The outcomes demonstrated a significant improvement, with results comparable to those achieved using an 80% aqueous ethanol solution. The UV-visible data was again cross-verified with the visible reflectance data as shown in **Figure 3.1.**

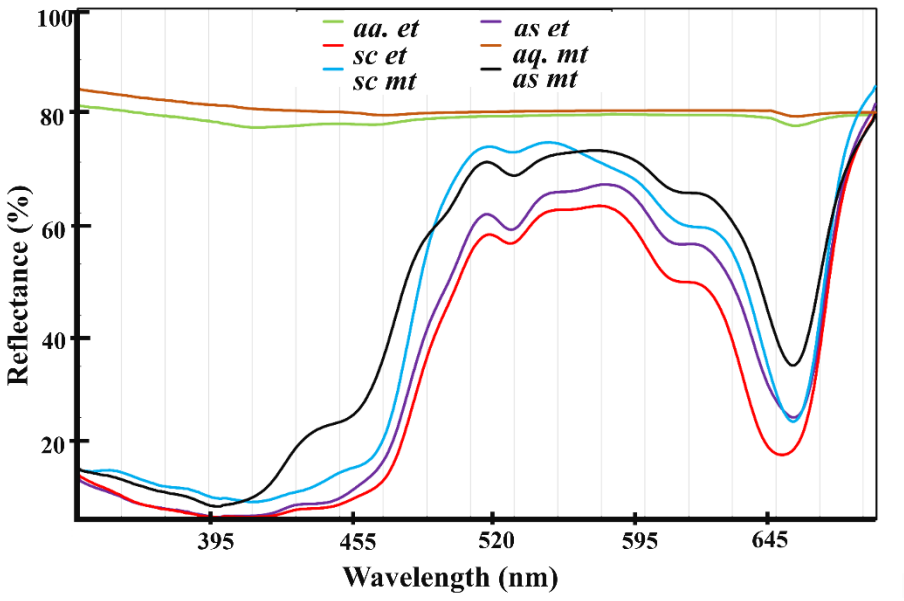

Figure 3.1. Visible region reflectance spectra of dyes from two microalgal species extracted in aqueous solvents of 80% ethanol and methanol separately utilizing hot solvent extraction.

The spectra of *sc* dye in aq. ethanol showed the least reflectance supporting the reason for its higher absorption in the particular range. The reflectance of ethanol with *as* dye was closely overlapped by the reflectance of *sc* dye in methanol in two particular regions of red and blue but does not do so in the green region due to less extraction of significant carotenoids via the solvent of methanol [Zhao et al., 2010; Duppeti et al., 2017]. Methanol was able to extract the least in the case of *as* dye.

3.3.2. UV- vis Photoelectron energy spectroscopy

The photoelectron spectrum originates from the analysis of the energy spectrum possessed by photoelectrons, which are electrons generated upon the impact of an energetic photon on a molecule as shown in **Figure 3.2.** for the two dyes.

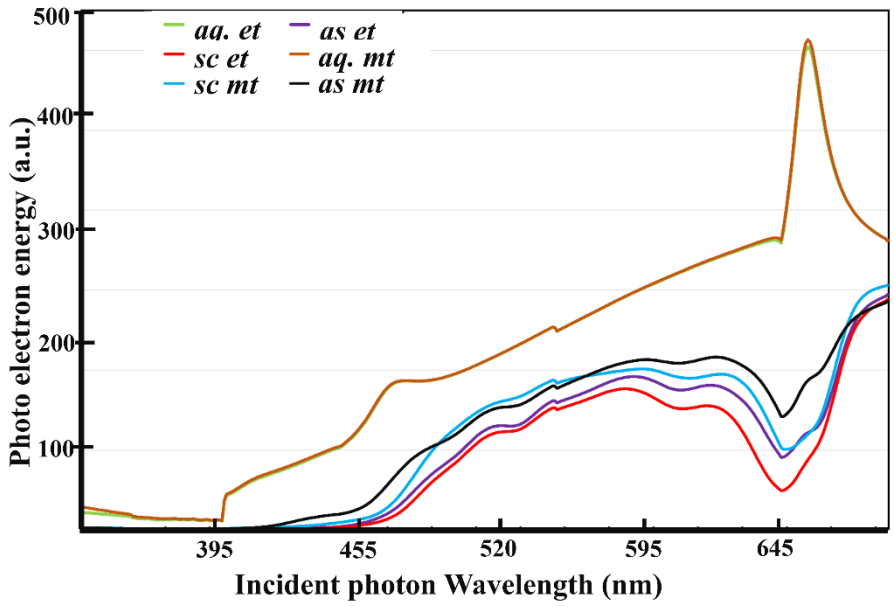

Figure 3.2. Visible region photo electron energy requirement for electron excitation vs wavelength of dyes from two microalgal species extracted in aqueous solvents of 80% ethanol and methanol separately utilizing hot solvent extraction.

The photoelectron energy spectra of *sc* dye in aq. ethanol showed the least need of energy to excite electrons to a higher state in the particular wavelength range. The energy of ethanol with *as* dye was closely followed by the energy gap of *sc* in methanol. *as* dye in methanol had the most requirement of energy for excitation.

The relationship between photon energy and wavelength can be described using the equation:

$$E = hc/\lambda \quad (11)$$

where E is the energy of a photon, h is Planck's constant (approximately 6.626×10^{-34} joule-seconds), c is the speed of light in a vacuum (approximately 3×10^{8} meters per second), and
λ is the wavelength of the photon.
The photon energy of a dye depends on the specific wavelength at which it absorbs light [Singh et al., 2020]. It's worth noting that while the basic molecular structures of ethanol and methanol are similar, subtle differences in their functional groups and molecular arrangements can lead to variations in their photoelectron energies and absorptionabsorbance spectra [Kosumi et al., 2012].
Dyes and solvents, such as methanol, can have different energy absorbance properties at a specific wavelength depending on their electronic structure and the presence of certain chromophores or functional groups that can interact with light [Kumar et al., 2021]. Dyes are specifically designed to have strong absorption at specific wavelengths, and they often contain conjugated systems or chromophores that exhibit electronic transitions that align with the energy level corresponding to a specific wavelength.

3.3.3. Fluorescence Spectroscopy

HORIBA Fluorolog-QM series modular research grade spectrofluorometer was used to measure the emission spectra of the microalgal dyes. The excited dye molecules that were exposed to the light of a specific wavelength had the dye's electrons promoted to higher energy levels and while they returned to their ground state, they released the excess energy in the form of photons [Yokono et al., 2011]. These emitted photons have longer wavelengths and correspond to specific colors of light. The spectrometer detects and measures the intensity of the emitted photons as shown in **Figure 3.3.** The scans were taken from ultraviolet (UV) to visible (Vis) and even near-infrared (NIR) region and the recorded intensity of emission is given in figure with plotted emission spectrum.

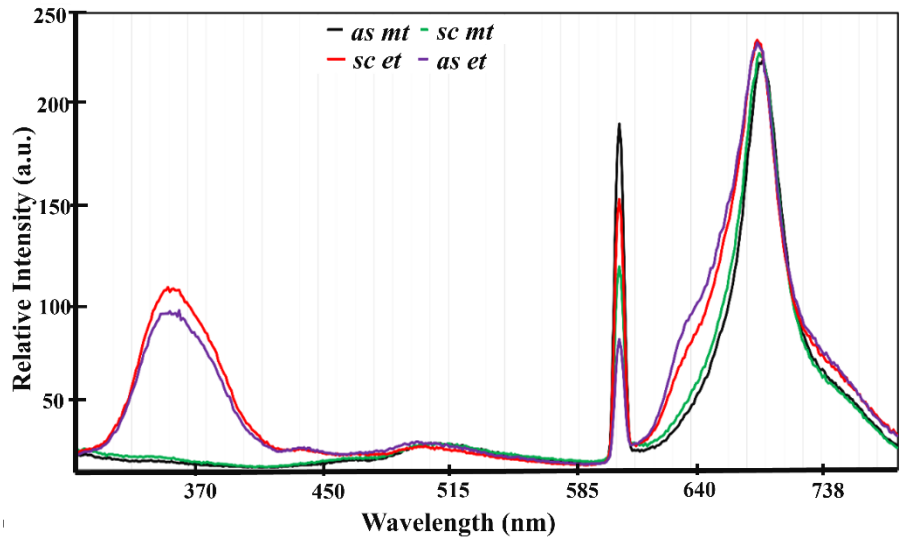

Figure 3.3. UV-visible region fluorescence vs wavelength of dyes from two microalgal species extracted in aqueous solvents of 80% ethanol and methanol separately utilizing hot solvent extraction.

The position and intensity of the peaks can indicate the efficiency of fluorescence emission. It is seen in **Figure 3.3.** that the significant emission points are almost common in all four dyes with varied intensity. The peaks at a wavelength of 601nm coincide in all four dyes in the high to low order of *mt as* > *et sc* > *mt sc* > *et as*. The peaks at

675nm are comparatively higher for *et sc* than *et as*. The peaks for dyes in methanol have a slight delay in emission and occur at 676 nm with similar peaks. The peak of *mt as* extends to 678nm from 676nm. Similarly in the blue region, the peaks of *et sc* also remain extended from 359 to 362nm along with that of *et as* from 362 to 365nm but with less relative intensity. Overall it can be summed up that *sc* is more efficient in electron emission and generation terms with more capacity to utilize the energy from photons.

3.3.4. Extraction Methods efficiency analysis via UV-visible spectroscopy

The dyes were generally extracted via a hot solvent extraction method at 100 °C with 80% concentration of solvents. The dyes extracted as per the literature review and practical extraction tests conducted were shown to get degraded and not able to extract temperature-sensitive pigments at this temperature value. So, two different temperature values were set to study the impact on extraction efficiency and degradation value to avoid these factors impacting dye utilization practically and on a large scale. The duration of extraction was kept the same as the original duration of 5 minutes and the concentration of solvent at 80%. The temperature of extraction was kept at 60 °C and 80 °C considering various points of literature like the boiling point of ethanol being 78.4 °C and methanol being 64.7 °C, the temperature of extraction being more than 60 °C being degrading for pigments and 80 °C able to work just sufficiently for extraction as it is just above the boiling point of all the employed solvents [Ngamwonglumlert et al., 2017].

The extraction test was carried out at both of these temperatures separately with four parts enclosed in each. For a fixed heating temperature of 60 °C and 80 °C it was done with a) *mt as* b) *mt sc* c) *et as* b) *et sc*. In each set, the control is of the duration of 5 minutes (min) of heating at the fixed heating temperature and the rest are varied with the duration of heating or sonication [Thankappan et al., 2013]. In

sonication-varied samples (so) at 10 min, 25 min, and 40 min, the heating duration is still fixed at 5 minutes whereas in heating-varied samples (ht) the heating duration changes to 10 min, 25 min, and 40 min [Ngamwonglumlert et al., 2017; Linares et al., 2022]. The results were obtained and plotted as shown in **Figure 3.4.a., 3.4.b., 3.4.c,** and **3.4.d.** and compared with control for inferencing the extraction efficiency of such variations concerning control.

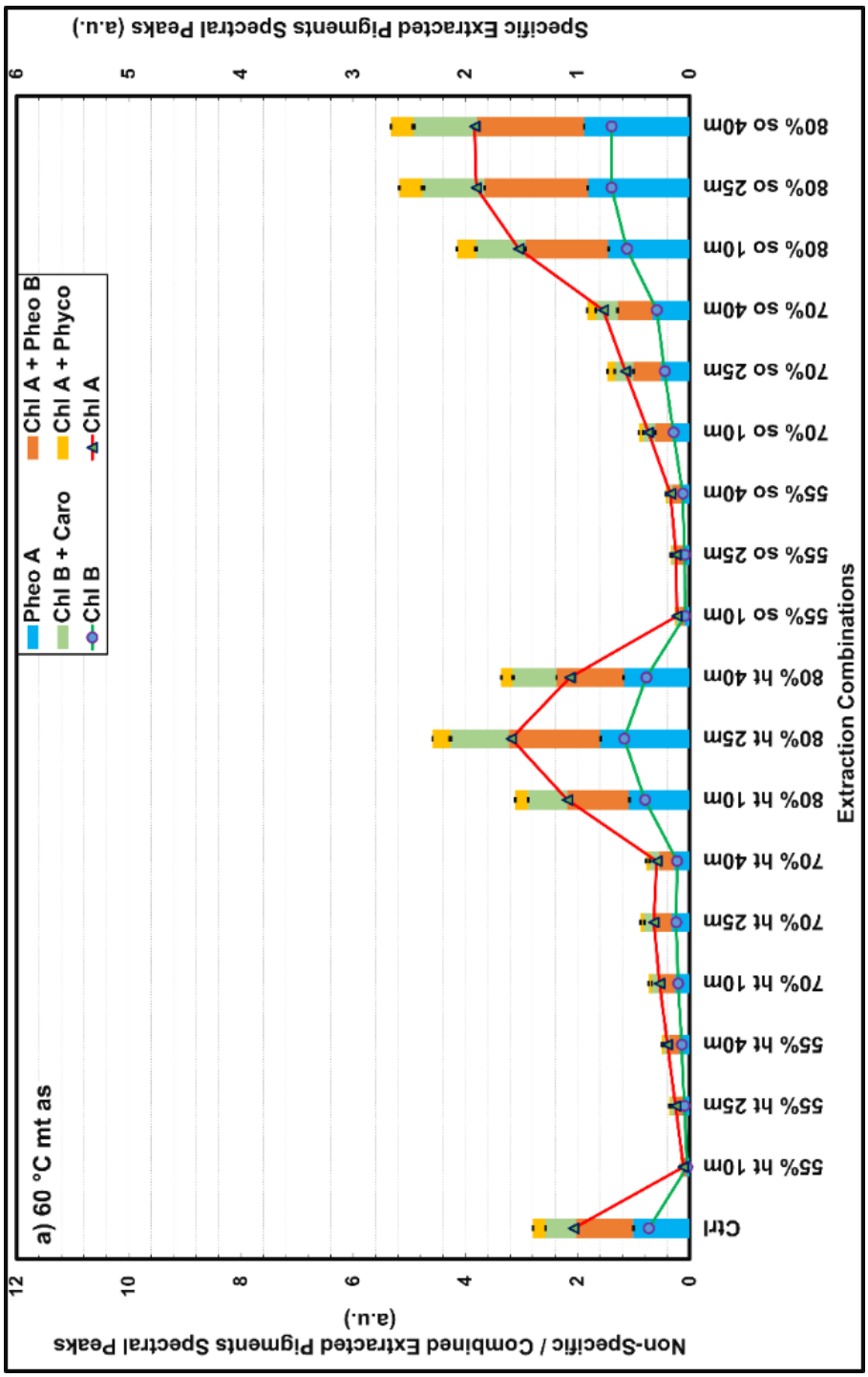
a) 60 °C mt as
Pheo A
Chl B + Caro
Chl B
Chl A + Pheo B
Chl A + Phyco
Chl A
Non-Specific / Combined Extracted Pigments Spectral Peaks (a.u.)
Specific Extracted Pigments Spectral Peaks (a.u.)
Extraction Combinations
Ctrl
55% ht 10m
55% ht 25m
55% ht 40m
70% ht 10m
70% ht 25m
70% ht 40m
80% ht 10m
80% ht 25m
80% ht 40m
55% so 10m
55% so 25m
55% so 40m
70% so 10m
70% so 25m
70% so 40m
80% so 10m
80% so 25m
80% so 40m

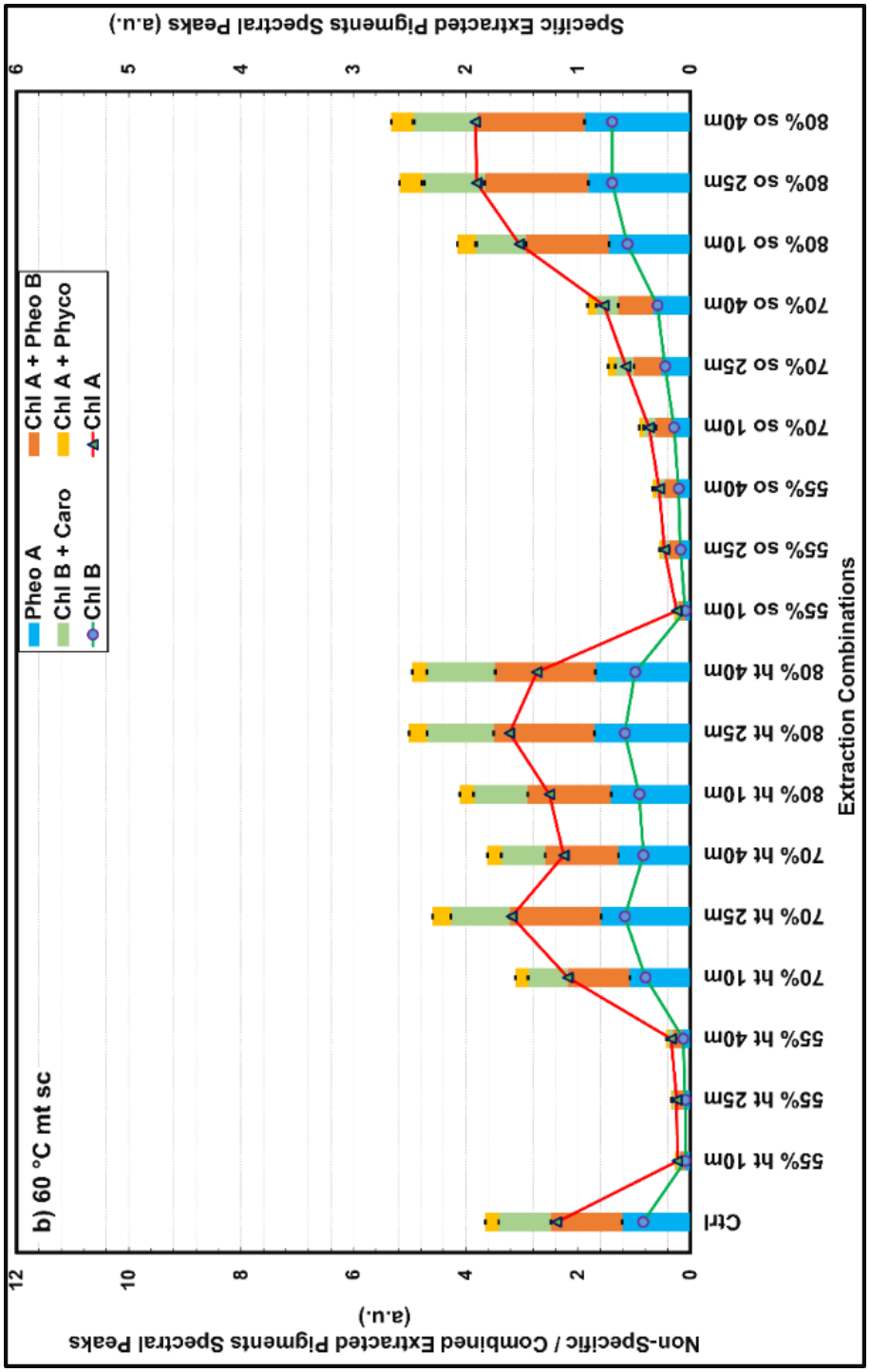
b) 60 °C mt sc
Pheo A
Chl B + Caro
Chl B
Chl A + Pheo B
Chl A + Phyco
Chl A
Non-Specific / Combined Extracted Pigments Spectral Peaks (a.u.)
Specific Extracted Pigments Spectral Peaks (a.u.)
Extraction Combinations
Ctrl
55% ht 10m
55% ht 25m
55% ht 40m
70% ht 10m
70% ht 25m
70% ht 40m
80% ht 10m
80% ht 25m
80% ht 40m
55% so 10m
55% so 25m
55% so 40m
70% so 10m
70% so 25m
70% so 40m
80% so 10m
80% so 25m
80% so 40m

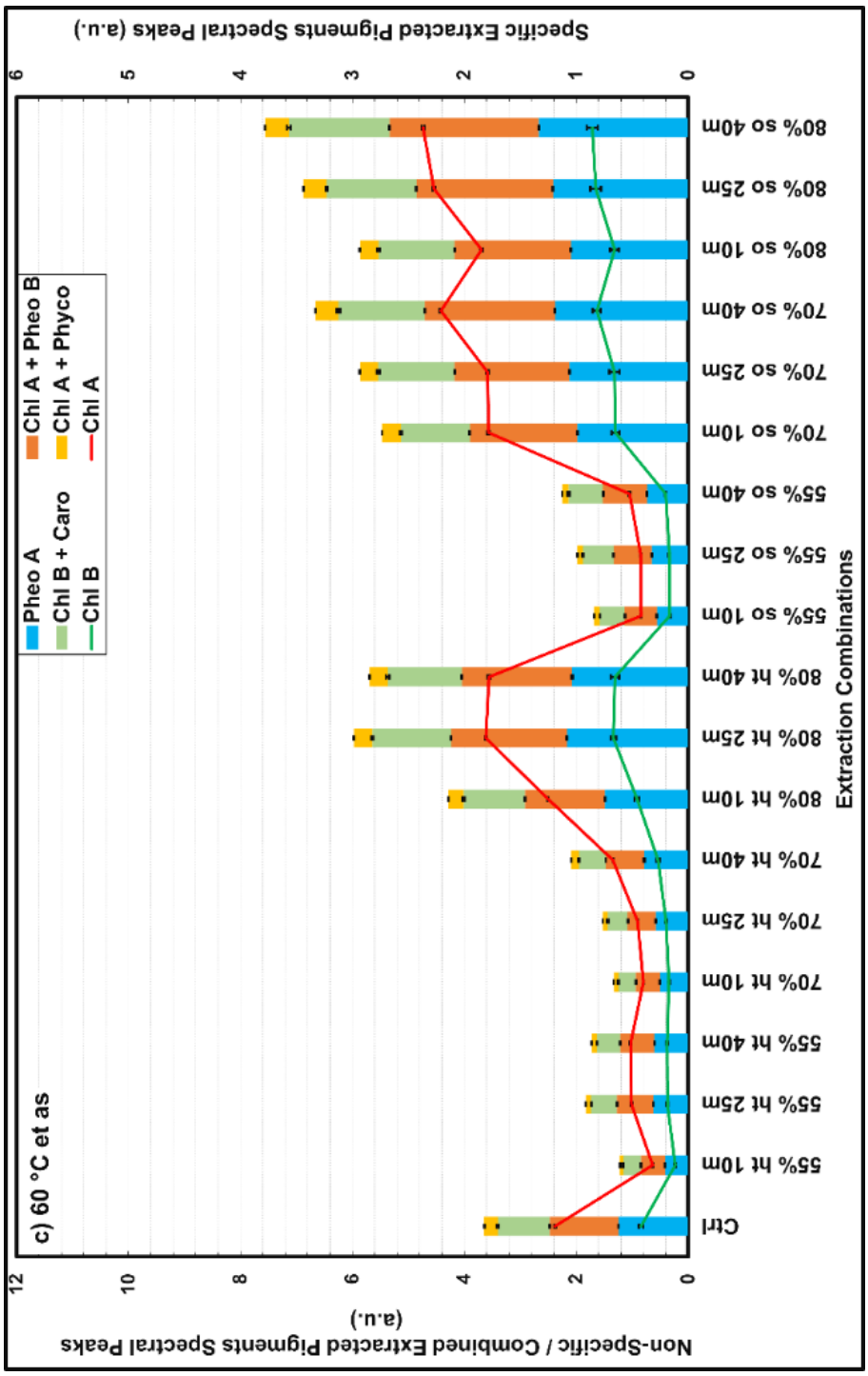
c) 60 °C et as
Pheo A
Chl B + Caro
Chl B
Chl A + Pheo B
Chl A + Phyco
Chl A
Non-Specific / Combined Extracted Pigments Spectral Peaks (a.u.)
Specific Extracted Pigments Spectral Peaks (a.u.)
Extraction Combinations
Ctrl
55% ht 10m
55% ht 25m
55% ht 40m
70% ht 10m
70% ht 25m
70% ht 40m
80% ht 10m
80% ht 25m
80% ht 40m
55% so 10m
55% so 25m
55% so 40m
70% so 10m
70% so 25m
70% so 40m
80% so 10m
80% so 25m
80% so 40m

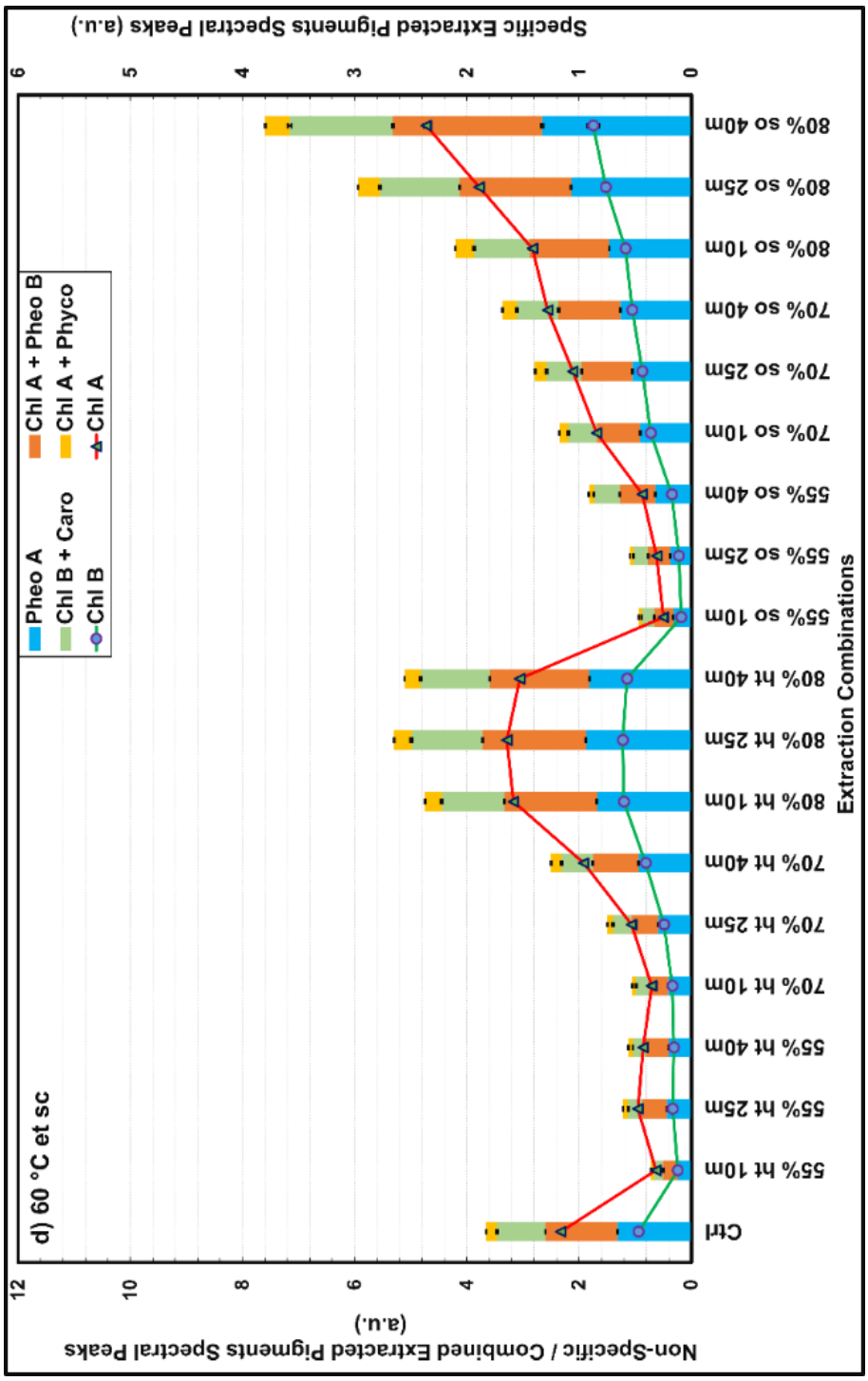

Figure 3.4. Comparative analysis of Non-Specific or Combined extracted pigments spectral peaks and Specific or defined extracted pigments spectral peaks w.r.t. different time-varying extraction techniques combinations at 60 °C.

It can be seen in **Figure 3.4.a.** that the combinations of *as* with methanol were effective in the extraction of dye with both heating and sonication at or above 80% concentration only. If the energy input and time taken parameters are considered then the best performance via heating is observed at 25 min after which the pigments start to degrade but efficiency remains higher than the control till 40 minutes. Whereas the extraction efficiency is constant after 25 minutes of sonication which means more duration of sonication will not show any significant effect in extracting [Das et al., 2022]. More dye was extracted by sonication in comparison to heating alone in comparison to their best performances [Sivakumar et al., 2009].

In **Figure 3.4.b.** which had the same combination with *sc,* it was seen that methanol was quite effective in the extraction for it compared to that of *as.*

The control itself was able to extract significantly more and good extraction peaks were even seen at 70% concentration with heating but was not so with sonication. Considering the heating combinations it was observed that combinations of 70% ht 25 min, 80% ht 10 min, 80% ht 25 min, and 80% ht 40 min performed better than the control. Whereas in sonication all the combinations with 80% solvent concentrations only could perform better than the control. But still, the sonication performance was better than the combinations of heating. It was understood that the sonication duration of a minimum of 25 min is enough to achieve efficient extraction, whereas heating after 25 minutes can deteriorate dyes [Das et al., 2022; Sivakumar et al., 2009].

In **Figure 3.4.c.** it was understood that ethanol with *as* dye in it, through intensification in temperature or sonication duration, becomes significantly effective in extraction in comparison to control. The pure heating method was only significant at a concentration at or above 80% whereas sonication was effective even at 70% or above concentrations. The optimum concentration of heating falls around somewhere between 25 min to 40 min proving that ethanol provides a

comparatively longer duration of heating tolerance over methanol at this temperature. In the sonication case, there is almost a 1.5-fold increase at 70 % concentration and the maximum extraction achieved at 80 % concentration with sonication for 40 min is almost a 2-fold increase w.r.t. control. However, an increase in sonication duration shows a slower increase in extraction efficiency but still is quite higher than the control [Zhong et al., 2019].

Figure 3.4.d. shows that *sc* dye at 80% or higher concentration has the extraction efficiency increased exponentially with sonication while below this concentration the extraction quantity remains below control at all durations. In the case of pure heating it is seen that heating for more than 10 min has no significant impact on pigment values and the optimum duration will lie between 10-25 min [Das et al., 2022; Sivakumar et al., 2009; Zhong et al., 2019].

It can be seen that the specific *Chl a* value is in agreement with the increase of non-specific *Chl a* value and the same goes for *Chl b* values for all the subfigures except with little insignificant deviation in the case of sonicated and heated dyes from *as* in ethanol for 80% concentration [Sivakumar et al., 2009; Zhong et al., 2019]. A significant increase in the ratio of pheophytin a to *Chl a* is also visible in the higher solvent concentration and with a temperature duration of more than 25 minutes.

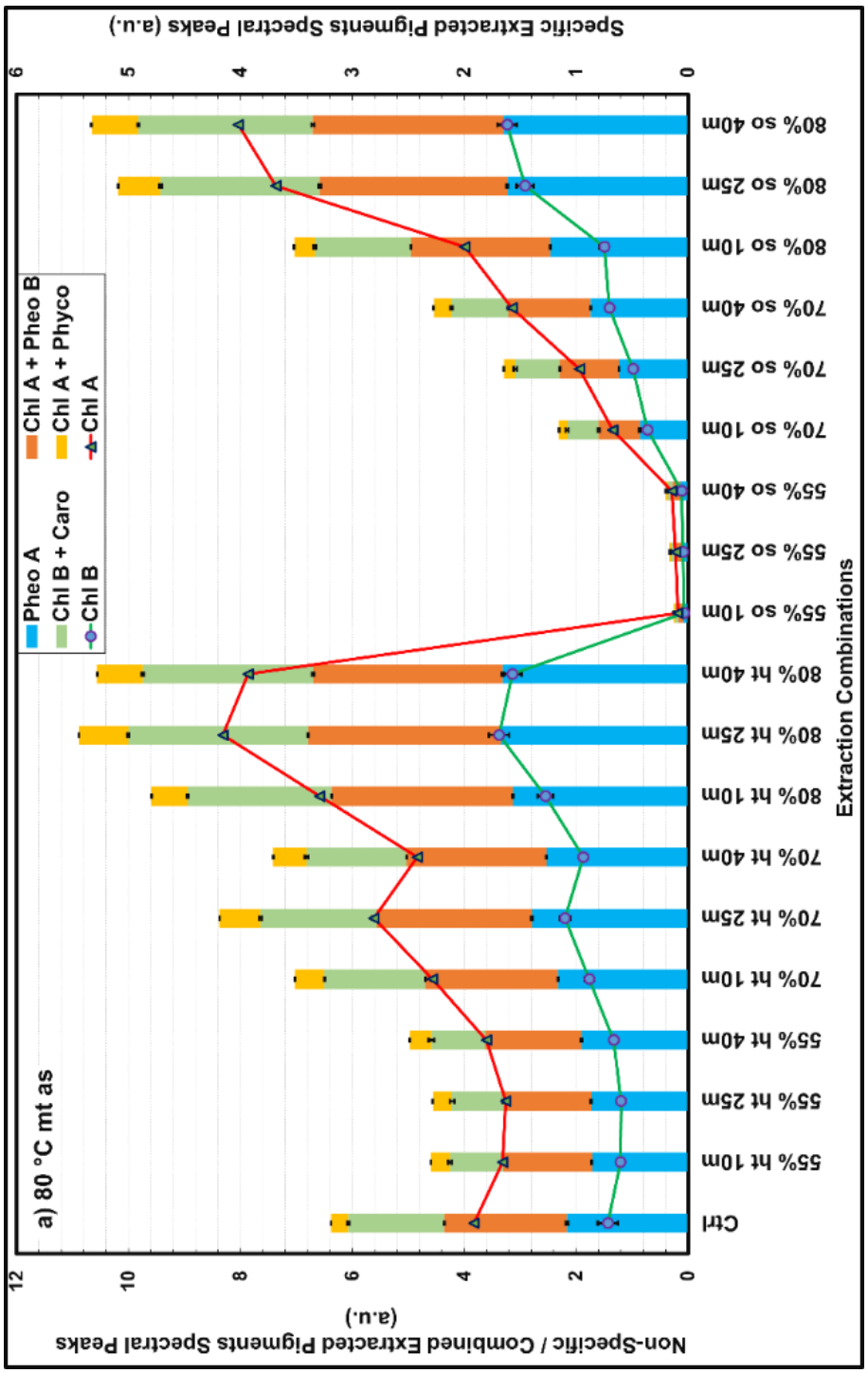
Non-Specific / Combined Extracted Pigments Spectral Peaks (a.u.)
Specific Extracted Pigments Spectral Peaks (a.u.)
a) 80 °C mt as
Pheo A
Chl B + Caro
Chl B
Chl A + Pheo B
Chl A + Phyco
Chl A
Extraction Combinations
Ctrl
55% ht 10m
55% ht 25m
55% ht 40m
70% ht 10m
70% ht 25m
70% ht 40m
80% ht 10m
80% ht 25m
80% ht 40m
55% so 10m
55% so 25m
55% so 40m
70% so 10m
70% so 25m
70% so 40m
80% so 10m
80% so 25m
80% so 40m

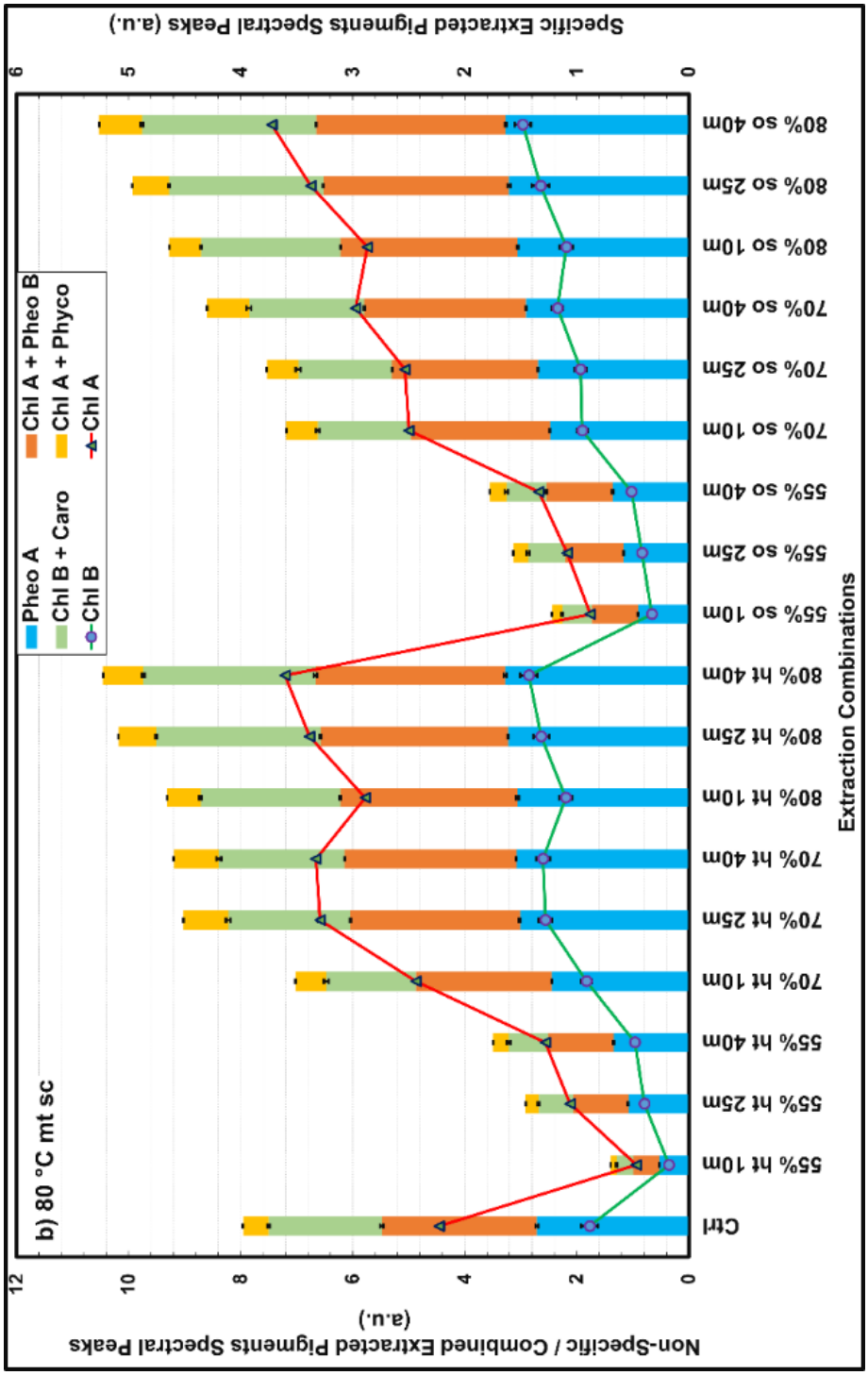
b) 80 °C mt sc
Pheo A
Chl B + Caro
Chl B
Chl A + Pheo B
Chl A + Phyco
Chl A
Non-Specific / Combined Extracted Pigments Spectral Peaks (a.u.)
Specific Extracted Pigments Spectral Peaks (a.u.)
Extraction Combinations
Ctrl
55% ht 10m
55% ht 25m
55% ht 40m
70% ht 10m
70% ht 25m
70% ht 40m
80% ht 10m
80% ht 25m
80% ht 40m
55% so 10m
55% so 25m
55% so 40m
70% so 10m
70% so 25m
70% so 40m
80% so 10m
80% so 25m
80% so 40m

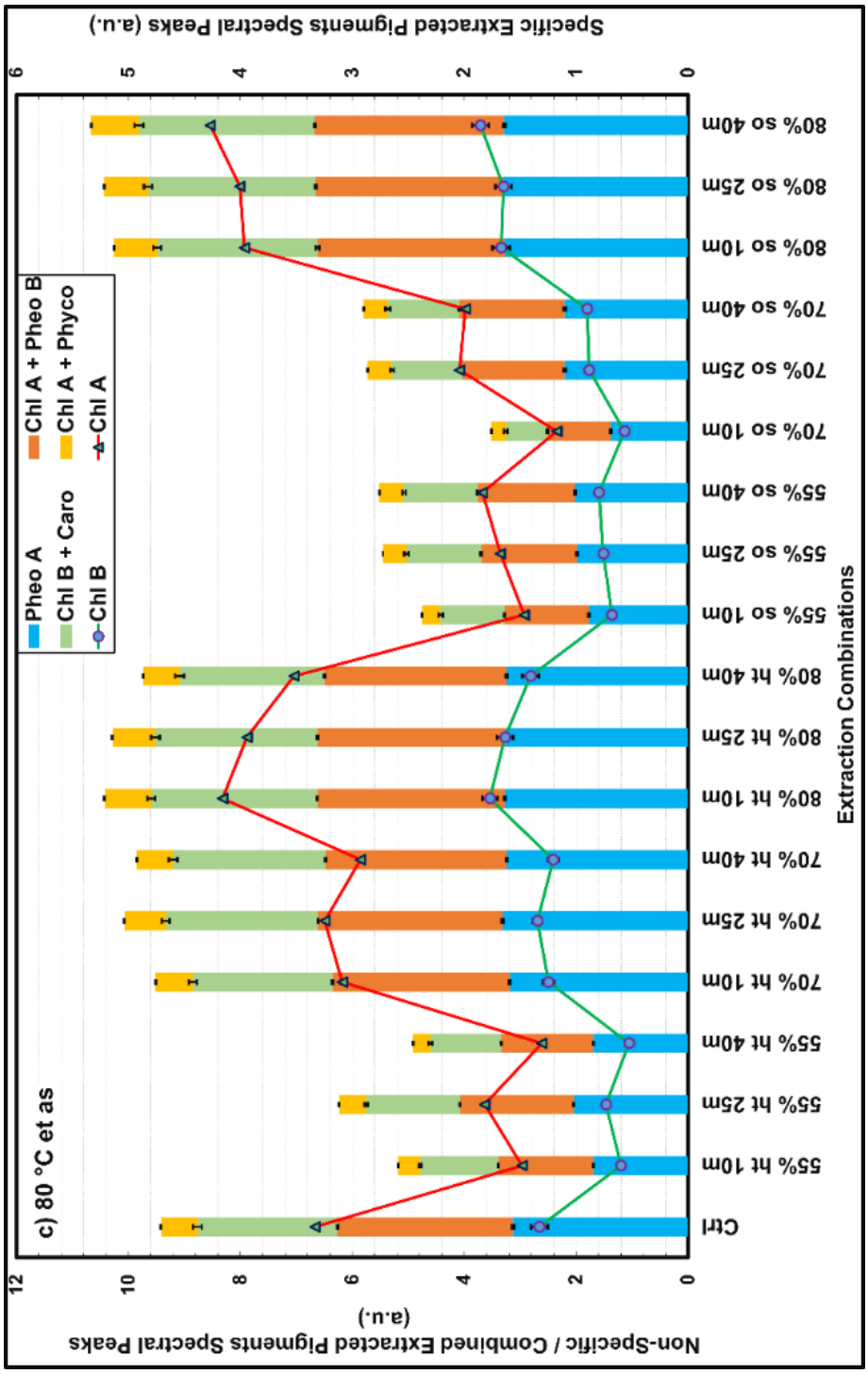
c) 80 °C et as
Pheo A
Chl B + Caro
Chl B
Chl A + Pheo B
Chl A + Phyco
Chl A
Non-Specific / Combined Extracted Pigments Spectral Peaks (a.u.)
Specific Extracted Pigments Spectral Peaks (a.u.)
Extraction Combinations
Ctrl
55% ht 10m
55% ht 25m
55% ht 40m
70% ht 10m
70% ht 25m
70% ht 40m
80% ht 10m
80% ht 25m
80% ht 40m
55% so 10m
55% so 25m
55% so 40m
70% so 10m
70% so 25m
70% so 40m
80% so 10m
80% so 25m
80% so 40m

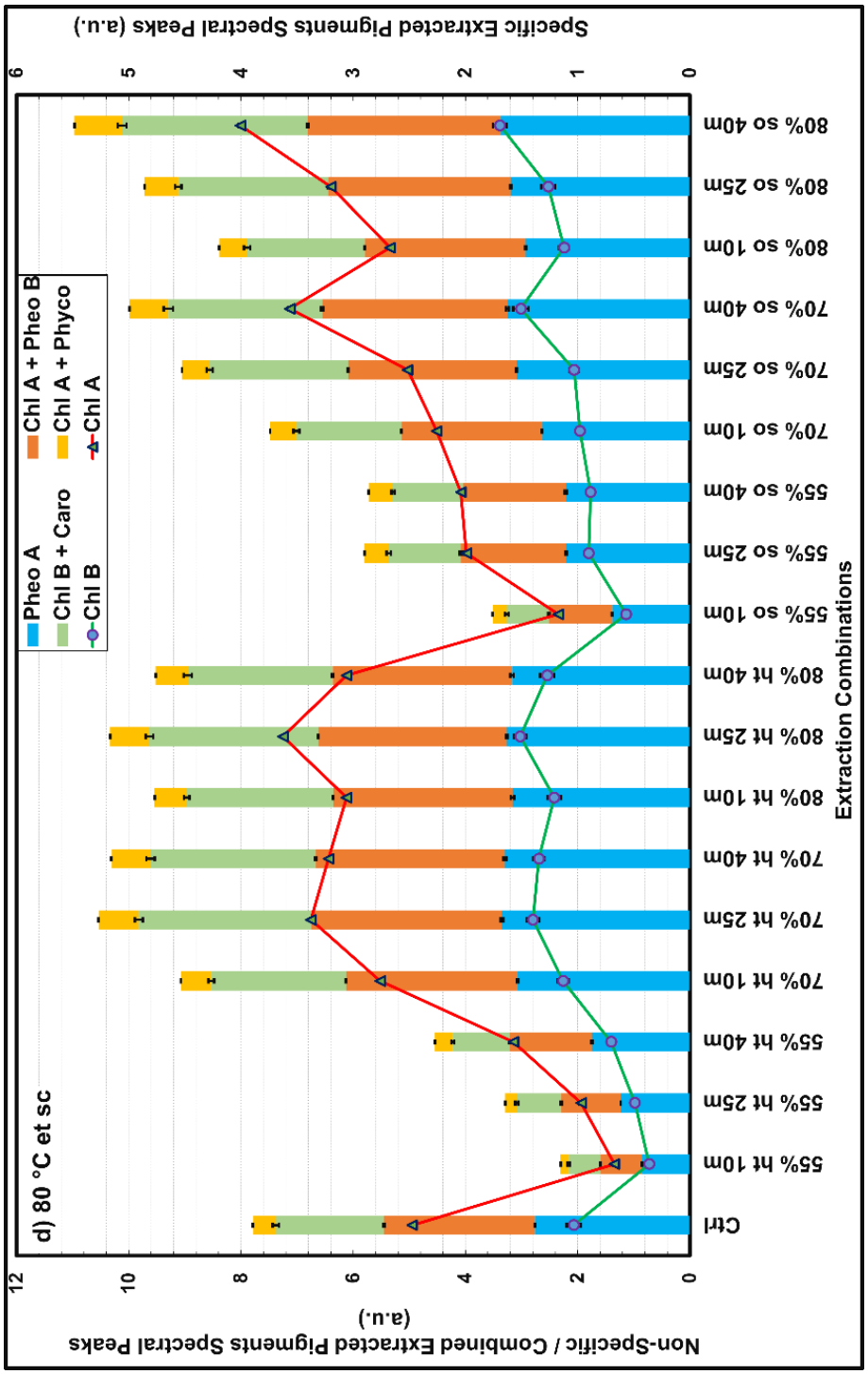

Figure 3.5. Comparative analysis of Non-Specific or Combined extracted pigments spectral peaks and Specific or defined extracted pigments spectral peaks w.r.t. different time-varying extraction techniques combinations at 80 °C.

The same extraction technique combinations were performed at 80 °C with both the species dye extracted in all three concentrations of both

solvents with different duration of sonication and heating and the results were plotted as shown in **Figure 3.5.** In **Figure 3.5.a** heating at 80 °C gets significantly central to extraction as above 70 % concentration all *as* dye get extracted more efficiently than control. At 70% concentration after 25 min heating is not profitable whereas at 80% concentration heating till 40 min does not create any significant reduction. Also, it is in agreement that heating at higher temperatures is vital to extract more pigment amount. The highest extraction was achieved with 25 min of heating at 80% concentration [Das et al., 2022; Sivakumar et al., 2009; Sakai et al., 2020]. Extraction with sonication flops to extract enough dye below 80% concentration clearing that solvent concentration is necessarily compulsory for sonication to be effective. Till 25 min of sonication, an exponential rate of extraction can be seen but it slows down with consistency after 25 min. Overall the extraction with both sonication and heating the extraction rates is more than 1.5-fold higher than the control.

As per **Figure 3.5.b** it can be seen that the control itself is at a higher extracted amount of *sc* dye in comparison to that of *as* dye in methanol. A concentration above 70% is only able to achieve efficiency above the control via heating alone if the duration is more than 25 minutes but shows no better efficiency than that even at more time of heating nor does it show degradation only and remains constant. A similar trend is seen at 80% concentration also. In the case of sonication, a steep rise is visible in the 80% concentration case till 40 min. 70% concentration with 40 min of sonication however shows promising extraction too [Sakai et al., 2020].

Figure 3.5.c shows that just 5 minutes of heating with ethanol for *as* dye is sufficient to get a high amount of extraction in comparison to methanol. More duration of heating has a slight effect on the enhancement of extraction but also starts to degrade as soon as it crosses the optimum mark which is 25 min for 70% concentration and 10 min for 80 % concentration. Sonication does not show any significant effect on the extraction process and shows only a minute

increase with an increased duration of sonication and is effective only at 80% concentration.

Figure 3.5.d. which depicts *sc* dye extraction in ethanol shows that ethanol is not as effective as extracting solvent for this species. The impact of heating duration plays a significant role at 70% and 80% concentrations. At 70% concentration, the dye starts degrading after 25 min, and at 80 % concentration, it might have started degrading even before 25 min as evident from the figure. Sonication is consistently enhancing extraction with an exponential rise in value at 70% and 80% concentration [Linares et al., 2022; Zhong et al., 2019; Sakai et al., 2020]. The best extraction performance observed overall is with 40 min of sonication at 80 % concentration in comparison to the control.

It is realized that the specific *Chl a* value is following the increase of non-specific chl a value and the same goes for *Chl b* values for all the subfigures.

3.3.5. Stability

The obtained dyes were evaluated for their stability at room temperature and the duration of their stability was recorded as shown in Table 1. The stability is considered till the time they stop showing any values of their pigments in terms of absorption. The light conditions are kept at an overcast light intensity of 1000 lux set artificially and it glows consistently. Stability readings were taken every 4 hours.

Table 3.1. Overview of stability at room temperature of various obtained dyes with different extraction techniques and duration of extraction in particular only the effective solvent concentrations considering only the enhanced extraction percentage from **Figure 3.4** and **Figure 3.5.**

Species dye and	**Concentration**	**Extraction technique**	**Increase %**	**Stability duration**

temperature	of solvent	duration	from control	(hrs)
Asterarcys quadricellulare at 60 °C	80% mt	Ht - 25 min	61	48
	80% mt	Ht - 40 min	16	36
	80% mt	So - 10 min	48	56
	80% mt	So - 25 min	85	56
	80% mt	So - 40 min	89	56
	80% et	Ht - 10 min	15	60
	80% et	Ht - 25 min	61	56
	80% et	Ht - 40 min	55	48
	70% et	So - 10 min	50	64
	70% et	So - 25 min	58	64
	70% et	So - 40 min	84	68
	80% et	So - 10 min	60	72
	80% et	So - 25 min	89	76
	80% et	So - 40 min	105	80
Scenedesmus sp. at 60 °C	70% mt	Ht - 25 min	28	52
	80% mt	Ht - 10 min	11	60
	80% mt	Ht - 25 min	37	56
	80% mt	Ht - 40 min	31	56
	80% mt	So - 10 min	17	60
	80% mt	So - 25 min	46	64
	80% mt	So - 40 min	50	64
	80% et	Ht - 10 min	31	68
	80% et	Ht - 25 min	44	64
	80% et	Ht - 40 min	38	64
	80% et	So - 10 min	17	76
	80% et	So - 25 min	62	80
	80% et	So - 40 min	106	80
Asterarcys quadricellulare at 80 °C	70% mt	Ht - 10 min	12	56
	70% mt	Ht - 25 min	35	56
	70% mt	Ht - 40 min	19	48
	80% mt	Ht - 10 min	55	60

	80% mt	Ht - 25 min	81	64
	80% mt	Ht - 40 min	75	64
	80% mt	So - 10 min	9	64
	80% mt	So - 25 min	67	68
	80% mt	So - 40 min	77	68
	80% et	Ht - 10 min	14	60
	80% et	Ht - 25 min	12	52
	80% et	Ht - 40 min	4	52
	80% et	So - 10 min	12	68
	80% et	So - 25 min	13	68
	80% et	So - 40 min	17	64
Scenedesmus	70% mt	Ht - 25 min	21	64
sp. at 80 °C	70% mt	Ht - 40 min	23	60
	80% mt	Ht - 10 min	20	64
	80% mt	Ht - 25 min	33	60
	80% mt	Ht - 40 min	38	60
	70% mt	So - 40 min	14	60
	80% mt	So - 10 min	19	64
	80% mt	So - 25 min	31	64
	80% mt	So - 40 min	40	64
	70% et	Ht - 10 min	15	68
	70% et	Ht - 25 min	36	64
	70% et	Ht - 40 min	32	64
	80% et	Ht - 10 min	23	68
	80% et	Ht - 25 min	36	64
	80% et	Ht - 40 min	23	64
	70% et	So - 25 min	13	72
	70% et	So - 40 min	32	72
	80% et	So - 10 min	8	72
	80% et	So - 25 min	26	76
	80% et	So - 40 min	46	76

It can be implied from Table 1 that the stability values fall between 36 hours to 80 hours. All the best-extracted dyes were consistently stable for the higher duration due to more presence of pigment amount in them. The dyes extracted via heating were consistently unstable due to degradation or due to less extraction of pigments, hence less amount also resulting in easy rapid degradation. It can be concluded that a longer duration of sonication will help extract higher amounts of pigments with promising stability too [Kumar et al., 2017]. But if the cost factors are taken into consideration and the natural sunlight is used for heating then not so long duration of heating with a high concentration of solvent volume can be a good inexpensive alternative.

3.4. Conclusions

The study helped to understand how these dyes interact with light and how their spectral characteristics vary across the electromagnetic spectrum. In the visible region reflectance spectra *sc* dye in ethanol performed better overall also it has the least requirement of energy for the excitation of photoelectrons and hence current generation. For the emission spectrum case, *sc* dye in ethanol, as well as *as* dye in ethanol, showed a high potential of transmitting photoelectric current within far visible wavelength region.

The performance of Dye-Sensitized Solar Cells (DSSCs) is intricately influenced by both the extraction procedure and solvent used in fabrication. These factors significantly impact the structural and morphological characteristics of the photoactive layers in the DSSC. The extraction procedure determines photosensitizer quality, affecting light absorption and charge transfer processes. Variations in extraction methodology lead to distinct molecular arrangements, influencing electronic structure and photovoltaic performance. Additionally, solvent choice affects photosensitizer solubility and reactivity, influencing adsorption onto the semiconductor surface. Solvent properties, like polarity and viscosity, alter dye loading kinetics and interfacial charge transfer dynamics, impacting overall DSSC

efficiency. The interplay between extraction procedure and solvent selection requires systematic investigation for optimal DSSC performance, emphasizing the need for a thorough understanding of their effects on reported performance for technology development and optimization.

The extraction temperature of 60 °C seems promising enough to extract dyes as an increase in temperature extracts more but comparatively extracts more but has a high probability of rapid degradation. Sonication for a longer duration of 40 min at a high concentration of 80% ethanol was able to extract 105% more dye for *as* and 106% more for *sc* with stability of almost 80 hours. The current research efforts in the chapter have successfully aimed and identified dyes that can be extracted at lower temperatures or that exhibit enhanced stability and performance under higher temperatures to develop into potential dyes for DSSCs. In the future, advancements in materials science, nanotechnology, and fabrication techniques could lead to more efficient and temperature-tolerant DSSCs using natural dyes, potentially opening up new economic opportunities. The next chapter deals with developing the DSSCs using novel algal and cyanobacterial dyes. Based on the findings of this chapter, pigment-forming dyes can replace hazardous chemical dyes and resolve problems in combination with CO_2 in the air and wastewater while growing. The microalgae, Asterarcys quadricellulare and Scenedesmus sp., were utilized in the extraction of the dyes. Followed by the coating with these dyes, the efficiency of DSSCs was investigated, with voltage, current, and fill factor being some of the performance parameters that were thoroughly evaluated.

CHAPTER 4

Utilization of Dyes in Natural Dye-Sensitized Solar cells (DSSCs)

CHAPTER 4

Utilization of Dyes in Natural Dye-Sensitized Solar cells (DSSCs)

4.1. Introduction

Solar energy holds immense potential to connect with a significant part of global energy needs using photovoltaic technology. Solar cells, like DSSCs, transform light into electricity by exciting electrons in a light-absorbing material, leading to their transition from the valence band to the conduction band. These energized electrons are then injected into the photoanode and transferred to an external circuit for practical use [Francis *et al*., 2021]. DSSCs, along with Perovskite solar cells, Inorganic solar cells, Polymer solar cells, Quantum dot solar cells, and hot carrier cells, are the key technologies of this PV generation. To convert solar energy, DSSC generally uses crystalline TiO_2 nanoparticle-type photoanodes that are dye-sensitized [O'Regan *et al*., 1991]. One noteworthy benefit of DSSC is that it may function effectively in low-irradiance scenarios, making it appropriate for a variety of locations. Additionally, both artificial and natural dyes can be used to sensitize DSSC, giving designers more material options. These characteristics have fuelled a great deal of excitement in DSSC and its prospects for use in solar energy harvesting [Teja, *et al*., 2023].

Natural pigments or dyes have several advantages over synthetic ones, including being more affordable, ease of extraction, biocompatible, high relative abundance, sustainable procurement, and non-toxic making them economically viable for large-scale production. Higher plants (such as their flowers, seeds, stems, leaves, petals, fruits, etc.) and microbes are two sources of these natural pigments for photo-harvesting [Ghosh *et al*., 2022]. These pigments can be processed and used well in DSSC applications because the extraction techniques are rather straightforward. Synthetic pigments have evolved as the favored option for light harvesting in DSSC due to their inherent availability and ability to capture light efficiently [Nandan Arka *et al*., 2021]. The

practical use of natural porphyrins and *Chls* for harvesting solar light was established by Kay and Grätzel in 1993 [Kay *et al*., 1993]. Subsequently, Tennakone and colleagues confirmed the efficacy of using cyanidin derived from anthurium flowers as an effective sensitizer [Tennakone *et al*., 1995].

Historically, pigments derived from higher plants have been the primary natural sensitizers for DSSC, but the consensus is that taller plants demand agricultural land, develop more slowly, and are more vulnerable to climate stressors. Other than this the natural sensitizers possess lower efficiency than silicon-based cells and degrade faster impacting long-term DSSC performance, composition differences due to growth conditions may affect consistency, narrower absorption range, and extraction complexities. The use of pigments derived from fungus, microbes, and algae, however, offers a more effective method. These microorganisms have large biomass outputs and quick doubling times, making the pigment extraction procedure more efficient [Di Bari *et al*., 2017]. Algae, fungi, and microbes can be grown in closely regulated surroundings, which means they cannot contend with taller plants for scarce cultivable land or have their growth considerably impacted by weather patterns [Orona-Navar *et al*., 2021].

Chl, carotenoids, and secondary metabolites are produced by microalgae and cyanobacteria since they are photosynthetic organisms. Certain bacteria, including purple and green bacteria, use bacteriochlorophyll, a type of chlorophyll, for anoxygenic photosynthesis [Nurachman *et al*., 2015]. Incongruously, Archaea uses retinal proteins to become accustomed to diffused light, extremely high temperatures, and high salt environments [Armendáriz-Mireles *et al*., 2023]. Through straightforward deposition processes with yield rates as high as 4.6%, the potential of pigments produced from micro-algae, cyanobacteria, etc., in DSSCs has been shown. Therefore, this article aims to analyze the new class of microalgae and cyanobacteria-based natural light harvesters extracted in two distinct solvents (ethanol and methanol). To give a thorough overview of possible applications in

solar energy harvesting, studies concentrating on the extraction and application of microalgae and cyanobacterial dyes were analyzed [Pagels *et al*., 2021]. The efficiency and stability of DSSCs using microalgal and cyanobacterial dyes in methanol and ethanol as sensitizers can depend on several factors like Spectral Absorption, Dye Adsorption, Electron Injection, Transport, Charge Recombination and Solvent Compatibility influencing dye extraction, adsorption, and overall device performance [Chauhan *et al*., 2022].

Microalgal and cyanobacterial pigments can cover a broader spectrum of light absorption compared to some synthetic dyes, potentially leading to enhanced light harvesting [Chauhan *et al*., 2023]. Efficient extraction and purification of the desired pigments from microalgae and cyanobacteria can be challenging and may impact overall cost-effectiveness. Ensuring the stability of natural dyes in DSSCs over time, especially in the presence of solvents like methanol and ethanol, is crucial for long-term device performance. Herein this work, we are going to examine the role of microalgae (*Asterarcys quadricellulare*: *as* and *Scenedesmus sp.*: *sc* based natural photo harvesters on the performance of DSSC.

4.2. Experimental Section

4.2.1. Chemicals Used

All the used materials were purchased from Sigma-Aldrich and used as it is without any further purification. The used materials are titanium diisopropoxide bis(acetylacetonate), titanium butoxide, 1-butanol, fluorine-doped tin oxide (FTO), hydrochloric acid (HCl, 37 wt%), ethanol (Absolute: 99.9%), methanol (Extra-pure AR 99.8%), carbon cloth, potassium iodide (KI), ethylene glycol, and iodine (I_2). The solvents were diluted by adding DI water following the experimental requirements, and a baseline was established for these solvents based on the specific measurements involved.

4.2.2. Synthesis of 1-D TiO_2 photoanodes

Herein, 1-D TiO_2 photoanodes were synthesized by using titanium diisopropoxide bis(acetylacetonate) which was accurately weighed and dissolved in 5 ml of 1-butanol to prepare two different molarity (0.1 and 0.2M) solutions for compact layer coating on cleaned FTO substrates. Before coating, these compact layer solutions were mixed in an ultra-sonicator for 30 minutes to ensure complete dissolution and homogeneity. First, we spin-coated the 0.1 M solution for 30 seconds at 3000 rpm, and seeded samples were heated at 120 °C for 30 minutes for proper adhesion of the compact layer. This process was repeated for the 0.2 M solution, with two additional spin-coating and heating cycles. The resulting films were subjected to a final annealing process at 450°C for 20 minutes to form a *c*-TiO_2 layer, which served as the seed layer for growing TiO_2 nanorods (NRs) using a hydrothermal method. For synthesizing 1-D TiO_2 nanorods, 60 ml of DI-water and HCl in a 1:1 volume ratio was mixed for 5 minutes. Then, 0.75 ml of titanium butoxide was added to the above-mentioned DI-water and HCl solution and stirred uniformly for 45 minutes to prepare a homogeneous solution. Further, this alike was poured into a 90 ml Teflon liner, up to two-thirds of its volume. The seeded samples were directly immersed in the teflon liner, sealed in a stainless-steel vessel, and placed in a muffle furnace at 150°C for 8 hours. After completion of the reaction, the samples were taken out of the autoclave and washed with DI water several times. After air-drying, the TiO_2 photoanodes were subjected to annealing at 450°C for 20 minutes to enhance crystallinity and eliminate excessive solvents from the TiO_2 nanorods' surface.

4.2.3. Dye Preparation

Two distinct indigenous, axenic freshwater microalgae species for our study: *Asterarcys quadricellulare* and *Scenedesmus sp*. The microalgal strains were cultivated in a standard BG-1 medium with a pH range of 7.2-7.4. To maintain this pH, we used dispersed HCl or base NaOH as per the requirement. The experiments were initiated by sub-culturing from the seed cultures of all four species, which had been grown in

Erlenmeyer flasks for a period of 10 days. For the microalgal species, we inoculated experimental culture flasks having a primary cell density of 0.1 at 680 nm and allowed them to grow for 30 days. Throughout the experiment, all cultures were perpetuated in a superintended culture room at a temperature of 27 ± 5 °C, with a 12-hour light photoperiod followed by a 12-hour dark period. To ensure proper growth, we maintained a light intensity of 3000 lux during the light period using white fluorescent lamps, positioning them at an appropriate distance from the culture flasks, each containing 250 ml [Stanier *et al.*, 1971].

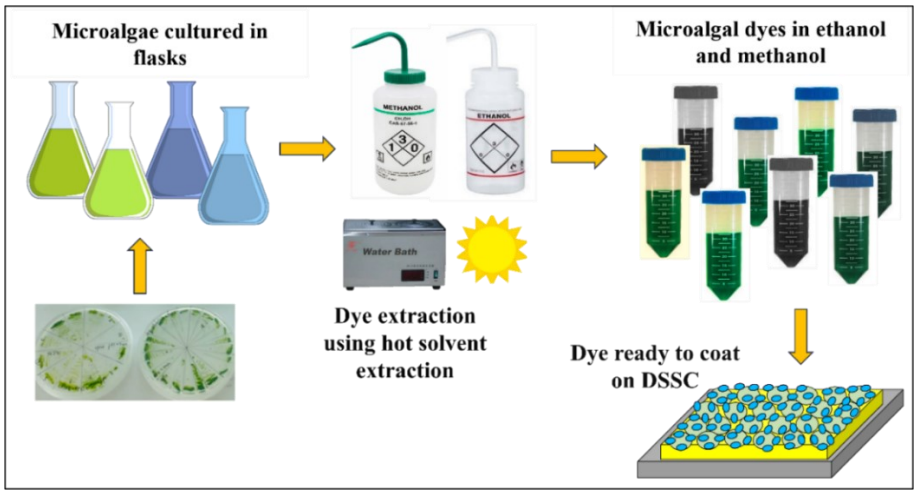

Figure 4.1. Typical schematic representation of microalgal-dye extraction process.

The microalgal species were collected on the 20th day, and we extracted their dyes using the hot solvent extraction method, employing both methanol and ethanol. Subsequently, we concentrated the extracted dyes according to their respective capacities. Finally, we quantified the contents in the dyes using spectrophotometric analysis. A systematic portrayal of typical dye preparation is depicted in **Figure 4.1**.

4.2.4. Fabrication of DSSC and Working Mechanism

The obtained 1-D TiO_2 photoanodes were sensitized by engulfing them in a dye solution containing natural dye (3.6 mg/ml) and direct dye (0.36 mg/ml) for 12 hours. After dye soaking, the films were washed

with DI ethanol/methanol and vacuum dried. **Figure 4.1.** displays the photographs of microalgal dyes in the ethanol and methanol solution and the natural dye-adsorbed photoanode, respectively. Carbon-based counter electrodes of size 1.5×1.5 cm^2 were prepared by cutting a carbon cloth. Initially, to fabricate the DSSC (active area: 1 × 1 cm^2), the dye-soaked photoanodes and the carbon-counter electrodes were sealed using binder clips. Further, I^-/I_3^- electrolyte was poured inside the coupled dye-loaded TiO_2 and carbon electrode. This electrolyte solution was prepared by mixing 0.05 M potassium iodide and 0.05 M iodine crystals in 5 ml ethylene glycol. A schematic of the DSSC fabrication is shown in **Figure 4.2**.

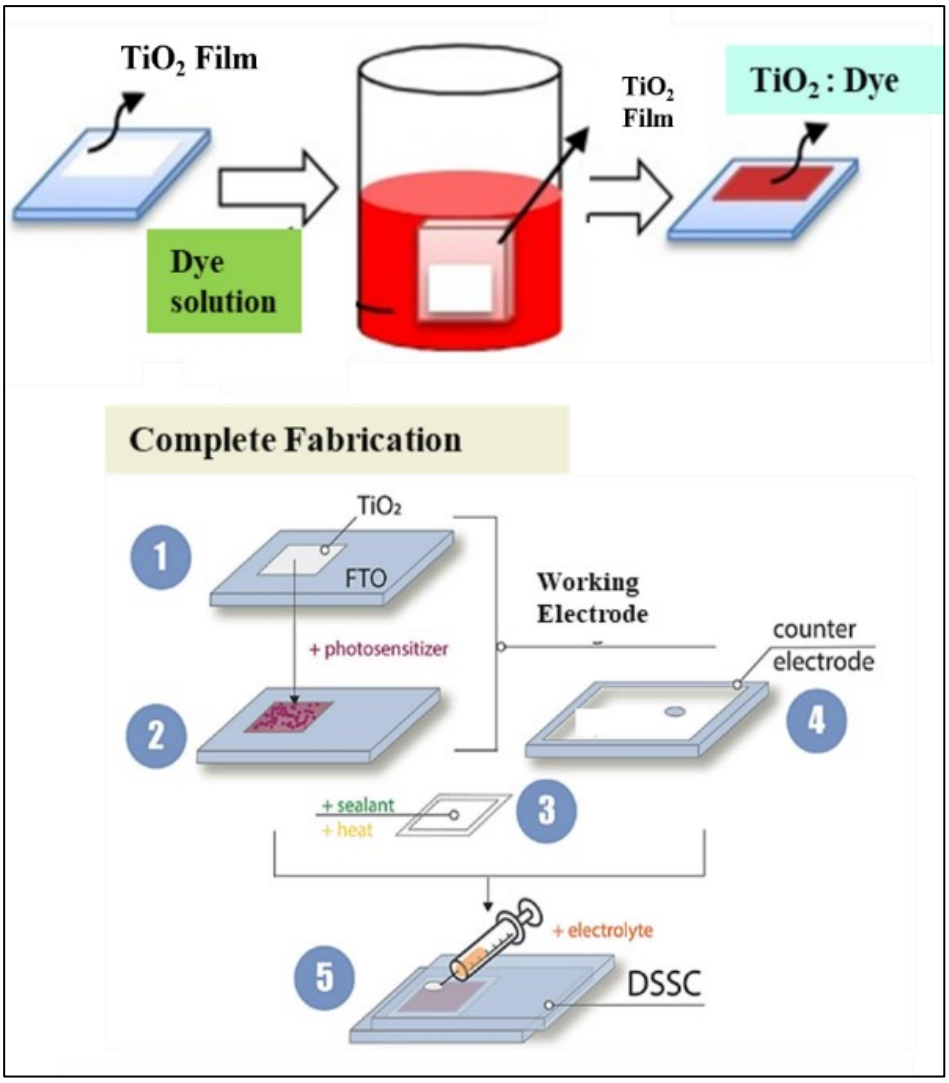

Figure 4.2. Step-wise schematic of the DSSC fabrication by utilizing microalgal dye and 0.05 M (I^-/I_3^-) electrolyte.

DSSCs differ from conventional semiconductor-based photovoltaic devices in their approach to light harvesting and transportation of charges. Herein, DSSC consists of 1-D TiO_2 nanorod photoanodes, which adsorb the dye molecules, while the counter electrode is typically made up of carbon cloth. Both the dye-soaked photoanode and counter electrode are immersed in an electrolyte encompassing an appropriate redox couple, such as (I^-/I_3^-). When the dye-electrolyte interface is exposed to solar irradiance having enough energy to excite the dye, electron-hole pairs are generated. The photogenerated electrons and holes were migrated towards the TiO_2 photoanode and semiconductor-electrolyte interface, respectively. As these photoanodes were synthesized on a transparent conducting substrate (FTO), these electrons were transported via an external load to the carbon electrode side, where they electrochemically interact with the electrolyte and perform redox reactions for dye regeneration. The uninterrupted flow of photocurrent is governed by the dye regeneration via reversible electrolytic redox couple, as shown in **Figure 4.3**.

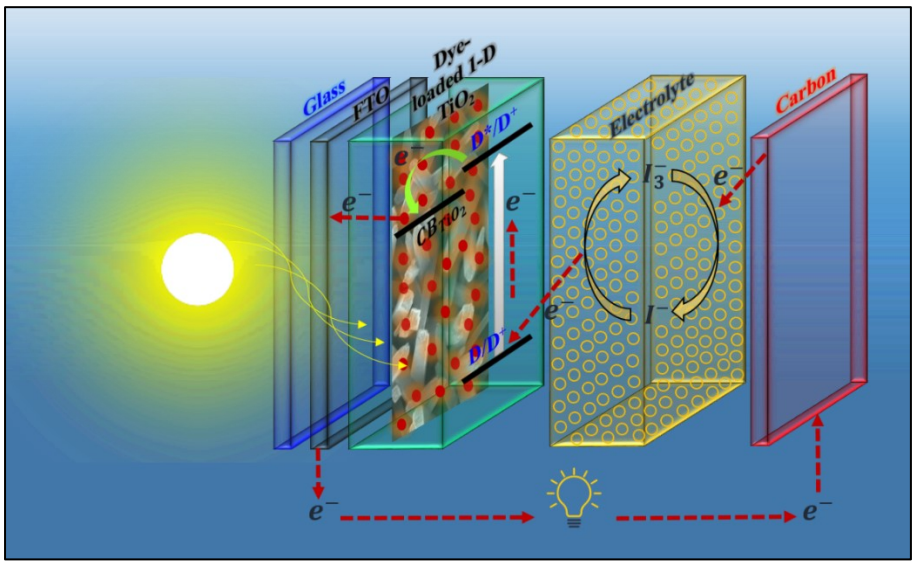

Figure 4.3. Typical schematics of DSSC include FTO, dye-loaded 1-D TiO_2 photo-anode matrix, electrolyte, and carbon counter electrode, depicting the working mechanism of the fabricated DSSC.

Several critical parameters are used to evaluate the effectiveness of a DSSC, namely open circuit voltage (V_{OC}), fill factor (FF), short circuit

current density (J_{SC}), and power conversion efficiency (η) **(Figure 4.4)**. These parameters are very decisive in the evaluation of the effectiveness of a DSSC operation and are as follows:

Open-Circuit Voltage: The V_{OC} of a solar cell refers to the maximum voltage achievable when any outer circuitry and load. This occurs when the solar cell junction is in a state of forward bias due to the photo-current. In other words, the V_{OC} reflects the degree of forward bias on the solar cell junction caused by the incident photo-current.

Short-Circuit Current Density: The J_{SC} of a solar cell corresponds to the photo-current flowing through the device when DSSC is short-circuited without connecting any load. Also at this point, the V_{OC} will reduce to zero. In this condition, the solar cell operates under a short-circuit condition, resulting in maximum current flow.

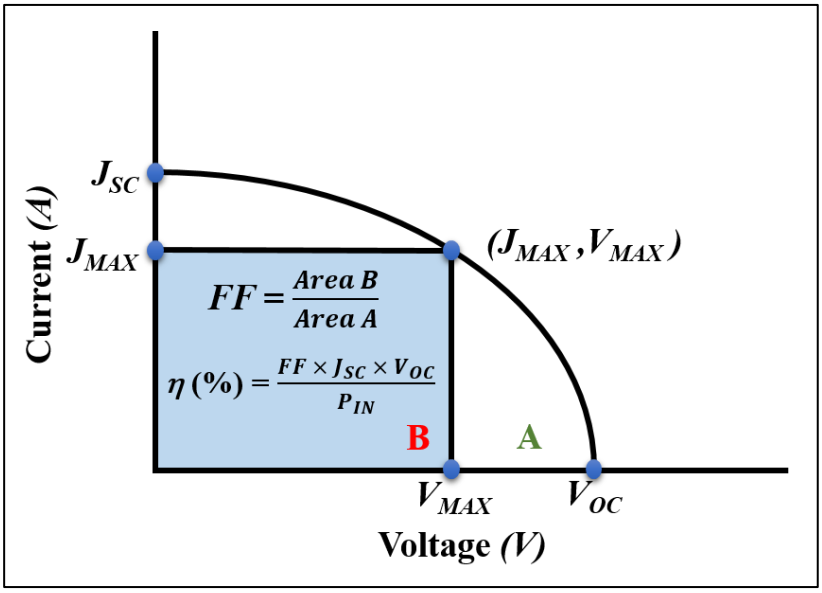

Figure 4.4. Schematic representation of different performance parameters for a general solar cell such as J_{SC}, J_{MAX}, V_{OC}, V_{MAX}, FF, and PCE (η).

Fill Factor: The FF of a DSSC is known as the ratio of the maximum output power (P_{max}) to the product of the I_{SC} and the V_{OC}. Mathematically, it can be represented as:

$$FF = \frac{P_{max}}{(I_{SC} \times V_{OC})} = \frac{I_m \times V_m}{I_{SC} \times V_{OC}} \qquad (12)$$

Power Conversion Efficiency (η): The η of a DSSC is the ratio of the P_{max} to the P_{in} subjected to the solar cell. Formula-wise, it can be expressed as:

$$\eta = \frac{P_{max}}{P_{in}} = \frac{I_{SC} \times V_{OC} \times FF}{P_{in}} \quad (13)$$

4.2.5. Characterization Tools

The crystalline properties of pristine 1-D TiO_2 photoanodes were investigated using XRD studies escorted using Cu-K_α radiation of wavelength, λ = 1.540 Å in the 2θ range of 10°–70° with a step size of 0.05 at room temperature. The morphological analysis of the compact-TiO_2 and 1-D TiO_2 photoanode film, chemical composition, and the grain size of TiO_2 nanorods were examined using a field emission scanning electron microscope (FESEM; JEOL: JSM-7610F PLUS). Absorption spectroscopy was performed with a UV/Vis/NIR absorption spectrophotometer (Shimadzu 2600). Further photovoltaic studies of DSSCs under irradiance were studied using a solar simulator (PET-#SS50AAA) calibrated to AM 1.5 G (1000 W/m^2) at room temperature.

4.3. Result and Discussions

4.3.1. XRD Analysis

The XRD pattern in **Figure 4.5.** displays several diffraction peaks at 2θ values of 26.27°, 27.21°, 35.87°, 37.48°, 41.04°, 54.19°, and 62.66°. These peaks correspond to the rutile phase of TiO_2, based on their crystallographic characteristics. The (hkl) planes associated with the diffraction peaks can be identified as (110), (121), (101), (200), (111), (211), and (002). The XRD pattern exhibited crystallinity, displaying well-defined characteristics that corresponded precisely to rutile TiO_2. Moreover, the 2θ values closely matched those found in the 21-1276 JCPDS data, further confirming the formation of rutile phase tetragonal 1D-TiO_2 nanorods. All FTO peaks are denoted by an asterisk (*). The XRD pattern confirms the tetragonal crystal structure with lattice constants a = b = 4.795 ± 0.003 Å, and c = 2.765 ± 0.005

Å, which are consistent with the earlier literature. All the calculations were performed by using **equations (3) and (4)**, given below.

$$d = \frac{n\lambda}{2\sin\theta} = \frac{1.5406\ \text{Å}}{2\sin\theta} \tag{14}$$

$$\frac{1}{d^2} = \frac{(h^2+k^2)}{a^2} + \frac{l^2}{c^2} \tag{15}$$

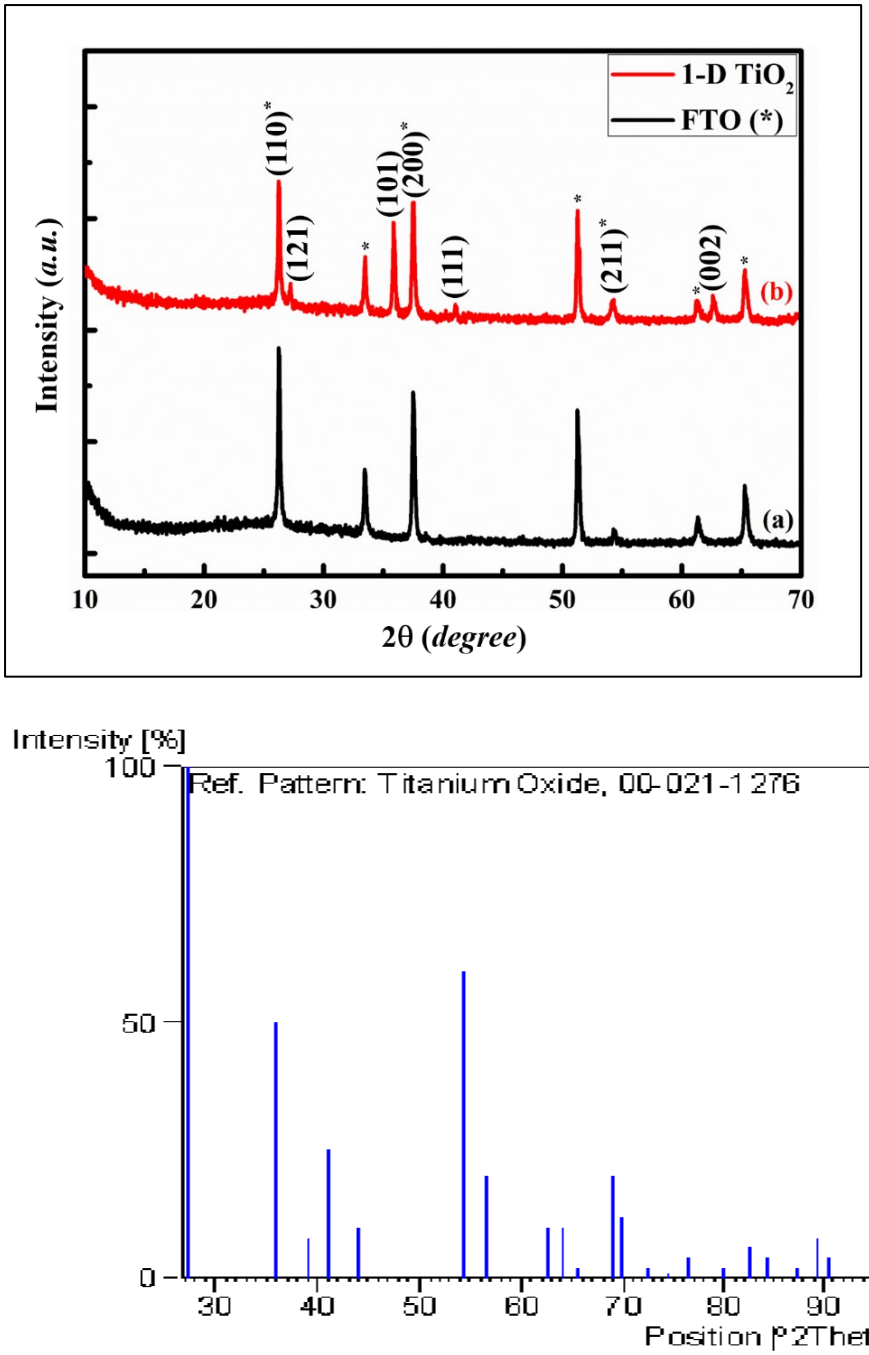

Figure 4.5. XRD pattern of (a) FTO substrate, and (b) 1-D TiO_2 nanorods, hydrothermally synthesized on the FTO substrate. (c) 21-1276 JCPDS data. FTO peaks are denoted by an asterisk (*).

Furthermore, the absence of any extra peaks or humps in the given XRD pattern indicates that the synthesized 1-D TiO_2 nanorods are pure phase. Apart from the FTO peaks, the (101) rutile phase diffraction peak is noticeably powerful and substantially higher than the other peaks. The other notable rutile diffraction peaks,

particularly the (110), and (200) planes, appear to be nearly suppressed, indicating the preferential formation of 1D rutile nanorods along the [001] direction.

4.3.2. Morphology

The 1-D TiO_2 arrays on FTO substrates were synthesized using the Hydrothermal method. A simple aqueous chemical growth approach was used to create vertically and randomly aligned TiO_2 nanorods on FTO, with a spin-coated compact TiO_2 layer serving as seed structures. **Figure 4.6.** depicts the top FESEM view of the synthesized TiO_2 nanorods matrix. A low-magnification view of the TiO_2 nanorods covering the whole FTO substrate is shown in **Figure 4.6.(*a*)**. A high magnification SEM view of the arrays is shown in **Figure 4.6.(*b*)**, which shows square-shaped top facets, which is consistent with the anticipated growth behaviour of tetragonal crystals [Wang *et al.*, 2011]. In the SEM image, the side facets of the 1-D TiO_2 nanorods seem very smooth. A cross-sectional FESEM image of the TiO_2 film grown is shown in **Figure 4.6.(*c*)**. A magnified cross-sectional view shows that the TiO_2 nanorods have a roughly vertical orientation possessing a length of around 1.8 ± 0.2 μm. The nanorods have an average facet size of 90 ± 5 nm at the bottom and 85 ± 5 nm at the top, with a practically comparable diameter from bottom to top.

On the top facets of the 1-D TiO_2 nanorods, there was a cascaded nano-dot-like structure. These nano-dot-like patterns increase surface area substantially, improving charge transfer ability. Previous papers have described the benefits of various semiconducting working electrodes, which include (i) a high aspect ratio (surface area), (ii) minimum grain boundaries and defect sites, which affect electron entrapment and scattering, and (iii) efficient charge carrier transportation. To improve dye loading, densely packed, large, and thin NR-like dye scaffolds with adequate charge carrier collection are required. These qualities are critical for maximizing the device's efficiency [Meng *et al.*, 2014].

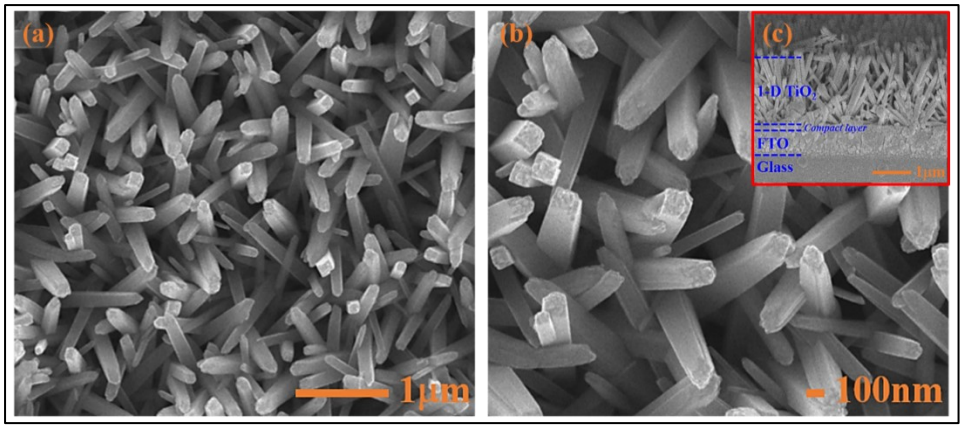

Figure 4.6. Morphology of hydrothermally grown TiO_2 nanorods, (a-b) FESEM-Top view of TiO_2 photoanodes at 15kX and 30kX magnifications, respectively, and (c) Cross-sectional-FESEM image showing the vertical aligned TiO_2 nanorods.

4.3.3. UV-Visible Analysis

UV-visible absorption spectroscopy of TiO_2 nanorods is crucial for their application in DSSCs. TiO_2 nanorods, with their high surface area and unique one-dimensional structure, are excellent photoanode materials. UV-visible spectroscopy is employed to investigate their optical properties, particularly their ability to absorb UV light and facilitate electron transport. The absorption spectrum provides insights into the band gap energy and the efficiency of light harvesting. Strong UV absorption by TiO_2 nanorods enhances the photocurrent generation in DSSCs by promoting efficient electron injection from the dye molecules into the conduction band of the TiO_2. This results in improved overall photovoltaic performance. Furthermore, UV analysis helps in understanding the impact of nanorod morphology and crystallinity on the photoelectrical properties, thereby guiding the optimization of TiO_2 nanorods for superior DSSC efficiency. The absorbance spectra of the TiO_2 nanorod sample, which is hydrothermally grown over the compact layer-coated FTO substrate, are shown in **Figure 4.7.(*a*)**. A pronounced absorption edge is observed at approximately 420 nm, indicative of the energy bandgap associated with rutile phase TiO_2. Given that the dimensions of the

TiO_2 nanorods surpass the Bohr exciton radius, no discernible blue shift attributable to quantum confinement effects is present. Significant light scattering from the one-dimensional TiO_2 photoanodes results in reduced absorbance, measured between 10% and 20%, within the 450 to 650 nm wavelength range. The optical energy band of corresponding 1D TiO_2 photoanodes was calculated using **equation 5** and shown in **Figure 4.7.(*b*)**.

$$\alpha = \frac{k(h\nu - E_g)^{n/2}}{h\nu} \qquad (5)$$

where k is a constant. The energy band gap (E_g) of the hydrothermally synthesized 1-D TiO_2 nanorods was evaluated using a Tauc plot in this study. The Tauc plot includes $(\alpha h\nu)^2$ versus photo-energy (hv) graph, where α and h are the absorptions and Planck's coefficient, respectively. The E_g for a direct energy band gap (n = 1) was calculated by locating the intercept of the tangent on the Tauc plot. The calculated energy band gap for one-dimensional TiO_2 nanorods is 3.0 eV, which corresponds to the energy band gap of rutile phase TiO_2. However, this value deviates slightly from the ideal band gap of 3.2 *eV*.

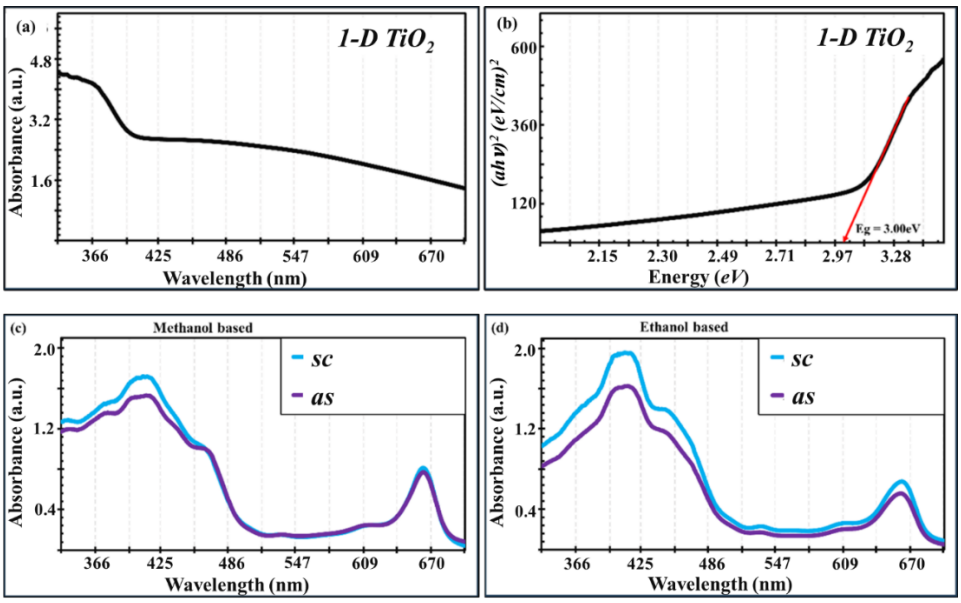

Figure 4.7. UV-visible absorption studies of (a) 1-D TiO_2 photoanodes and (b) Corresponding Tauc's plot for estimation of the bandgap,

which is 3.00 eV (as observed). (c-d) Absorption spectra of microalgae-based dyes extracted in methanol and ethanol solvents, respectively.

The further specified pH range of all the species taken in both the solvents (pH was measured just after extraction) is mentioned in **Table 4.1**. There were a total of 3 replication or review cycles at the time of preparation of the photosensitizer (photosensitizing dye). Further UV-visible spectra of *as*, and *sc*-dyes extracted in two different alcoholic solvents (ethanol and methanol) were recorded from 335 to 700 nm to estimate the light harnessing capabilities of these natural photo harvesters as shown in **Figure 4.7.(c-d)**.

Table 4.1. Mean pH range for both the *as* and *sc* dye species extracted in ethanol and methanol.

Solvent Used	Dye name (species)	Mean pH
Ethanol	*as* (*Asterarcys quadricellulare*)	7.2 ± 0.3
	sc (*Scenedesmus sp*.)	7.3 ± 0.2
Methanol	*as* (*Asterarcys quadricellulare*)	7.1 ± 0.2
	sc (*Scenedesmus sp*.)	7.3 ± 0.3

All these four microalgal dyes show very good absorption around the wavelength of 640-680 nm and below 500 nm under visible light. The absorption range and maximum absorption peaks at particular wavelengths were separately mentioned in **Table 4.2**. It is very interesting to see that all the micro-algae dyes were showing better visible light absorption in ethanol as compared to methanol which also reflects in the fabricated DSSCs performance. In **Table 4.3**, we comprised the previous reports regarding dye absorption capability, range, and parameters that are affecting the performance of DSSC.

Table 4.2. Absorption range and maximum absorption point obtained microalgal dyes.

Solvent Used	Dye Name	Absorption Range (nm)	Max. Absorption point (nm)
Ethanol	*as*	≤ 500 and 640-680	410
	sc		412
Methanol	*as*	≤ 490 and 650-680	403
	sc		405

Table 4.3. Comparative analysis of different natural pigments explored as natural light harvesters and a variety of parameters that affect the DSSC's performance.

Natural Dye	Source	Absorption Wavelength (nm)	Conversion Efficiency (%)	Parameters Affecting Efficiency	Ref.
Anthocyanins	Berries, Flowers	260-280 nm and 490-550 nm	Low to Moderate	electron injection efficiency, Absorption spectrum	Saha *et al.*, 2021
Chl	Green Plants, Algae	*Chl-a*: 420-450 nm and 640-680 nm, *Chl-b*:450-470 nm, and 640-660 nm, *Chl-c*:	Low	energy mismatch, Exciton injection,	Sanchini *et al.*, 2020 Castill

		Varies among subtypes		electron transport	o-Robles *et al.*, 2021
Betalains	Beets (*Beta vulgaris*), Cacti	Betacyanins: 535-540 nm Betaxanthins: 480-485 nm	Low to Moderate	electron transport, Sensitizer adsorption	Aztatzi-Rugerio *et al.*, 2019 Adhikary, *et al.*, 2020 Isah *et al.*, 2015
Curcumin	Turmeric (*Curcuma longa*)	Absorption peak wavelength: 420-430 nm	Low	recombination rate, Electron injection,	Rapalli *et al.*, 2020 Purnama *et al.*, 2021
Anthraquinones	Various Plant Sources	Absorption peak wavelength: 400-420 nm	Low to Moderate	recombination, Absorption	MacHatova *et al.*, 2016 Tissier *et al.*, 2022 Li *et al.*,

					2007
Natural Carotenoids	Fruits, Vegetables	Soret Band: 400-450 nm Q Bands: 450-550 nm	Low to Moderate	Exciton injection	Melén dez-Martínez *et al.*, 2019 Maddah *et al.*, 2020
Microalgal dyes	Micro algae	Absorption peak wavelength: 421, 435, 467, 618, 652 & 665nm	Low to Moderate	Better Solubility, Large range visible light absorption, etc.	**This Work**

4.3.4. J-V analysis

Figure 4.8. depicts the J-V performance of the DSSCs fabricated via *as* and *sc* micro-algae that were extracted in ethanol and methanol solvents, respectively. The DSSC performance was analyzed using a PET Solar Simulator (Model No: #SS50AAA) calibrated to AM 1.5 G (1000 W/m^2) at room temperature, and a Kethley meter source was used for J-V data acquisition. As dyes were extracted in two different solvents (i.e., ethanol and methanol), herein we plotted J-V plots separately for these solvents shown in **Figure 4.8.(a-b)**, respectively. In all the DSSCs reported, the DSSC architecture Glass/FTO/*c*-TiO_2/1-D TiO_2/*sc* (ethanol)/electrolyte/carbon was shown maximum PCE of

0.25% with maximum V_{OC} = 651 mV and J_{SC} = 639 µA/cm^2, respectively. Further, **Table 4.4** shows all the photovoltaic parameters, such as V_{OC}, J_{SC}, FF, and η etc. For all the DSSC having 1-D TiO_2 photoanodes sensitized with *as* and *sc* natural dyes, respectively.

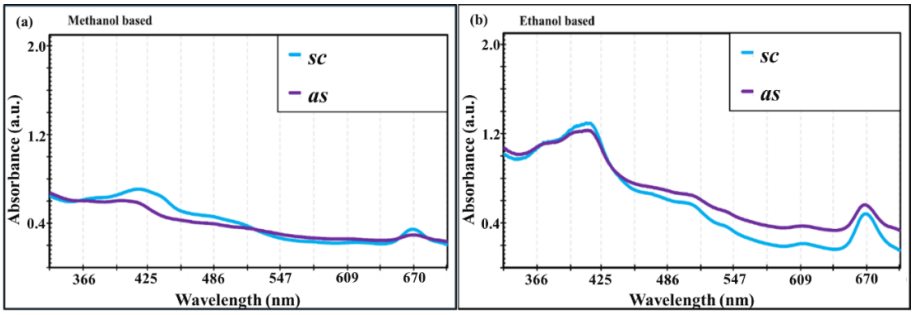

Figure 4.8. Absorption spectra of microalgae-based dyes extracted and coated on TiO_2 respectively.

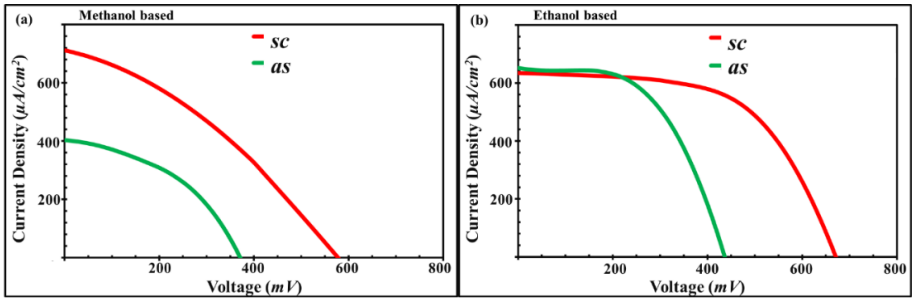

Figure 4.9. J-V analysis of the fabricated DSSC by utilizing micro-algae (*as* and *sc*) natural photo harvesters, which are extracted in (a) ethanol, and (b) methanol.

In contrast to previously reported efficiencies, the Asterarcys quadricellulare and Scenedesmus sp. microalgae natural dye-DSSCs employed in this study demonstrate a noteworthy improvement, achieving a maximum PCE of 0.25%. This enhanced efficiency observed in such DSSCs can likely be attributed to the following factors:

- The improvement in photoelectrode design, transitioning from nanoparticles to nanorods, serves to mitigate electron recombination by facilitating direct electron transfer.
- Substituting ethanol with methanol as the solvent for extracting microalgal dyes has the potential to substantially enhance both the anthocyanin and *Chl - a/ b/ c* content, better solubility, and the color stability of the resulting *as* and *sc* dyes.
- Better and optimum dye loading is one other aspect of this enhanced PCE.

Table 4.4. Comparative analysis of various PV parameters obtained by microalgae-dye-based natural-DSSC.

Dye	**Solar Intensity (W/m^2)**	V_{OC} **(mV)**	J_{SC} **(mA/cm^2)**	P_{MAX} **(mW)**	**FF**	**η (%)**
sc et	996.2	651.176	0.639	0.252	0.61	**0.25**
as et	996	427.255	0.653	0.177	0.63	**0.18**
sc mt	1053.4	566.080	0.695	0.225	0.57	**0.14**
as mt	1050.2	382.135	0.411	0.123	0.78	**0.08**

As can be seen, the absorption spectra somewhat correlate to the efficiency obtained, and it is checked that it can be due to the semiconducting surface compatibility issue. Also, the efficiency of this cell is affected by several factors, other than the type of dye used as the sensitizer. When comparing methanol-based and ethanol-based dyes, it can be seen that the solubility of algal natural dye molecules in methanol is excellent, which can help dissolve a wide range of dye molecules. This high solubility can facilitate the even distribution of the dye on the semiconductor surface, enhancing light absorption and electron injection efficiency. This can lead to issues with dye

aggregation or uneven distribution, negatively impacting the overall efficiency of the solar cell. Methanol typically has a lower viscosity than ethanol, allowing for better diffusion of dye molecules. Improved diffusion is crucial for the efficient penetration of the dye into the porous semiconductor material in DSSCs, leading to more effective light absorption and charge separation. The choice of solvent can also affect the composition of the electrolyte in DSSCs. Methanol is often preferred for use in iodide-based electrolytes, which are commonly employed in DSSCs due to their good conductivity and stability.

Table 4.5 presents the comparative photovoltaic performance metrics of DSSCs using various natural dyes as sensitizers, including *Chl* dyes, delonix regia flower, codiaeum variegatum leaf, beta vulgaris, and combinations of beta vulgaris with other dyes, as well as Scenedesmus sp and Asterarcys quadricellulare in ethanol and methanol. For *Chl* dyes, Ammar *et al.* (2019) reported a J_{SC} of 410 µA/cm², V_{OC} of 590 mV, FF of 0.58, and PCE of 0.172%, while Sengupta *et al.* (2015) achieved a J_{SC} of 678 µA/cm², V_{OC} of 397 mV, FF of 0.55, and PCE of 0.148%, suggesting the improved dye absorption on the TiO_2 surface and enhanced light scattering. Djibrilla *et al.* (2021) noted that DSSCs using delonix regia flower exhibited a J_{SC} of 81 µA/cm², V_{OC} of 420 mV, FF of 0.29, and PCE of 0.10%, manifesting better charge separation and transportation form anthocyanin pigments dominantly present in the delonix flower. Yusoff *et al.* (2014) found that Codiaeum variegatum leaf-based DSSCs achieved a J_{SC} of 403 µA/cm², V_{OC} of 435 mV, FF of 0.55, and efficiency of 1.08%. Sinha *et al.* (2018) reported that Beta vulgaris-based DSSCs showed a J_{SC} of 720 µA/cm², V_{OC} of 460 mV, FF of 0.51, and efficiency of 0.1788%. Combining Beta vulgaris with purple cabbage resulted in a J_{SC} of 1120 µA/cm², V_{OC} of 560 mV, FF of 0.60, and PCE of 0.3824%. A blend of 80% Beta vulgaris and 20% spinach, as reported by Bashar *et al.* (2019), achieved a remarkable J_{SC} of 4650 µA/cm², V_{OC} of 386.7 mV, FF of 0.55, and PCE of 0.99%. These mixed dyes were shown to improve dye soaking and the synergistic effect of both dyes. This work

also explored Scenedesmus sp and Asterarcys quadricellulare microalgal dyes extracted in ethanol and methanol solvents. Scenedesmus sp (ethanol) yielded a J_{SC} of 639 µA/cm², V_{OC} of 651.176 mV, FF of 0.61, and PCE of 0.25%, whereas Asterarcys quadricellulare (ethanol) achieved a J_{SC} of 653 µA/cm², V_{OC} of 427.255 mV, FF of 0.63, and PCE of 0.18%. In the case of methanol extraction, the results are not good enough, suggesting that methanol is not a good extraction solvent. The data highlights significant variability in DSSC performance based on the dye used, underscoring the importance of selecting an optimal sensitizer to enhance solar cell efficiency.

Table 4.5. Comparative study of previously reported photovoltaic performances of *Chl* and other dyes-based DSSC.

Dyes	J_{SC} **(µA/cm²)**	V_{OC} **(mV)**	***FF***	η **(%)**	**Ref.**
Chl dyes	410	590	0.58	0.172	(Ammar *et al.*, 2019)
	678	397	0.55	0.148	(Sengupta *et al.*, 2015)
Delonix Regia Flower	81	0.42	29	0.10	(Djibrilla *et al.*, 2021)
Codiaeum Variegatum Leaf	403	0.435	0.55	*1.08*	(Yusoff *et al.*, 2014)
Beta Vulgaris	720	460	0.51	0.1788	(Sinha *et al.*, 2018)
Purple Cabbage + Beta Vulgaris	1120	560	0.60	0.3824	
80% BV + 20% spinach	4650	386.7	0.55	0.99	(Bashar *et al.*, 2019)
Scenedesmus sp (ethanol)	639	651.176	0.61	0.25	**This Work**
Asterarcys	653	427.255	0.63	0.18	**This**

quadricellulare (ethanol)					**Work**
Scenedesmus sp (methanol)	695	566.080	0.57	0.14	**This Work**
Asterarcys quadricellulare (methanol)	411	382.135	0.78	0.08	**This Work**

4.4. Future Perspective

The prospects for algae-based photo harvesters are exciting and multifaceted. Their inherent ability to efficiently capture sunlight across a broad spectrum opens doors to unprecedented energy conversion efficiency. Scientists aim to optimize photon absorption in these devices, potentially elevating their performance to rival or surpass conventional silicon-based solar cells. Additionally, algae's intricate light-harvesting structures inspire biomimetic designs for future solar cell technology, paving the way for a new era of sustainable and high-performance bio-inspired systems and can enhance energy capture in diverse geographic regions, bolstering the global viability of solar energy. Furthermore, integrating algae-based light harvesters with other renewable technologies, such as wastewater treatment, presents symbiotic opportunities that address both energy and environmental challenges [Fabris *et al.*, 2020][Krishna *et al.*, 2021]. Algae's unique carbon sequestration capacity holds promise for transforming algae-based DSSCs into carbon-neutral systems, actively mitigating greenhouse gas concentrations. Beyond traditional solar panels, transparent and flexible algae-based DSSCs offer urban and architectural integration, enabling aesthetically pleasing structures that simultaneously generate electricity [Sarwer *et al.*, 2022][Abdelfattah *et al.*, 2023]. To realize their commercial potential and global energy accessibility, further research will focus on scalability, affordability, and streamlined production techniques. This decentralized energy production method could revolutionize energy access in off-the-grid

and isolated areas, promoting a more equitable distribution of the world's energy resources [Pessarrodona *et al.*, 2023][Biloria *et al.*, 2020][Vo *et al.*, 2018].

4.5. Conclusion

Herein this research, we replaced the hazardous synthetic dyes with Asterarcys quadricellulare and Scenedesmus sp. microalgae-based photo harvesters and analyzed their effect on the DSSC's performance. We successfully demonstrated a very economical and reproducible hydrothermal method to synthesize the 1-D TiO_2 photoanodes and studied the role of solvents that were used to extract the dyes. Different physicochemical characterizations were performed to understand the phase purity, morphology, and UV-visible absorption of the prepared photoanodes and dyes. Further J-V analysis was done to test the performance of the fabricated devices and reported very interesting results. Herein the DSSC configuration comprising Glass/FTO/c-TiO_2/1-D TiO_2/*sc* (*et*)/electrolyte/carbon consistently achieved the highest PCE of 0.25%. It also demonstrated an impressive V_{OC} of 651.176 mV and a high J_{SC} of 639 μA/cm^2 for the same species in ethanol devices. After the short efficient period of dye in DSSCs, more dye can be extracted from the microbial green cells, and this can be reloaded onto the cells again and again as this dye is abundant in nature.

CHAPTER 5

Optimization and Storage in coordination with different Pigmental Analysis

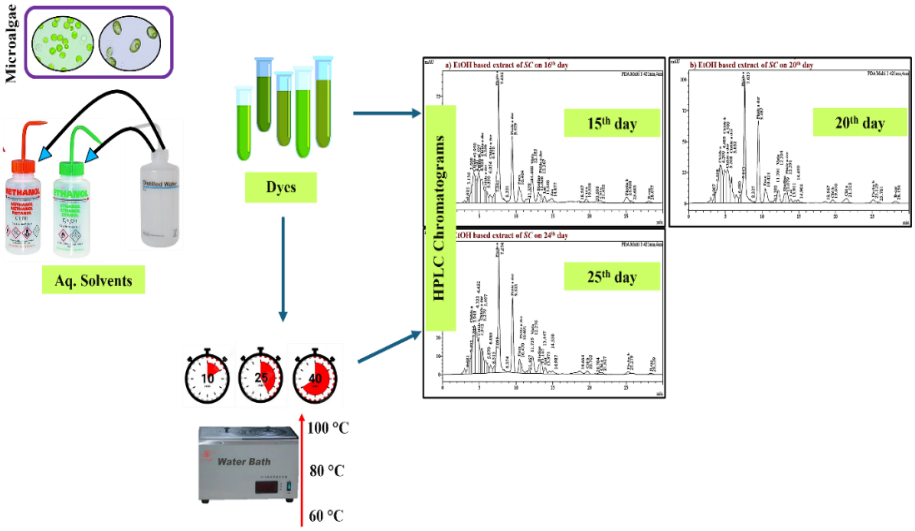

CHAPTER 5

Optimization and Storage in coordination with different Pigmental Analysis

5.1. Introduction

Microalgal pigments have emerged as promising candidates for dye-sensitized solar cells (DSSCs) owing to their ample accessibility, eco-friendly characteristics, and cost-effective production, alongside their demonstrated resilience under dissimilar conditions [Chauhan et al., 2022]. Dyes (mixture of pigments in natural case) from microalgae can be sensitive to various factors like light, temperature, pH, and oxygen levels as per studies and may involve testing under different conditions for suitability [Chauhan et al., 2023; Chauhan et al., 2024a]. Various techniques have been employed to incorporate natural dyes in DSSCs, including the addition of co-pigments and the blending of different dyes. These approaches aim to enhance stability and broaden the spectrum of light absorption, ultimately improving the overall efficiency [Chauhan et al., 2024b].

The dyes are particularly shortlisted with spectrophotometry but to outdo some of the shortfalls of microscopy and spectrophotometry, high-performance liquid chromatography (HPLC) pigment analysis methods have been examined in current years to gain both precise pigment data and comprehensive evidence about the conformation [Jodłowska & Latała, 2011; Picazo et al., 2013]. HPLC is used for both qualitative and quantitative analysis of dyes due to the intricate nature of dye extracts and the subtle distinctions among various *Chls*, isolating individual pigments can be challenging [Zhang & Laursen, 2009]. Also, a significant portion of recent efforts in the analytical HPLC of *Chls* has been directed towards distinguishing mono-vinyl [MV]-pigments from their corresponding di-vinyl [DV]-analogues [Sanz et al., 2015]. Researchers also seek to stabilize *Chls* for stable natural dyes and strategies include metal substitution, encapsulation,

and microencapsulation. As *Chl* comprises tetrapyrrole rings with various substituents, including chlorins, phorbins, and porphins, however photosynthetically active *Chls* are magnesium complexes with specific ring structures and a phytyl group.

This approach makes it easier to confirm the important roles played by the pigments and their derivatives and make them known without being shadowed in terms of absorption spectra. The development of new Reverse phase (RP)-HPLC methods alongside columns like Monomeric octadecyl silica (ODS, C18) hydrophobic columns remain the most frequently used stationary phases for the analysis of *Chls* and also their combination with alcohol groups, and the same goes for carotenoids which are much less affected by degrading factors [Ligor et al., 2014; Turcsi et al., 2016]. A significant advancement is anticipated with the establishment of monolithic columns, characterized by a single rod of continuous porous silica containing large through-pores and mesopores. This structure leads to increased permeability, producing columns with high efficiency and low back-pressure, operable at high flow rates. These features enhance separation speed while maintaining an efficiency comparable to that of particulate materials smaller than 3 μm. [Cabrera et al., 2000; Rieux et al., 2005]. As a result, the separation of *Chls*, which previously required lengthy analysis periods with traditional packed columns, can now be completed in significantly shorter times. The efficiency of pigment extraction and detection can vary based on factors such as solvent properties, extraction duration, cell concentration, algae species, and the use of mechanical disruption. Common physical methods to avoid extraction-based degradation of pigments include grinding, bath sonication, high-power sonication, and soaking.

Identifying pigments through HPLC entails the precise characterization of pigments present in a given sample with accurate measurement of pigment concentrations and also gives a clear distinction between which factors are creating what changes in the pigments [Picazo et al., 2013]. In qualitative terms, HPLC and Mass Spectrometry, LC-MS enable the identification of pigments based on their unique retention

times and mass spectra. The separation achieved by HPLC allows for the isolation of individual pigments, while LC-MS provides additional specificity through mass-to-charge ratio information [Mantoura & Llewellyn, 1983; Airs & Garrido, 2011]. Distinctions between common *Chls* and carotenoids can be established during HPLC from online UV/visible (UV/Vis) spectra, or co-elution with valid standards [Airs & Garrido, 2011].

This comprehensive approach facilitates the elucidation of pigment composition in complex mixtures, contributing to a deeper understanding of the sample's chemical makeup. By employing calibration curves and standard reference materials, the HPLC analyses can be quantified, providing valuable insights into the relative abundance of different pigments [Eckardt et al., 1990]. To enhance the accuracy of structure prediction using HPLC data, specific techniques such as matching retention times with standards for initial chemical insights are useful.

Wright and colleagues extensively explored the use of various extraction solvents, particularly highlighting acetone and methanol, which are widely employed in extracting algal pigments [Jeffrey et al., 1997]. Although methanol, when paired with mechanical disruption, generally yields the highest extraction efficiency, the stability of pigments in methanol is notably low [Chen et al., 2003]. It is often implicated in promoting *Chl a* allomerization, a concern underscored by Mantoura and Llewellyn's findings on the formation of *Chl a* derivative products in methanol [Mantoura & Llewellyn, 1983]. However, research indicates that certain *Chls* and carotenoids are more effectively extracted with methanol other than Dimethyl sulfoxide (DMF) [Jeffrey, 1974]. Despite sharing the same polarity index as methanol, acetone exhibits greater eluotrophic strength for carbon-rich substrates. Furthermore, it induces fewer artifacts compared to methanol and DMF, with *Chl a* derivatives, mainly *Chl a* allomer, and epimer, detected at only up to 5% of measured *Chl a* levels [Bowles et al., 1985].

5.2. Experimentation

5.2.1. Reagents

The solvents consumed were of Sigma-Aldrich, with test specifications as Ethanol (C_2H_6O), and Methanol (CH_4O), both ≥ 99.8% pure.

The concentration of the subsequent solvents was maintained by the additive of deionized distilled water as per the needs of the testing. The overall mixtures had in strength of 80%.

5.2.2. Conditions of Growth and Culture

In this scientific investigation, two distinct uncontaminated cultures of indegenous freshwater microalgae, specifically *Asterarcys quadricellulare*, and *Scenedesmus sp.* were utilized. These microorganisms were cultured in a standard BG-11 medium, with careful pH maintenance within the range of 7.2 - 7.4, achieved by the use of diluted hydrochloric acid (HCl) or sodium hydroxide (NaOH) [Chauhan et al., 2023; Chauhan et al., 2024a; Chauhan et al., 2024b].

The initial cultures of both species were cultivated in Erlenmeyer flasks for a period of 10 days, following which axenic subcultures were derived from these primary cultures. Subsequent experiments involved inoculating similar culture flasks and growth assessments were conducted at 24-hour intervals until the 30th day of cultivation. These cultures were housed in a dedicated culture room, maintaining a stable temperature of 27 ± 5 °C. A 12-hour light photoperiod was followed by a 12-hour dark phase [Stanier et al., 1971]. To ensure optimal growth, white fluorescent lamps were positioned at an applicable expanse from the cultures during the light phase, maintaining a light intensity of 3000 lux. After collecting the microalgal cell biomass on the 15^{th}, 20^{th}, and 25^{th} day, the dyes were extracted from the algae and were subjected to analysis for absorbance spectra and underwent other requisite characterizations.

5.2.3. Methodology

5.2.3.1. Dye extraction

The dye extraction on the 15th, 20th, and 25th day with ethanol and methanol was done separately. Three triplicates of methanol and ethanol were taken for dissolving pigments at 80%.

5.2.3.2. Extraction techniques

The hot solvent extraction method was performed with a known volume of the particular microalgal species culture. These cultures were centrifuged, and the obtained residue was blended with 80% ethanol and methanol separately, and then heated for 5 minutes in a boiling water bath at three different temperatures as per the requirement. The solution is once again centrifuged and the obtained green-colored supernatant is separately collected [Pápista et al., 2002; Henriques et al., 1970].

5.3. Instruments and Characterization

Photosynthetic pigments obtained here were sensitive to oxygen, heat, and light. All operations were executed under a dim or diffused or no light condition and kept at a reasonable laboratory temperature.

HPLC System: Shimadzu Prominence-i LC-2030C 3D Plus Liquid Chromatograph with C18 column (a straight 18-long fully saturated carbon chain, called octadecyl silyl (ODS))

Measurements were performed using the HPLC system, which included a 717 plus autosampler, an RF-20A prominence fluorescence photodiode array detector, and a 4 μm C-18 reverse phase column (Ascentis® C18 HPLC Column pore size 120 Å, 5 μm particle size, L × I.D. 25 cm × 4.6 mm | Supelco Analytical). The pump's flow rate was 0.6 mL/min. The column temperature used was 40 °C. Pigments were detected in the range of 300 nm to 800 nm. The injection was automated by an autosampler SIL–20AC XR (Shimadzu) and 20 μL pigment solution was subjected to analysis [Loh et al., 2012; Garrido et al., 2003].

HPLC analysis was performed by the isocratic method using a mobile phase consisting of 100% *mt*. 30 min were required per measurement. PTFE syringe filters were used with 0.22 µm pore size to clarify extracts before injecting them into the HPLC system.

The diode array detector was programmed to get a full visible spectrum at selected chromatographic points, particularly at 421nm, 435nm, 467 nm, 652nm, and 665nm. These help to provide a chromatographic indication which increases the sensitivity of the detection [Edelenbos et al., 2001].

5.4. Pigment identification

Pigments were identified by their retention behavior, comparing pigment retention times with profiles from standard cultures. Since multiple pigments can share the same retention time if they coelute in a single peak, additional identification criteria are required. Intermediary reactions and compound formations in the dye sample can also cause variable retention times, leading to inconsistent results. To characterize pigments and assess peak purity, the full visible spectrum was examined in different sections of each peak. Selective detection was accomplished by extracting chromatograms at specific wavelengths [Sartory, 1985; Kuczynska et al., 2015].

Since methanolic extracts are known to promote *Chl* allomerization during extended storage, samples should be injected immediately after extraction. To prevent peak shape distortion caused by "viscous fingering" phenomena in less retained pigments, it is essential to mix the extracts with water to match the injection solvent's viscosity with that of the eluent. Additionally, low polarity pigments may be lost due to their limited solubility in aqueous solvents [Wright et al., 1991].

5.5. Result and Discussion

The pigments were coded so for ease of imprinting in the chromatograms obtained and as it has been used in previously customary papers [Roy & Garrido, 2013; Schmid & Stich, 1995]. Little bit different color codes or colors have been provided for some extraordinary chromatograms. The retention times were thoroughly compared to the previously published papers for accurately predicting and confirming the peaks that which peak is of which pigment. The data is originally taken for 6 wavelengths which was later reduced to 5 due to the presence of two much-deviating baselines on a particular wavelength. [Nakamura & Watanabe, 1998; Bidigare et al., 2005; Phytoplankton pigment analysis, 2002]

5.5.1. HPLC Chromatograms analysis

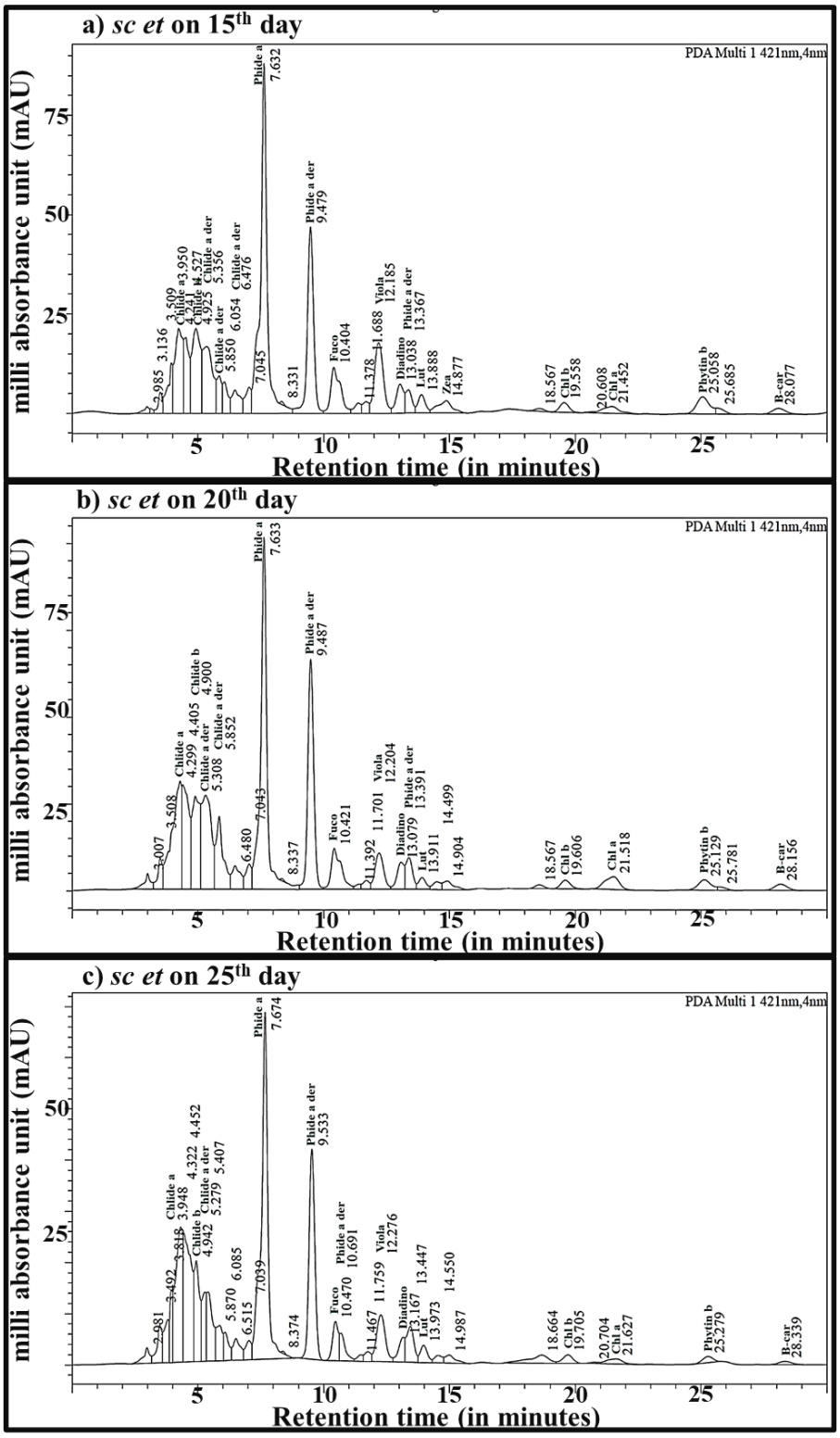

i. *sc* dye spectra at 421 nm

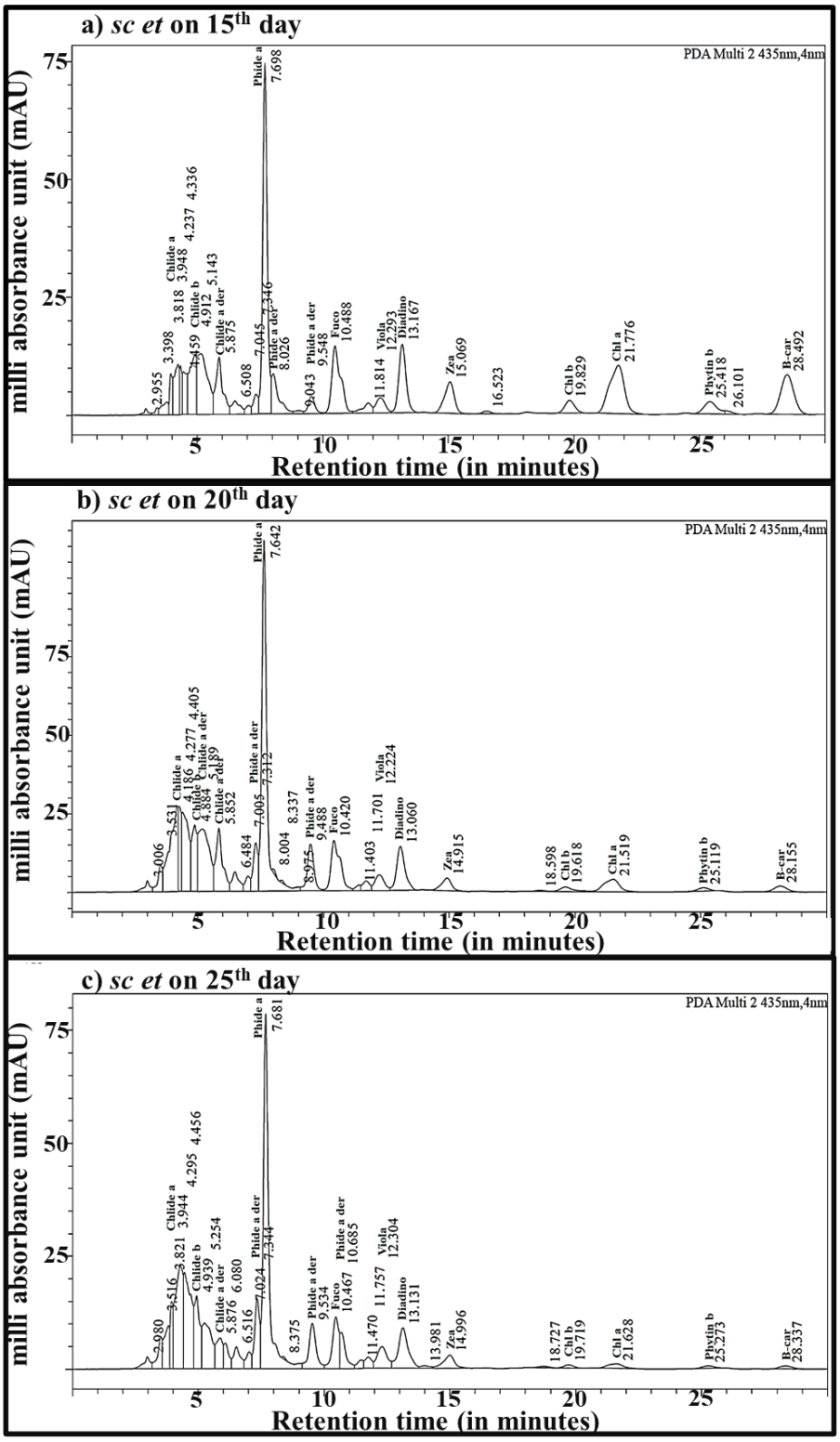

ii. *sc* dye spectra at 435 nm

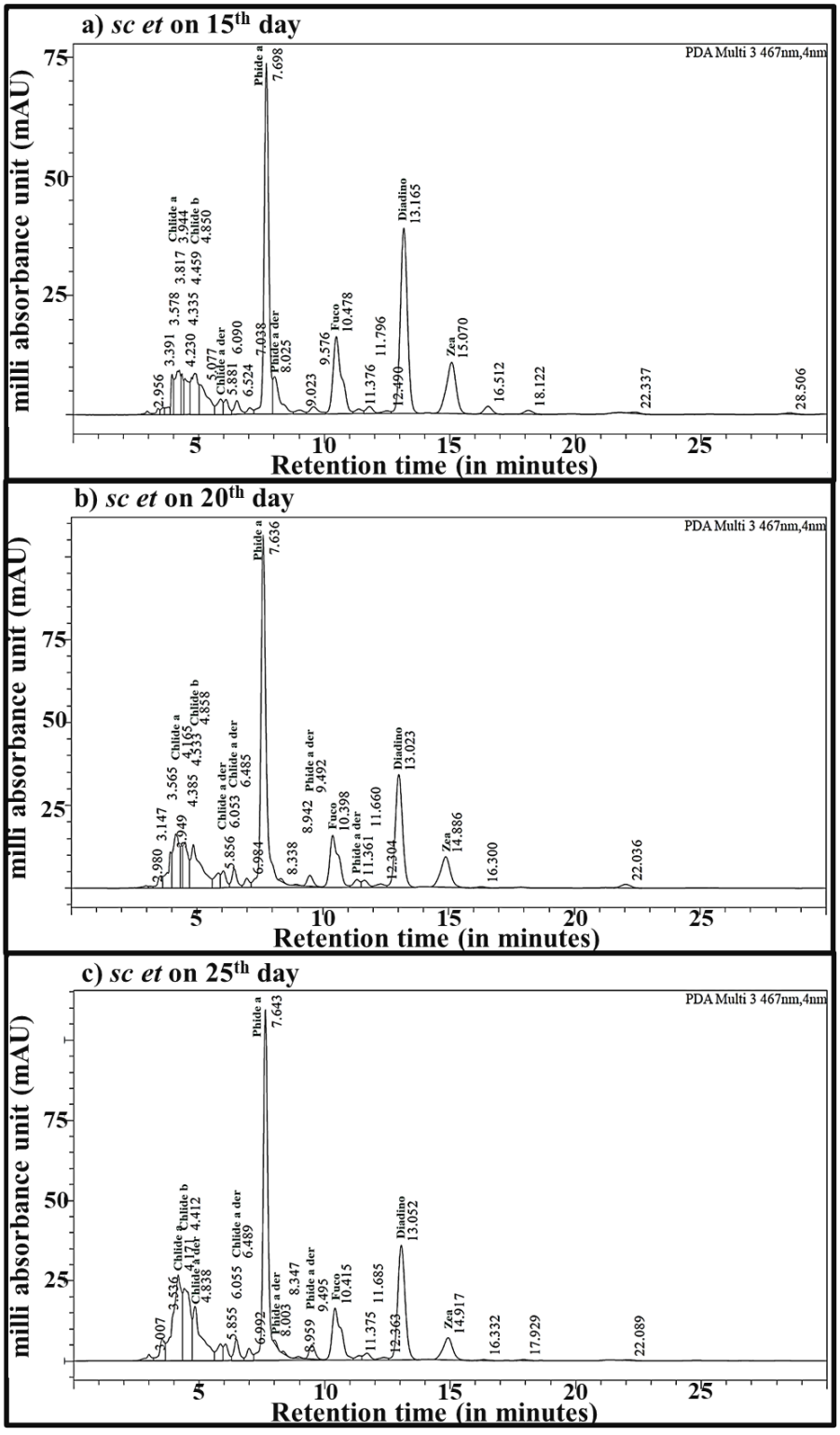

iii. *sc* dye spectra at 467 nm

Figure 5.1. *sc* dye spectra at i) 421 nm ii) 435 nm and iii) 467 nm were detected on a) the 15th day b) the 20th day and c) the 25th day of extraction via 80 % *et* as solvent at 80 °C.

When the filtered dye from *sc* was observed through a chromatogram format in **Figure 5.1.** on the following three wavelengths, the presence of *Phide a* at a retention time of around 7.63 to 7.69 was the maximum on all the three days of extraction followed by the *Phide a* derivative as the second best at 421nm [Kraay et al., 1992; Jeffrey et al., 1999]. The other most significant pigment is *Chlide a* and *Chlide b* and their derivative. In terms of pigments quantity in **Figure 5.1.i**. it can be seen that the pigments are maximum overall as well as individually on the 20^{th} day of extraction. The highest height possessed by the *Phide a* is 101287mAU on the 20^{th} day of extraction, followed by 88061 mAU and 67753 mAU on the 15^{th} and 25^{th} day of extraction, and is similarly reciprocated in terms of area at 421nm. Here, It can be understood that the extra addition of *Chl* derivatives by using ethanol at a high temperature also causes loss of magnesium ions from *Chl* hence making them less stable for utilization as DSSC dye. On 421nm on the 25^{th} day as expected the carotenoids peaks remain significantly high in comparison to *Chl* derivatives, when evaluated concerning the 15^{th} and 25^{th} day. Also, they may be able to resist more temperature-based degradation of pigment at this stage than at other days. However there is a high difference in the data in **Figure 5.1.ii.** at 435nm when seen on the 25^{th} day the peaks of carotenoids are not that high on the 25^{th} day and reduce in comparison to that on the 15^{th} and 20^{th} day, which may be due to unfavorable wavelength point. But here it can be seen that *Chlide* and its derivatives are significantly high in comparison to that of the 15^{th} day. The *Chl a* has reduced or most probably converted to *phide* or *Chlide* on the 20^{th} day or their mixing and overlapping of retention time of compounds due to excess of the same point eluting compounds. The elution is far clearer in **Figure 5.1.ii.a.** with *B-car* being visible smoothly along with other carotenoids, similarly for ii. b. where *Fuco, Viola, Diadino,* and *Zea* are very well eluted and marked on both the chromatograms.

In **Figure 5.1.iii.a., b.,** and **c**. at 467 nm other than the phide a, the compound eluting significantly is that of diadino which remains almost consistent in the dye. Alongside *Diadino* other carotenoids also had a significant peak value while *Chls* and *B-car* were not able to mark even their presence in the run [Wright & Shearer, 1984; Zapata et al., 2000].

So overall it can be quantified and concluded that the significant denaturation by the method of extraction which involves heating can be a significant reason for less presence of *Chl a* and more of *Phide a* and *Chlide a* and their derivative. The excess recovery of *Chl* in a short time by using *et* based heating method at 80° C can cause more extraction but significantly more denaturation, ultimately causing loss of magnesium ions and removal or detachment of the phytol chain. But overall the quantity of the *Chl* and its derivatives remains a significant high comparatively [Wright & Shearer, 1984; Zapata et al., 2000; Van Heukelem & Thomas, 2001].

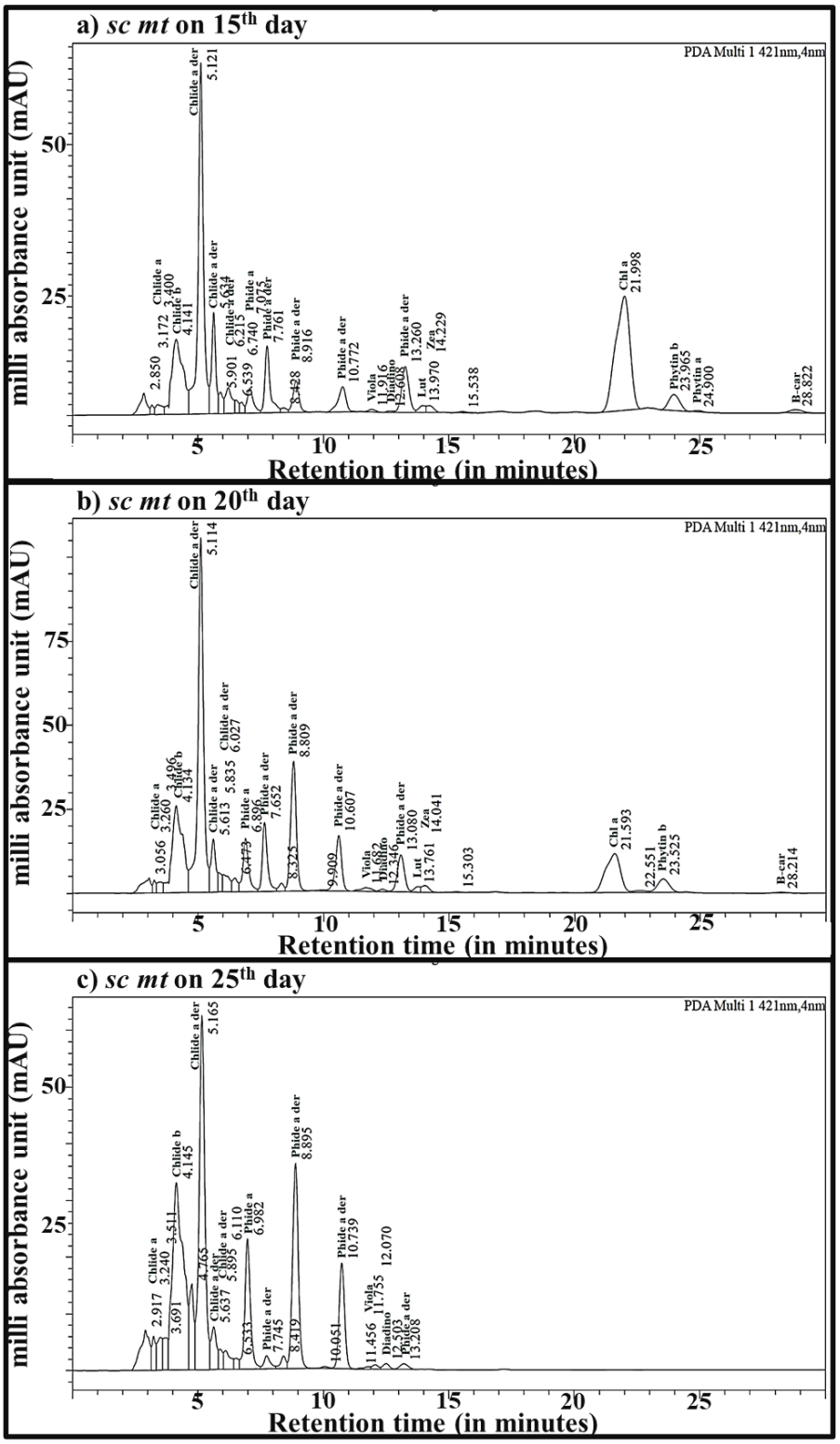

i. *sc* dye spectra at 421 nm

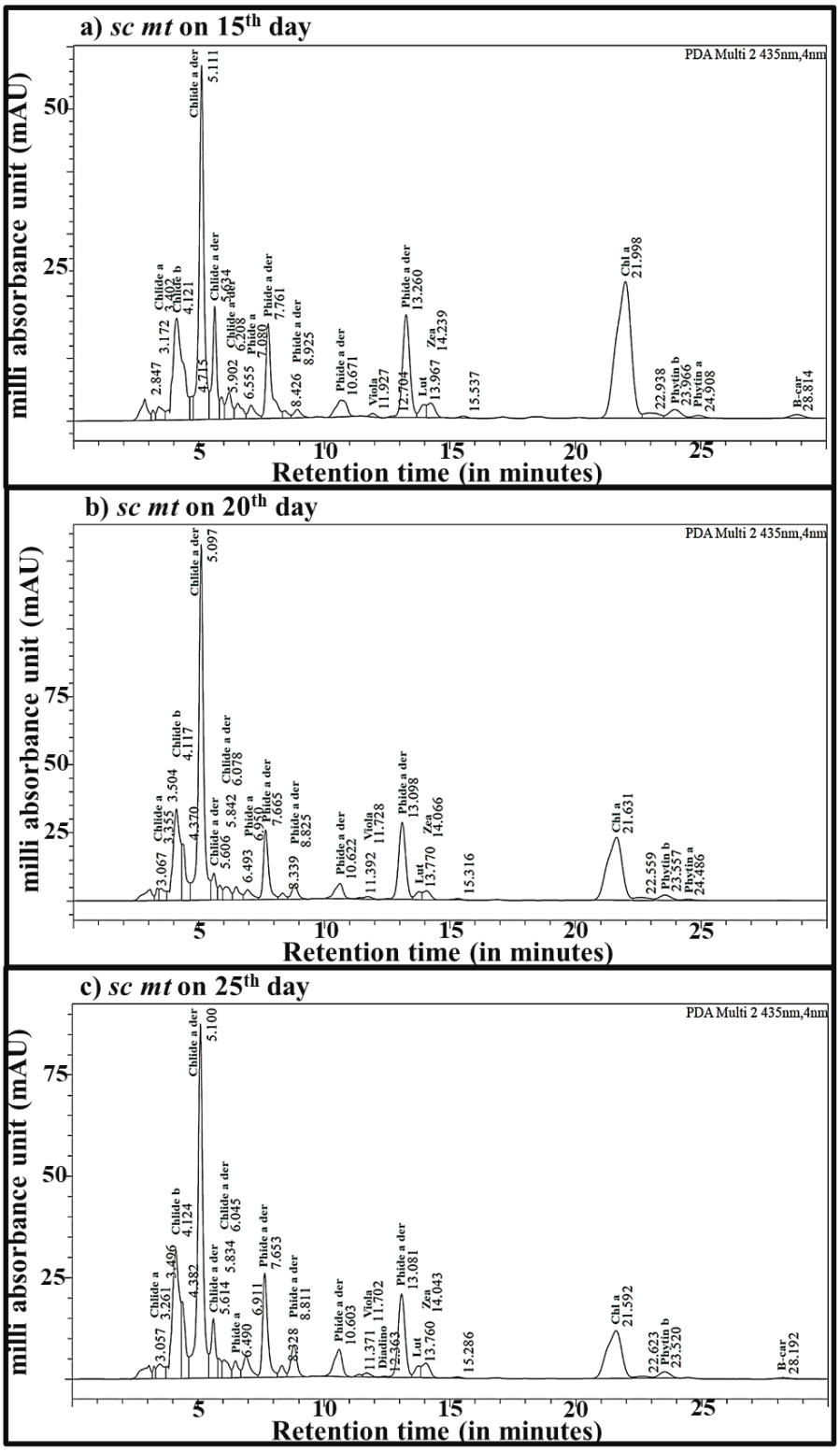

ii. *sc* dye spectra at 435 nm

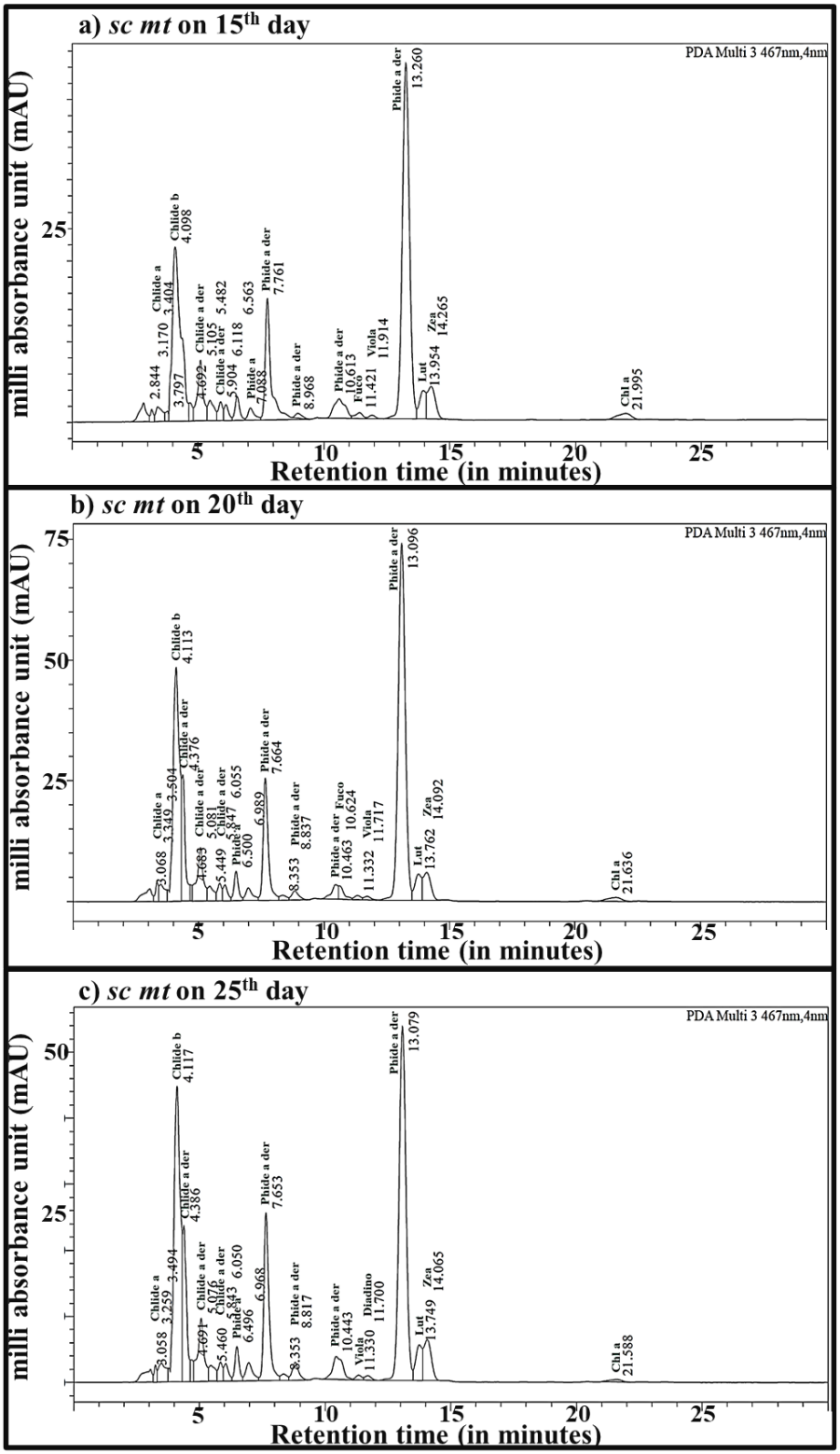

iii. *sc* dye spectra at 467 nm

Figure 5.2. *sc* dye spectra at i) 421 nm ii) 435 nm and iii) 467 nm were detected on a) the 15th day b) the 20th day and c) the 25th day of extraction via 80 % *mt* as solvent at 60 °C.

In **Figure 5.2.i.a**. on the 15th day extraction *Chl a* is relatively high w.r.t. to its converted derivative of *Chlide a* closing on the detachment of phytol tail without the loss of magnesium ions. This trend is also visible in **Figure 5.2.i.b.** whereby 20th day the *Chl a* production also kind of pauses and *Chl a* turns weaker and causes self degradation by removing the phytol chain. It is possible because of using a relatively lower temperature with *mt* in comparison to that used with *et*. There is also a significant formation of *Phide a* derivative as well probably due to the oxidation nature of *mt* by supplying hydroxide and methyl groups. Also here it can be seen that the extraction of carotenoids has not been significant on all days due to the use of *mt* denaturing properties. In **Figure 5.2.i.c.** it can be seen that the *Chl a* is more of turning to *Phide a* and its derivatives on the 25th day and hence their concentration comparatively shows an increase. *Chlide b* concentration as expected keeps on increasing with an increase in days with conversion of *Chl a* to *Chl b* for phytoprotection. **Figure 5.2. ii. a, b, c** also shows a similar trend at 435nm as it was at 421nm. In **Figure 5.2.iii.c** some evident presence of *Lut* and *Zea* can be seen but here the lead is with *Phide a* derivatives in comparison to *Chlides*. At 467nm it can be seen that *Chlide b* is substantially high which makes *Phide a* der less dominant.

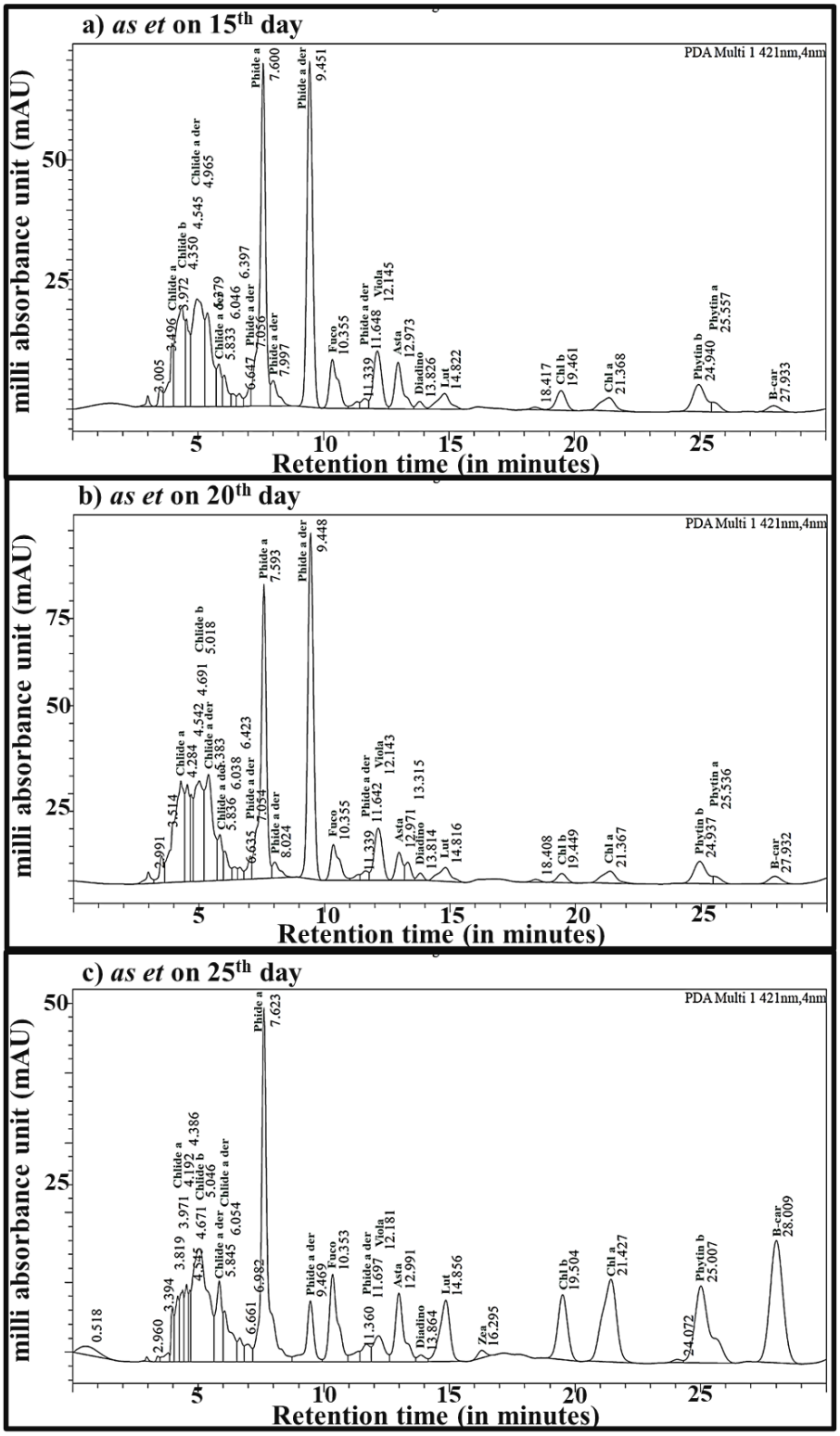

i. *as* dye spectra at 421 nm

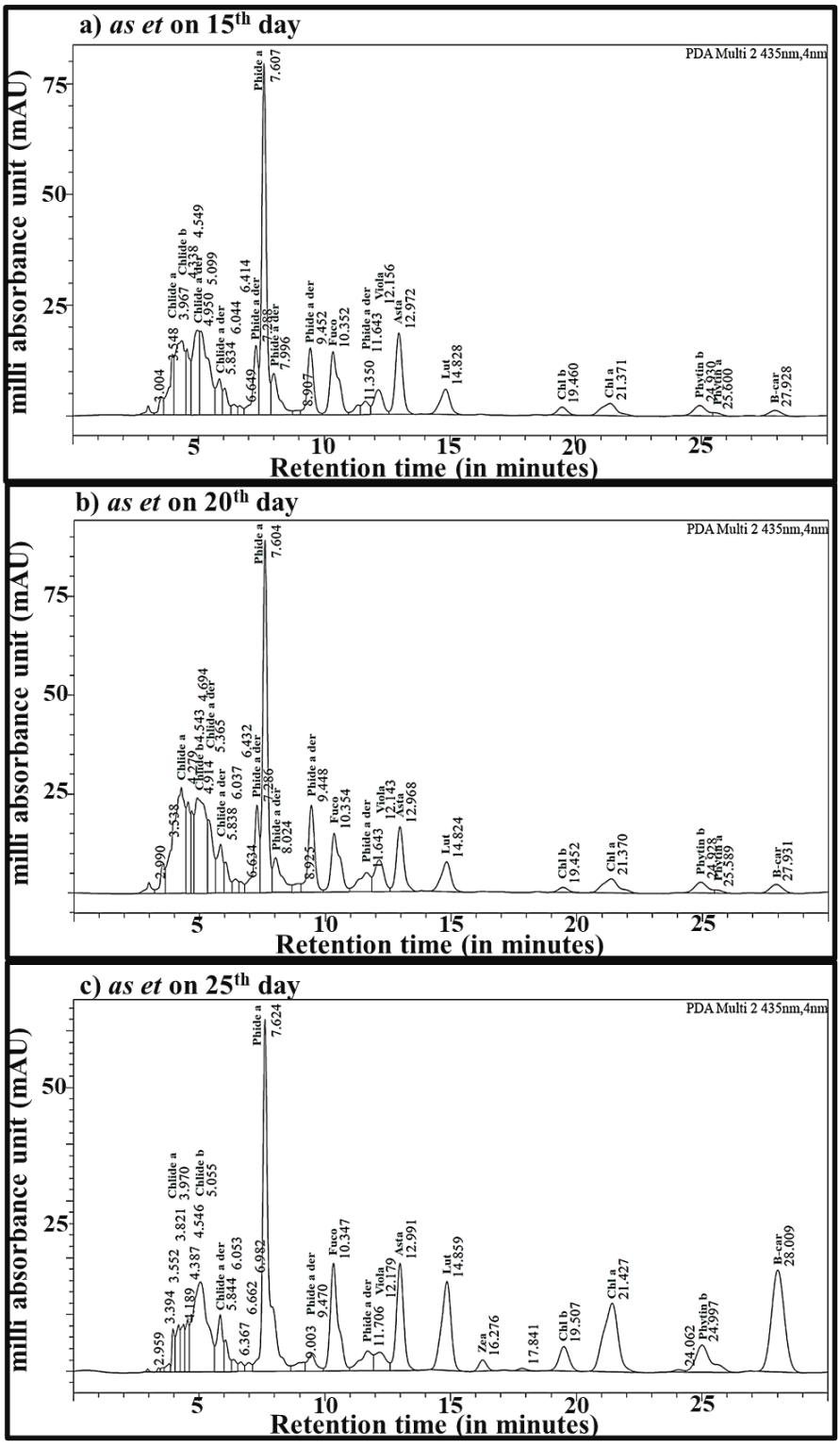

ii. *as* dye spectra at 435 nm

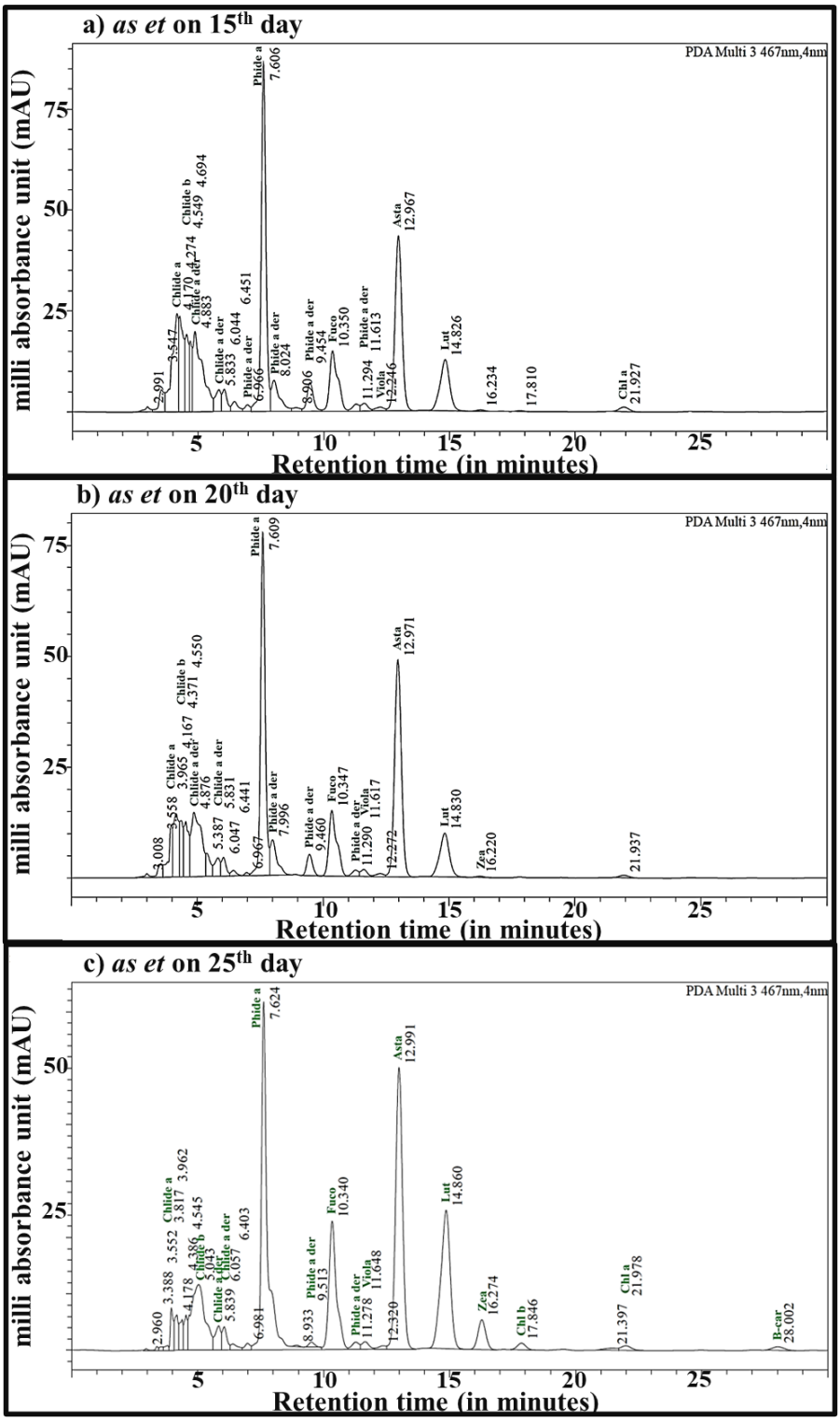

iii. *as* dye spectra at 467 nm

Figure 5.3. *as* dye spectra at i) 421 nm ii) 435 nm and iii) 467 nm were detected on a) the 15th day b) the 20th day and c) the 25th day of extraction via 80 % *et* as solvent at 80 °C.

In **Figure 5.3.i.a** and **b**, it can be seen that there is more creation of *Phytin* from *Chl*, and it can be assumed that there is more severity of loss of magnesium ions than that of losing the phytol tail. Here the phides are not so strong and stable as they are forming bonds due to oxidation of *Phide* molecules by readily available hydroxide through *et*. Here there is comparatively greater extraction of carotenoids like *Fuco*, *Viola,* and *Asta* in comparison to *sc*. It can be seen that the conversion to *Chlide* or *Phide* is in proportion and *Chl b* also displays a similar breakdown but generates only *Chlide* and *Phytin b*. The peak areas are significantly broader with chances of overlapping of peaks too. In **Figure 5.3.i.c.** the peaks are low in mAU but show relative stability of pigments like *B-car*, *Chlide b*, and *Phytin b* which play crucial roles in avoiding photodegradation and are also supported by *Fuco*, *Asta*, and *Lut*. It can also be understood that all other pigments derived from *Chl a* have reached a significant downfall on the 25th day and stable pigments remain alone. In **Figure 5.3.ii**. it can be seen that there is a rapid breakdown to *Phide a* as well as oxidation to derivatives of *Chlide* and *Phide a*. *Phide a* leads significantly in **Figure 5.3.ii.a** and **b** with other major peaks being of *Fuco*, *Asta*, and *Lut*. **Figure 5.3.ii.c** the *Chl b* and derived pigments of *Chlide b* and *Phytin b* gets somewhat stable by the 25th day as the species is in stationary cum declining phase of growth then. **Figure 5.3.iii.** of 467nm has a remarkable extraction of asta comparatively higher than *Chlides* but it is not free from doubt that it might have an overlapping of *Phide a* derivative as this much mAU peak is little doubtful. *Phide a* as usual leads on all three days with a similar leading performance from *Fuco* and *Lut* too. *Zea* is also visible on the 25th day.

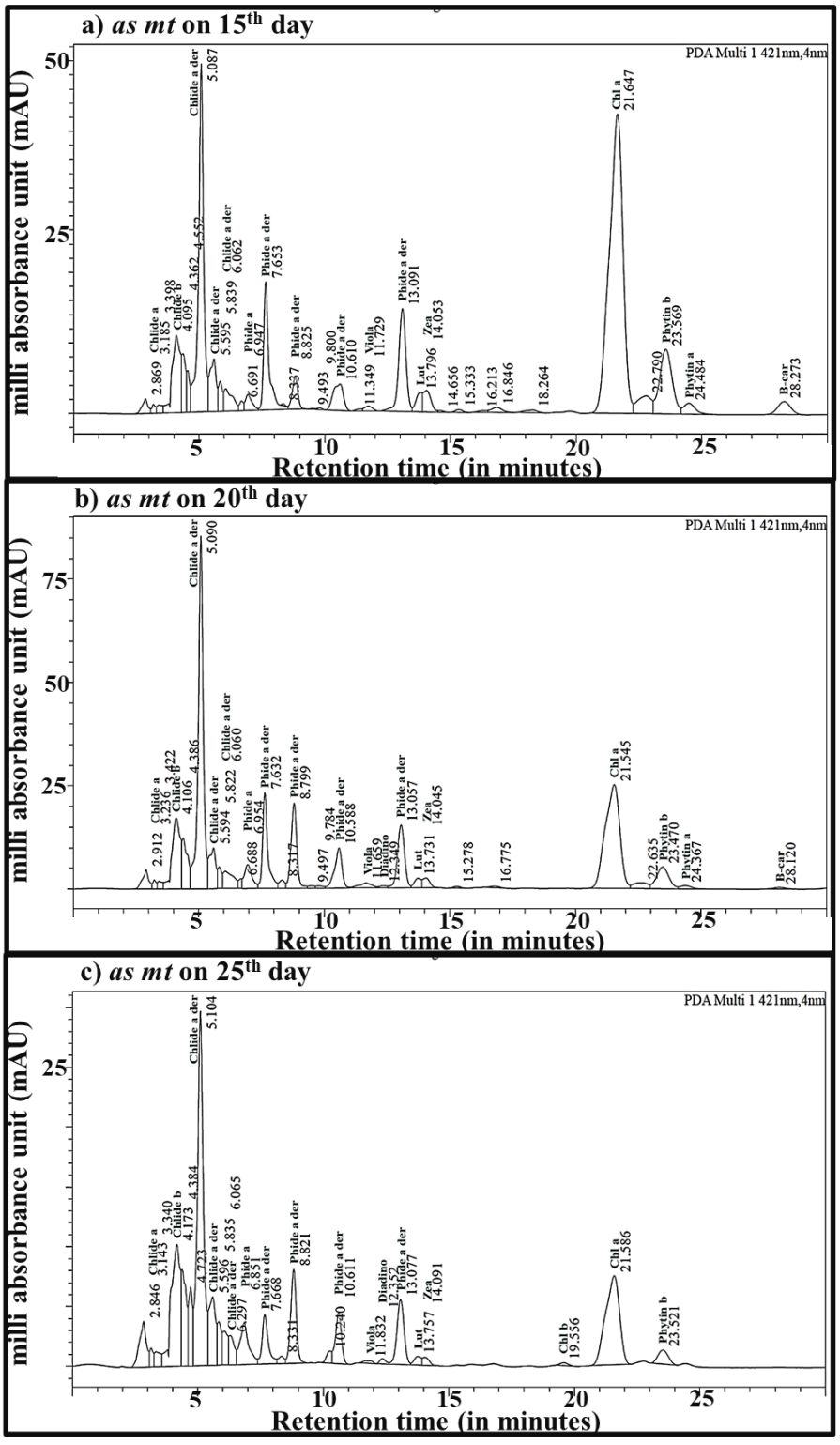

i. *as* dye spectra at 421 nm

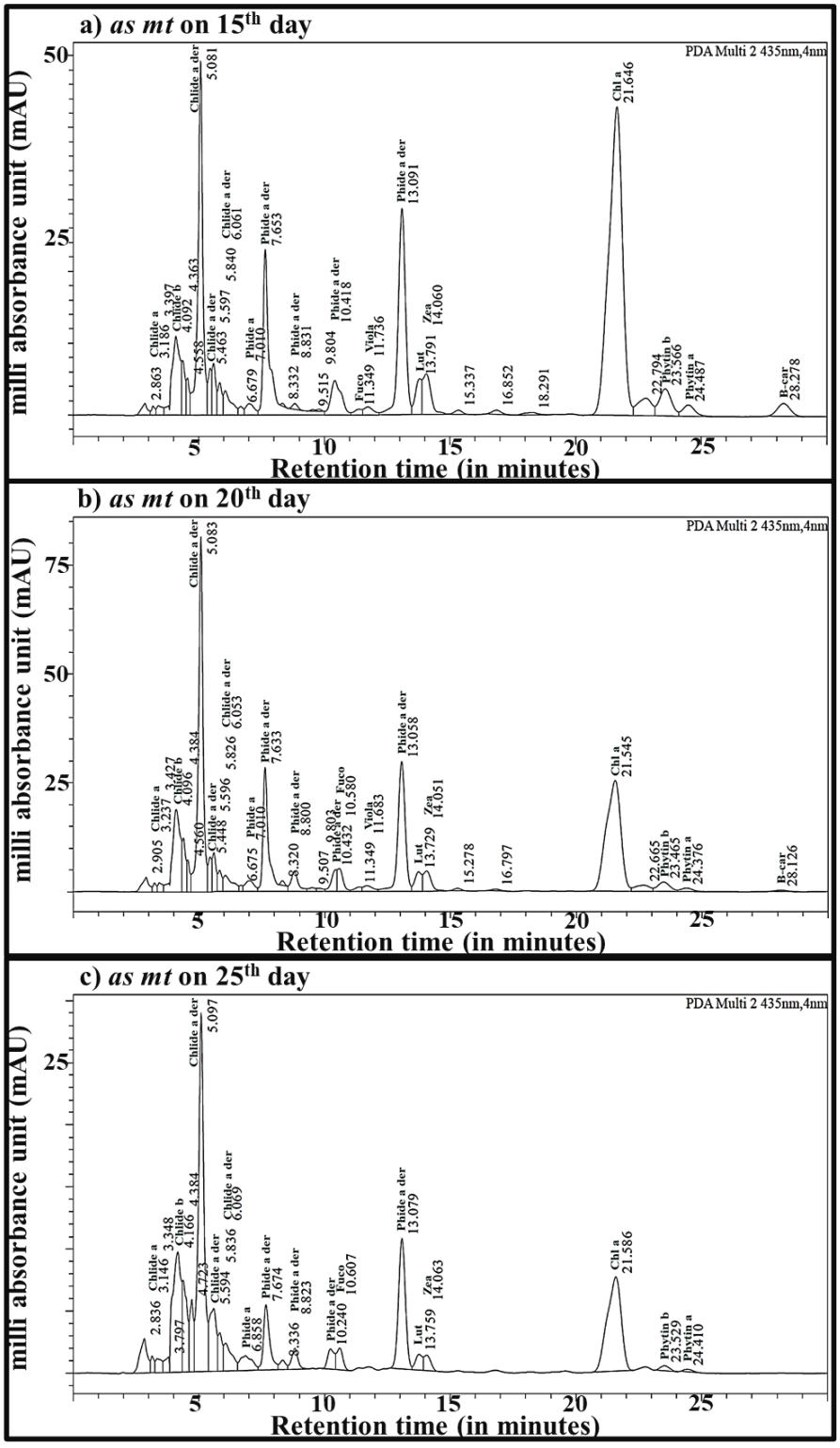

ii. *as* dye spectra at 435 nm

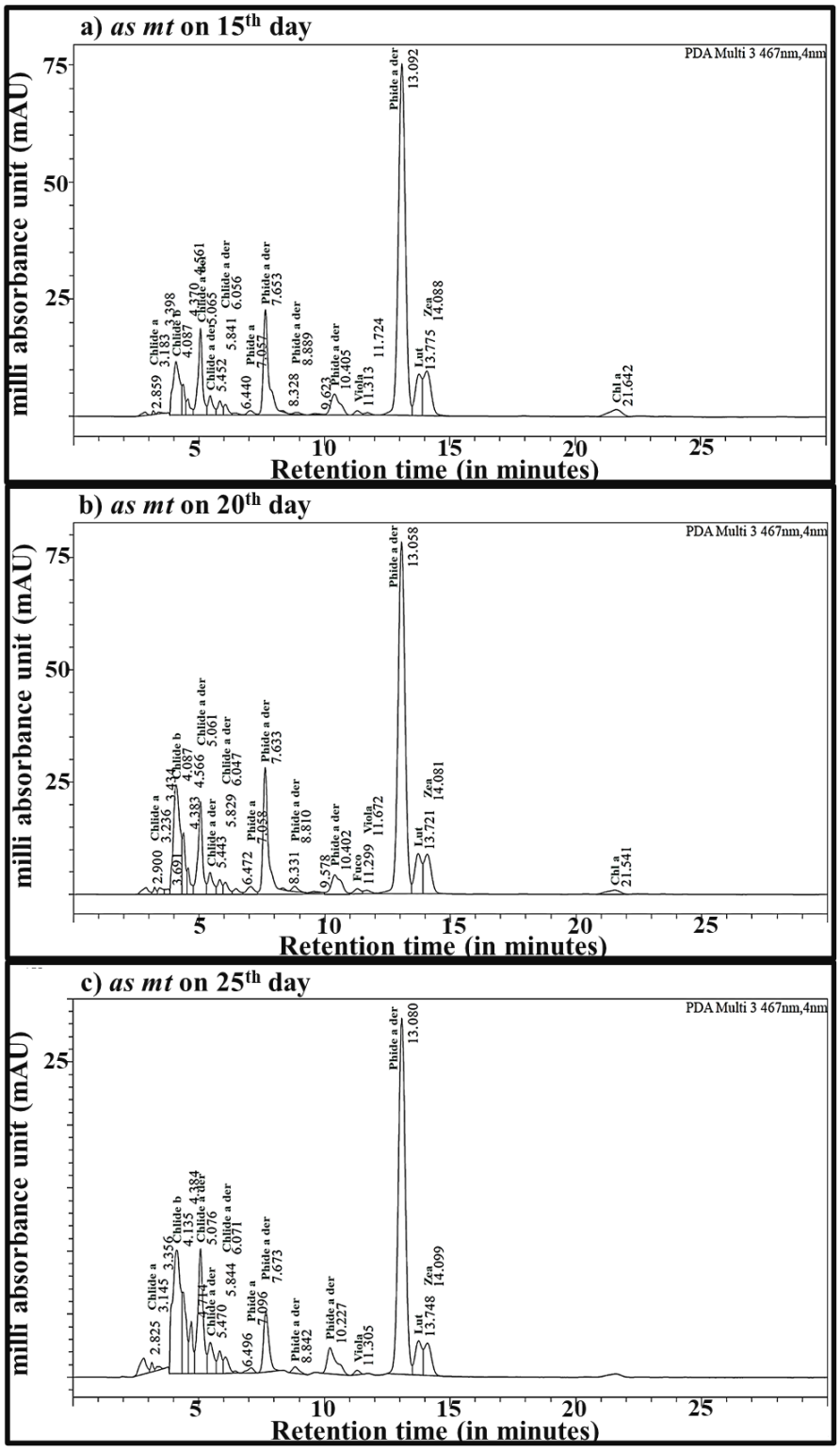

iii. *as* dye spectra at 467 nm

Figure 5.4. *as* dye spectra at i) 421 nm ii) 435 nm and iii) 467 nm were detected on a) the 15th day b) the 20th day and c) the 25th day of growth and extracted via 80 % *mt* as solvent at 60 °C.

In **Figure 5.4.i.a., b.,** and **c**. *Chl a* remains a good high without much degradation. In **Figure 5.4.i.a**. *Chlide a* is almost equivalent to *Chl a* as there is less natural degradation which is prevalent on the 20th day, where the *Chlide a* peaks more than three times *Chl a* due to a significant increase and even more conversion of *Chl a*. In **Figure 5.4.i.** *mt* can resist magnesium ions loss as well as allow less formation of phides and their derivatives. *Chl b* is significantly present in its forms of *Chlide b* and *Phytin b* as presumed. At a wavelength of 435nm, there are almost similar results except the phides start to rise notably on all three days. In **Figure 5.4.iii.** It can be seen that the phides derivatives are the leading peaks on all days as apparent but carotenoids of *Lut* and *Zea* make their presence known along with *Chlide b* and *Chlide a* der [Kraay et al., 1992; Jeffrey et al., 1999; Wright & Shearer, 1984; Zapata et al., 2000; Van Heukelem & Thomas, 2001].

Considering these four figures it can be supposed that the high temperature and type of solvent play a big role in extraction for less unfavorable alignment and without denaturation other than the factor of species pigmental tolerance towards these factors. Here *mt* seems more promising in extracting *Chl* as such with less degradation but *et* seems better in terms of quantity of extraction but in terms of *Chl* degraded derived products of *Chlide* and *Phide*. *mt* can preserve more magnesium ions embedded in *Chl*-derived pigments than *et*. But *et* can dissolve and not degrade more carotenoids as evident in *as* species-derived dye and also gets a higher pigment extraction mAU altogether in comparison.

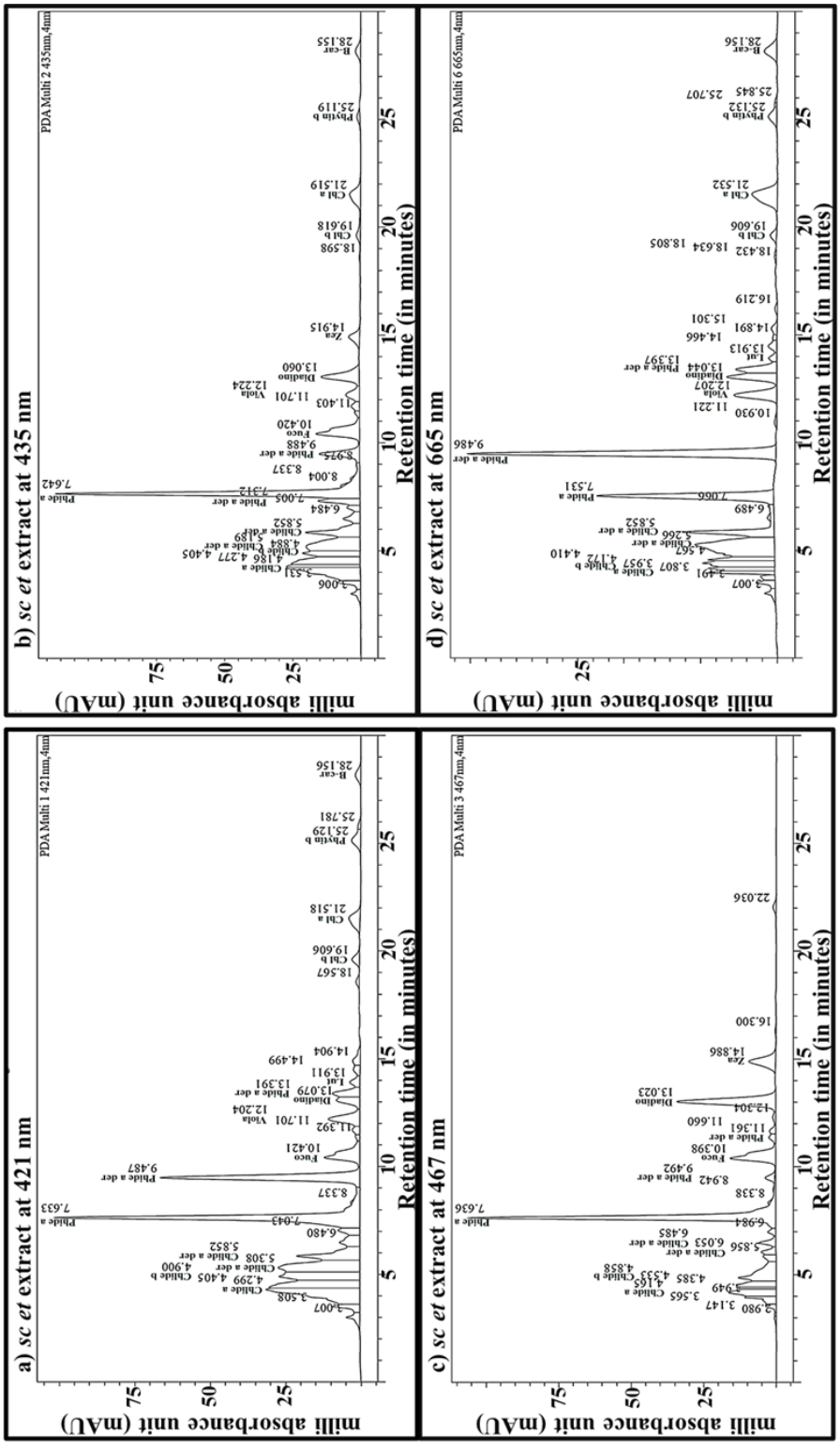

i. *sc* dye spectra extracted in *et*

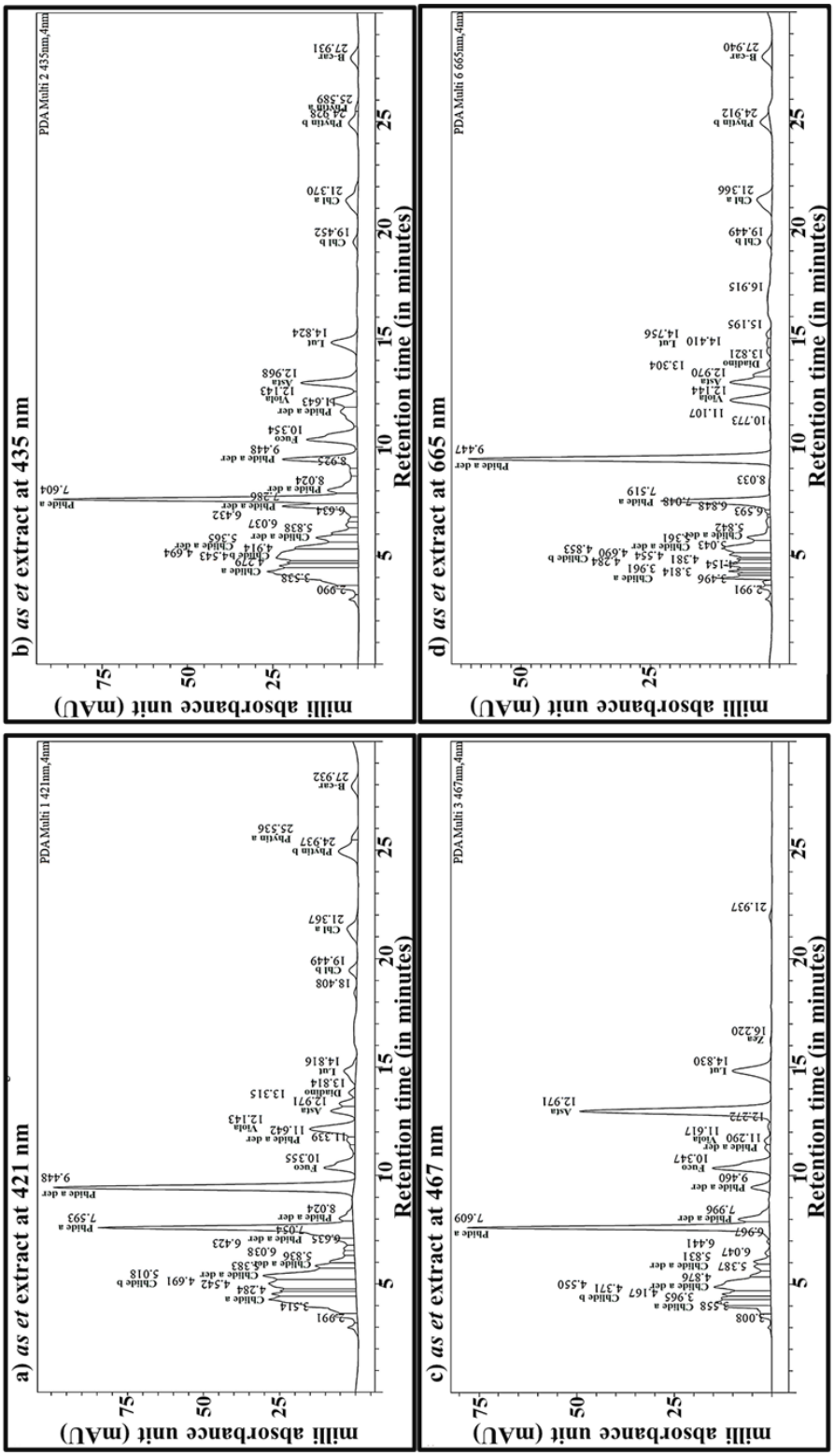

ii. *as* dye spectra extracted in *et*

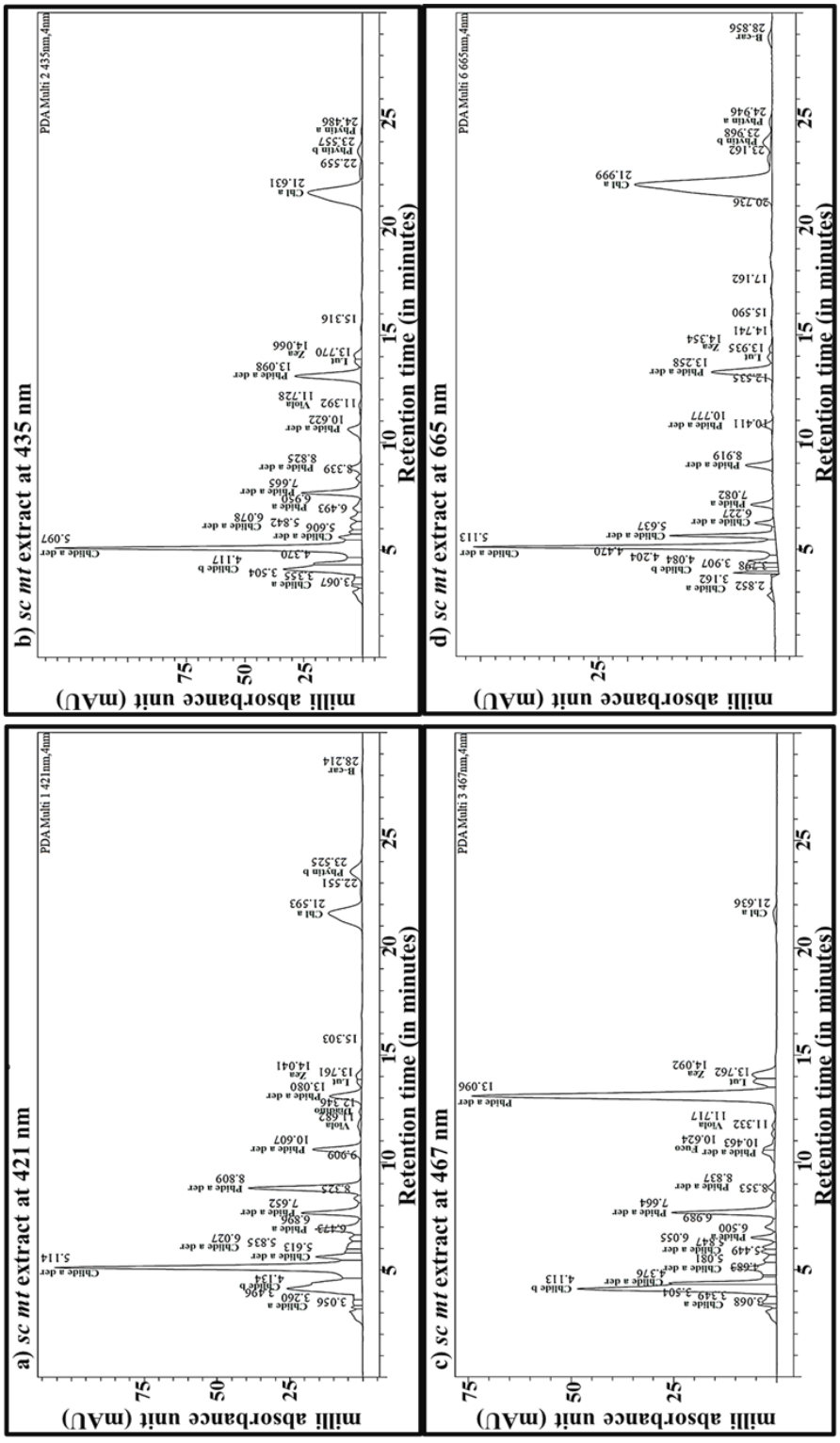

iii. *sc* dye spectra extracted in *mt*

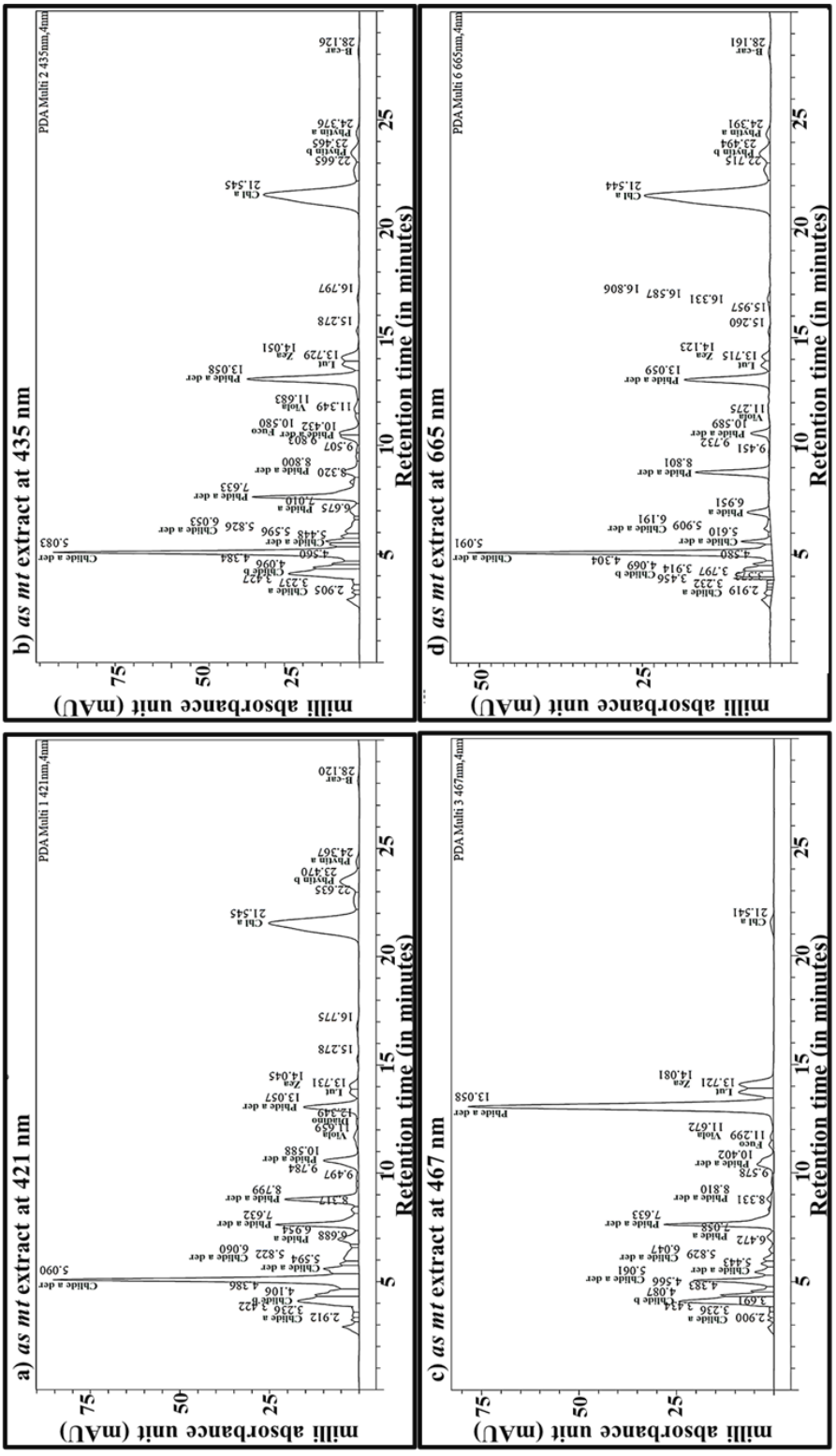

iv. *as* dye spectra extracted in *mt*

Figure 5.5. *sc* and *as* dye spectra when extracted on the selected 20th day of growth in *et* and *mt* at a) 421 nm b) 435 nm c) 467 nm and d)

665nm were detected through 80 % *mt* as solvent at 60 °C and 80 % *et* as solvent at 80 °C.

Here in **Figure 5.5.i.** if we compare the peak value change w.r.t. to the change in wavelength then it can be seen that *Phide* continues to dominate throughout the 20th-day extraction which is found to be the best out of the three in the previous figures. Except at 421nm and 665 nm where alongside *Phide a* and its derivative is also noticeable well to the mark. Rest remains more or less similar with prominent pigments being that of *Chlide a* and b, *Chl a* and *Chl b* cum *Phytin b*. In the carotenoids major peaks that remained consistent in 421nm and 435nm are of *Fuco*, *Viola,* and *Diadino* whereas in 467nm *Zea* arises with the decline of *Viola,* and in 665nm *Viola* arises again with the decline of *Zea*. At 665nm *Chlide a* possesses a big area peak hence proposing a high amount of it too or can be significant overlapping.

In **Figure 5.5.ii.** if it can be seen that the *as* present *Phide a* derivative supersedes the *Phide a* compound itself at 421nm and 665nm, whereas in c. and d. the *Phide a* dominates the peaks. *Chlide a* and *Chlide b* remain high consistently throughout the chromatograms. The other significant peaks ensuing of *Fuco*, *Asta,* and *Lut* at 421nm, 435nm, and 467nm wherein *Asta* being as high as 50 mAU at 467nm but at 665nm *Viola* and *Asta* remain below 10mAU.

In the methanolic extract of *sc,* it can be seen that *Chlide a* derivatives of small molecular weight has a significant amount in the extract as seen on 421nm, 435nm, and 665nm. It is followed by *Phide a* derivatives and then *Chlide b*. Carotenoids are not that prevalent except at a few places, with no significant peaks. At 665 nm, there are baseline fluctuations but still, the only established broad peak is of *Chl a*.

mt was able to extract the pigments in *as* well in comparison to *sc* with less degradation as the amount of *Chl a* is significantly high better achieved than anywhere else. Also, it is supported by the claim that there is a formation of *Chlide* and not *Phide* alone here and even very

little of *Phytin*. The other pigments are of *Lut* and *Zea* at 665nm following the trend of a, b, and c.

5.6. Stability

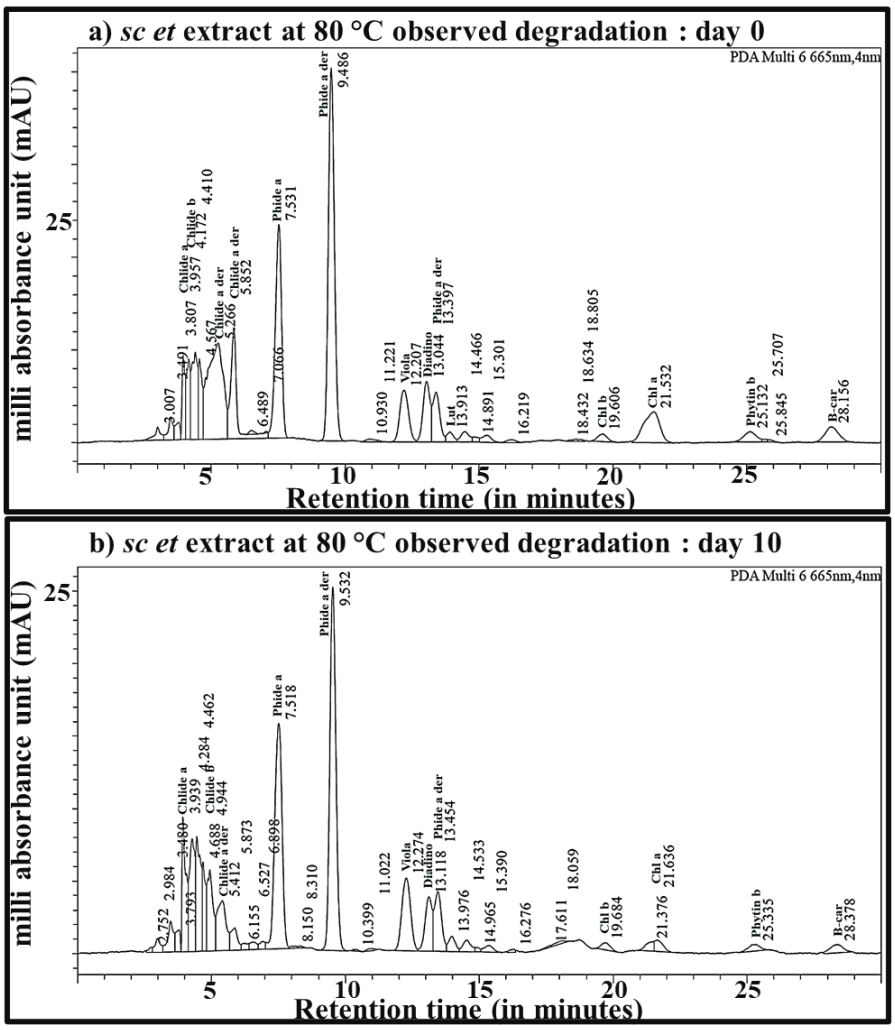

i. *sc* dye degradation at 665nm in *et*

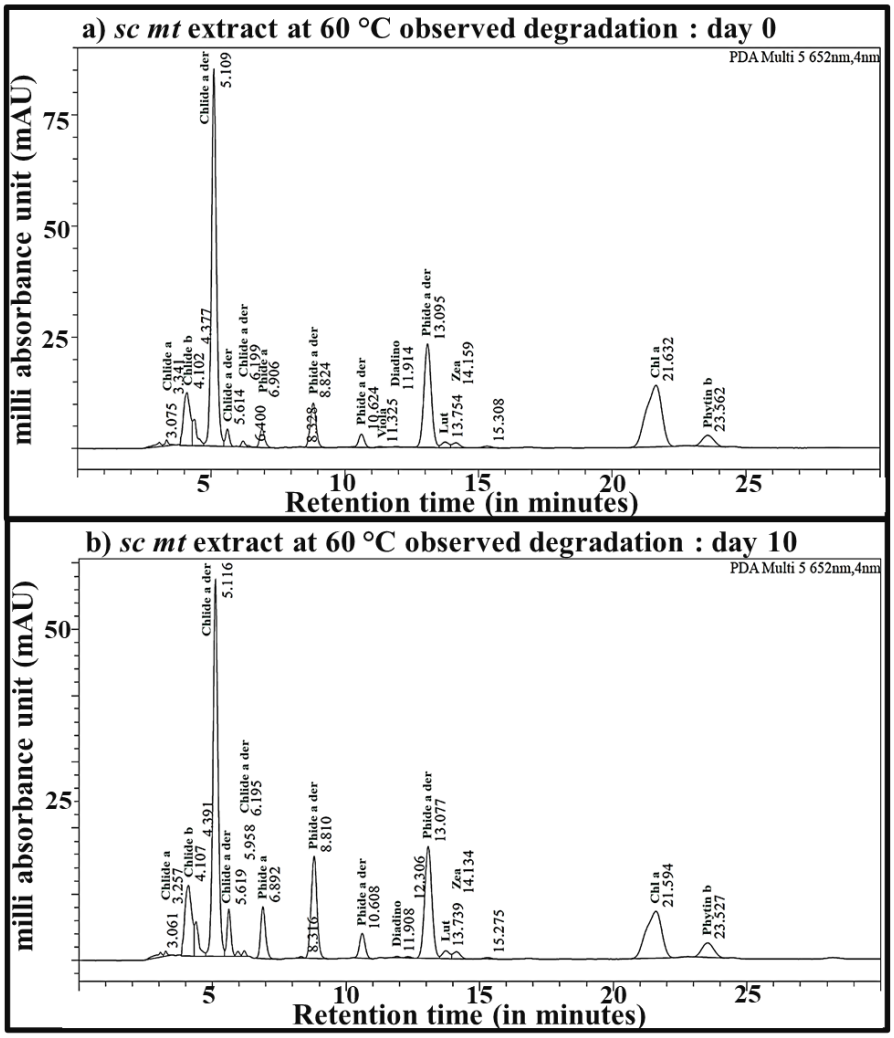

ii. *sc* dye degradation at 652nm in *mt*

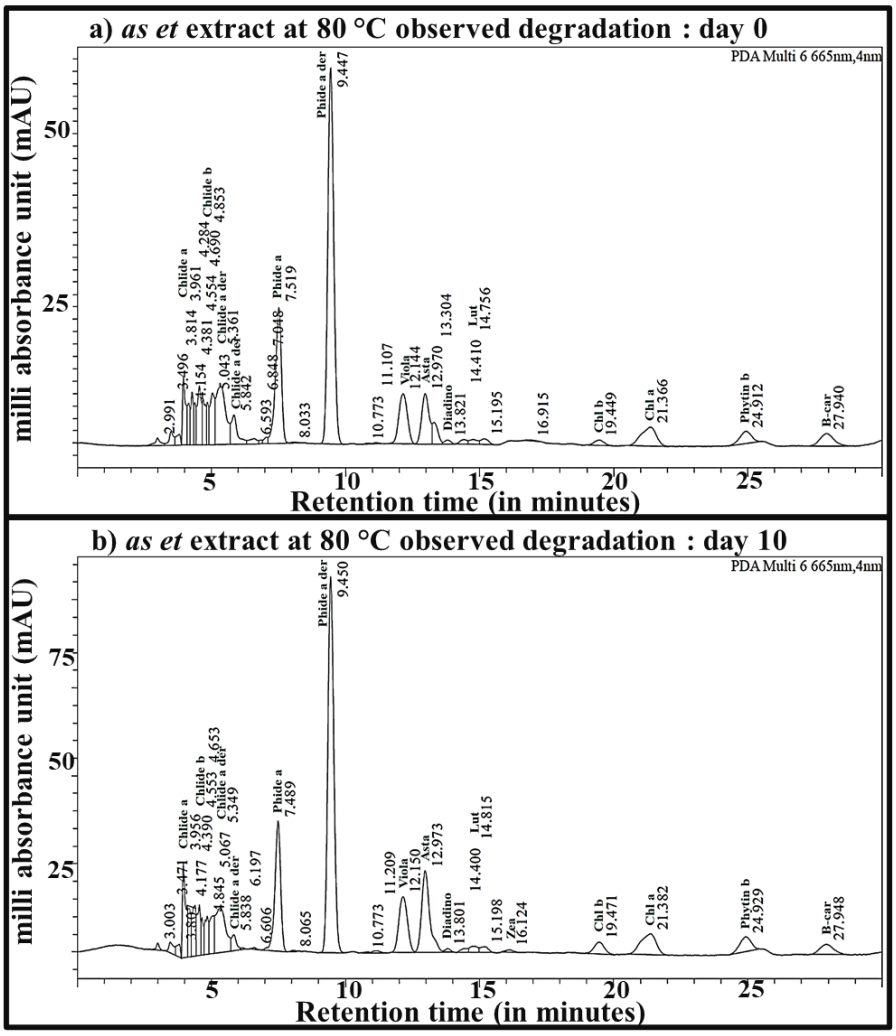

iii. *as* dye degradation at 665nm in *et*

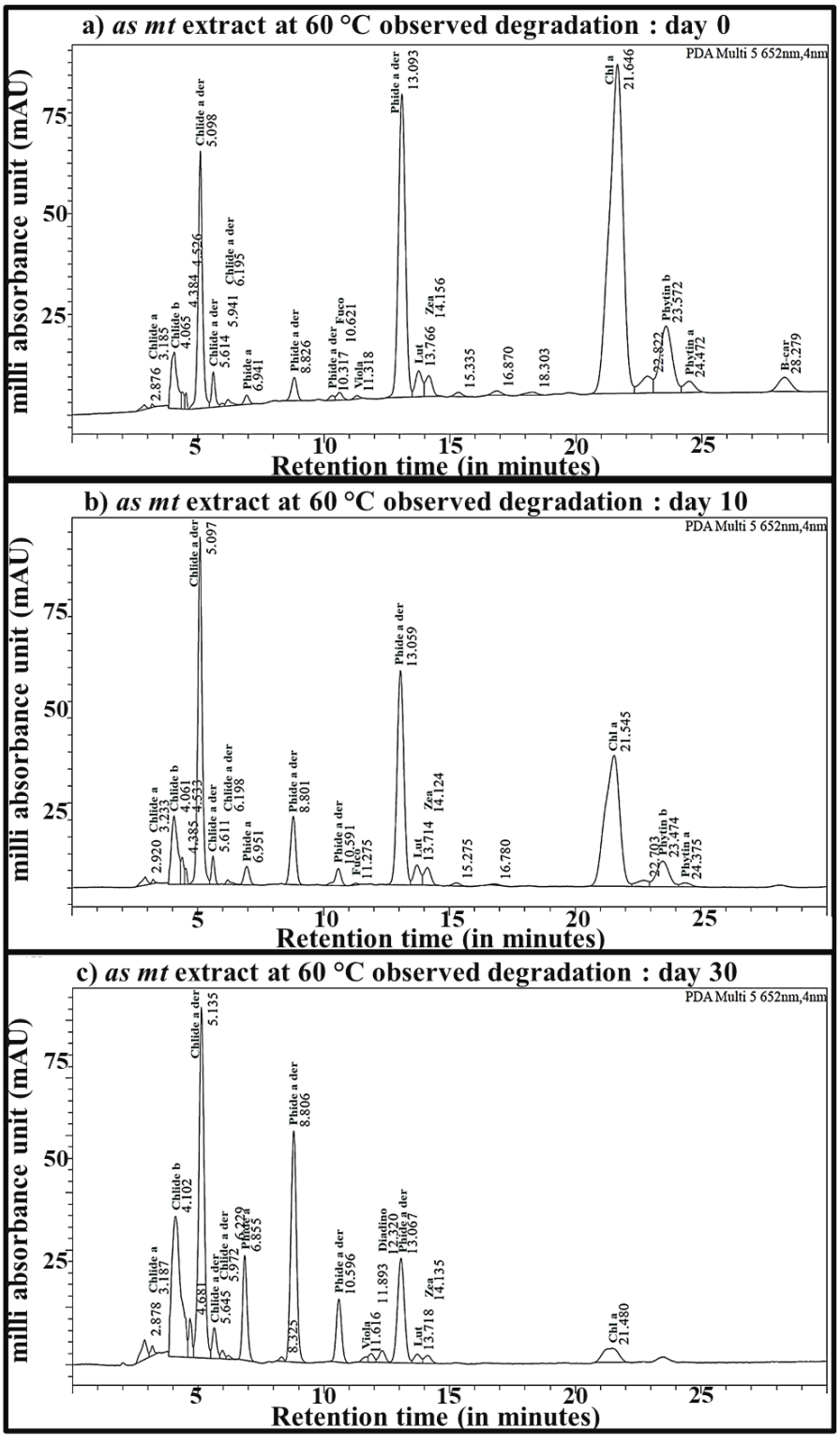

iv. *as* dye degradation at 652nm in *mt*

Figure 5.6. Spectra for stability of *sc* and *as* dyes at room temperature after extraction in *et* at 80 °C (665nm) and in *mt* at 60 °C (652nm) on a) 0th day b) the 10th day and c) the 30th day.

When the samples extracted from *sc* and *as* in **Figure 5.5.** were put to room temperature without any light for 10 days to 30 days the following changes as shown in **Figure 5.6.** were observed. **Figure 5.6.i.b.** shows the degradation at 665nm with *Chl a* content reducing drastically along with *Phide a* and its derivative. Other carotenoids also showed a peak reduction like that of *Viola* and *Diadino* but comparing all it can be understood that *Chl* was much less stable than others. The reduction can be an indicator that the pigment bonding has weakened due to high temperature-based extraction with *et*.

In **Figure 5.6.ii.** at 652nm which was far more favorable than 665nm due to lesser baseline fluctuations in the chromatograms, it was observed that *Chl a* degradation has turned more to *Phide a* derivative due to easy availability of hydroxide molecule within the *mt* solvent for this much longer duration. *Chlides* remained a constant somehow reducing only partially as probable with time and converting with phides.

In *as* dye *Chl a*, *Chl b*, *Phytin b*, and *B-car* remained somewhat constant while there was a reduction in peaks of *Phide a* derivative and *Chlides* alone. Also, *Viola* reduced slightly below *Asta* after 10 days. It can be understood that the intensity of reduction is not equal for all pigments but is selective on a few which are having higher presence in the dye.

In **Figure 5.6.iv.** there was a different kind of reduction in the peaks as we see in the a and b part of it at 652nm. In **Figure 5.6.iv.b.** it can be seen that *Chl a* has reduced but it is making *Chlide a* derivative on reduction and hence further adding to *Chlide a* derivative mAU value. Similarly, *Chl b* reduction has added to *Chlide b* enhancement. There were no major changes in carotenoids except the *B-car* going to complete extinction by day 10. Here, we have also added the data for day 30 to understand further the degradation after that and on day 30 it can be seen that *Chl a* reduced considerably and pigments like that of phytins have gone extinct. There is a huge reduction in the peak strength of *Phide a* and *Chlide a* derivatives throughout too [Zapata et al., 1987; Mendes et al., 2007; Nakamura et al., 2001].

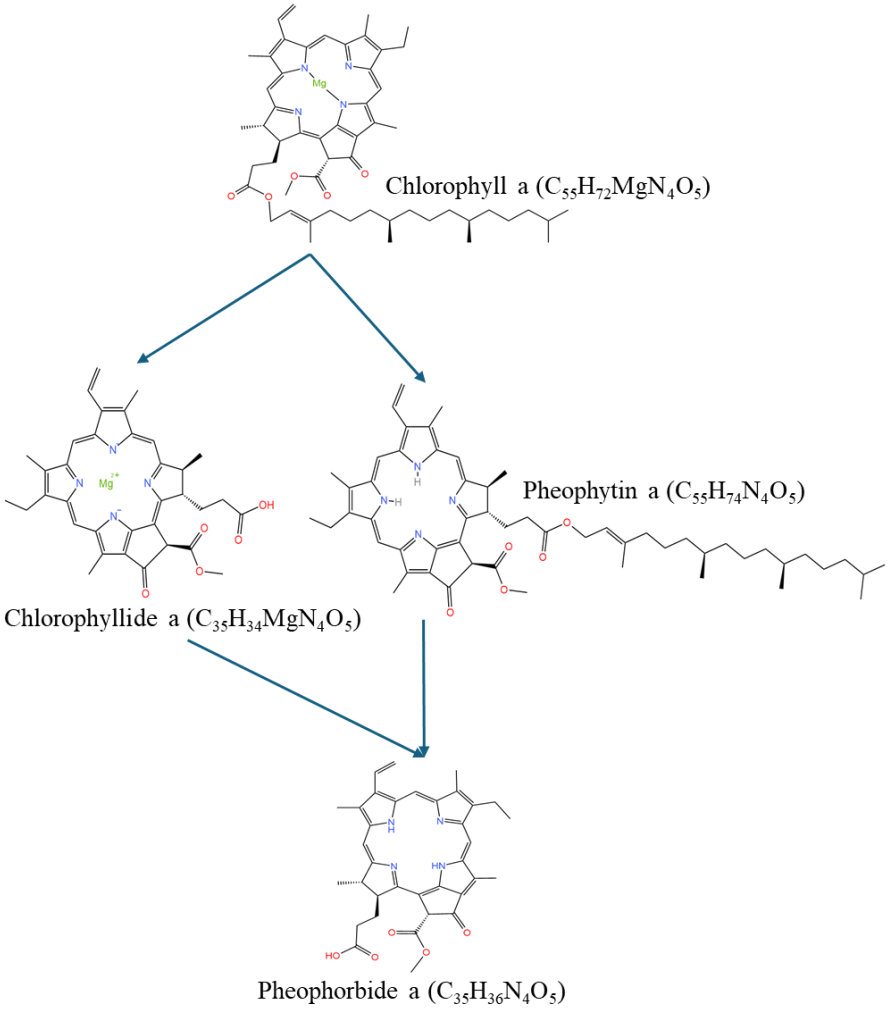
Chlorophyll a ($C_{55}H_{72}MgN_4O_5$)
Chlorophyllide a ($C_{35}H_{34}MgN_4O_5$)
Pheophytin a ($C_{55}H_{74}N_4O_5$)
Pheophorbide a ($C_{35}H_{36}N_4O_5$)

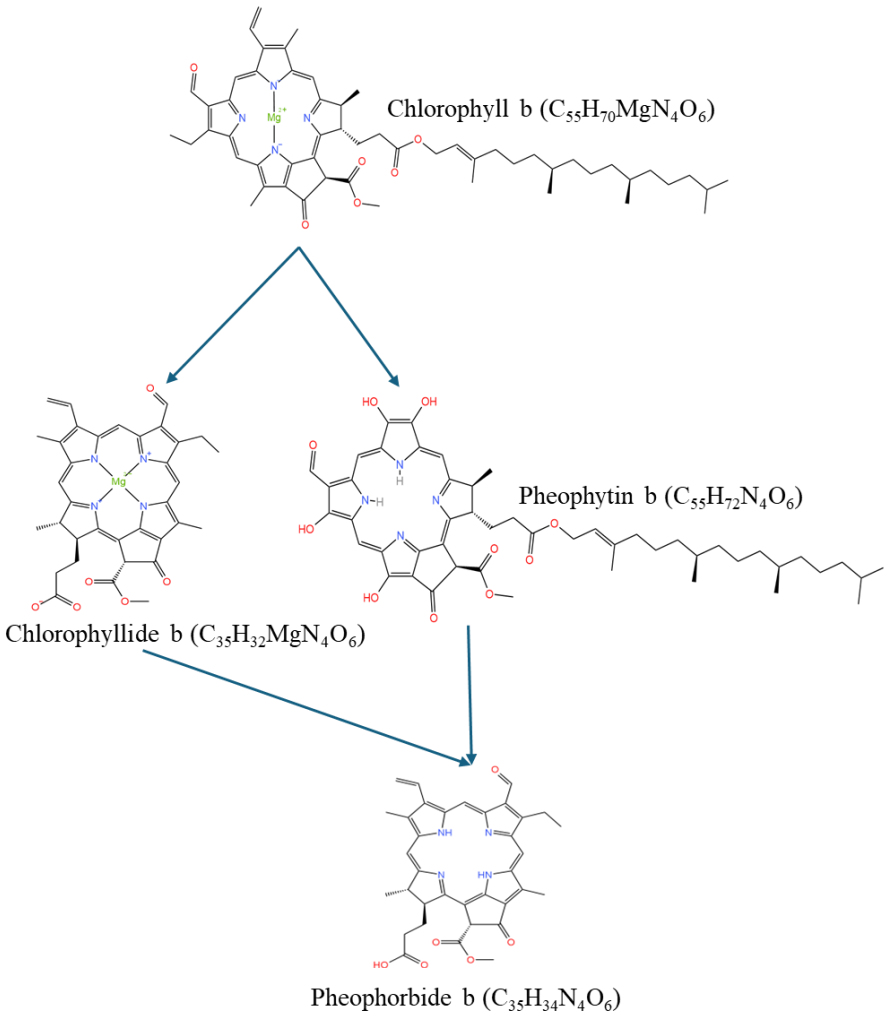

i. *Chl a* and b reactions with subsequent compound formation in dyes during extraction and storage.

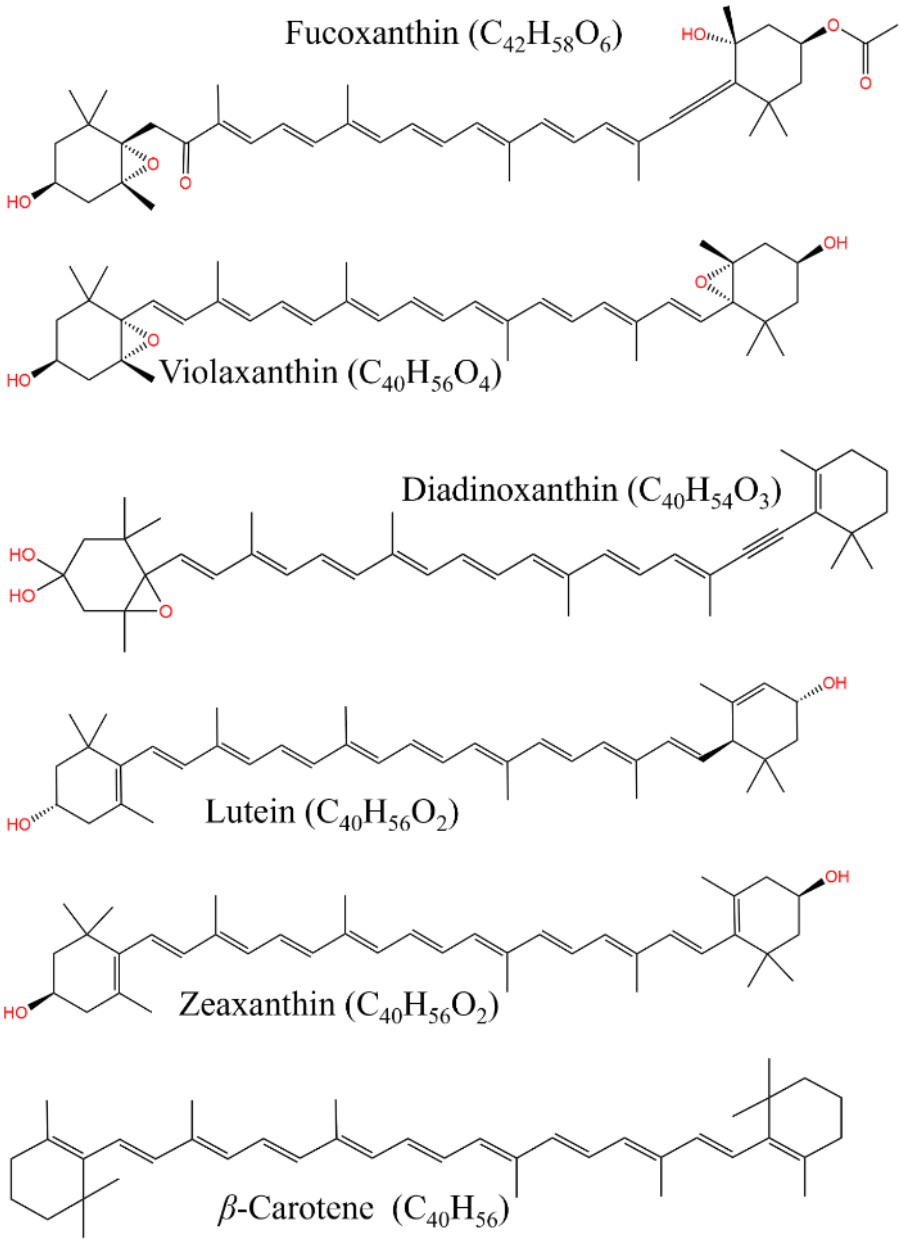

ii. Carotenoids present in dyes

Figure 5.7. *sc* and *as* dye pigments types and the degradation reaction taking place in the extracts.

So overall we have analyzed the formation of the following pigments as given in **Figure 5.7.** and the process taking place in the *Chl*-based pigments as mentioned in **Figure 5.7.i.** which is clear on the degradation happening during extraction and storage. It can be understood that *Chlide* and *Phide* are more constant in reduction. And if we extract more *Chl* than other degraded compounds then we can get

that dye to get more time to take for subsequent conversion to *Chlide*, *Phytin*, and finally *Phide* [Nakamura et al., 2001; Hu et al., 2013; Scheepers et al., 2011].

Overall during different solvent-based extractions, it can be understood that no substantial effect on the total *Chlide* concentration but just the *Phide* concentrations increased, respectively from the degradation of original *Chls, Chlides,* or *Phytins*. As *Chlide a* and b have the identical absorption spectrum as natural *Chls*, the conversion to these compounds will not affect the visible green color. In difference, the removal of magnesium ions from the green *Chls* heading to *Phytin a* and *b* may impact the color because pheophytins are somewhat brown and have a little varying absorption spectrum [Edelenbos et al., 2001; Van Heukelem & Thomas, 2001; Mendes et al., 2007].

5.7. Conclusions

Our research demonstrated that temperatures above 60 °C were not beneficial for the stability and extraction efficiency of *Chls* and other pigments. Also, several key aspects obtained underline the importance of utilizing different wavelengths in a photodiode array (PDA) detector for effective *Chl* identification:

a. Different *Chls*, exhibit distinct absorption spectra. Utilizing various wavelengths facilitates the identification of specific *Chl* types based on their characteristic absorption peaks. Optimizing the detection at their respective absorption maxima through different wavelengths enhances the accuracy and precision of quantitative analysis in *Chl*-containing samples.
b. *Chls* often coexist with other pigments. Multiple wavelengths help assess the purity of *Chl* by confirming the absence of interfering compounds through their unique absorption profiles.
c. In complex samples such as this, *Chl* peaks may overlap with other compounds. Scanning at various wavelengths helps

resolve these overlapping peaks, ensuring accurate identification and quantification of *Chls*.

d. Different extraction methods may influence *Chl* spectra. Multiple wavelengths help validate extraction methods by ensuring consistent and reliable identification of *Chl*.

This approach ensures reliable and accurate analysis, particularly when high temperatures above 60 °C are not suitable for maintaining *Chl* stability and extraction efficiency [Indriatmoko et al., 2015; Fernandes et al., 2020]. This has a connected significant impact on the longer duration of storage of the dye too as evaluated.

CHAPTER 6

Exploring the stability of extracted Dye Component Compounds

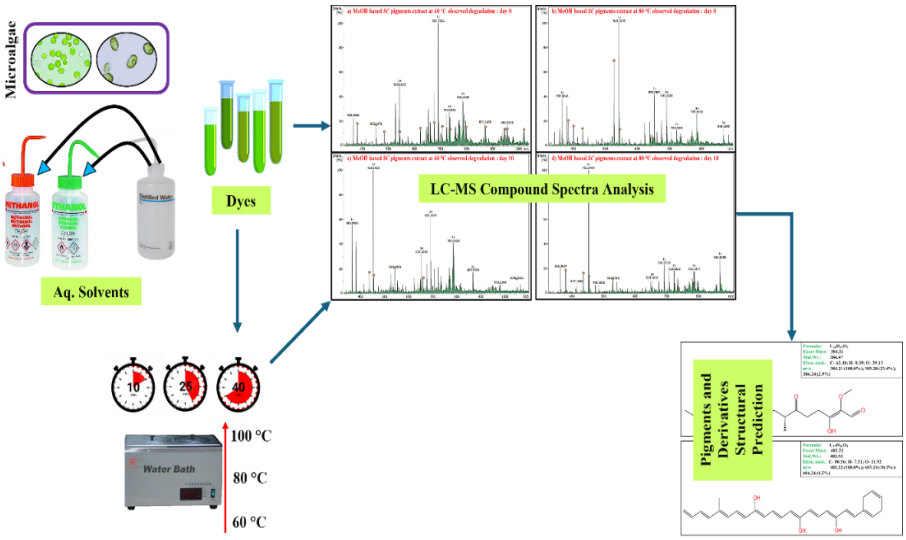

CHAPTER 6

Exploring the stability of extracted Dye Component Compounds

6.1. Introduction

Microalgal dyes hold promise for incorporation into dye-sensitized solar cells (DSSCs) owing to their generous abundance, eco-sustainable nature, and inexpensive fabrication [Chauhan et al., 2022]. These dyes are a mixture of pigments obtained from microalgae that can be sensitive to various factors like light, and temperature [Chauhan et al., 2023]. The use of natural dyes in DSSC has been countered by not enough provision of stability and narrow light absorption spectra hence not resulting in better efficiency [Karki et al., 2013].

The dyes are predominantly qualified with spectrophotometry but to overcome some of the inadequacies high-performance liquid chromatography (HPLC) has been investigated to obtain accurate data on causal photons absorbing pigments [van Leeuwe et al., 2006]. Liquid chromatography-mass spectrometry (LC-MS) combined with HPLC is used to avoid the confusion of subtle distinctions among various *Chls* but collecting HPLC's separated eluents of the individual pigments can be challenging [Jackson, 1979].

LC-MS has played a crucial role in gaining structural insights and this integrated tactic makes it comfortable to authorize the chief roles played by the pigments cum derivatives hence making them acknowledged and not blotted out in footings of spectra. LC-MS, in its entirety, enhances specificity by leveraging mass-to-charge ratio data [Huang et al., 2008].

LC-MS clarifies pigment composition in complex dye mixtures, deepening understanding of the sample's chemical makeup by determining the pigment's molecular weight. Further analysis of fragmentation patterns provides insights into its structural elements. By employing standard reference materials, the relative abundance and

breakdown of different comparative pigments can be known better [Canjura et al., 1991a]. Further facilitating LC-MS steps includes interpreting mass spectra for fragment ions, isotopic patterns, and adduct formations, and then searching databases for matches with observed LC-MS data. It further uses isotope labeling to distinguish between structural options and confirm proposed structures [Milenković et al., 2012].

Chl a and *b* pigments, exist in a typical ratio of 3 to 1 and contribute to the green color of all microalgae [Nwoba et al., 2020]. *Phytins* are *Chl* derivatives lacking the central magnesium atom and are formed during thermal activity or via the acidic environment when the magnesium atom in the center of the *Chl* porphyrin ring is substituted by hydrogen atoms, consequentially forming an olive-brown color [Mackinney & Joslyn, n.d.]. *Chlides* are formed when the phytol chain is removed from *Chl* and can further degrade to *Phide* under heat or acidic conditions. Pyropheophytins, formed during prolonged heat treatments are decarbomethoxylated derivatives of *Phytins* [Nowruzi et al., 2019]. *Chl* is significantly susceptible to these changes when heated above 80°C. The kinetics of *Chl* degradation follow a first-order model where *Chl a* degrades several times faster than *Chl b*.

Chlides are assumed to be more stable than *Chls*, and this approach showed minimal improvement in green color preservation due to the small amount of *Chlides* produced [Canjura et al., 1991a]. However, studies indicate that *Chlides* are less stable than *Chls* during thermal processing [Gupte et al., 1964]. In the mass spectrum of *Chl a*, the peak at m/z 893.8 corresponds to the molecular ion peak, and its fragmentation yields ions at around m/z 555.7 and at around 639.0, hence indicating the presence of specific molecular fragments [Müller et al., 2014]. Similarly, the mass spectrum of *Phytin a* shows a peak at m/z 871.7, confirming the removal of the magnesium atom from *Chl a*, and its fragmentation produces ions at m/z 533.5 and 593.3 [Wei & O'Connor, 2015]. The peak at m/z 614.2 of *Chlide a* yields ions at m/z 583.1 and 555.2 on fragmentation [Van Breemen et al., 1991].

6.2. Experimental Section

6.2.1. Materials and Reagents

The solvents of ethanol C_2H_6O, ≥ 99.8% pure, and methanol CH_4O, ≥ 99.8% pure were used. The concentration of the solvents was maintained at 80% by DI water addition.

6.2.2. Microalgal cultivation

Axenic cultures of freshwater microalgae species, *Scenedesmus sp.* (*sc*), and *Asterarcys quadricellulare* (*as*) were used. These were cultured in a standard BG-11 medium, a pH range of 7.2 to 7.4, [Chauhan et al., 2023; Chauhan et al., 2024a; Chauhan et al., 2024b].
The initial cultures were grown in Erlenmeyer flasks for 10 days after which derived axenic subcultures were used as primary cultures for subsequent experiments. Growth assessments were performed every 24 hours until the designated days for cultivation and dye extraction. These cultures were maintained in a dedicated culture room at a stable temperature of 27 ± 5 °C with a 12:12-hour photoperiod and dark phase [Stanier et al., 1971]. To ensure optimal growth, white fluorescent lamps were positioned at an appropriate distance from the cultures during the light phase, providing a light intensity of 3000 lux. The flasks containing these species were sampled for dye extraction on the 15^{th}, 20^{th}, and 25^{th} days, using *et* and *mt* separately.

6.2.3. Extraction

The hot solvent extraction method was applied to a known volume of the microalgal culture of a specific species. The solution was then centrifuged, and the supernatant was collected [Chauhan et al., 2024a; Chauhan et al., 2024b]. Photosynthetic pigments are sensitive to light, oxygen, and heat, as well as to bases and acids. All operations were done under dim light and keeping a reasonable laboratory temperature.

6.2.4. Instruments and Characterization

Bruker micrOTOF-Q II Daltonik Benchtop LC-MS spectrometer was used. The mobile phase was 100% *mt*. PTFE syringe filters were used with 0.22 μm pore size to clear up extracts before filling into the vial.

6.2.5. Pigment standards and Pigment identification

0.5 mg/ml of *B-car* standard (std.) in 80% ethanol and methanol was prepared separately for testing through LC-MS. Pigments were identified by their close peaks m/z value. Considering that the same pigment can be modified into several pigment derivatives with different values. Because methanolic extracts are known to promote *Chl* allomerization with prolonged storage, the samples were injected almost immediately after extraction and elution [LaJOLLO et al., 1971].

6.3. Result and Discussion

The pigments obtained were analyzed based on the following table 1.

Table 6.1. List of evaluated pigmental compounds with their basic descriptive information.

Compound Abbreviation	Molar Mass	Molecular Formula
Chlide a	615.9 g/mol	$C_{35}H_{34}MgN_4O_5$
Chlide b	614.9 g/mol	$C_{35}H_{32}MgN_4O_6$
Chlide a der	varies	varies
Phide a	592.7 g/mol	$C_{35}H_{36}N_4O_5$
Phide a der	varies	varies
Fuco	658.9 g/mol	$C_{42}H_{58}O_6$
Viola	600.9 g/mol	$C_{40}H_{56}O_4$
Diadino	582.9 g/mol	$C_{40}H_{54}O_3$
Lut	568.9 g/mol	$C_{40}H_{56}O_2$
Zea	568.9 g/mol	$C_{40}H_{56}O_2$
Chl b	907.5 g/mol	$C_{55}H_{70}MgN_4O_6$
Chl a	893.5 g/mol	$C_{55}H_{72}MgN_4O_5$

Phytin b	885.2 g/mol	$C_{55}H_{72}N_4O_6$
Phytin a	871.2 g/mol	$C_{55}H_{74}N_4O_5$
B-car	536.9 g/mol	$C_{40}H_{56}$

B-car std. when evaluated through LC-MS the peaks were as shown in **Figure 6.1.i**. It shows that the *B-car* std. in *et* had almost a fixed set of compound evolution with a significant value from the breakdown positioned at around an m/z value of 325. Whereas *mt* -extracted and stored compounds were seen as having multiple compound formations with 4 possessing a significant m/z value peak height positioned at 325 (with 100% intensity), 403, 301, and 279. These obtained peaks were used to reach the compound formed by using the "Process mass spectrum analyses with Bruker Compass Data Analysis" software and the compound library embedded in the in-house copy of the software of Bruker LC-MS [Zhang & Laursen, 2009; Airs & Garrido, 2011].

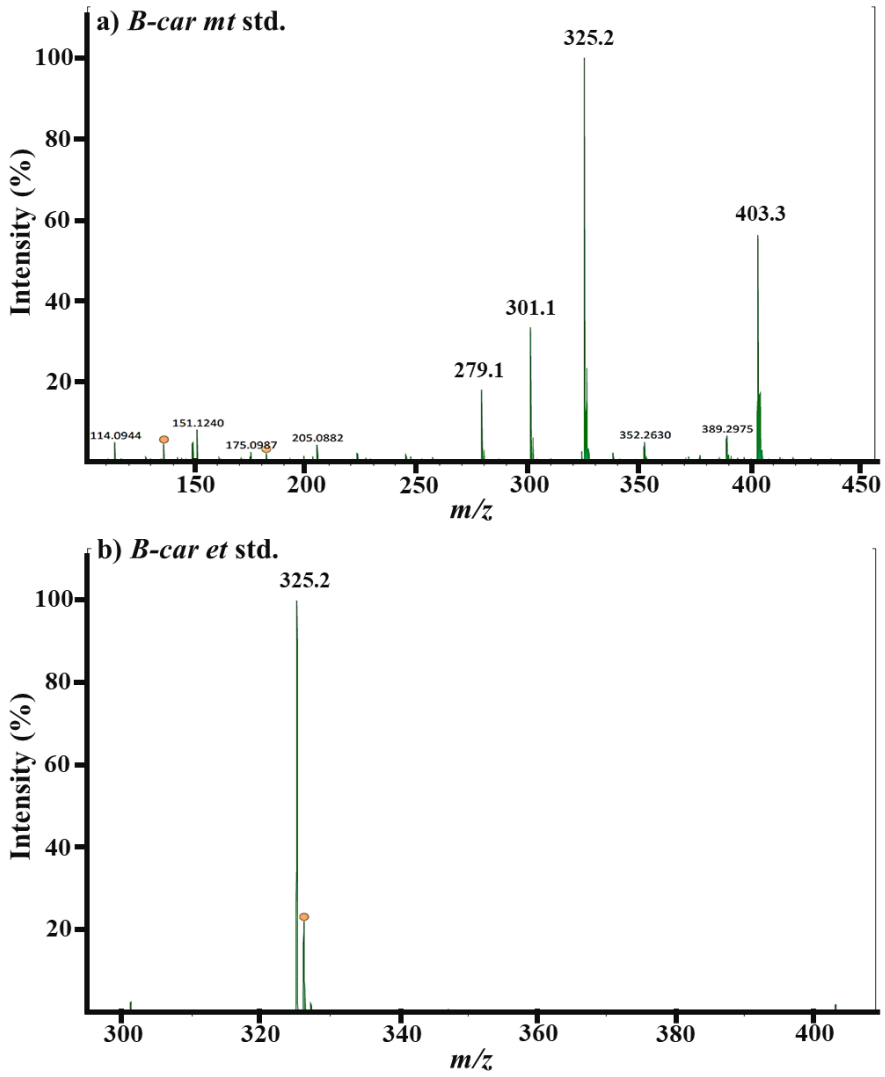

i. Compound Spectra of *B-car* std.

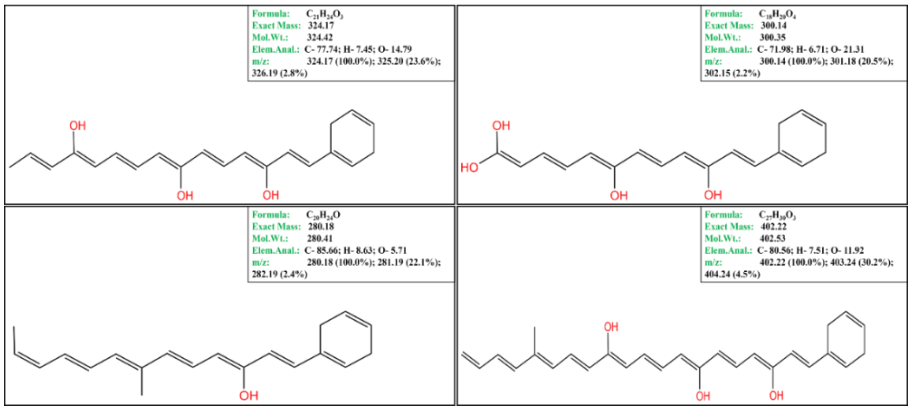

ii. Predicted structural compounds with chemical formula, molecular weight, elemental analysis, and m/z values derived from *B-car* std.

Figure 6.1. Std. *B-car* compound peaks with the added supplement of predicted degradation-based compound formation analysis in *et* and *mt*.

Now used the same software and similar pattern analysis by first going to the obtained chromatogram, then selecting range cum view spectra, and clicking on the peak of the chromatograph. Next to spectrum view, then copy to compound spectra as a compound. When Spectrum data is visible with the mass list, go to compound spectra and select smooth. Further, do smart formula manually, select both, adducts all, automatically locate isotopic peak and all. Then at compound spectra select deconvolute and on the right side spectrum data should have deconvolution results. Next in compound spectra select a smart formula and calculate the best possible structure with the elemental number that fits [Eckardt et al., 1990]. The obtained data is assembled and mentioned at the end for the structures and in the supplementary file too for values of the obtained peaks with the data connected to them.

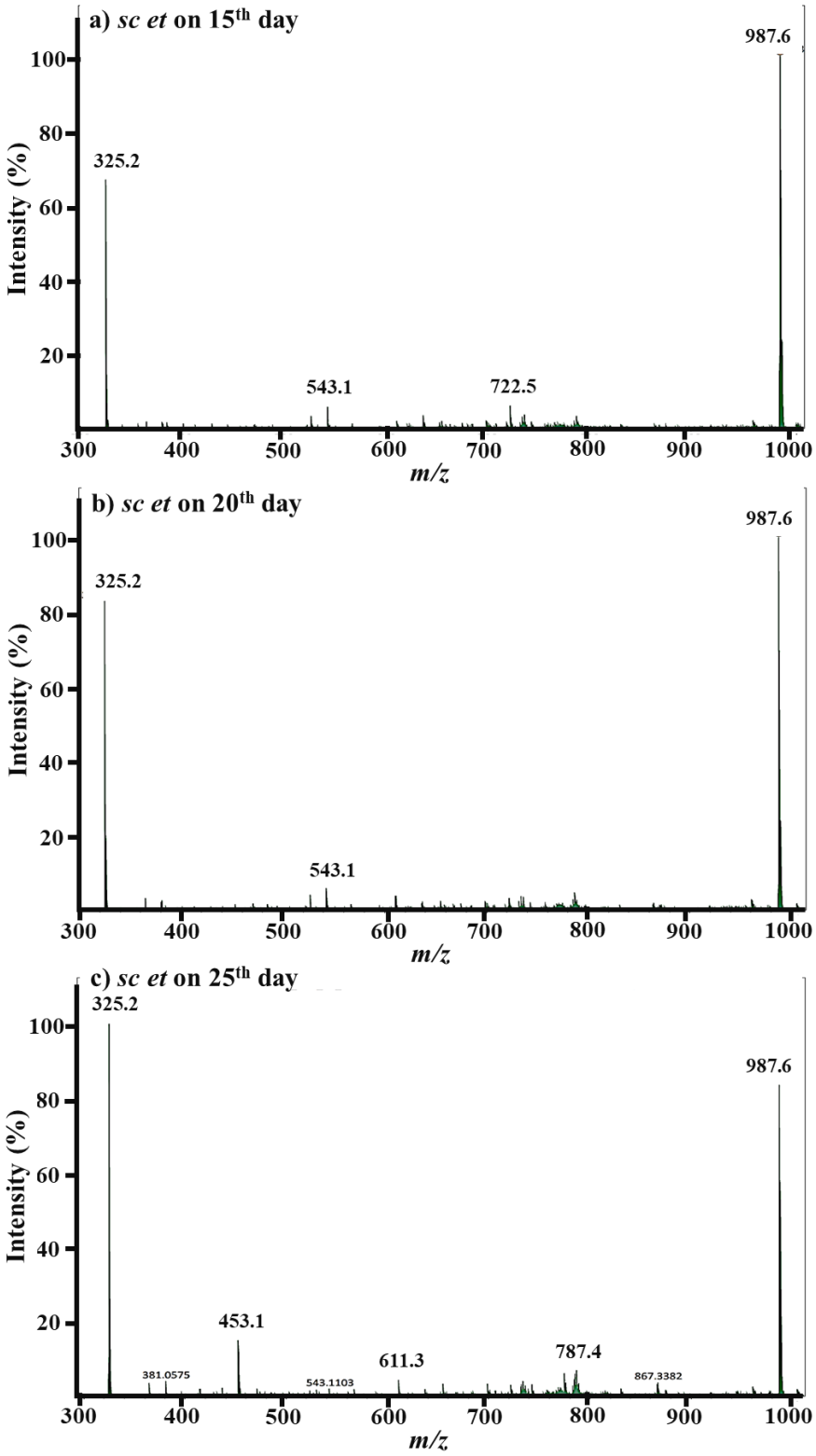

i. *sc* dye mass spectra was detected on the 15th, 20th, and 25th day of extraction via 80 % *et* as solvent at 80 °C.

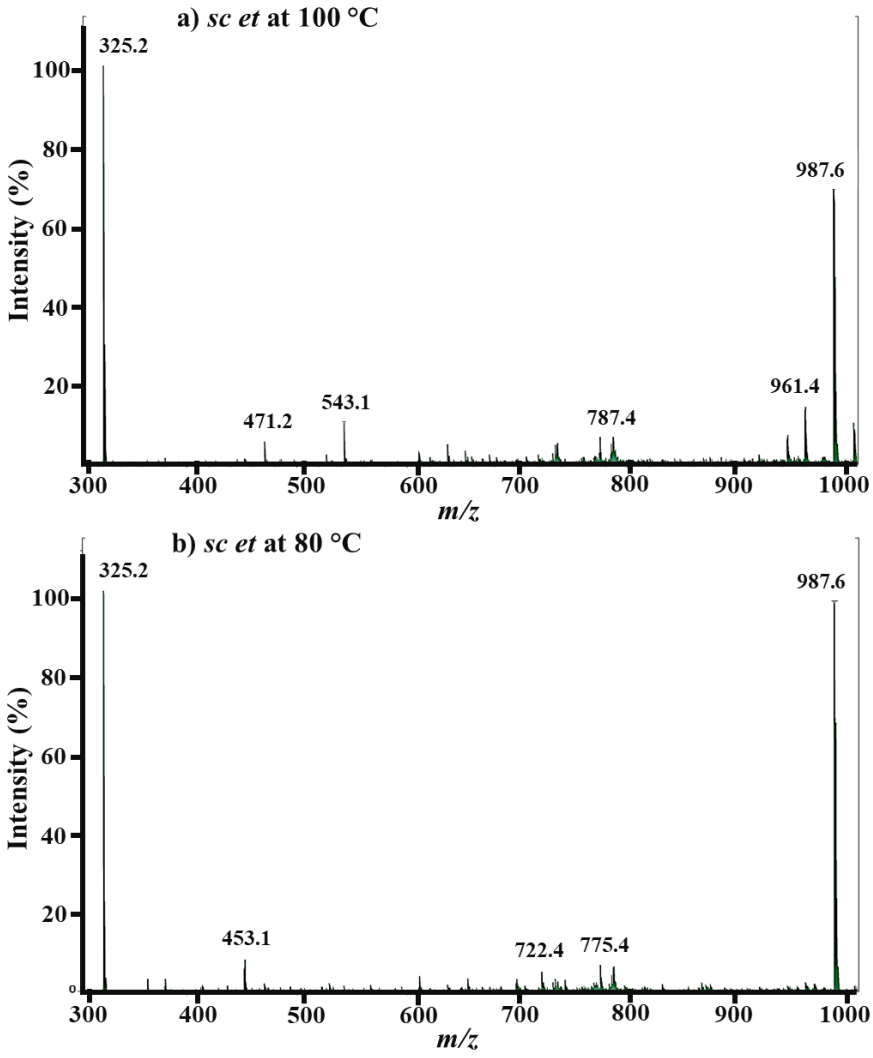

ii. *sc* dye mass spectra comparison with different temperature-based extractions of the same amount of biomass with the same duration of temperature.

Figure 6.2. Growth-oriented extraction and temperature-oriented extraction's compound formation analysis in *et* and *mt*.

In **Figure 6.2.i**. it can be seen that the pigment peaks dominate 2 positions in particular on all three days which are 325 and 987. If we go by the *Chl a* production rate, it is known to be maximum on the 20th day and reduces thereafter or gets a C*hl b* or other carotenoid conversion further. As it can be seen here too, the peak at 987 which is of a *Chl* oxidized derivative drops after the 20th day. Also, it can be

seen that the peak at 325 keeps on increasing throughout which symbolizes continuous weakening of *Chl* and breakdown to smaller molecular compounds or more conversion to carotenoids. The intermediate peaks also start to shift towards low molecular weight compounds formed by either breakdown or natural growth. For understanding the role of temperature it is shown by **Figure 6.2.ii.** where the peak at 987 has reduced at 100 °C and there is the formation of close peaks around 961 and at 941-943 due to that peak halt at an intensity of 67 % along with the rise of a noteworthy peak at 543. It is visually recognizable that the width of the peak at 325 has increased surely due to the formation and add-up of smaller compounds at that position consecutively [Fernandes et al., 2020]. 80 °C extraction seems to be preserving more of the heavy molecular weight or unfragmented structure of the pigmental compounds as intermediate compounds are also less.

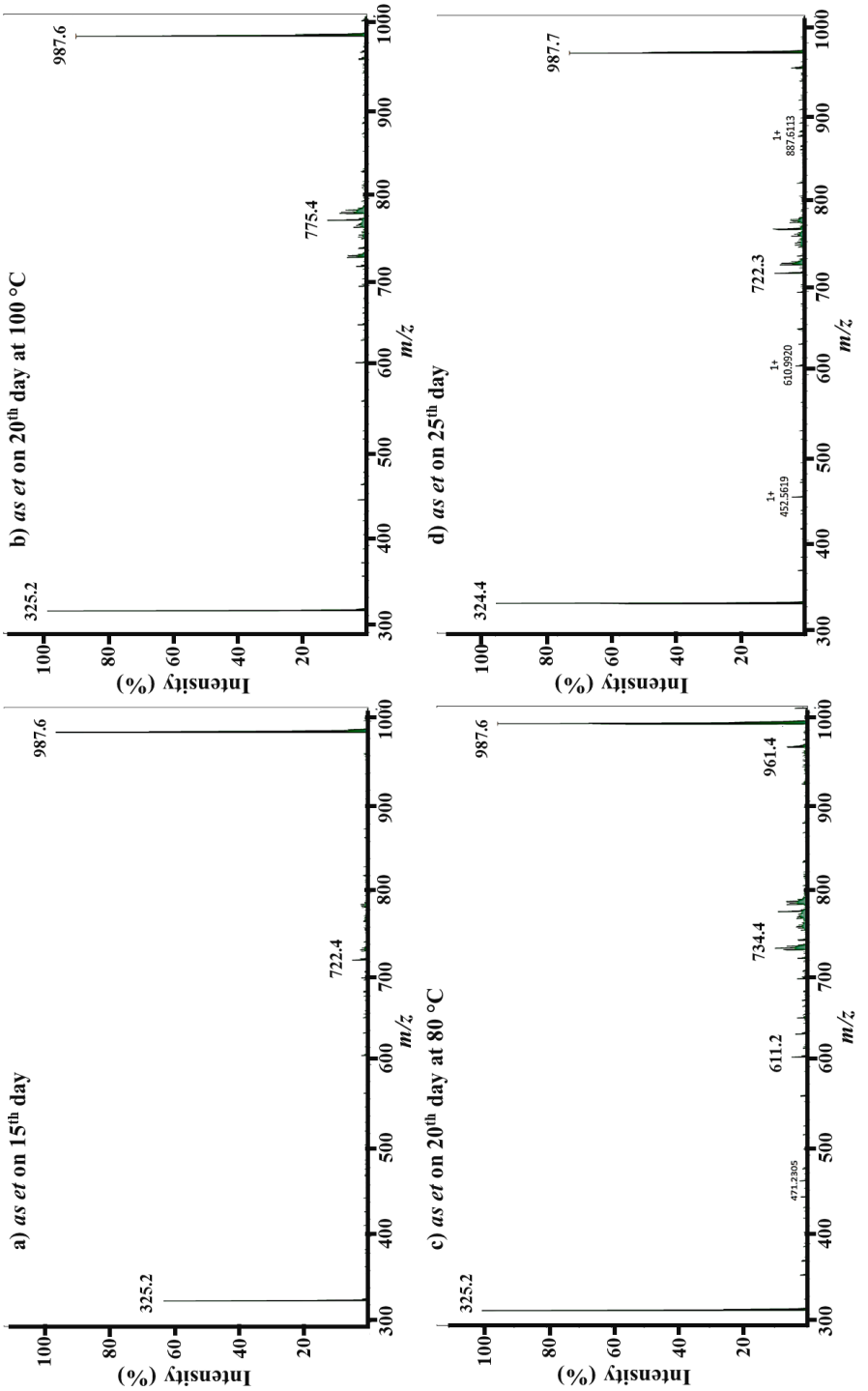

Figure 6.3. *as* dye mass spectra was detected on the 15th, 20th, and 25th day of extraction via 80 % *et* as solvent at 80 and 100 °C for the 20th day.

Figure 6.3. displays that the rate of *Chl* formation and degradation in *as* is as per that of *sc*. The 20th day as usual shows an overall

significant peak but the *Chl* derivatives remain the highest at 987 on the 15th day as confirmed by the thickness level and height of the peak there. It is also due to the loss of some peak to 961 m/z value at 80 °C as seen in c) subpart. *Chl* derivatives keep on decreasing with a continuous increase of the peak at 325 position, along with thickness, and intermediate products. The intermediary compounds formed out of degradation or oxidization are simply more in no. and heavy in molecular weight at 80 °C than at 100 °C as inferred from the figure. Overall it can be understood that *et*, breaks the compounds or aggregates them to a certain peak position as not many pigments can be recognized due to the specificity of compound breakdown based on molecular weights or m/z ratios [Walker et al., 2003; Loh et al., 2012]. However many formulas ought to be calculated based on these molecular weights alone for different pigment compounds.

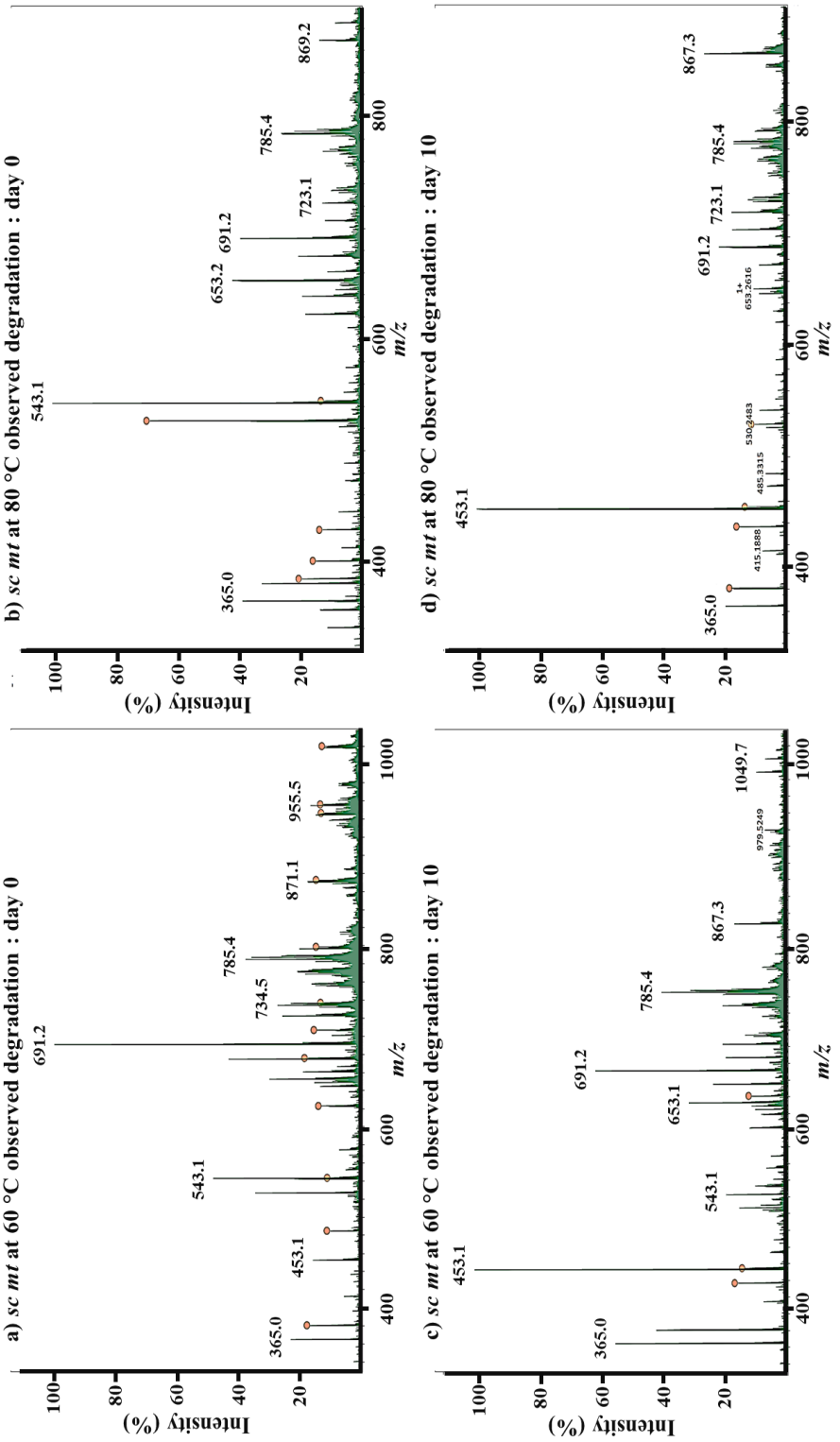

Figure 6.4. *sc* dye mass spectra extraction via 80 % *mt* as solvent at 80 and 60 °C for the 20th day and with storage for 10 days.

Figure 6.4. shows the difference in compound formation that is occurring during extraction based on temperature and storage. A

temperature of 60 °C is more favorable for extraction to safeguard more pigmental compounds of comparable high molecular weight as there are peaks at 691 and less significantly at 543 and 785. Whereas at 80 °C it is at 543 and 523, also at 691 and 653 but less significantly, and overall peaks are thinner in intensity. When tested again after 10 days it can be understood that the pigments at 80 °C that remained after extraction were in a fragile or unstable state and broke down to lower mass compounds as indicated by the complete absence of 543 and 523 m/z value compounds [Schwartz & Lorenzo, 1991]. Also, the compounds are trying to stabilize at 453 and other values like 867. At 60 °C the stabilisation also takes place at 453 and 867 but peaks at 691, 365, and 785 did not get eroded much.

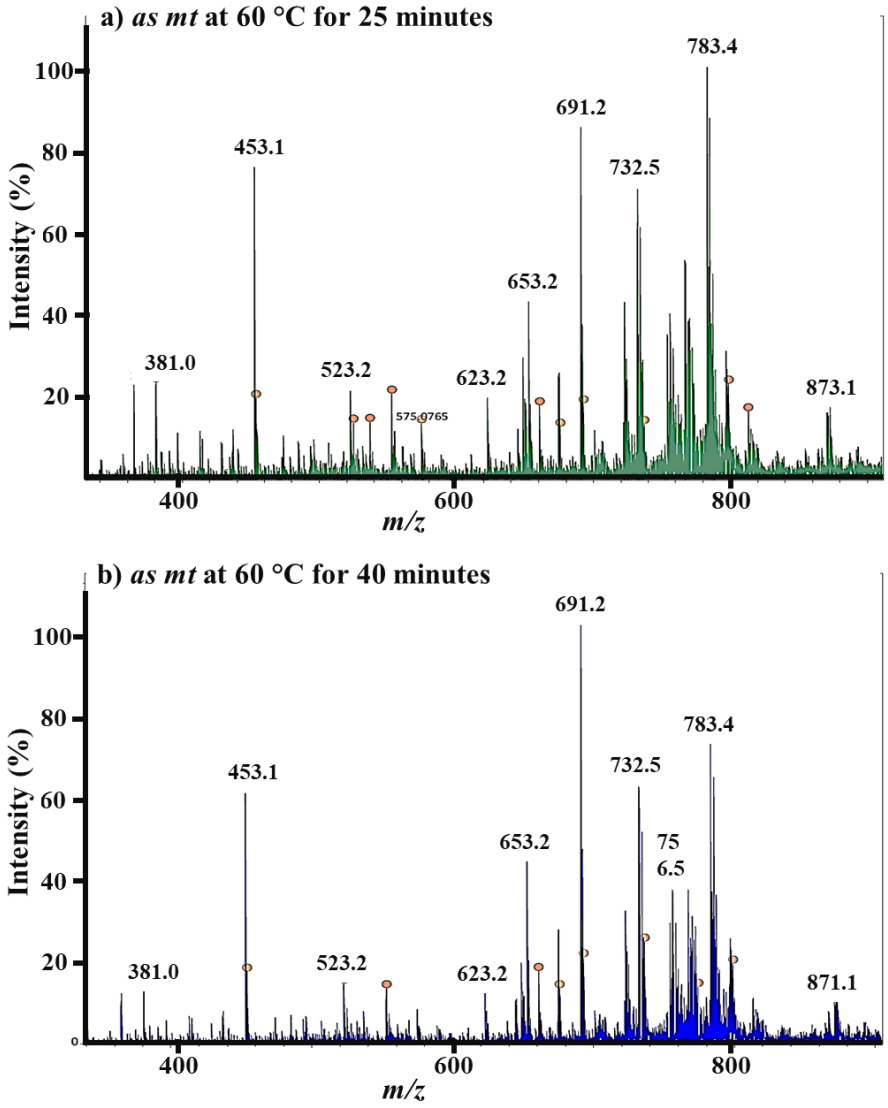

i. *as* dye extraction in *mt* via change of heating duration

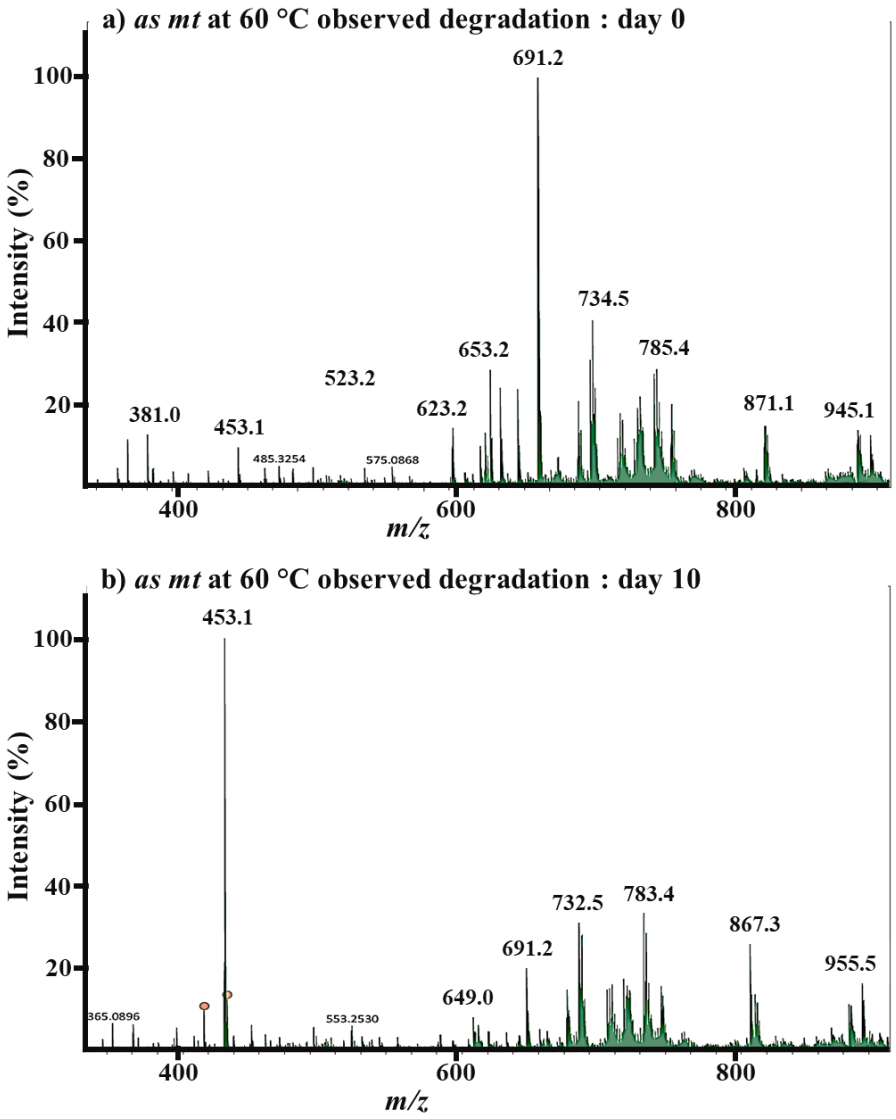

ii. *as* dye 10 days storage-based degradation analysis.

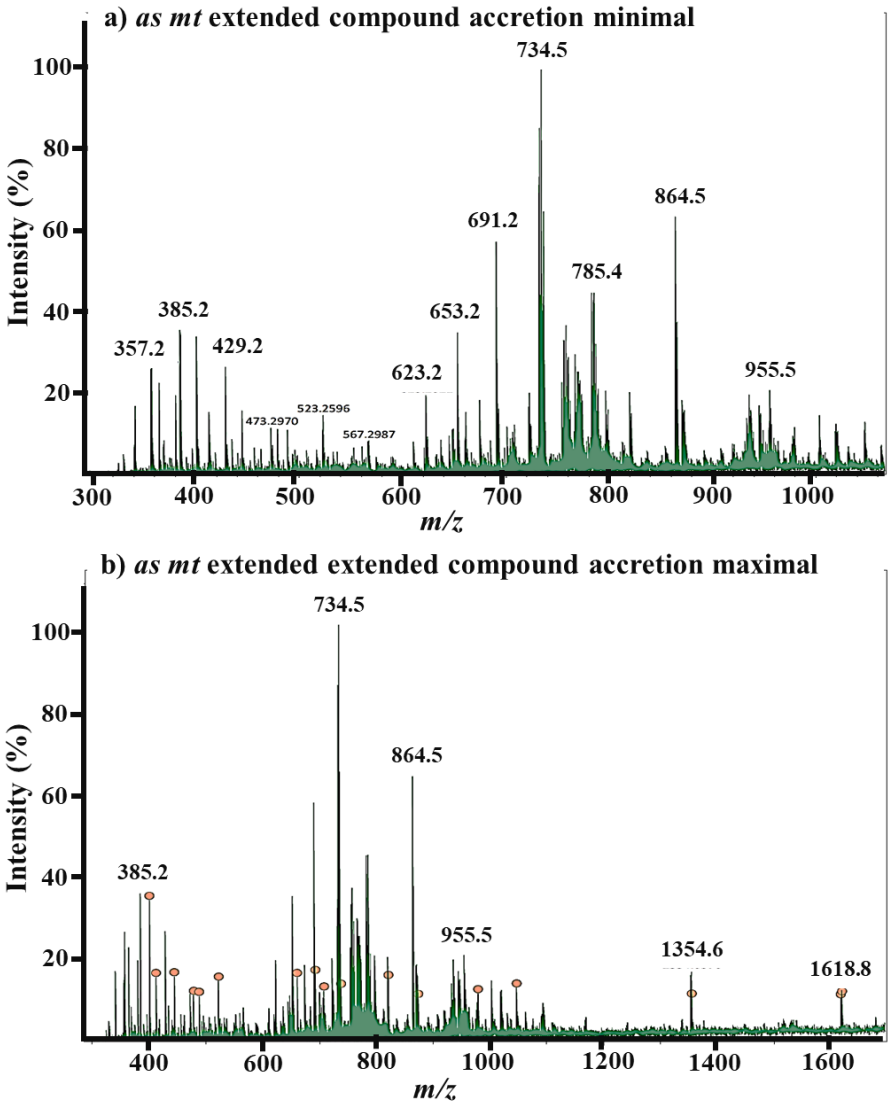

iii. *as* dye overall m/z range of compound formation by accretion

Figure 6.5. *as* dye mass spectra extraction via 80 % *mt* as solvent at 60 °C for the 20th day for 25 and 40 minutes of testing along with 25 minutes of extracted samples storage-based degradation observed for 10 days.

In **Figure 6.5.i.a.** it can be seen that the peaks are quite densely packed between 650 to 800 m/z value range which is more than the peaks in the same range in **Figure 6.5.ii.b**.. Particularly in this range, it can be seen that the 100% intensity peak has shifted to 691 from that of 783, after just 25 minutes of heating. They also get less and less broad

showing the possibility of settling with stability or degradation, along with a decrease in height of all major peaks even 453 [Buckle & Edwards, 1970].

Figure 6.5.ii. displays that the major peak value has shifted from 691 to 453 alongside losing the peak thickness too, infering a peak value shift and mass decline of almost 250 m/z value. Other peaks remain somewhat the same and show a minor shift towards lower molar mass in terms of intensity and thickness.

Figure 6.5.iii. is just an overview of the accretion range that needs to be taken into account but is not easily possible and we could just guess the best possibility ranges to be able to rightfully display convenient results. There is no pure peak gap among peaks and hence it is very tough to recognise which compound peak is a part of which breakdown or accretion of compound [Schanderl et al., 1962]. One more drawback of taking a bigger range is the loss of specificity of peak value cum isotope differentiation cum formula identifier or automatic labeling by the software. So the peaks below 5 % intensity were naturally ignored and all above were only taken into consideration in the supplementary file for calculating the formula and hence identifying the closest possibly formed compound.

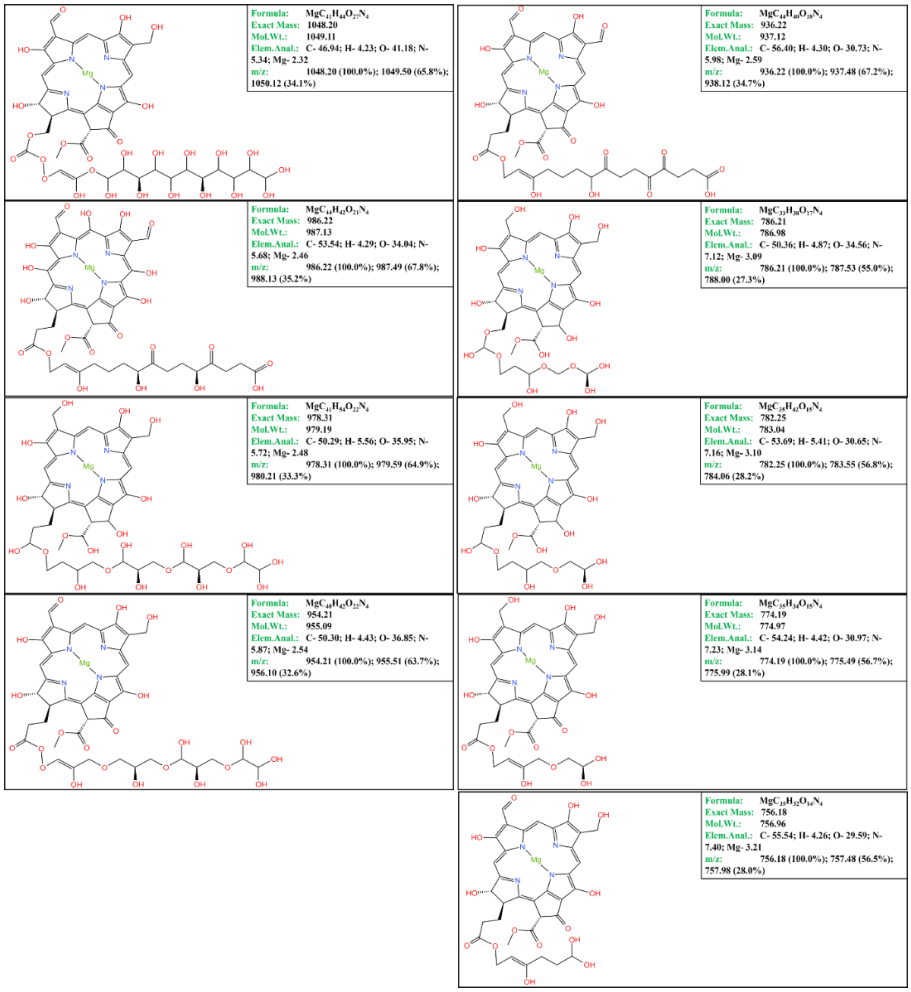

i. *Chl a* degraded and oxidized byproducts

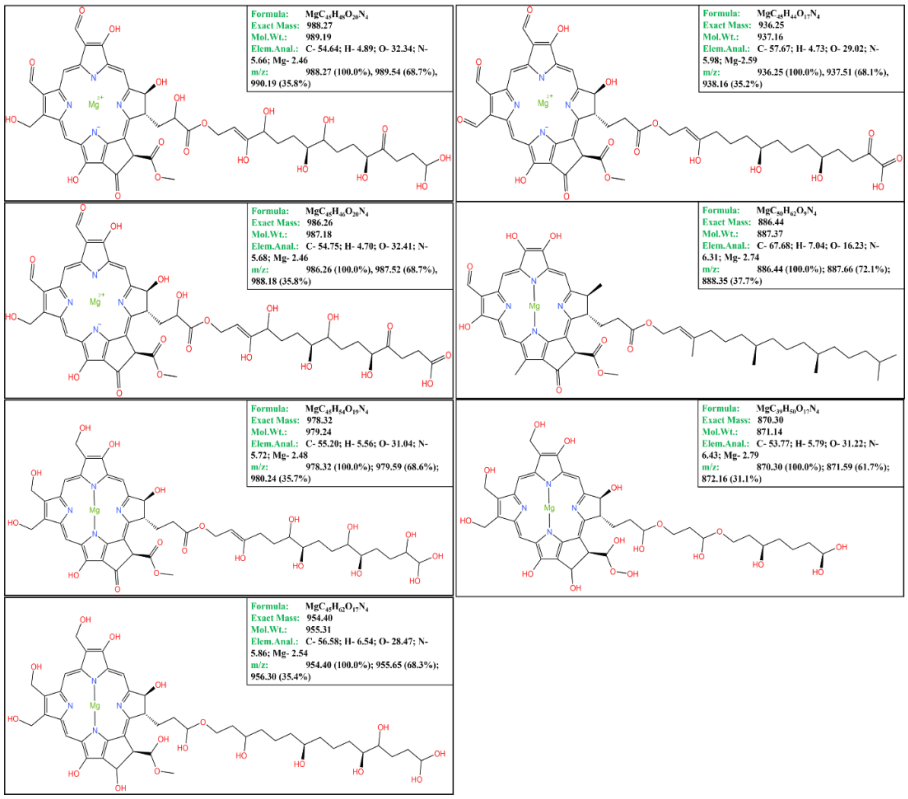

ii. *Chl b* degraded and oxidized byproducts

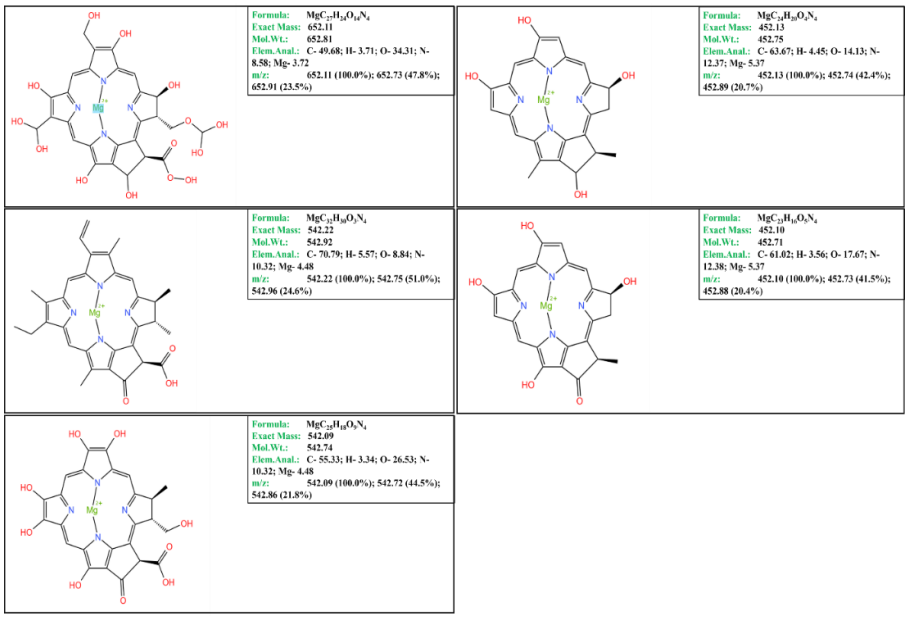

iii. *Chlide a* byproducts

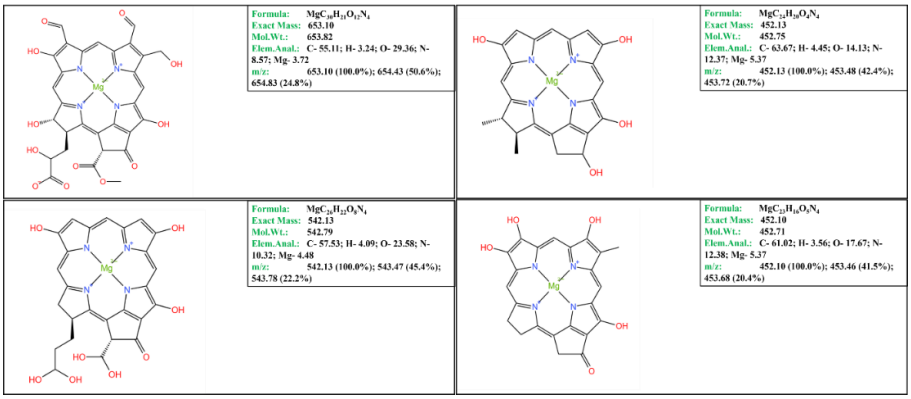

iv. *Chlide b* byproducts

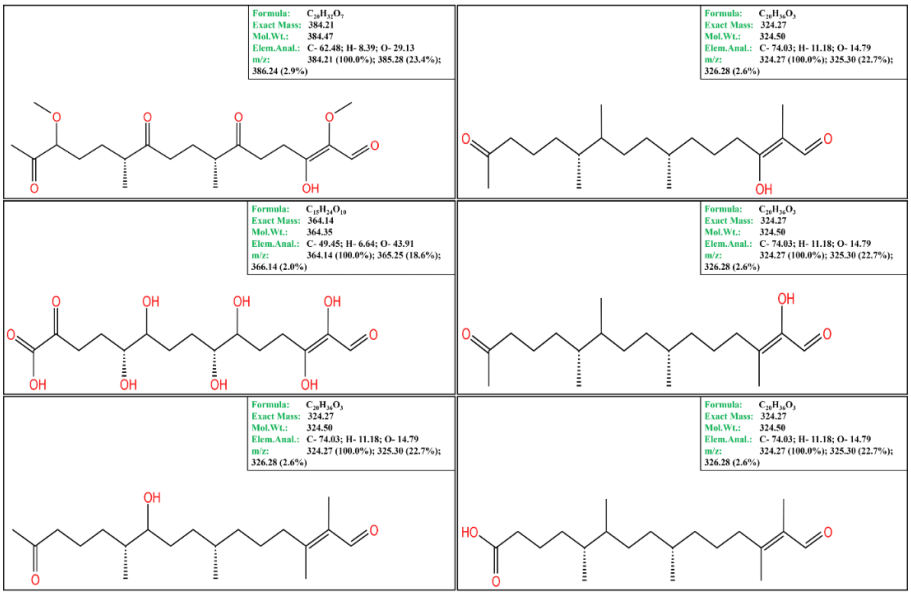

v. *Phytol* oxidized byproducts

Figure 6.6. Best possible structure formations of *Chl* and their derivatives and their shortlisted predicted characteristics based on the data of m/z value, peak intensity, elemental number, and chemical formula to mass [Suzuki et al., 2009; Diop et al., 2023].

6.4. Conclusions

Regarding the heat stability of *Chl a* and *Chl b*, it is evident that *Chl a* is less stable and thus degrades more quickly than *Chl b*. The higher

thermal stability of *Chl b* is due to the electron-withdrawing effect of its C-3 formyl group. *Chl* remains stable at relatively low extraction temperatures. The conversion of *Chl* to Phytin is visibly responsible for the color change from bright green to dull olive green. All the derived identified compound structures developed were based on parent peak, isotopes, electron difference, or 1 mass unit heavier than compounds strategy and resemble huge closeness to the actual possible compounds. These derived compounds like *Chlides* have similar porphyrin rings that empower them to precisely extract the same amount of energy when incorporated into DSSC dye. These microalgal dyes are hence capable of performing well in moderate temperature conditions and are less stable at high temperatures, longer storage, and high temperature-oriented extraction duration which can lead to degradation and reduced efficiency, otherwise, they maintain their structural integrity and continue to function effectively. This makes them attractive for large-scale applications in DSSCs, especially in regions with abundant natural resources. Extraction process improvement can enhance the molecular structure of natural dyes and develop better thermal encapsulation techniques to increase their efficiency and stability, overall, and finally far more stable natural DSSCs [Dutton et al., 1943; Wang et al., 2007].

CHAPTER 7

Conclusion and Future Perspectives

CHAPTER 7

Conclusions and Future Perspectives

7.1. Conclusions

The investigation of using microalgal dyes for dye-sensitized solar cells (DSSCs) has yielded significant insights and promising results. This study not only validated the potential of specific microalgal species as sources for efficient and stable dyes but also optimized the extraction methods to enhance their performance in DSSCs.

The study has successfully demonstrated the viability of microalgal dyes for DSSCs, offering a promising, sustainable, and eco-friendly alternative to synthetic dyes. The findings provide a strong foundation for further research and development, paving the way for more efficient and stable natural dye-based solar cells. Continued innovation and optimization will be essential in unlocking the full potential of microalgal dyes for renewable energy solutions.

The research highlights the significant potential of microalgal dyes in solar energy applications, with promising results that address key challenges in the field. By building on these findings and exploring new avenues for improvement, the future of microalgal dye-based DSSCs looks bright, offering a sustainable and efficient solution for renewable energy.

Here are the summarized key findings and discussion for the future directions that could further improve and scale the application of these natural dyes in solar energy harvesting.

7.2. Key Findings:

7.2.1. Effective Microalgal Species and Solvent Selection:

The screening process identified six microalgal species for their potential in dye extraction. Among these, *Scenedesmus sp.* and *Asterarcys quadricellulare* emerged as the most promising candidates

due to their superior photosensitizing properties. The UV-Vis spectroscopic analysis confirmed the presence of key pigments, such as chlorophyll a, chlorophyll b, and carotenoids, with absorption peaks well-suited for solar energy conversion.

Ethanol, particularly at an 80% concentration, was found to be the optimal solvent for extracting these dyes. This solvent consistently outperformed acetone and methanol, with methanol showing effectiveness only at higher concentrations. Ethanol provided the best balance between extraction efficiency and dye stability, making it the preferred choice for further studies.

7.2.2. Optimization of Extraction Conditions and other characteristics:

The efficiency of pigment extraction was closely tied to the growth period of the microalgae, with the 20^{th} day being optimal. This timing was crucial for achieving maximum pigment yield before degradation processes began. The study compared cold and hot solvent extraction methods, revealing that hot extraction significantly increased pigment yield and stability, especially when combined with sonication. Sonication at 80% ethanol concentration, in particular, extracted significantly more dye compared to traditional methods, with the dyes remaining stable for nearly 80 hours.

Reflectance spectroscopy showed that *Scenedesmus* sp. pigment in aqueous ethanol had the least reflectance, indicating higher light absorption efficiency. This was further supported by photoelectron energy spectroscopy, where *Scenedesmus* sp. dye required the least energy for electron excitation, demonstrating its effectiveness as a photosensitizer.

7.2.3. Structural and Morphological Characteristics of DSSC and efficiency:

The photoanode preparation involved developing a semiconducting layer on glass substrates using TiO_2 nanorods. These nanorods,

synthesized via the hydrothermal method, exhibited high purity and crystallinity, as confirmed by X-ray diffraction analysis and scanning electron microscopy. The vertical alignment and increased surface area of the nanorods facilitated better light absorption and electron transport.

Integrating microalgal dyes into these photoanodes resulted in a maximum power conversion efficiency (PCE) of 0.25%. This performance, although modest, demonstrated the feasibility of using natural dyes in DSSCs and highlighted the need for further optimization to improve efficiency.

7.2.4. Degradation and Storage Analysis:

HPLC and LC-MS analyses provided detailed insights into the degradation and stability of the extracted dyes. *Scenedesmus* sp. dye showed significant peaks corresponding to stable pigment compounds, with storage tests indicating notable pigment degradation over time, especially when stored at room temperature in darkness. Ethanol extraction yielded higher but more degraded products than methanol, which better-preserved pigment stability.

It was also observed in the study that elevated extraction temperatures above 60 °C were found to be detrimental to chlorophyll stability, leading to rapid degradation. Lower extraction temperatures and prolonged sonication preserved dye stability, with *Scenedesmus* sp. dye extracted at 80 °C in ethanol showing consistently higher compound formations over time.

- **Optimization and Stability:**
  Chromatographic and spectroscopic analyses identified optimal extraction periods and highlighted the effects of storage conditions on dye stability. Methanol preserved pigment stability better than ethanol, although ethanol-extracted dyes yielded higher pigment amounts.
- **Degradation and Compound Formation:**

Elevated extraction temperatures led to rapid degradation of chlorophylls, underscoring the need for lower-temperature extraction methods. LC-MS analysis revealed the formation of various degradation products, providing insights into the stability challenges and potential improvements for dye longevity.

7.3. Implications for Future Microalgal DSSC Development

1. **Dye Stability and Extraction Optimization**
2. Optimize microalgal dye stability with eco-friendly additives and low extraction temperatures to extend dye lifespan in continuous bio-reactor solar cells.**Extraction Conditions**

   Fine-tune solvent concentration, temperature, and duration for efficient dye extraction, using hot solvent extraction and sonication to maximize yield and stability.
3. **DSSC Component Improvement**

   Improve DSSC components (electrolytes, counter electrodes) for better performance. Carbon counter electrodes reduce costs but may limit efficiency, requiring further optimization.
4. **Direct Energy Production from Microalgae**

   Harness microalgae for direct energy production, mimicking photosynthesis to enhance solar energy harvesting efficiency and sustainability in bio-reactor systems.
5. **Biomaterials and Fabrication Innovations**

   Develop advanced biomaterials and fabrication techniques to improve light absorption, electron transport, and temperature tolerance in bio-reactor solar cells.
6. **Scaling Up Production**

   Scale microalgal dye production for large-scale, cost-effective, and sustainable bio-reactor solar cells to meet energy demands.
7. **Environmental and Economic Viability**

   Use microalgal dyes as eco-friendly alternatives to synthetic dyes, focusing on cost-efficient production and disposal for long-term viability and adoption.

REFERENCES

- Abdelfattah, A., Ali, S. S., Ramadan, H., El-Aswar, E. I., Eltawab, R., Ho, S.-H., Elsamahy, T., Li, S., El-Sheekh, M. M., Schagerl, M., Kornaros, M., & Sun, J. (2023). Microalgae-based wastewater treatment: Mechanisms, challenges, recent advances, and future prospects. Environmental Science and Ecotechnology, 13, 100205. https://doi.org/10.1016/j.ese.2022.100205
- Acemoglu, M., Uebelhart, P., Rey, M., & Eugster, C. H. (1988). Synthese von Enantiomerenreinen Violaxanthinen und Verwandten Verbindungen. Helvetica Chimica Acta, 71(5), 931–956. https://doi.org/10.1002/hlca.19880710502
- Adhikary, D., Forsyth, J. A., Murch, S. J., & Deyholos, M. K. (2020). Impact of betacyanins on responses to ultraviolet radiation inamaranthus tricolorL. Journal of Plant Interactions, 15(1), 117–126. https://doi.org/10.1080/17429145.2020.1766584
- Aftabuzzaman, M., & Kim, H. (2018). Porous Carbon Materials as Supreme Metal-Free Counter Electrode for Dye-Sensitized Solar Cells. Emerging Solar Energy Materials. https://doi.org/10.5772/intechopen.75398
- Ahmad, S., Yum, J., Butt, H., Nazeeruddin, M., & Grätzel, M. (2010). Efficient Platinum-Free Counter Electrodes for Dye-Sensitized Solar Cell Applications. Chemphyschem, 11(13), 2814-2819. https://doi.org/10.1002/cphc.201000612
- Airs, R. L., & Garrido, J. L. (2011). Liquid chromatography-mass spectrometry for pigment analysis. Phytoplankton Pigments, 314–342. https://doi.org/10.1017/cbo9780511732263.011
- Alami, A., Rajab, B., Abed, J., Faraj, M., Hawili, A., & Alawadhi, H. (2019). Investigating various copper oxides-based counter electrodes for dye sensitized solar cell applications. Energy, 174, 526-533. https://doi.org/10.1016/j.energy.2019.03.011
- Alamri, S. (2003). The growth of CdTe thin film by close space sublimation system. Physica Status Solidi (A), 200(2), 352-360. https://doi.org/10.1002/pssa.200306691

- Alexis De Vos. (1983). The fill factor of a solar cell from a mathematical point of view. Solar Cells, 8(3), 283-296. https://doi.org/10.1016/0379-6787(83)90067-4
- Aly, A. (2017). Performance Evaluation of Nanostructured Solar Cells. Nanostructured Materials - Fabrication to Applications. https://doi.org/10.5772/67405
- Anand, M., & Suresh, S. (2015). Marine seaweed Sargassum wightii extract as a low-cost sensitizer for ZnO photoanode based dye-sensitized solar cell. Advances in Natural Sciences: Nanoscience and Nanotechnology, 6(3), 035008. https://doi.org/10.1088/2043-6262/6/3/035008
- Arkan, F., & Izadyar, M. (2017). The role of solvent and structure in the kinetics of the excitons in porphyrin-based hybrid solar cells. Solar Energy, 146, 368-378. https://doi.org/10.1016/j.solener.2017.03.006
- Armeli Minicante, S., Ambrosi, E., Back, M., Barichello, J., Cattaruzza, E., & Gonella, F. et al. (2016). Development of an eco-protocol for seaweed chlorophylls extraction and possible applications in dye sensitized solar cells. Journal of Physics D: Applied Physics, 49(29), 295601. https://doi.org/10.1088/0022-3727/49/29/295601
- Armendáriz-Mireles, E. N., Calles-Arriaga, C. A., Pech-Rodríguez, W., Castillo-Robles, A., & Rocha-Rangel, E. (2023). Alternative sources of natural photosensitizers: Role of algae in dye-sensitized solar cell. Colorants, 2(1), 137–150. https://doi.org/10.3390/colorants2010010
- Arnon, D. I. (1949). Copper enzymes in isolated chloroplasts. Polyphenoloxidase in beta vulgaris. Plant Physiology, 24(1), 1–15. https://doi.org/10.1104/pp.24.1.1
- Arslan, B., Güzel, E., Kaya, T., Durmaz, V., Keskin, M., & Avcı, D. et al. (2019). Novel D-π-A organic dyes for DSSCs based on dibenzo [b,h][1,6]naphthyridine as a π-bridge. Dyes and Pigments, 164, 188-197. https://doi.org/10.1016/j.dyepig.2019.01.027

- Asbury, J., Hao, E., Wang, Y., Ghosh, H., & Lian, T. (2001). Ultrafast Electron Transfer Dynamics from Molecular Adsorbates to Semiconductor Nanocrystalline Thin Films. The Journal of Physical Chemistry B, 105(20), 4545-4557. https://doi.org/10.1021/jp003485m
- Avetta, P., Bella, F., Bianco Prevot, A., Laurenti, E., Montoneri, E., Arques, A., & Carlos, L. (2013). Waste Cleaning Waste: Photodegradation of Monochlorophenols in the Presence of Waste-Derived Photosensitizer. ACS Sustainable Chemistry & Engineering, 1(12), 1545-1550. https://doi.org/10.1021/sc400294z
- Aztatzi-Rugerio, L., Granados-Balbuena, S. Y., Zainos-Cuapio, Y., Ocaranza-Sánchez, E., & Rojas-López, M. (2019). Analysis of the degradation of Betanin obtained from beetroot using Fourier transform infrared spectroscopy. Journal of Food Science and Technology, 56(8), 3677–3686. https://doi.org/10.1007/s13197-019-03826-2
- B., H., S., A., Shanmukappagouda, J., K., Devaiah C., T., R., S., Balakrishna, R. G., & T.N., A. (2019). New 2-methoxy-4,6-bis(4-(4-nitrostyryl)phenyl)nicotinonitrile: Synthesis, characterization and DSSC study. Journal of Photochemistry and Photobiology A: Chemistry, 377, 75–79. https://doi.org/10.1016/j.jphotochem.2019.03.032
- Baby, R., Nixon, P., Kumar, N., Subathra, M., & Ananthi, N. (2021). A comprehensive review of dye-sensitized solar cell optimal fabrication conditions, natural dye selection, and application-based future perspectives. Environmental Science And Pollution Research. https://doi.org/10.1007/s11356-021-16976-8
- Baran, W., Makowski, A., & Wardas, W. (2008). The effect of UV radiation absorption of cationic and anionic dye solutions on their photocatalytic degradation in the presence of TiO2. Dyes and Pigments, 76(1), 226–230. https://doi.org/10.1016/j.dyepig.2006.08.031
- Bashar, H., Bhuiyan, M., Hossain, M., Kabir, F., Rahaman, M., Manir, M., & Ikegami, T. (2019). Study on combination of natural

red and green dyes to improve the power conversion efficiency of dye sensitized solar cells. Optik, 185, 620-625. https://doi.org/10.1016/j.ijleo.2019.03.043

- Basu, P., Pujahari, R., Kaur, H., Singh, D., Varandani, D., & Mehta, B. (2010). Impact of surface roughness on the electrical parameters of industrial high efficiency NaOH–NaOCl textured multicrystalline silicon solar cell. Solar Energy, 84(9), 1658-1665. https://doi.org/10.1016/j.solener.2010.06.001
- Baumeler, A., Zerbe, O., Kunz, R., & Eugster, C. H. (1994). (6R,9'z)-Neoxanthin: Synthese, Schmelzverhalten, Spektren und Konformationsberechnungen. Helvetica Chimica Acta, 77(4), 909–930. https://doi.org/10.1002/hlca.19940770405
- Bella, F., Gerbaldi, C., Barolo, C., & Grätzel, M. (2015). Aqueous dye-sensitized solar cells. Chemical Society Reviews, 44(11), 3431-3473. https://doi.org/10.1039/c4cs00456f
- Beretta, G. (2007). World energy consumption and resources: an outlook for the rest of the century. International Journal of Environmental Technology and Management, 7(1/2), 99. https://doi.org/10.1504/ijetm.2007.013239
- Bidigare, R. R., Van Heukelem, L., & Trees, C. C. (2005). Analysis of algal pigments by high-performance liquid chromatography. Algal Culturing Techniques, 327–345. https://doi.org/10.1016/b978-012088426-1/50021-4
- Bist, A., & Chatterjee, S. (2021). Review on Efficiency Enhancement Using Natural Extract Mediated Dye-Sensitized Solar Cell for Sustainable Photovoltaics. Energy Technology, 9(8), 2001058. https://doi.org/10.1002/ente.202001058
- Boschloo, G., Häggman, L., &Hagfeldt, A. (2006). Quantification of the Effect of 4-tert-Butylpyridine Addition to I-/I3-Redox Electrolytes in Dye-Sensitized Nanostructured TiO2Solar Cells. The Journal of Physical Chemistry B, 110(26), 13144-13150. https://doi.org/10.1021/jp0619641
- Bowles, N. D., Paerl, H. W., & Tucker, J. (1985). Effective solvents and extraction periods employed in phytoplankton

carotenoid and chlorophyll determinations. Canadian Journal of Fisheries and Aquatic Sciences, 42(6), 1127–1131. https://doi.org/10.1139/f85-139

- Bramhankar, T., Pawar, S., Shaikh, J., Gunge, V., Beedri, N., & Baviskar, P. et al. (2020). Effect of Nickel–Zinc Co-doped TiO2 blocking layer on performance of DSSCs. Journal of Alloys and Compounds, 817, 152810. https://doi.org/10.1016/j.jallcom.2019.152810
- Brown, T., De Rossi, F., Di Giacomo, F., Mincuzzi, G., Zardetto, V., Reale, A., & Di Carlo, A. (2014). Progress in flexible dye solar cell materials, processes and devices. J. Mater. Chem. A, 2(28), 10788-10817. https://doi.org/10.1039/c4ta00902a
- Buckle, K. A., & Edwards, R. A. (1970). Chlorophyll, colour and pH changes in H.T.S.T. processed green pea puree. International Journal of Food Science & Technology, 5(2), 173–186. https://doi.org/10.1111/j.1365-2621.1970.tb01555.x
- Burak, H., Dunbar, A., & Gilmour, D. (2019). Enhancement of Dunaliella salina growth by using wavelength shifting dyes. Journal of Applied Phycology, 31(5), 2791-2796. https://doi.org/10.1007/s10811-019-01819-4
- Cabrera, K., Lubda, D., Eggenweiler, H.-M., Minakuchi, H., & Nakanishi, K. (2000). A new monolithic-type HPLC column for fast separations. Journal of High-Resolution Chromatography, 23(1), 93–99. https://doi.org/10.1002/(SICI)1521-4168(20000101)23:1%3C93::AID-JHRC93%3E3.0.CO;2-2
- Caimi, S., Klaue, A., Wu, H., & Morbidelli, M. (2018). Effect of SiO2 Nanoparticles on the Performance of PVdF-HFP/Ionic Liquid Separator for Lithium-Ion Batteries. Nanomaterials, 8(11), 926. https://doi.org/10.3390/nano8110926
- Canjura, F. L., Schwartz, S. J., & Nunes, R. V. (1991). Degradation kinetics of chlorophylls and chlorophyllides. Journal of Food Science, 56(6), 1639–1643. https://doi.org/10.1111/j.1365-2621.1991.tb08660.x

- Castillo-Robles, J. A., Rocha-Rangel, E., Ramírez-de-León, J. A., Caballero-Rico, F. C., & Armendáriz-Mireles, E. N. (2021). Advances on dye-sensitized solar cells (dsscs) nanostructures and natural colorants: A Review. Journal of Composites Science, 5(11), 288. https://doi.org/10.3390/jcs5110288
- Chang, W., Lee, C., Yu, W., & Lin, C. (2012). Optimization of dye adsorption time and film thickness for efficient ZnO dye-sensitized solar cells with high at-rest stability. Nanoscale Research Letters, 7(1), 688. https://doi.org/10.1186/1556-276x-7-688
- Chauhan, R. (2022). Scanning prevalent technologies to promote scalable devising of DSSCs: An emphasis on dye component precisely with a shift to ambient algal dyes. Inorganic Chemistry Communications, 139, 109368. https://doi.org/10.1016/j.inoche.2022.109368
- Chauhan, R., Shirage, P. M., & Bala, K. (2023). Unravelling the spectral enigma with enhanced extraction of algal dyes: A sustainable energy tactic. Journal of Photochemistry and Photobiology A: Chemistry, 444, 115006. https://doi.org/10.1016/j.jphotochem.2023.115006
- Chauhan, R., Shirage, P. M., & Bala, K. (2024). Delving into judiciously extracted inexpensive micro-algal dyes for DSSCs: Spectral decipherment and time-oriented extraction systems. Sustainable Energy Technologies and Assessments, 64, 103746. https://doi.org/10.1016/j.seta.2024.103746
- Chauhan, R., Srivastava, A., Shirage, P. M., & Bala, K. (2024). Innovating Dye-Sensitized Solar Cells through Novel Microalgal and Cyanobacterial Species Extricated Dyes: A sustainable tack for material scarce earth. Solar Energy, 270, 112369. https://doi.org/10.1016/j.solener.2024.112369
- Chellamuthu, J., Nagaraj, P., Chidambaram, S., Sambandam, A., & Muthupandian, A. (2016). Enhanced photocurrent generation in bacteriorhodopsin based bio-sensitized solar cells using gel electrolyte. Journal of Photochemistry and Photobiology B:

Biology, 162, 208-212. https://doi.org/10.1016/j.jphotobiol.2016.06.044

- Chen, K.-F., Liu, C.-H., Huang, H.-K., Tsai, C.-H & Chen, Fu-Rong. (2013). Polyvinyl Butyral-Based Thin Film Polymeric Electrolyte for Dye-Sensitized Solar Cell with Long-Term Stability. International Journal of Electrochemical Science, 8. 3524-3539.
- Chen, N., Bianchi, T. S., & Bland, J. M. (2003). Novel decomposition products of chlorophyll-a in continental shelf (Louisiana Shelf) sediments: Formation and transformation of carotenol chlorin esters. Geochimica et Cosmochimica Acta, 67(11), 2027–2042. https://doi.org/10.1016/s0016-7037(02)01297-8
- Cheng, X., Pan, J., Zhao, Y., Liao, M., & Peng, H. (2017). Gel Polymer Electrolytes for Electrochemical Energy Storage. Advanced Energy Materials, 8(7), 1702184. https://doi.org/10.1002/aenm.201702184
- Choi, H., Raabe, I., Kim, D., Teocoli, F., Kim, C., & Song, K. et al. (2010). High Molar Extinction Coefficient Organic Sensitizers for Efficient Dye-Sensitized Solar Cells. Chemistry - A European Journal, 16(4), 1193-1201. https://doi.org/10.1002/chem.200902197
- Cisneros, R., Beley, M., & Lapicque, F. (2016). A study of the impact of co-adsorbents on DSSC electron transfer processes: anti-π-stacking vs. shield effect. Physical Chemistry Chemical Physics, 18(14), 9645-9651. https://doi.org/10.1039/c6cp00077k
- Constantino-Robles, C. D., Romero-Eredia, J. A., Sevilla-Camacho, P. Y., Robles-Ocampo, J. B., Sol-Montejo, L. J., Rodríguez-Reséndiz, J., & Perez-Sariñana, B. Y. (2022). Novel hybrid solar dryer for medicinal plants: An experimental evaluation (Tithonia diversifolia gray). Sustainable Energy Technologies and Assessments, 51, 101950. https://doi.org/10.1016/j.seta.2022.101950

- da Silva, L., & Freeman, H. (2019). Variation in hydrophobic chain length of co-adsorbents to improve dye-sensitized solar cell performance. Physical Chemistry Chemical Physics, 21(30), 16771-16778. https://doi.org/10.1039/c9cp02439e
- Daeneke, T., Mozer, A., Uemura, Y., Makuta, S., Fekete, M., & Tachibana, Y. et al. (2012). Dye Regeneration Kinetics in Dye-Sensitized Solar Cells. Journal of The American Chemical Society, 134(41), 16925-16928. https://doi.org/10.1021/ja3054578
- Das, P., Nayak, P. K., & Kesavan, R. krishnan. (2022). Ultrasound assisted extraction of food colorants: Principle, mechanism, extraction technique and applications: A review on recent progress. Food Chemistry Advances, 1, 100144. https://doi.org/10.1016/j.focha.2022.100144
- Data & Statistics - IEA. IEA. (2020). Retrieved 14 April 2020, from https://www.iea.org/statistics/renewables/
- Dayan, S., Kayaci, N., & Kalaycioğlu Özpozan, N. (2020). Improved performance with molecular design of Ruthenium (II) complexes bearing diamine-based bidentate ligands as sensitizer for dye-sensitized solar cells (DSSC). Journal of Molecular Structure, 1209, 127920. https://doi.org/10.1016/j.molstruc.2020.127920
- Desilvestro, J., Graetzel, M., Kavan, L., Moser, J., & Augustynski, J. (1985). Highly efficient sensitization of titanium dioxide. Journal of the American Chemical Society, 107(10), 2988-2990. https://doi.org/10.1021/ja00296a035
- Desta, M., Liao, C., & Sun, S. (2017). A General Strategy to Enhance the Performance of Dye-Sensitized Solar Cells by Incorporating a Light-Harvesting Dye with a Hydrophobic Polydiacetylene Electrolyte-Blocking Layer. Chemistry - An Asian Journal, 12(6), 690-697. https://doi.org/10.1002/asia.201601722
- Di Bari, C., Forni, C., Di Carlo, A., Barrajón-Catalán, E., Micol, V., Teoli, F., Nota, P., Matteocci, F., Frattarelli, A., Caboni, E., & Lucioli, S. (2017). Pigments for natural dye-sensitized solar cells

from in vitro grown shoot cultures. Journal of Photonics for Energy, 7(2), 025503. https://doi.org/10.1117/1.jpe.7.025503

- Diantoro, M., Maftuha, D., Suprayogi, T., Reynaldi Iqbal, M., Solehudin, & Mufti, N. et al. (2019). Performance of Pterocarpus Indicus Willd Leaf Extract as Natural Dye TiO2-Dye/ITO DSSC. Materials Today: Proceedings, 17, 1268-1276. https://doi.org/10.1016/j.matpr.2019.06.015
- Didden, A., Hillebrand, P., Dam, B., & van de Krol, R. (2015). Photo corrosion Mechanism of TiO2-Coated Photoanodes. International Journal of Photoenergy, 2015, 1-8. https://doi.org/10.1155/2015/457980
- Diop, M., El-Hayek, M., Attard, J., Muhieddine, A., Veremeienko, V., Soorkia, S., Carbonnière, P., De La Lande, A., Soep, B., & Shafizadeh, N. (2023). Chlorophyll and pheophytin protonated and deprotonated ions: Observation and theory. Journal of Chemical Physics Online/ the Journal of Chemical Physics/Journal of Chemical Physics, 159(19). https://doi.org/10.1063/5.0174351
- Distributed Solar PV – Renewables 2019 – Analysis - IEA. IEA. (2020). Retrieved 14 April 2020, from https://www.iea.org/reports/renewables-2019/distributed-solar-pv#forecast-overview
- Duan, Y., Tang, Q., Chen, Y., Zhao, Z., Lv, Y., & Hou, M. et al. (2015). Solid-state dye-sensitized solar cells from poly (ethylene oxide)/polyaniline electrolytes with catalytic and hole-transporting characteristics. Journal of Materials Chemistry A, 3(10), 5368-5374. https://doi.org/10.1039/c4ta06393g
- Dumbrava, A., Lungu, J., & Ion, A. (2016). Green seaweeds extract as co-sensitizer for dye sensitized solar cells. Scientific Study and Research: Chemistry And Chemical Engineering, Biotechnology, Food Industry, 17, 13-25
- Duppeti, H., Chakraborty, S., Das, B. S., Mallick, N., & Kotamreddy, J. N. R. (2017). Rapid assessment of algal biomass and pigment contents using diffuse reflectance spectroscopy and

chemometrics. Algal Research, 27, 274–285. https://doi.org/10.1016/j.algal.2017.09.016

- Dutton, H. J., Manning, W. M., & Duggar, B. M. (1943). Chlorophyll fluorescence and energy transfer in the diatom Nitzschia closterium. Journal of Physical Chemistry, 47(4), 308–313. https://doi.org/10.1021/j150427a002
- Eaves, S., & Eaves, J. (2004). A cost comparison of fuel-cell and battery electric vehicles. Journal of Power Sources, 130(1-2), 208-212. https://doi.org/10.1016/j.jpowsour.2003.12.016
- Eckardt, C. B., Carter, J. F., & Maxwell, J. R. (1990). Combined liquid chromatography/mass spectrometry of tetrapyrroles of sedimentary significance. Energy & Fuels, 4(6), 741–747. https://doi.org/10.1021/ef00024a021
- Edelenbos, M., Christensen, L. P., & Grevsen, K. (2001). HPLC determination of chlorophyll and carotenoid pigments in processed green pea cultivars (pisum sativum L.). Journal of Agricultural and Food Chemistry, 49(10), 4768–4774. https://doi.org/10.1021/jf010569z
- Elmorsy, M., Abdel-Latif, E., Badawy, S., & Fadda, A. (2020). Molecular geometry, synthesis and photovoltaic performance studies over 2-cyanoacetanilides as sensitizers and effective co-sensitizers for DSSCs loaded with HD-2. Journal of Photochemistry and Photobiology A: Chemistry, 389, 112239. https://doi.org/10.1016/j.jphotochem.2019.112239
- Elumalai, N., & Uddin, A. (2016). Open circuit voltage of organic solar cells: an in-depth review. Energy & Environmental Science, 9(2), 391-410. https://doi.org/10.1039/c5ee02871j
- Enciso, P., & Cerdá, M. (2016). Solar cells based on the use of photosensitizers obtained from Antarctic red algae. Cold Regions Science and Technology, 126, 51-54. https://doi.org/10.1016/j.coldregions.2016.04.002
- Enciso, P., Cabrerizo, F., Gancheff, J., Denis, P., & Cerdá, M. (2013). Phycocyanin as Potential Natural Dye for its Use in

Photovoltaic Cells. Journal of Applied Solution Chemistry and Modelling. https://doi.org/10.6000/1929-5030.2013.02.04.3

- Enciso, P., Decoppet, J., Moehl, T., Grätzel, M., Wörner, M., & Cerdá, M. (2016). Influence of the Adsorption of Phycocyanin on the Performance in DSS Cells: and Electrochemical and QCM Evaluation. International Journal of Electrochemical Science, 11, 3604-3614. https://doi.org/10.20964/110443
- Eriksen, N. T. (2008). Production of phycocyanin—a pigment with applications in biology, biotechnology, Foods, and Medicine. Applied Microbiology and Biotechnology, 80(1), 1–14. https://doi.org/10.1007/s00253-008-1542-y
- Fabris, M., Abbriano, R. M., Pernice, M., Sutherland, D. L., Commault, A. S., Hall, C. C., Labeeuw, L., McCauley, J. I., Kuzhiuparambil, U., Ray, P., Kahlke, T., & Ralph, P. J. (2020). Emerging Technologies in Algal Biotechnology: Toward the establishment of a sustainable, algae-based bioeconomy. Frontiers in Plant Science, 11. https://doi.org/10.3389/fpls.2020.00279
- Fernandes, A. S., Petry, F. C., Mercadante, A. Z., Jacob-Lopes, E., & Zepka, L. Q. (2020). HPLC-PDA-MS/ms as a strategy to characterize and quantify natural pigments from microalgae. Current Research in Food Science, 3, 100–112. https://doi.org/10.1016/j.crfs.2020.03.009
- Ferreira, F., Babu, R., de Barros, A., Raja, S., da Conceição, L., & Mattoso, L. (2020). Photoelectric performance evaluation of DSSCs using the dye extracted from different color petals of Leucanthemum vulgare flowers as novel sensitizers. Spectrochimica Acta Part A: Molecular and Biomolecular Spectroscopy, 233, 118198. https://doi.org/10.1016/j.saa.2020.118198
- Fleury, D. (2017). A Modular Photosynthetic Microbial Fuel Cell with Interchangeable Algae Solar Compartments. https://doi.org/10.1101/166793

- Francis, O. I., & Ikenna, A. (2021). Review of dye-sensitized solar cell (dsscs) development. Natural Science, 13(12), 496–509. https://doi.org/10.4236/ns.2021.1312043
- Fu, Q., Zhao, C., Yang, S., & Wu, J. (2014). The photoelectric performance of dye-sensitized solar cells fabricated by assembling pigment–protein complexes of purple bacteria on nanocrystalline photoelectrode. Materials Letters, 129, 195-197. https://doi.org/10.1016/j.matlet.2014.05.054
- Galagan, Y. (2018). Flexible Solar Cells. Roll-To-Roll Manufacturing, 325-362. https://doi.org/10.1002/9781119163824.ch11
- Gantt, E. (1980). Structure and Function of Phycobilisomes: Light Harvesting Pigment Complexes in Red and Blue-Green Algae. International Review of Cytology, 45-80. https://doi.org/10.1016/s0074-7696(08)61971-3
- Garner, S., Glaesemann, S., & Li, X. (2014). Ultra-slim flexible glass for roll-to-roll electronic device fabrication. Applied Physics A, 116(2), 403-407. https://doi.org/10.1007/s00339-014-8468-2
- Garrido, J., Rodriguez, F., Campana, E., & Zapata, M. (2003). Rapid separation of chlorophylls A and B and their demetallated and dephytylated derivatives using a monolithic silica C18 column and a pyridine-containing mobile phase. Journal of Chromatography A, 994(1–2), 85–92. https://doi.org/10.1016/s0021-9673(03)00486-2
- Gáspár, C.-L., Panea, I., & Bâldea, I. (2008). Solvent and temperature effects on the electronic transitions of 3-h-Indolo-2-dimethinehemicyanine dyes. Dyes and Pigments, 76(2), 455–462. https://doi.org/10.1016/j.dyepig.2006.10.001
- Gautam, S., Kashyap, M., Gupta, S., Kumar, V., Schoefs, B., & Gordon, R. et al. (2016). Metabolic engineering of TiO2 nanoparticles in Nitzschia palea to form diatom nanotubes: an ingredient for solar cells to produce electricity and biofuel. RSC Advances, 6(99), 97276-97284. https://doi.org/10.1039/c6ra18487a

- Ghann, W., Chavez-Gil, T., Goede, C., Kang, H., Khan, S., & Sobhi, H. et al. (2017). Photophysical, Electrochemical and Photovoltaic Properties of Porphyrin-Based Dye Sensitized Solar Cell. Advances in Materials Physics and Chemistry, 07(05), 148-172. https://doi.org/10.4236/ampc.2017.75013
- Ghosh, A., Selvaraj, P., Sundaram, S., & Mallick, T. (2018). The colour rendering index and correlated colour temperature of dye-sensitized solar cell for adaptive glazing application. Solar Energy, 163, 537-544. https://doi.org/10.1016/j.solener.2018.02.021
- Ghosh, S., Sarkar, T., Das, A., & Chakraborty, R. (2022). Natural colorants from plant pigments and their encapsulation: An emerging window for the food industry. LWT, 153, 112527. https://doi.org/10.1016/j.lwt.2021.112527
- Gnanasekar, S., Kollu, P., Jeong, S., & Grace, A. (2019). Pt-free, low-cost and efficient counter electrode with carbon wrapped VO2 (M) nanofiber for dye-sensitized solar cells. Scientific Reports, 9(1). https://doi.org/10.1038/s41598-019-41693-1
- Gondi, R., Kavitha, S., Yukesh Kannah, R., Kumar, G., & Rajesh Banu, J. (2022). Wastewater based microalgae valorization for biofuel and value-added products recovery. Sustainable Energy Technologies and Assessments, 53, 102443. https://doi.org/10.1016/j.seta.2022.102443
- Gopal Krishna, B., & Tiwari, S. (2021). Bioinspired solar cells: Contribution of biology to light harvesting systems. Sustainable Material Solutions for Solar Energy Technologies, 593–632. https://doi.org/10.1016/b978-0-12-821592-0.00006-6
- Green, M. (1981). Solar cell fill factors: General graph and empirical expressions. Solid-State Electronics, 24(8), 788-789. https://doi.org/10.1016/0038-1101(81)90062-9
- Gregg, B. (2003). Excitonic Solar Cells. The Journal of Physical Chemistry B, 107(20), 4688-4698. https://doi.org/10.1021/jp022507x
- Groeneveld, I., Kanelli, M., Ariese, F., & van Bommel, M. R. (2023). Parameters that affect the photodegradation of dyes and

pigments in solution and on substrate – an overview. Dyes and Pigments, 210, 110999. https://doi.org/10.1016/j.dyepig.2022.110999

- Gullace, S., Nastasi, F., Puntoriero, F., Trusso, S., & Calogero, G. (2020). A platinum-free nanostructured gold counter electrode for DSSCs prepared by pulsed laser ablation. Applied Surface Science, 506, 144690. https://doi.org/10.1016/j.apsusc.2019.144690
- Guo, H., Zhu, Y., Li, W., Zheng, H., Wu, K., & Ding, K. et al. (2015). Synthesis of highly effective Pt/carbon fiber composite counter electrode catalyst for dye-sensitized solar cells. Electrochimica Acta, 176, 997-1000. https://doi.org/10.1016/j.electacta.2015.07.103
- Gupte, S. M., El-bisi, H. M., & Francis, F. J. (1964). Kinetics of thermal degradation of chlorophyll in spinach pureea. Journal of Food Science, 29(4), 379–382. https://doi.org/10.1111/j.1365-2621.1964.tb01747.x
- Habib, K., Husain, A., & Al-Hazza, A. (2015). Degradation/oxidation susceptibility of organic photovoltaic cells in aqueous solutions. Review of Scientific Instruments, 86(12), 124101. https://doi.org/10.1063/1.4936593
- Hagberg, D., Marinado, T., Karlsson, K., Nonomura, K., Qin, P., & Boschloo, G. et al. (2007). Tuning the HOMO and LUMO Energy Levels of Organic Chromophores for Dye Sensitized Solar Cells. The Journal of Organic Chemistry, 72(25), 9550-9556. https://doi.org/10.1021/jo701592x
- Hagfeldt, A., Cappel, U., Boschloo, G., Sun, L., Kloo, L., Pettersson, H., & Gibson, E. (2018). Dye-Sensitized Photoelectrochemical Cells. Mcevoy's Handbook of Photovoltaics, 503-565. https://doi.org/10.1016/b978-0-12-809921-6.00014-8
- Hagfeldt, A., Cappel, U., Boschloo, G., Sun, L., Kloo, L., Pettersson, H., & Gibson, E. (2013). Dye-Sensitized Photoelectrochemical Cells. Solar Cells, 385-441. https://doi.org/10.1016/b978-0-12-386964-7.00013-5

- Hamed, N., Ahmad, M., Urus, N., Mohamad, F., Nafarizal, N., & Ahmad, N. et al. (2017). Performance comparison between silicon solar panel and dye-sensitized solar panel in Malaysia. https://doi.org/10.1063/1.5002047
- Hara, K., Wang, Z., Sato, T., Furube, A., Katoh, R., & Sugihara, H. et al. (2005). Oligothiophene-Containing Coumarin Dyes for Efficient Dye-Sensitized Solar Cells. The Journal of Physical Chemistry B, 109(32), 15476-15482. https://doi.org/10.1021/jp0518557
- Hardin, B., Sellinger, A., Moehl, T., Humphry-Baker, R., Moser, J., & Wang, P. et al. (2011). Energy and Hole Transfer between Dyes Attached to Titania in Cosensitized Dye-Sensitized Solar Cells. Journal of The American Chemical Society, 133(27), 10662-10667. https://doi.org/10.1021/ja2042172
- Haugan, J.A., & Liaaen-Jensen, S. (1989). Improved isolation procedure for fucoxanthin. Phytochemistry, 28(10), 2797–2798. https://doi.org/10.1016/s0031-9422(00)98091-9
- He, C., Zhao, L., Zheng, Z., & Lu, F. (2008). Determination of Electron Diffusion Coefficient and Lifetime in Dye-Sensitized Solar Cells by Electrochemical Impedance Spectroscopy at High Fermi Level Conditions. The Journal of Physical Chemistry C, 112(48), 18730-18733. https://doi.org/10.1021/jp8085733
- Henriques, M., Silva, A. M. S., & Rocha, J. (1970, January 1). [pdf] extraction and quantification of pigments from a marine microalga: A simple and reproducible method: Semantic scholar. [PDF] Extraction and quantification of pigments from a marine microalga: a simple and reproducible method | Semantic Scholar. https://www.semanticscholar.org/paper/Extraction-and-quantification-of-pigments-from-a-a-Henriques-Silva/8df0bc0596e3ef04447550a03238731f08ce6de0
- Heo, N., Jun, Y., & Park, J. (2013). Dye molecules in electrolytes: new approach for suppression of dye-desorption in dye-sensitized solar cells. Scientific Reports, 3(1). https://doi.org/10.1038/srep01712

- Hertzberg, S., & Liaaen-Jensen, S. (1969). The structure of myxoxanthophyll. Phytochemistry, 8(7), 1259–1280. https://doi.org/10.1016/s0031-9422(00)85566-1
- Hosseinnezhad, M., Gharanjig, K., Ghahari, M., & Nasiri, S.. Investigation of Photo-electrode and Counter Electrode Effect on DSSCs Based on Indoline Dyes. The Progress in Color, Colorants and Coatings Journal, 17, (2024) 121–132. https://doi.org/https://doi.org/10.30509/pccc.2023.167159.1230
- Hosseinpanahi, K., Golzarian, M., Abbaspour-Fard, M., & Feizy, J. (2019). Improving The Efficiency of DSSC with A Novel Multi-dye layers Approach. Optik, 164068. https://doi.org/10.1016/j.ijleo.2019.164068
- Hu, X., Tanaka, A., & Tanaka, R. (2013). Simple extraction methods that prevent the artifactual conversion of chlorophyll to chlorophyllide during pigment isolation from leaf samples. Plant Methods, 9(1). https://doi.org/10.1186/1746-4811-9-19
- Huang, S., Hung, C., Wu, W., & Chen, B. (2008). Determination of chlorophylls and their derivatives in Gynostemma pentaphyllum Makino by liquid chromatography–mass spectrometry. Journal of Pharmaceutical and Biomedical Analysis, 48(1), 105–112. https://doi.org/10.1016/j.jpba.2008.05.009
- Hui, Z., Xiong, Y., Heng, L., Yuan, L., & Yu-Xiang, W. (2007). Explanation of Effect of Added Water on Dye-Sensitized Nanocrystalline TiO2 Solar Cell: Correlation between Performance and Carrier Relaxation Kinetics. Chinese Physics Letters, 24(11), 3272-3275. https://doi.org/10.1088/0256-307x/24/11/068
- Huo, J., Zheng, M., Tu, Y., Wu, J., Hu, L., & Dai, S. (2015). A high performance cobalt sulfide counter electrode for dye-sensitized solar cells. Electrochimica Acta, 159, 166-173. https://doi.org/10.1016/j.electacta.2015.01.214
- Idigoras, J., Tena-Zaera, R., & Anta, J. (2014). Control of the recombination rate by changing the polarity of the electrolyte in dye-sensitized solar cells. Phys. Chem. Chem. Phys., 16(39), 21513-21523. https://doi.org/10.1039/c4cp03303e

- Iftikhar, H., Sonai, G., Hashmi, S., Nogueira, A., & Lund, P. (2019). Progress on Electrolytes Development in Dye-Sensitized Solar Cells. Materials, 12(12), 1998. https://doi.org/10.3390/ma12121998
- Indriatmoko, Shioi, Y., Brotosudarmo, T. H., & Limantara, L. (2015). Separation of photosynthetic pigments by high-performance liquid chromatography: Comparison of column performance, mobile phase, and temperature. Procedia Chemistry, 14, 202–210. https://doi.org/10.1016/j.proche.2015.03.029
- Isah, K. U., Ahmadu, U., Idris, A., Kimpa, M. I., Uno, U. E., Ndamitso, M. M., & Alu, N. (2014). Betalain pigments as natural photosensitizers for dye-sensitized solar cells: The effect of dye ph on the photoelectric parameters. Materials for Renewable and Sustainable Energy, 4(1). https://doi.org/10.1007/s40243-014-0039-0
- Isler, O., Lindlar, H., Montavon, M., Rüegg, R., Saucy, G., & Zeller, P. (1956). Synthesen in der carotinoid-reihe mitteilung. Totalsynthese von Zeaxanthin und physalien. Helvetica Chimica Acta, 39(7), 2041–2053. https://doi.org/10.1002/hlca.19560390717
- Jackson, A. H. (1979). Applications of mass spectrometry in studies of porphyrins and related tetrapyrroles. Philosophical Transactions of the Royal Society of London. Series a, Mathematical and Physical Sciences, 293(1400), 21–37. https://doi.org/10.1098/rsta.1979.0077
- Jamalullail, N., Mohamad, I., Norizan, M., Baharum, N., & Mahmed, N. (2017). Short review: Natural pigments photosensitizer for dye-sensitized solar cell (DSSC). 2017 IEEE 15Th Student Conference On Research And Development (Scored). https://doi.org/10.1109/scored.2017.8305367
- Janfaza, S., Molaeirad, A., Mohamadpour, R., Khayati, M., & Mehrvand, J. (2013). Efficient Bio-Nano Hybrid Solar Cells via Purple Membrane as Sensitizer. Bionanoscience, 4(1), 71-77. https://doi.org/10.1007/s12668-013-0118-1

- Jeffrey, S. W. (1972). Preparation and some properties of crystalline chlorophyll c1 and c2 from marine algae. Biochimica et Biophysica Acta (BBA) - General Subjects, 279(1), 15–33. https://doi.org/10.1016/0304-4165(72)90238-3
- Jeffrey, S. W. (1974). Profiles of photosynthetic pigments in the ocean using thin-layer chromatography. Marine Biology, 26(2), 101–110. https://doi.org/10.1007/bf00388879
- Jeffrey, S. W., & Humphrey, G. F. (1975). New spectrophotometric equations for determining chlorophylls a, b, C1, and C2 in higher plants, algae, and natural phytoplankton. Biochemie Und Physiologie Der Pflanzen, 167(2), 191–194. https://doi.org/10.1016/s0015-3796(17)30778-3
- Jeffrey, S. W., Wright, S. W., & Zapata, M. (1999). Recent advances in HPLC pigment analysis of phytoplankton. Marine and Freshwater Research. https://doi.org/10.1071/mf99109
- Jeon, I., Kim, H., Choi, I., Lim, K., Ko, J., & Kim, J. et al. (2015). High-performance dye-sensitized solar cells using edge-halogenated graphene nanoplatelets as counter electrodes. Nano Energy, 13, 336-345. https://doi.org/10.1016/j.nanoen.2015.02.037
- Jiang, Q., Li, W., Wu, J., Cheng, W., Zhu, J., & Yan, Z. et al. (2019). Electrodeposited cobalt and nickel selenides as high-performance electrocatalytic materials for dye-sensitized solar cells. Journal of Materials Science: Materials In Electronics, 30(10), 9429-9437. https://doi.org/10.1007/s10854-019-01273-5
- Jie, J., Xu, Q., Yang, G., Feng, Y., & Zhang, B. (2020). Porphyrin sensitizers involving a fluorine-substituted benzothiadiazole as auxiliary acceptor and thiophene as π bridge for use in dye-sensitized solar cells (DSSCs). Dyes and Pigments, 174, 107984. https://doi.org/10.1016/j.dyepig.2019.107984
- Jin, L., Greene, G., MacFarlane, D., & Pringle, J. (2016). Redox-Active Quasi-Solid-State Electrolytes for Thermal Energy Harvesting. ACS Energy Letters, 1(4), 654-658. https://doi.org/10.1021/acsenergylett.6b00305

- Jodłowska, S., & Latała, A. (2011). The comparison of spectrophotometric method and high-performance liquid chromatography in photosynthetic pigments analysis. OnLine Journal of Biological Sciences, 11(2), 63–69. https://doi.org/10.3844/ojbsci.2011.63.69
- Johansen, J. E., Svec, W. A., Liaaen-Jensen, S., & Haxo, F. T. (1974). Carotenoids of the Dinophyceae. Phytochemistry, 13(10), 2261–2271. https://doi.org/10.1016/0031-9422(74)85038-7
- Johari, R., Khan, M., Gupta, P., Parvaz, M., Ahmad, S., & Singh, P. et al. (2017). Natural and environment favourable Dye Used as Light Sensitizer in Dye Sensitized Solar Cell: A Critical Review. Journal of Materials Science & Surface Engineering, 5(8), 722-728. https://doi.org/10.jmsse/2348-8956/5-8.3
- Joshi, P., Korfiatis, D., Potamianou, S., & Thoma, K. (2011). Oxide thickness and roughness factor as parameters for TiO2-dye sensitized solar cells performance. Russian Journal of Electrochemistry, 47(5), 517-521. https://doi.org/10.1134/s102319351105003x
- Juozapavicius, M., Kaucikas, M., van Thor, J., & O'Regan, B. (2012). Observation of Multiexponential Pico- to Sub nanosecond Electron Injection in Optimized Dye-Sensitized Solar Cells with Visible-Pump Mid-Infrared-Probe Transient Absorption Spectroscopy. The Journal of Physical Chemistry C, 117(1), 116-123. https://doi.org/10.1021/jp309732z
- Kabir, F., Bhuiyan, M., Hossain, M., Bashar, H., Rahaman, M., & Manir, M. et al. (2019). Effect of combination of natural dyes and post-TiCl4 treatment in improving the photovoltaic performance of dye-sensitized solar cells. Comptes Rendus Chimie, 22(9-10), 659-666. https://doi.org/10.1016/j.crci.2019.08.002
- Kabir, F., Nazmus Sakib, S., Shehab Uddin, S., Tawsif Efaz, E., & Farhan Himel, Md. T. (2019). Enhance cell performance of DSSC by Dye Mixture, carbon nanotube and post Ticl4 treatment along with degradation study. Sustainable Energy Technologies and

Assessments, 35, 298–307. https://doi.org/10.1016/j.seta.2019.07.011

- Kakiage, K., Aoyama, Y., Yano, T., Oya, K., Fujisawa, J., & Hanaya, M. (2015). Highly-efficient dye-sensitized solar cells with collaborative sensitization by silyl-anchor and carboxy-anchor dyes. Chemical Communications, 51(88), 15894-15897. https://doi.org/10.1039/c5cc06759f
- Kargul, J., Janna Olmos, J., & Krupnik, T. (2012). Structure and function of photosystem I and its application in biomimetic solar-to-fuel systems. Journal of Plant Physiology, 169(16), 1639-1653. https://doi.org/10.1016/j.jplph.2012.05.018
- Karki, I., Nakarmi, J., Mandal, P., & Chatterjee, S. (2013). Absorption spectra of natural dyes and their effect on efficiency of zno based dye-sensitized solar cells. Nepal Journal of Science and Technology, 13(1), 179–185. https://doi.org/10.3126/njst.v13i1.7457
- Katoh, R., Furube, A., Kasuya, M., Fuke, N., Koide, N., & Han, L. (2007). Photoinduced electron injection in black dye sensitized nanocrystalline TiO2 films. Journal of Materials Chemistry, 17(30), 3190. https://doi.org/10.1039/b702805a
- Katoh, R., Furube, A., Mori, S., Miyashita, M., Sunahara, K., Koumura, N., & Hara, K. (2009). Highly stable sensitizer dyes for dye-sensitized solar cells: role of the oligothiophene moiety. Energy & Environmental Science, 2(5), 542. https://doi.org/10.1039/b900372j
- Kawashima, T., Ezure, T., Okada, K., Matsui, H., Goto, K., & Tanabe, N. (2004). FTO/ITO double-layered transparent conductive oxide for dye-sensitized solar cells. Journal of Photochemistry and Photobiology A: Chemistry, 164(1-3), 199-202. https://doi.org/10.1016/j.jphotochem.2003.12.028
- Kay, A., & Graetzel, M. (1993) Artificial photosynthesis. 1. Photosensitization of titania solar cells with chlorophyll derivatives and related natural porphyrins, J. Phys. Chem. 97 6272–6277. https://doi.org/https://doi.org/10.1021/j100125a029.

- Koops, S., O'Regan, B., Barnes, P., & Durrant, J. (2009). Parameters Influencing the Efficiency of Electron Injection in Dye-Sensitized Solar Cells. Journal of the American Chemical Society, 131(13), 4808-4818. https://doi.org/10.1021/ja8091278
- Kosumi, D., Kita, M., Fujii, R., Sugisaki, M., Oka, N., Takaesu, Y., Taira, T., Iha, M., & Hashimoto, H. (2012). Excitation Energy-transfer dynamics of brown algal photosynthetic antennas. The Journal of Physical Chemistry Letters, 3(18), 2659–2664. https://doi.org/10.1021/jz300612c
- Kraay, G. W., Zapata, M., & Veldhuis, M. J. (1992). Separation of chlorophylls c1, c2, and c3 of marine phytoplankton by reversed-phase-c18-high-performance liquid chromatography1. Journal of Phycology, 28(5), 708–712. https://doi.org/10.1111/j.0022-3646.1992.00708.x
- Kranz, L., Gretener, C., Perrenoud, J., Schmitt, R., Pianezzi, F., & La Mattina, F. et al. (2013). Doping of polycrystalline CdTe for high-efficiency solar cells on flexible metal foil. Nature Communications, 4(1). https://doi.org/10.1038/ncomms3306
- Kroeze, J., Hirata, N., Koops, S., Nazeeruddin, M., Schmidt-Mende, L., Grätzel, M., & Durrant, J. (2006). Alkyl Chain Barriers for Kinetic Optimization in Dye-Sensitized Solar Cells. Journal of the American Chemical Society, 128(50), 16376-16383. https://doi.org/10.1021/ja065653f
- Kuczynska, P., Jemiola-Rzeminska, M., & Strzalka, K. (2015). Photosynthetic pigments in diatoms. Marine Drugs, 13(9), 5847–5881. https://doi.org/10.3390/md13095847
- Kumar, A., Dixit, U., Singh, K., Prakash Gupta, S., & S. Jamal Beg, M. (2021). Structure and properties of dyes and pigments. Dyes and Pigments - Novel Applications and Waste Treatment. https://doi.org/10.5772/intechopen.97104
- Kumar, P., Kumar, S., Ghosh, S., & Pal, S. (2016). Femtosecond insights into direct electron injection in dye anchored ZnO QDs following charge transfer excitation. Physical Chemistry Chemical Physics, 18(30), 20672-20681. https://doi.org/10.1039/c6cp01721e

- Kumar, S. N., Ritesh, S. K., Sharmila, G., & Muthukumaran, C. (2017). Extraction optimization and characterization of water soluble red purple pigment from floral bracts of bougainvillea glabra. Arabian Journal of Chemistry, 10. https://doi.org/10.1016/j.arabjc.2013.07.047
- Kumar, V., Gupta, R., & Bansal, A. (2020). Role of chenodeoxycholic acid as co-additive in improving the efficiency of DSSCs. Solar Energy, 196, 589-596. https://doi.org/10.1016/j.solener.2019.12.034
- Kumara, N., Lim, A., Lim, C., Petra, M., & Ekanayake, P. (2017). Recent progress and utilization of natural pigments in dye sensitized solar cells: A review. Renewable And Sustainable Energy Reviews, 78, 301-317. https://doi.org/10.1016/j.rser.2017.04.075
- Kunzmann, A., Valero, S., Sepúlveda, Á., Rico-Santacruz, M., Lalinde, E., & Berenguer, J. et al. (2018). Hybrid Dye-Titania Nanoparticles for Superior Low-Temperature Dye-Sensitized Solar Cells. Advanced Energy Materials, 8(12), 1702583. https://doi.org/10.1002/aenm.201702583
- LaJOLLO, F., Tannenbaum, S. R., & Labuza, T. P. (1971). REACTION AT LIMITED WATER CONCENTRATION. 2. Chlorophyll degradation. Journal of Food Science, 36(6), 850–853. https://doi.org/10.1111/j.1365-2621.1971.tb15542.x
- Lamnatou, Chr., & Chemisana, D. (2023). Photovoltaics for buildings and greenhouses: Organic solar cells and other technologies. Sustainable Energy Technologies and Assessments, 56, 103062. https://doi.org/10.1016/j.seta.2023.103062
- Le Bahers, T., Labat, F., Pauporté, T., & Ciofini, I. (2010). Effect of solvent and additives on the open-circuit voltage of ZnO-based dye-sensitized solar cells: a combined theoretical and experimental study. Physical Chemistry Chemical Physics, 12(44), 14710. https://doi.org/10.1039/c004358c
- Leandri, V., Ellis, H., Gabrielsson, E., Sun, L., Boschloo, G., & Hagfeldt, A. (2014). An organic hydrophilic dye for water-based

dye-sensitized solar cells. Phys. Chem. Chem. Phys., 16(37), 19964-19971. https://doi.org/10.1039/c4cp02774d

- Lee, C., & Hyun, Y. (2016). Preparation and Characterization of Carbon Nanofibers and its Composites by Chemical Vapor Deposition. Chemical Vapor Deposition - Recent Advances and Applications in Optical, Solar Cells and Solid-State Devices. https://doi.org/10.5772/63755
- Li, C., Yang, X., Chen, R., Pan, J., Tian, H., Zhu, H., Wang, X., Hagfeldt, A., & Sun, L. (2007). Anthraquinone dyes as photosensitizers for dye-sensitized solar cells. Solar Energy Materials and Solar Cells, 91(19), 1863–1871. https://doi.org/10.1016/j.solmat.2007.07.002
- Li, Z., Chen, T., & Liao, Y. (2015). Performance enforcement of gel polymer electrolyte for lithium-ion battery with co-doping silicon dioxide and zirconium dioxide nanoparticles. Ionics, 21(10), 2763-2770. https://doi.org/10.1007/s11581-015-1478-z
- Lichtenthaler, H. K. (1987). [34] Chlorophylls and Carotenoids: Pigments of Photosynthetic Biomembranes. Methods in Enzymology, 350–382. https://doi.org/10.1016/0076-6879(87)48036-1
- Lichtenthaler, H. K., & Wellburn, A. R. (1983). Determinations of total carotenoids and chlorophylls a and b of leaf extracts in different solvents. Biochemical Society Transactions, 11(5), 591–592. https://doi.org/10.1042/bst0110591
- Ligor, M., Kováčová, J., Gadzała-Kopciuch, R. M., Studzińska, S., Bocian, Sz., Lehotay, J., & Buszewski, B. (2014). Study of RP HPLC retention behaviours in analysis of carotenoids. Chromatographia, 77(15–16), 1047–1057. https://doi.org/10.1007/s10337-014-2657-1
- Lim, A., Haji Manaf, N., Tennakoon, K., Chandrakanthi, R., Lim, L., Bandara, J., & Ekanayake, P. (2015). Higher Performance of DSSC with Dyes from Cladophora sp. as Mixed Cosensitizer through Synergistic Effect. Journal of Biophysics, 2015, 1-8. https://doi.org/10.1155/2015/510467

- Linares, G., & Rojas, M. L. (2022). Ultrasound-assisted extraction of natural pigments from food processing by-products: A Review. Frontiers in Nutrition, 9. https://doi.org/10.3389/fnut.2022.891462
- Liska, P., Vlachopoulos, N., Nazeeruddin, M., Comte, P., & Graetzel, M. (1988). cis-Diaquabis(2,2'-bipyridyl-4,4'-dicarboxylate) ruthenium (II) sensitizes wide band gap oxide semiconductors very efficiently over a broad spectral range in the visible. Journal of The American Chemical Society, 110(11), 3686-3687. https://doi.org/10.1021/ja00219a068
- Liu, B., & Aydil, E. S. (2009). Growth of oriented single-crystalline rutile tio2 nanorods on transparent conducting substrates for dye-sensitized solar cells. Journal of the American Chemical Society, 131(11), 3985–3990. https://doi.org/10.1021/ja8078972
- Liu, I., Hou, Y., Li, C., & Lee, Y. (2017). Highly electrocatalytic counter electrodes based on carbon black for cobalt (iii)/ (ii)-mediated dye-sensitized solar cells. Journal of Materials Chemistry A, 5(1), 240-249. https://doi.org/10.1039/c6ta08818j
- Liu, Y., Liu, X., Cui, Y., & Yuan, W. (2022). Ultrasound for microalgal cell disruption and product extraction: A Review. Ultrasonics Sonochemistry, 87, 106054. https://doi.org/10.1016/j.ultsonch.2022.106054
- Liu, Y., Ye, X., An, Q., Lei, B., Sun, W., & Sun, Z. (2018). A novel synthesis of the bottom-straight and top-bent dual TiO2 nanowires for dye-sensitized solar cells. Advanced Powder Technology, 29(6), 1455-1462. https://doi.org/10.1016/j.apt.2018.03.008
- Loh, C. H., Inbaraj, B. S., Liu, M. H., & Chen, B. H. (2012). Determination of chlorophylls in taraxacum formosanum by high-performance liquid chromatography–diode array detection–mass spectrometry and preparation by column chromatography. Journal of Agricultural and Food Chemistry, 60(24), 6108–6115. https://doi.org/10.1021/jf301422m
- Lu, H., Shen, T., Huang, S., Tung, Y., & Yang, T. (2011). The degradation of dye sensitized solar cell in the presence of water

isotopes. Solar Energy Materials and Solar Cells, 95(7), 1624-1629. https://doi.org/10.1016/j.solmat.2011.01.014

- Machatová, Z., Barbieriková, Z., Poliak, P., Jančovičová, V., Lukeš, V., & Brezová, V. (2016). Study of natural anthraquinone colorants by EPR and UV/Vis Spectroscopy. Dyes and Pigments, 132, 79–93. https://doi.org/10.1016/j.dyepig.2016.04.046
- Macht, B., Turrión, M., Barkschat, A., Salvador, P., Ellmer, K., & Tributsch, H. (2002). Patterns of efficiency and degradation in dye sensitization solar cells measured with imaging techniques. Solar Energy Materials and Solar Cells, 73(2), 163-173. https://doi.org/10.1016/s0927-0248(01)00121-0
- Mackinney, G. (1941). Absorption of light by Chlorophyll Solutions. Journal of Biological Chemistry, 140(2), 315–322. https://doi.org/10.1016/s0021-9258(18)51320-x
- Mackinney, G., & Joslyn, M. A. (n.d.). Chlorophyll-Pheophytin: temperature coefficient of the rate of pheophytin formation. Journal of the American Chemical Society, 63(9), 2530–2531. https://doi.org/10.1021/ja01854a507
- Maddah, H. A., Berry, V., & Behura, S. K. (2020). Biomolecular photosensitizers for dye-sensitized solar cells: Recent developments and Critical Insights. Renewable and Sustainable Energy Reviews, 121, 109678. https://doi.org/10.1016/j.rser.2019.109678
- Maddah, H., Berry, V., & Behura, S. (2020). Biomolecular photosensitizers for dye-sensitized solar cells: Recent developments and critical insights. Renewable and Sustainable Energy Reviews, 121, 109678. https://doi.org/10.1016/j.rser.2019.109678
- Magis, G., Olsen, J., Reynolds, N., Leggett, G., Hunter, C., Aartsma, T., & Frese, R. (2011). Use of Engineered Unique Cysteine Residues to Facilitate Oriented Coupling of Proteins Directly to a Gold Substrate. Photochemistry and Photobiology, 87(5), 1050-1057. https://doi.org/10.1111/j.1751-1097.2011.00948.x

- Mahabaduge, H., Rance, W., Burst, J., Reese, M., Meysing, D., & Wolden, C. et al. (2015). High-efficiency, flexible CdTe solar cells on ultra-thin glass substrates. Applied Physics Letters, 106(13), 133501. https://doi.org/10.1063/1.4916634
- Maiaugree, W., Lowpa, S., Towannang, M., Rutphonsan, P., Tangtrakarn, A., &Pimanpang, S. et al. (2015). A dye sensitized solar cell using natural counter electrode and natural dye derived from mangosteen peel waste. Scientific Reports, 5(1). https://doi.org/10.1038/srep15230
- Manthou, V., Pefkianakis, E., Falaras, P., & Vougioukalakis, G. (2015). Co-Adsorbents: A Key Component in Efficient and Robust Dye-Sensitized Solar Cells. Chemsuschem, 8(4), 588-599. https://doi.org/10.1002/cssc.201403211
- Mantoura, R. F. C., & Llewellyn, C. A. (1983). The rapid determination of algal chlorophyll and carotenoid pigments and their breakdown products in natural waters by reverse-phase high-performance liquid chromatography. Analytica Chimica Acta, 151, 297–314. https://doi.org/10.1016/s0003-2670(00)80092-6
- Marchini, E., Darari, M., Lazzarin, L., Boaretto, R., Argazzi, R., & Bignozzi, C. et al. (2020). Recombination and regeneration dynamics in FeNHC (ii)-sensitized solar cells. Chemical Communications, 56(4), 543-546. https://doi.org/10.1039/c9cc07794d
- Margulis, G., Lim, B., Hardin, B., Unger, E., Yum, J., & Feckl, J. et al. (2013). Highly soluble energy relay dyes for dye-sensitized solar cells. Physical Chemistry Chemical Physics, 15(27), 11306. https://doi.org/10.1039/c3cp51018b
- Markvart, T., & Castañer, L. (2013). Principles of Solar Cell Operation. Solar Cells, 3-25. https://doi.org/10.1016/b978-0-12-386964-7.00001-9
- Marri, A., Black, F., Mallows, J., Gibson, E., & Fielden, J. (2019). Pyridinium p-DSSC dyes: An old acceptor learns new tricks. Dyes and Pigments, 165, 508-517. https://doi.org/10.1016/j.dyepig.2019.02.044

- Mattioli, G., Melis, C., Malloci, G., Filippone, F., Alippi, P., & Giannozzi, P. et al. (2012). Zinc Oxide–Zinc Phthalocyanine Interface for Hybrid Solar Cells. The Journal of Physical Chemistry C, 116(29), 15439-15448. https://doi.org/10.1021/jp303781v
- McMillon-Brown, L., Mariano, M., Lin, Y., Li, J., Hashmi, S., & Semichaevsky, A. et al. (2017). Light-trapping in polymer solar cells by processing with nanostructured diatomaceous earth. Organic Electronics, 51, 422-427. https://doi.org/10.1016/j.orgel.2017.09.009
- Meléndez-Martínez, A. J., Stinco, C. M., & Mapelli-Brahm, P. (2019). Skin carotenoids in public health and nutricosmetics: The emerging roles and applications of the UV radiation-absorbing colourless carotenoids phytoene and phytofluene. Nutrients, 11(5), 1093. https://doi.org/10.3390/nu11051093
- Mendes, C. R., Cartaxana, P., & Brotas, V. (2007). HPLC determination of phytoplankton and microphytobenthos pigments: Comparing resolution and sensitivity of a C18 and a C8 method. Limnology and Oceanography: Methods, 5(10), 363–370. https://doi.org/10.4319/lom.2007.5.363
- Meng, L., Chen, H., Li, C., & dos Santos, M. P. (2014). Growth of the [110] oriented tio2 nanorods on ITO substrates by sputtering technique for dye-sensitized solar cells. Frontiers in Materials, 1. https://doi.org/10.3389/fmats.2014.00014
- Mihi, A., & Míguez, H. (2005). Origin of Light-Harvesting Enhancement in Colloidal-Photonic-Crystal-Based Dye-Sensitized Solar Cells. The Journal of Physical Chemistry B, 109(33), 15968-15976. https://doi.org/10.1021/jp051828g
- Mihi, A., López-Alcaraz, F., & Míguez, H. (2006). Full spectrum enhancement of the light harvesting efficiency of dye sensitized solar cells by including colloidal photonic crystal multilayers. Applied Physics Letters, 88(19), 193110. https://doi.org/10.1063/1.2200746
- Milenković, S. M., Zvezdanović, J. B., Anđelković, T. D., & Dejan, Z. (2012). THE IDENTIFICATION OF CHLOROPHYLL

AND ITS DERIVATIVES IN THE PIGMENT MIXTURES: HPLC-CHROMATOGRAPHY, VISIBLE AND MASS SPECTROSCOPY STUDIES. Savremene Tehnologije, 1(1), 16–24. http://www.tf.ni.ac.rs/casopis/sveska1/c2.pdf

- Mittal, R., Tavanandi, H. A., Mantri, V. A., & Raghavarao, K. S. M. S. (2017). Ultrasound assisted methods for enhanced extraction of phycobiliproteins from marine macro-algae, Gelidium Pusillum (Rhodophyta). Ultrasonics Sonochemistry, 38, 92–103. https://doi.org/10.1016/j.ultsonch.2017.02.030
- Miyashita, H., Adachi, K., Kurano, N., Ikemot, H., Chihara, M., & Miyach, S. (1997). Pigment composition of a novel oxygenic photosynthetic prokaryote containing chlorophyll d as the major chlorophyll. Plant and Cell Physiology, 38(3), 274–281. https://doi.org/10.1093/oxfordjournals.pcp.a029163
- Mohammadpour, R., Janfaza, S., & Abbaspour-Aghdam, F. (2014). Light harvesting and photocurrent generation by nanostructured photoelectrodes sensitized with a photosynthetic pigment: A new application for microalgae. Bioresource Technology, 163, 1-5. https://doi.org/10.1016/j.biortech.2014.04.003
- Molaeirad, A., Janfaza, S., Karimi-Fard, A., & Mahyad, B. (2014). Photocurrent generation by adsorption of two main pigments of Halobacterium salinarum on TiO2 nanostructured electrode. Biotechnology and Applied Biochemistry, 62(1), 121-125. https://doi.org/10.1002/bab.1244
- Montagni, T., Enciso, P., Marizcurrena, J., Castro-Sowinski, S., Fontana, C., Davyt, D., & Cerdá, M. (2018). Dye sensitized solar cells based on Antarctic Hymenobacter sp. UV11 dyes. Environmental Sustainability, 1(1), 89-97. https://doi.org/10.1007/s42398-018-0007-1
- Müller, T., Vergeiner, S., & Kräutler, B. (2014). Structure elucidation of chlorophyll catabolites (phyllobilins) by ESI-mass spectrometry—Pseudo-molecular ions and fragmentation analysis of a nonfluorescent chlorophyll catabolite (NCC). International

Journal of Mass Spectrometry, 365–366, 48–55. https://doi.org/10.1016/j.ijms.2013.12.028

- Musazade, E., Voloshin, R., Brady, N., Mondal, J., Atashova, S., & Zharmukhamedov, S. et al. (2018). Biohybrid solar cells: Fundamentals, progress, and challenges. Journal of Photochemistry and Photobiology C: Photochemistry Reviews, 35, 134-156. https://doi.org/10.1016/j.jphotochemrev.2018.04.001
- N. Biloria, Y. Thakkar, Integrating algae building technology in the built environment: A cost and benefit perspective, Front. Archit. Res. 9 (2020) 370–384. https://doi.org/10.1016/j.foar.2019.12.004.
- Nahar, K. (2021). A Review on Natural Dye Sensitized Solar Cells: Dye Extraction, Application and Comparing the Performance. Advanced Engineering Forum, 39, 63-73. https://doi.org/10.4028/www.scientific.net/aef.39.63
- Nakade, S., Makimoto, Y., Kubo, W., Kitamura, T., Wada, Y., & Yanagida, S. (2005). Roles of Electrolytes on Charge Recombination in Dye-Sensitized TiO2Solar Cells (2): The Case of Solar Cells Using Cobalt Complex Redox Couples. The Journal of Physical Chemistry B, 109(8), 3488-3493. https://doi.org/10.1021/jp046002d
- Nakamura, A., & Watanabe, T. (1998). HPLC determination of photosynthetic pigments during greening of etiolated barley leaves. FEBS Letters, 426(2), 201–204. https://doi.org/10.1016/s0014-5793(98)00344-5
- Nakamura, A., Tanaka, S., & Watanabe, T. (2001). Normal-phase HPLC separation of possible biosynthetic intermediates of Pheophytin A and chlorophyll a′. Analytical Sciences, 17(4), 509–513. https://doi.org/10.2116/analsci.17.509
- Nandan Arka, G., Bhushan Prasad, S., & Singh, S. (2021). Comprehensive study on dye sensitized solar cell in subsystem level to Excel Performance Potential: A Review. Solar Energy, 226, 192–213. https://doi.org/10.1016/j.solener.2021.08.037

- Nanostructured Solar Cells. Google Books. (2017). Retrieved 18 April 2020, from https://books.google.co.in/books?id=GsOQDwAAQBAJ
- Nemala, S., Kartikay, P., Agrawal, R., Bhargava, P., Mallick, S., & Bohm, S. (2018). Few layers graphene based conductive composite inks for Pt free stainless steel counter electrodes for DSSC. Solar Energy, 169, 67-74. https://doi.org/10.1016/j.solener.2018.02.061
- Neville, R. (1995). SOLAR CELL CONFIGURATION AND PERFORMANCE. Solar Energy Conversion, 197-256. https://doi.org/10.1016/b978-044489818-0/50006-5
- Ng, F., Phang, S., Periasamy, V., Yunus, K., & Fisher, A. (2017). Enhancement of Power Output by using Alginate Immobilized Algae in Biophotovoltaic Devices. Scientific Reports, 7(1). https://doi.org/10.1038/s41598-017-16530-y
- Ngamwonglumlert, L., Devahastin, S., & Chiewchan, N. (2017). Natural colorants: Pigment stability and extraction yield enhancement via utilization of appropriate pretreatment and Extraction Methods. Critical Reviews in Food Science and Nutrition, 57(15), 3243–3259. https://doi.org/10.1080/10408398.2015.1109498
- Non-Conventional Energy Resources. Google Books. (2015). Retrieved 18 April 2020, from https://books.google.co.in/books?id=B7_ODAAAQBAJ
- Nowruzi, B., Sattari, T. N., & Jokela, J. (2019). A Report on Finding a New Peptide Aldehyde from Cyanobacterium Nostoc sp. Bahar M by LC-MS and Marfey's Analysis. Iranian Journal of Biotechnology, 17(2), 71–78. https://doi.org/10.21859/ijb.1853
- Nurachman, Z., H, H., Rahmaniyah, W. R., Kurnia, D., Hidayat, R., Prijamboedi, B., Suendo, V., Ratnaningsih, E., Panggabean, L. M., & Nurbaiti, S. (2015). Tropical Marine Chlorella SP.. PP1 as a source of photosynthetic pigments for dye-sensitized solar cells. Algal Research, 10, 25–32. https://doi.org/10.1016/j.algal.2015.04.009

- Nurachman, Z., H, H., Rahmaniyah, W., Kurnia, D., Hidayat, R., & Prijamboedi, B. et al. (2015). Tropical marine Chlorella sp. PP1 as a source of photosynthetic pigments for dye-sensitized solar cells. Algal Research, 10, 25-32. https://doi.org/10.1016/j.algal.2015.04.009
- Nwoba, E. G., Ogbonna, C. N., Ishika, T., & Vadiveloo, A. (2020). Microalgal pigments: a source of natural food colors. In Springer eBooks (pp. 81–123). https://doi.org/10.1007/978-981-15-0169-2_3
- Ocakoglu, K., Krupnik, T., van den Bosch, B., Harputlu, E., Gullo, M., & Olmos, J. et al. (2014). Photosystem I-based Biophotovoltaics on Nanostructured Hematite. Advanced Functional Materials, 24(47), 7467-7477. https://doi.org/10.1002/adfm.201401399
- Önen, T., Karakuş, M., Coşkun, R., & Çetin, H. (2019). Reaching stability at DSSCs with new type gel electrolytes. Journal of Photochemistry and Photobiology A: Chemistry, 385, 112082. https://doi.org/10.1016/j.jphotochem.2019.112082
- Órdenes-Aenishanslins, N., Anziani-Ostuni, G., Vargas-Reyes, M., Alarcón, J., Tello, A., & Pérez-Donoso, J. (2016). Pigments from UV-resistant Antarctic bacteria as photosensitizers in Dye Sensitized Solar Cells. Journal of Photochemistry and Photobiology B: Biology, 162, 707-714. https://doi.org/10.1016/j.jphotobiol.2016.08.004
- O'Regan, B., & Grätzel, M. (1991). A low-cost, high-efficiency solar cell based on dye-sensitized colloidal TiO2 films. Nature, 353(6346), 737-740. https://doi.org/10.1038/353737a0
- Orona-Navar, A., Aguilar-Hernández, I., Cerdán-Pasarán, A., López-Luke, T., Rodríguez-Delgado, M., & Cárdenas-Chávez, D. et al. (2017). Astaxanthin from Haematococcus pluvialis as a natural photosensitizer for dye-sensitized solar cell. Algal Research, 26, 15-24. https://doi.org/10.1016/j.algal.2017.06.027
- Orona-Navar, A., Aguilar-Hernández, I., López-Luke, T., Zarazúa, I., Romero-Arellano, V., Guerrero, J., & Ornelas-Soto, N. (2020).

Photoconversion efficiency of Titania solar cells co-sensitized with natural pigments from cochineal, papaya peel and microalga Scenedesmus obliquus. Journal of Photochemistry and Photobiology A: Chemistry, 388, 112216. https://doi.org/10.1016/j.jphotochem.2019.112216

- Orona-Navar, A., Aguilar-Hernández, I., Nigam, K. D. P., Cerdán-Pasarán, A., & Ornelas-Soto, N. (2021). Alternative sources of natural pigments for dye-sensitized solar cells: Algae, cyanobacteria, Bacteria, Archaea and fungi. Journal of Biotechnology, 332, 29–53. https://doi.org/10.1016/j.jbiotec.2021.03.013
- Ortiz-Torres, M., Fernández-Niño, M., Cruz, J., Capasso, A., Matteocci, F., & Patiño, E. et al. (2020). Rational Design of Photo-Electrochemical Hybrid Devices Based on Graphene and Chlamydomonas reinhardtii Light-Harvesting Proteins. Scientific Reports, 10(1). https://doi.org/10.1038/s41598-020-60408-5
- Pagels, F., Pereira, R. N., Vicente, A. A., & Guedes, A. C. (2021). Extraction of pigments from microalgae and cyanobacteria—a review on current methodologies. Applied Sciences, 11(11), 5187. https://doi.org/10.3390/app11115187
- Pagels, F., Pereira, R. N., Vicente, A. A., & Guedes, A. C. (2021). Extraction of pigments from microalgae and cyanobacteria—a review on current methodologies. Applied Sciences, 11(11), 5187. https://doi.org/10.3390/app11115187
- Pal, M. (1965). Effects of differently hydrophobic solvents on the aggregation of cationic dyes as measured by quenching of fluorescence and/or metachromasia of the dyes. Histochemie, 5(1), 24-31. https://doi.org/10.1007/bf00307889
- Pápista, É., Ács, É., & Böddi, B. (2002). Hydrobiologia, 485(1/3), 191–198. https://doi.org/10.1023/a:1021329602685
- Parisi, M. L., Sinicropi, A., & Basosi, R. (2011). Life cycle assessment of gratzel-type cell production for non-conventional photovoltaics from novel organic dyes. International Journal of Heat and Technology, 29(2), 161-169

- Pashaei, B., & Shahroosvand, H. (2020). Molecularly engineered ruthenium polypyridyl complexes for using in dye-sensitized solar cell. Inorganic Chemistry Communications, 112, 107737. https://doi.org/10.1016/j.inoche.2019.107737
- Pazoki, M., Cappel, U., Johansson, E., Hagfeldt, A., & Boschloo, G. (2017). Characterization techniques for dye-sensitized solar cells. Energy & Environmental Science, 10(3), 672-709. https://doi.org/10.1039/c6ee02732f
- Pessarrodona, A., Franco-Santos, R. M., Wright, L. S., Vanderklift, M. A., Howard, J., Pidgeon, E., Wernberg, T., & Filbee-Dexter, K. (2023). Carbon sequestration and climate change mitigation using macroalgae: A State of Knowledge Review. Biological Reviews, 98(6), 1945–1971. https://doi.org/10.1111/brv.12990
- Pez Jaeschke, D., Rocha Teixeira, I., Damasceno Ferreira Marczak, L., & Domeneghini Mercali, G. (2021). Phycocyanin from spirulina: A review of extraction methods and stability. Food Research International, 143, 110314. https://doi.org/10.1016/j.foodres.2021.110314
- Phytoplankton pigment analysis by HPLC and its application in algal community investigations. (2002, October 1). https://ejournal.sinica.edu.tw/bbas/content/2002/4/bot434-05.html
- Picazo, A., Rochera, C., Vicente, E., Miracle, Maria R. M., & Camacho, A. (2013). Spectrophotometric methods for the determination of photosynthetic pigments in Stratified Lakes: A critical analysis based on comparisons with HPLC determinations in a Model Lake. Limnetica, (32), 139–158. https://doi.org/10.23818/limn.32.13
- Pinto, A., Cruz, L., Gomes, V., Cruz, H., Calogero, G., & de Freitas, V. et al. (2019). Catechol versus carboxyl linkage impact on DSSC performance of synthetic pyranoflavylium salts. Dyes and Pigments, 170, 107577. https://doi.org/10.1016/j.dyepig.2019.107577
- Porra, R. J., Thompson, W. A., & Kriedemann, P. E. (1989). Determination of accurate extinction coefficients and simultaneous

equations for assaying chlorophylls a and B extracted with four different solvents: Verification of the concentration of chlorophyll standards by atomic absorption spectroscopy. Biochimica et Biophysica Acta (BBA) - Bioenergetics, 975(3), 384–394. https://doi.org/10.1016/s0005-2728(89)80347-0

- Pugliese, D., Lamberti, A., Bella, F., Sacco, A., Bianco, S., & Tresso, E. (2014). TiO_2 nanotubes as flexible photoanode for back-illuminated dye-sensitized solar cells with hemi-squaraine organic dye and iodine-free transparent electrolyte. Organic Electronics, 15(12), 3715-3722. https://doi.org/10.1016/j.orgel.2014.10.018
- Pujiarti, H., Arsyad, W., Wulandari, P., & Hidayat, R. (2014). The effect of ionic liquid electrolyte concentrations in dye sensitized solar cell using gel electrolyte. https://doi.org/10.1063/1.4897099
- Purnama, H., Prabowo, B. A., Hanif, L. N., Ridwan, I., & Hidayati, N. (2021). Effect of sintering temperature in curcumin dye-sensitized solar cell using Ito Glass. Journal of Physics: Conference Series, 1858(1), 012059. https://doi.org/10.1088/1742-6596/1858/1/012059
- Puspitasari, N., Nurul Amalia, S., Yudoyono, G., & Endarko. (2017). Effect of Mixing Dyes and Solvent in Electrolyte Toward Characterization of Dye Sensitized Solar Cell Using Natural Dyes as The Sensitizer. IOP Conference Series: Materials Science and Engineering, 214, 012022. https://doi.org/10.1088/1757-899x/214/1/012022
- PVWatts Calculator. Pvwatts.nrel.gov. (2020). Retrieved 14 April 2020, from https://pvwatts.nrel.gov/
- Qin, Q., Tao, J., & Yang, Y. (2010). Preparation and characterization of polyaniline film on stainless steel by electrochemical polymerization as a counter electrode of DSSC. Synthetic Metals, 160(11-12), 1167-1172. https://doi.org/10.1016/j.synthmet.2010.03.003
- Qin, R., Yang, W., Li, S., Lau, T., Yu, Z., & Liu, Z. et al. (2019). Enhanced intramolecular charge transfer of unfused electron

acceptors for efficient organic solar cells. Materials Chemistry Frontiers, 3(3), 513-519. https://doi.org/10.1039/c8qm00609a

- Raïssi, M., Pellegrin, Y., Lefevre, F., Boujtita, M., Rousseau, D., Berthelot, T., & Odobel, F. (2020). Digital printing of efficient dye-sensitized solar cells (DSSCs). Solar Energy, 199, 92-99. https://doi.org/10.1016/j.solener.2020.02.004
- Ramanujam, J., & Singh, U. (2017). Copper indium gallium selenide based solar cells – a review. Energy & Environmental Science, 10(6), 1306-1319. https://doi.org/10.1039/c7ee00826k
- Rapalli, V. K., Kaul, V., Gorantla, S., Waghule, T., Dubey, S. K., Pandey, M. M., & Singhvi, G. (2020). UV spectrophotometric method for characterization of curcumin loaded nanostructured lipid nanocarriers in simulated conditions: Method development, in-vitro and ex-vivo applications in topical delivery. Spectrochimica Acta Part A: Molecular and Biomolecular Spectroscopy, 224, 117392. https://doi.org/10.1016/j.saa.2019.117392
- Rapsomanikis, A., Sygkridou, D., Voutsinas, E., & Stathatos, E. (2016). Transparent quasi-solid-state dye-sensitized solar cells sensitized with naturally derived pigment extracted from red seaweed. Current Applied Physics, 16(6), 651-657. https://doi.org/10.1016/j.cap.2016.03.018
- Rath, J., Brinza, M., Liu, Y., Borreman, A., & Schropp, R. (2010). Fabrication of thin film silicon solar cells on plastic substrate by very high frequency PECVD. Solar Energy Materials and Solar Cells, 94(9), 1534-1541. https://doi.org/10.1016/j.solmat.2010.01.013
- Ravi Kumar, V., Verma, C., & Umapathy, S. (2016). Molecular dynamics and simulations study on the vibrational and electronic solvatochromism of benzophenone. The Journal of Chemical Physics, 144(6), 064302. https://doi.org/10.1063/1.4941058
- Ren, X., Chen, S., Lee, H., Mei, D., Engelhard, M., & Burton, S. et al. (2018). Localized High-Concentration Sulfone Electrolytes for

High-Efficiency Lithium-Metal Batteries. Chem, 4(8), 1877-1892. https://doi.org/10.1016/j.chempr.2018.05.002

- Renewables 2019 – Analysis - IEA. IEA. (2020). Retrieved 14 April 2020, from https://www.iea.org/renewables2019/
- Renita. A, A., & Davuluri, D. (2015). Extraction of dye from marine macroalgae. International Journal of Chemtech Research, 8(3), 1060-1063. Retrieved 21 April 2020, from http://sphinxsai.com/2015/ch_vol8_no3/2/(1060-1063)V8N3.pdf
- Richhariya, G., Kumar, A., Tekasakul, P., & Gupta, B. (2017). Natural dyes for dye sensitized solar cell: A review. Renewable And Sustainable Energy Reviews, 69, 705-718. https://doi.org/10.1016/j.rser.2016.11.198
- Rieux, L., Niederländer, H., Verpoorte, E., & Bischoff, R. (2005). Silica monolithic columns: Synthesis, characterisation and applications to the analysis of biological molecules. Journal of Separation Science, 28(14), 1628–1641. https://doi.org/10.1002/jssc.200500146
- Risbridger, T., Castro, F., & Cameron, P. (2012). Two-Dimensional Photocurrent and Transmission Mapping of Aqueous Dye-Sensitized Solar Cells. The Journal of Physical Chemistry C, 116(42), 22253-22260. https://doi.org/10.1021/jp308238p
- Ritchie, R. J. (2006). Consistent sets of spectrophotometric chlorophyll equations for acetone, methanol, and ethanol solvents. Photosynthesis Research, 89(1), 27–41. https://doi.org/10.1007/s11120-006-9065-9
- Rowan, K. S. (1989). Photosynthetic pigments of algae. Cambridge University Press.
- Roy, S., & Garrido, J. L. (2013). Pigments | liquid chromatography. Reference Module in Chemistry, Molecular Sciences and Chemical Engineering. https://doi.org/10.1016/b978-0-12-409547-2.04878-2
- Ruess, R., Nguyen, T., & Schlettwein, D. (2018). Metal Complexes as Redox Shuttles in Dye-Sensitized Solar Cells Based on Electrodeposited ZnO: Tuning Recombination Kinetics and

Conduction Band Energy. Journal of the Electrochemical Society, 165(4), H3115-H3121. https://doi.org/10.1149/2.0131804jes

- Ruthenium (Ru) - Chemical properties, Health and Environmental effects. Lenntech.com. (2020). Retrieved 17 April 2020, from https://www.lenntech.com/periodic/elements/ru.htm#Health%20effects%20of%20ruthenium
- S.W. Jeffrey, R.F.C. Mantoura, S.W. Wright, editors. phytoplankton pigments in oceanography: Guidelines to modern methods. 661P. Paris: UNESCO Publishing, 1997. (monographs on Oceanographic Methodology No. 10). price $64.00. (1997). Journal of the Marine Biological Association of the United Kingdom, 77(3), 918–918. https://doi.org/10.1017/s0025315400036389
- Saeed, M., Usman, M., & Haq, A. (2018). Catalytic Degradation of Organic Dyes in Aqueous Medium. Photochemistry and Photophysics - Fundamentals To Applications. https://doi.org/10.5772/intechopen.75008
- Saha, S., Singh, J., Paul, A., Sarkar, R., Khan, Z., & Banerjee, K. (2020). Anthocyanin profiling using UV-vis spectroscopy and liquid chromatography mass spectrometry. Journal of AOAC INTERNATIONAL, 103(1), 23–39. https://doi.org/10.5740/jaoacint.19-0201
- Saito, H., Uegusa, S., Murakami, T., Kawashima, N., & Miyasaka, T. (2004). Fabrication and Efficiency Enhancement of Water-based Dye-Sensitized Solar Cells by Interfacial Activation of TiO2 Mesopores. Electrochemistry, 72(5), 310-316. https://doi.org/10.5796/electrochemistry.72.310
- Sakai, H., Ono, K., Tokunaga, S., Sharmin, T., Aida, T. M., & Mishima, K. (2020a). Extraction of natural pigments from gardenia jasminoides j.ellis fruit pulp using CO2-expanded liquids and direct sonication. Separations, 8(1), 1. https://doi.org/10.3390/separations8010001
- Salvatori, P., Marotta, G., Cinti, A., Anselmi, C., Mosconi, E., & De Angelis, F. (2013). Supramolecular Interactions of Chenodeoxycholic Acid Increase the Efficiency of Dye-Sensitized

Solar Cells Based on a Cobalt Electrolyte. The Journal of Physical Chemistry C, 117(8), 3874-3887. https://doi.org/10.1021/jp4003577

- Sánchez, E., & Araújo, G. (1987). On the analytical determination of solar cell fill factor and efficiency. Solar Cells, 20(1), 1-11. https://doi.org/10.1016/0379-6787(87)90015-9
- Sanchini, A., & Grosjean, M. (2020). Quantification of chlorophyll a, chlorophyll b and pheopigments a in lake sediments through deconvolution of bulk UV–vis absorption spectra. Journal of Paleolimnology, 64(3), 243–256. https://doi.org/10.1007/s10933-020-00135-z
- Sanz, N., García-Blanco, A., Gavalás-Olea, A., Loures, P., & Garrido, J. L. (2015). Phytoplankton pigment biomarkers: hplc separation using a pentafluorophenyloctadecyl silica column. Methods in Ecology and Evolution, 6(10), 1199–1209. https://doi.org/10.1111/2041-210x.12406
- Sartory, D. P. (1985). The determination of algal chlorophyllous pigments by high performance liquid chromatography and Spectrophotometry. Water Research, 19(5), 605–610. https://doi.org/10.1016/0043-1354(85)90066-1
- Sarwer, A., Hamed, S. M., Osman, A. I., Jamil, F., Al-Muhtaseb, A. H., Alhajeri, N. S., & Rooney, D. W. (2022). Algal biomass valorization for biofuel production and carbon sequestration: A Review. Environmental Chemistry Letters, 20(5), 2797–2851. https://doi.org/10.1007/s10311-022-01458-1
- Scendo, M., & Uznanska, J. (2011). The Effect of Ionic Liquids on the Corrosion Inhibition of Copper in Acidic Chloride Solutions. International Journal of Corrosion, 2011, 1-13. https://doi.org/10.1155/2011/718626
- Schanderl, S. H., Chichester, C. O., & Marsh, G. L. (1962). Degradation of chlorophyll and several derivatives in acid solution. Journal of Organic Chemistry, 27(11), 3865–3868. https://doi.org/10.1021/jo01058a025

- Scheepers, J. C., Dyk, S. V., Preez, J. L. D., & Malan, S. F. (2011). The High Performance Liquid Chromatography (HPLC) analysis of ultraviolet (UV) irradiated chlorophyll a and secondary plant compounds. AFRICAN JOURNAL OF BIOTECHNOLOGY, 10(74). https://doi.org/10.5897/ajb11.1999
- Schlichthörl, G., Park, N., & Frank, A. (1999). Evaluation of the Charge-Collection Efficiency of Dye-Sensitized Nanocrystalline TiO2 Solar Cells. The Journal of Physical Chemistry B, 103(5), 782-791. https://doi.org/10.1021/jp9831177
- Schmid, H., & Stich, H. B. (1995). HPLC-analysis of algal pigments: Comparison of columns, column properties and eluents. Journal of Applied Phycology, 7(5), 487–494. https://doi.org/10.1007/bf00003933
- Schwartz, S., & Lorenzo, T. (1991). Chlorophyll stability during continuous aseptic processing and storage. Journal of Food Science, 56(4), 1059–1062. https://doi.org/10.1111/j.1365-2621.1991.tb14641.x
- Scott, M., Woodhouse, M., Parkinson, B., & Elliott, C. (2008). Spatially Resolved Current-Voltage Measurements—Evidence for Non uniform Photocurrents in Dye-Sensitized Solar Cells. Journal of the Electrochemical Society, 155(3), B290. https://doi.org/10.1149/1.2830944
- Shah, Z., Zaib, K., & M, K. (2017). Dye Sensitized Solar Cells Based on Different Solvents: Comparative Study. Journal of Fundamentals of Renewable Energy and Applications, 07(04). https://doi.org/10.4172/2090-4541.1000234
- Shalini, S., Balasundara prabhu, R., Prasanna, S., Mallick, T., & Senthilarasu, S. (2015). Review on natural dye sensitized solar cells: Operation, materials and methods. Renewable And Sustainable Energy Reviews, 51, 1306-1325. https://doi.org/10.1016/j.rser.2015.07.052
- Shalini, S., Balasundaraprabhu, R., Kumar, T., Prabavathy, N., Senthilarasu, S., & Prasanna, S. (2016). Status and outlook of sensitizers/dyes used in dye sensitized solar cells (DSSC): a

review. International Journal of Energy Research, 40(10), 1303-1320. https://doi.org/10.1002/er.3538

- Shinnar, R. (2003). The hydrogen economy, fuel cells, and electric cars. Technology in Society, 25(4), 455-476. https://doi.org/10.1016/j.techsoc.2003.09.024
- Singh, S., Maurya, I. C., Sharma, S., Srivastava, P., & Bahadur, L. (2020). Effect of dye extraction solvent on the photovoltaic performance of Tecoma Stans-sensitized solar cells. Journal of Electronic Materials, 49(7), 4355–4363. https://doi.org/10.1007/s11664-020-08154-2
- Sivakumar, V., Anna, J. L., Vijayeeswarri, J., & Swaminathan, G. (2009). Ultrasound assisted enhancement in natural dye extraction from beetroot for industrial applications and natural dyeing of leather. Ultrasonics Sonochemistry, 16(6), 782–789. https://doi.org/10.1016/j.ultsonch.2009.03.009
- Song, J., Li, G., Wu, C., & Gao, X. (2014). Metal sulfide counter electrodes for dye-sensitized solar cells: A balanced strategy for optical transparency and electrochemical activity. Journal of Power Sources, 266, 464-470. https://doi.org/10.1016/j.jpowsour.2014.05.062
- Soundarrajan, P., Sankarasubramanian, K., Logu, T., Sethuraman, K., & Ramamurthi, K. (2014). Growth of rutile tio2 nanorods on Tio2 seed layer prepared using facile low cost chemical methods. Materials Letters, 116, 191–194. https://doi.org/10.1016/j.matlet.2013.11.026
- Stamford, L., & Azapagic, A. (2018). Environmental Impacts of Photovoltaics: The Effects of Technological Improvements and Transfer of Manufacturing from Europe to China. Energy Technology, 6(6), 1148-1160. https://doi.org/10.1002/ente.201800037
- Stanier, R. Y., Kunisawa, R., Mandel, M., & Cohen-Bazire, G. (1971). Purification and Properties of Unicellular Blue-Green Algae (Order Chroococcales). Bacteriological Reviews, 35(2), 171–205. https://doi.org/10.1128/br.35.2.171-205.1971

- Steephen, A., Saini, K., Suvitha, A., Vivek, P., Arumanayagam, T., Rekha, M., & Madhavan, B. (2023). Investigational, computational explorations on Betanin, lycopene, cyanidin, and peonidin organic photo sensitizers for green energy harvesting. Sustainable Energy Technologies and Assessments, 60, 103451. https://doi.org/10.1016/j.seta.2023.103451
- Strickland, J. D., & Parsons, T. R. (1968). A practical handbook of seawater analysis: By J.D.H. Strickland and T.R. Parsons. Fisheries Research Board of Canada.
- Sun, K., Sahito, I., Noh, J., Yeo, S., Im, J., & Yi, S. et al. (2016). Highly efficient and durable dye-sensitized solar cells based on a wet-laid PET membrane electrolyte. Journal of Materials Chemistry A, 4(2), 458-465. https://doi.org/10.1039/c5ta07720f
- Suzuki, T., Midonoya, H., & Shioi, Y. (2009). Analysis of chlorophylls and their derivatives by matrix-assisted laser desorption/ionization–time-of-flight mass spectrometry. Analytical Biochemistry, 390(1), 57–62. https://doi.org/10.1016/j.ab.2009.04.005
- Takekuma, Y., Ochiai, T., & Nagata, M. (2018). Immobilization of Rhodamine B Isothiocyanate on TiO2 for Light Harvesting in Zinc Phthalocyanine Dye-sensitized Solar Cells. Chemistry Letters, 47(2), 225-227. https://doi.org/10.1246/cl.171024
- Talaei, M., Mahdavinejad, M., Azari, R., Haghighi, H. M., & Atashdast, A. (2022). Thermal and energy performance of a user-responsive microalgae bioreactive façade for climate adaptability. Sustainable Energy Technologies and Assessments, 52, 101894. https://doi.org/10.1016/j.seta.2021.101894
- Tauc, J., Grigorovici, R., & Vancu, A. (1966). Optical properties and electronic structure of amorphous germanium. Physica Status Solidi (b), 15(2), 627–637. https://doi.org/10.1002/pssb.19660150224
- Taya, S., El-Agez, T., El-Ghamri, H., & Abdel-Latif, M. (2013). Dye-Sensitized Solar Cells Using Fresh and Dried Natural Dyes.

International Journal of Materials Science and Applications, 2(2), 37. https://doi.org/10.11648/j.ijmsa.20130202.11

- Teja, A. S., Srivastava, A., Satrughna, J. A., Tiwari, M. K., Kanwade, A., Chand Yadav, S., & Shirage, P. M. (2023). Optimal processing methodology for futuristic natural dye-sensitized solar cells and novel applications. Dyes and Pigments, 210, 110997. https://doi.org/10.1016/j.dyepig.2022.110997
- Tennakone, K., Kumara, G. R., Kumarasinghe, A. R., Wijayantha, K. G., & Sirimanne, P. M. (1995). A dye-sensitized nano-porous solid-state photovoltaic cell. Semiconductor Science and Technology, 10(12), 1689–1693. https://doi.org/10.1088/0268-1242/10/12/020
- Thankappan, A., Thomas, S., & Nampoori, V. P. N. (2013). Solvent effect on the third order optical nonlinearity and optical limiting ability of Betanin natural dye extracted from red beet root. Optical Materials, 35(12), 2332–2337. https://doi.org/10.1016/j.optmat.2013.06.032
- Tissier, R.-C., Rigaud, B., Thureau, P., Huix-Rotllant, M., Jaber, M., & Ferré, N. (2022). Stressing the differences in alizarin and purpurin dyes through UV-visible light absorption and1H-NMR spectroscopies. Physical Chemistry Chemical Physics, 24(32), 19452–19462. https://doi.org/10.1039/d2cp00520d
- Tourlouki, K., Tsavatopoulou, V., Alexandropoulos, D., Manariotis, I. D., & Mazzucato, S. (2020). A novel Microalgae harvesting method using laser micromachined glass fiber reinforced polymers. Photonics, 7(2), 42. https://doi.org/10.3390/photonics7020042
- Tractz, G., Viomar, A., Dias, B., de Lima, C., Banczek, E., & da Cunha, M. et al. (2018). Recombination Study of Dye Sensitized Solar Cells with Natural Extracts. Journal of the Brazilian Chemical Society. https://doi.org/10.21577/0103-5053.20180186
- Turcsi, E., Nagy, V., & Deli, J. (2016). Study on the elution order of carotenoids on endcapped C18 and C30 reverse silica stationary

phases. A review of the database. Journal of Food Composition and Analysis, 47, 101–112. https://doi.org/10.1016/j.jfca.2016.01.005

- Tzima, S., Georgiopoulou, I., Louli, V., & Magoulas, K. (2023). Recent advances in supercritical CO2 extraction of pigments, lipids, and bioactive compounds from microalgae. Molecules, 28(3), 1410. https://doi.org/10.3390/molecules28031410
- UNESCO. (1966). Determination of photosynthetic pigments in seawater (Ser. Monographs on oceanographic methodology).
- Urbani, M., Ragoussi, M., Nazeeruddin, M., & Torres, T. (2019). Phthalocyanines for dye-sensitized solar cells. Coordination Chemistry Reviews, 381, 1-64. https://doi.org/10.1016/j.ccr.2018.10.007
- US20100307571A1 - Using energy relay dyes to increase light absorption in dye-sensitized solar cells - Google Patents. Patents.google.com. (2010). Retrieved 20 April 2020, from https://patents.google.com/patent/US20100307571
- V., K. K., K., M. mohan, Gunaseelan, K., & Gajalakshmi, S. (2021). Insights into the role of bioinspiration, photosynthetic organisms, and biomass-derived electrodes/membranes in the development of Bioelectrochemical Systems. Sustainable Energy Technologies and Assessments, 48, 101570. https://doi.org/10.1016/j.seta.2021.101570
- Van Breemen, R. B., Canjura, F. L., & Schwartz, S. J. (1991). Identification of chlorophyll derivatives by mass spectrometry. Journal of Agricultural and Food Chemistry, 39(8), 1452–1456. https://doi.org/10.1021/jf00008a018
- Van Heukelem, L., & Thomas, C. S. (2001). Computer-assisted high-performance liquid chromatography method development with applications to the isolation and analysis of phytoplankton pigments. Journal of Chromatography A, 910(1), 31–49. https://doi.org/10.1016/s0378-4347(00)00603-4
- van Leeuwe, M. A., Villerius, L. A., Roggeveld, J., Visser, R. J. W., & Stefels, J. (2006). An optimized method for automated

analysis of algal pigments by HPLC. Marine Chemistry, 102(3–4), 267–275. https://doi.org/10.1016/j.marchem.2006.05.003

- Velusamy, M., Justin Thomas, K., Lin, J., Hsu, Y., & Ho, K. (2005). Organic Dyes Incorporating Low-Band-Gap Chromophores for Dye-Sensitized Solar Cells. Organic Letters, 7(10), 1899-1902. https://doi.org/10.1021/ol050417f
- Virkki, K., Tervola, E., Ince, M., Torres, T., & Tkachenko, N. (2018). Comparison of electron injection and recombination on TiO 2 nanoparticles and ZnO nanorods photosensitized by phthalocyanine. Royal Society Open Science, 5(7), 180323. https://doi.org/10.1098/rsos.180323
- Vlachopoulos, N., Liska, P., Augustynski, J., & Graetzel, M. (1988). Very efficient visible light energy harvesting and conversion by spectral sensitization of high surface area polycrystalline titanium dioxide films. Journal of the American Chemical Society, 110(4), 1216-1220. https://doi.org/10.1021/ja00212a033
- Vo Hoang Nhat, P., Ngo, H. H., Guo, W. S., Chang, S. W., Nguyen, D. D., Nguyen, P. D., Bui, X. T., Zhang, X. B., & Guo, J. B. (2018). Can algae-based technologies be an affordable green process for biofuel production and wastewater remediation? Bioresource Technology, 256, 491–501. https://doi.org/10.1016/j.biortech.2018.02.031
- Waghmare, A., Nagula, K., Pandit, A., & Arya, S. (2019). Hydrodynamic cavitation for energy efficient and scalable process of microalgae cell disruption. Algal Research, 40, 101496. https://doi.org/10.1016/j.algal.2019.101496
- Walker, J. S., Jie, C., & Keely, B. J. (2003). Identification of diastereomeric chlorophyll allomers by atmospheric pressure chemical ionisation liquid chromatography/tandem mass spectrometry. Rapid Communications in Mass Spectrometry/RCM. Rapid Communications in Mass Spectrometry, 17(11), 1125–1131. https://doi.org/10.1002/rcm.1015

- Wang, H., Bai, Y., Wu, Q., Zhou, W., Zhang, H., Li, J., & Guo, L. (2011). Rutile tio2 nano-branched arrays on FTO for dye-sensitized solar cells. Physical Chemistry Chemical Physics, 13(15), 7008. https://doi.org/10.1039/c1cp20351g
- Wang, H., Wang, H., Gao, B., Wang, L., Yang, Z., & Du, X. et al. (2011). Exciton diffusion and charge transfer dynamics in nano phase-separated P3HT/PCBM blend films. Nanoscale, 3(5), 2280. https://doi.org/10.1039/c0nr01002b
- Wang, L., Tian, L., Deng, X., Zhang, M., Sun, S., Zhang, W., & Zhao, L. (2014). Photosensitizers from Spirulina for Solar Cell. Journal of Chemistry, 2014, 1-5. https://doi.org/10.1155/2014/430806
- Wang, X., Koyama, Y., Wada, Y., Sasaki, S., & Tamiaki, H. (2007). A dye-sensitized solar cell using pheophytin–carotenoid adduct: Enhancement of photocurrent by electron and singlet-energy transfer and by suppression of singlet–triplet annihilation due to the presence of the carotenoid moiety. Chemical Physics Letters, 439(1–3), 115–120. https://doi.org/10.1016/j.cplett.2007.03.064
- Wang, X., Wang, L., Wang, Z., Wang, Y., Tamai, N., Hong, Z., & Kido, J. (2013). Natural Photosynthetic Carotenoids for Solution-Processed Organic Bulk-Heterojunction Solar Cells. The Journal of Physical Chemistry C, 117(2), 804-811. https://doi.org/10.1021/jp309773b
- Wang, X., Xiang, J., Wang, P., Koyama, Y., Yanagida, S., & Wada, Y. et al. (2005). Dye-sensitized solar cells using a chlorophyll a derivative as the sensitizer and carotenoids having different conjugation lengths as redox spacers. Chemical Physics Letters, 408(4-6), 409-414. https://doi.org/10.1016/j.cplett.2005.04.067
- Wang, X., Zhan, C., Maoka, T., Wada, Y., & Koyama, Y. (2007). Fabrication of dye-sensitized solar cells using chlorophylls c1 and c2 and their oxidized forms c1’ and c2’ from Undaria pinnatifida

(Wakame). Chemical Physics Letters, 447(1-3), 79-85. https://doi.org/10.1016/j.cplett.2007.08.097

- Wei, J., & O'Connor, P. B. (2015). Extensive fragmentation of pheophytin-a by infrared multiphoton dissociation tandem mass spectrometry. Rapid Communications in Mass Spectrometry/RCM. Rapid Communications in Mass Spectrometry, 29(24), 2411–2418. https://doi.org/10.1002/rcm.7391
- Weng, B., Qi, M., Han, C., Tang, Z., & Xu, Y. (2019). Photo corrosion Inhibition of Semiconductor-Based Photocatalysts: Basic Principle, Current Development, and Future Perspective. ACS Catalysis, 9(5), 4642-4687. https://doi.org/10.1021/acscatal.9b00313
- Wiberg, J., Marinado, T., Hagberg, D., Sun, L., Hagfeldt, A., & Albinsson, B. (2009). Effect of Anchoring Group on Electron Injection and Recombination Dynamics in Organic Dye-Sensitized Solar Cells. The Journal of Physical Chemistry C, 113(9), 3881-3886. https://doi.org/10.1021/jp8101139
- Williams, B., Major, J., Bowen, L., Phillips, L., Zoppi, G., Forbes, I., & Durose, K. (2014). Challenges and prospects for developing CdS/CdTe substrate solar cells on Mo foils. Solar Energy Materials and Solar Cells, 124, 31-38. https://doi.org/10.1016/j.solmat.2014.01.017
- Woronowicz, K., Ahmed, S., Biradar, A., Biradar, A., Birnie, D., Asefa, T., & Niederman, R. (2012). Near-IR Absorbing Solar Cell Sensitized with Bacterial Photosynthetic Membranes. Photochemistry and Photobiology, 88(6), 1467-1472. https://doi.org/10.1111/j.1751-1097.2012.01190.x
- Wright, S. W., & Shearer, J. D. (1984a). Rapid extraction and high-performance liquid chromatography of chlorophylls and carotenoids from marine phytoplankton. Journal of Chromatography A, 294, 281–295. https://doi.org/10.1016/s0021-9673(01)96134-5
- Wright, S., Jeffrey, S., Mantoura, R., Llewellyn, C., Bjornland, T., Repeta, D., & Welschmeyer, N. (1991). Improved HPLC method

for the analysis of chlorophylls and carotenoids from marine phytoplankton. Marine Ecology Progress Series, 77, 183–196. https://doi.org/10.3354/meps077183

- Wu, C., Chang, T., Teng, H., & Lee, Y. (2016). High performance carbon black counter electrodes for dye-sensitized solar cells. Energy, 115, 513-518. https://doi.org/10.1016/j.energy.2016.09.052
- Wu, J., Lan, Z., Lin, J., Huang, M., & Li, P. (2007). Effect of solvents in liquid electrolyte on the photovoltaic performance of dye-sensitized solar cells. Journal of Power Sources, 173(1), 585-591. https://doi.org/10.1016/j.jpowsour.2007.04.085
- Wu, J., Lan, Z., Lin, J., Huang, M., Huang, Y., Fan, L., & Luo, G. (2015). Electrolytes in Dye-Sensitized Solar Cells. Chemical Reviews, 115(5), 2136-2173. https://doi.org/10.1021/cr400675m
- Xu, B., Tian, L., Etman, A., Sun, J., & Tian, H. (2019). Solution-processed nanoporous NiO-dye-ZnO photocathodes: Toward efficient and stable solid-state p-type dye-sensitized solar cells and dye-sensitized photoelectrosynthesis cells. Nano Energy, 55, 59-64. https://doi.org/10.1016/j.nanoen.2018.10.054
- Xue, G., Guo, Y., Yu, T., & Guan, J., Yu, X., Zhang, J., Liu, J., & Zou, Z. (2012). Degradation Mechanisms Investigation for Long-term Thermal Stability of Dye-Sensitized Solar Cells. International Journal of Electrochemical Science. 7.
- Yang, J., Bao, C., Zhu, K., Yu, T., Li, F., & Liu, J. et al. (2014). High catalytic activity and stability of nickel sulfide and cobalt sulfide hierarchical nanospheres on the counter electrodes for dye-sensitized solar cells. Chem. Commun., 50(37), 4824-4826. https://doi.org/10.1039/c4cc00001c
- Yang, J., Ganesan, P., Teuscher, J., Moehl, T., Kim, Y., & Yi, C. et al. (2014). Influence of the Donor Size in D−π–A Organic Dyes for Dye-Sensitized Solar Cells. Journal of the American Chemical Society, 136(15), 5722-5730. https://doi.org/10.1021/ja500280r
- Yañuk, J., Cabrerizo, F., Dellatorre, F., & Cerdá, M. (2020). Photosensitizing role of R-phycoerythrin red protein and β-

carboline alkaloids in Dye sensitized solar cell. Electrochemical and spectroscopic characterization. Energy Reports, 6, 25-36. https://doi.org/10.1016/j.egyr.2019.10.045

- Yehezkeli, O., Tel-Vered, R., Michaeli, D., Nechushtai, R., & Willner, I. (2013). Photosystem I (PSI)/Photosystem II (PSII)-Based Photo-Bioelectrochemical Cells Revealing Directional Generation of Photocurrents. Small, 9(17), 2970-2978. https://doi.org/10.1002/smll.201300051
- Yella, A., Lee, H., Tsao, H., Yi, C., Chandiran, A., & Nazeeruddin, M. et al. (2011). Porphyrin-Sensitized Solar Cells with Cobalt (II/III)-Based Redox Electrolyte Exceed 12 Percent Efficiency. Science, 334(6056), 629-634. https://doi.org/10.1126/science.1209688
- Yin, X., Zhao, H., Chen, L., Tan, W., Zhang, J., & Weng, Y. et al. (2007). The effects of pyridine derivative additives on interface processes at nanocrystalline TiO2 thin film in dye-sensitized solar cells. Surface and Interface Analysis, 39(10), 809-816. https://doi.org/10.1002/sia.2594
- Yokono, M., Murakami, A., & Akimoto, S. (2011). Excitation energy transfer between Photosystem II and photosystem I in red algae: Larger amounts of phycobilisome enhance spillover. Biochimica et Biophysica Acta (BBA) - Bioenergetics, 1807(7), 847–853. https://doi.org/10.1016/j.bbabio.2011.03.014
- Yu, D. Y., Zhang, J., Unsworth, L. D., & Zhang, S. G. (2008). Chlorin e6 sensitized ZnO nanowires coupling with phycobilisome: a novel approach obtaining high efficiency for dye-sensitized solar cells. In Proc. Int. Conf. Biomass Energy Tech (Vol. 2, pp. 536-540).
- Yu, D., Wang, M., Zhu, G., Ge, B., Liu, S., & Huang, F. (2015). Enhanced photocurrent production by bio-dyes of photosynthetic macromolecules on designed TiO2 film. Scientific Reports, 5(1). https://doi.org/10.1038/srep09375

- Yu, K., & Chen, J. (2008). Enhancing Solar Cell Efficiencies through 1-D Nanostructures. Nanoscale Research Letters, 4(1), 1-10. https://doi.org/10.1007/s11671-008-9200-y
- Yu, Z., Gorlov, M., Boschloo, G., & Kloo, L. (2010). Synergistic Effect of N-Methylbenzimidazole and Guanidinium Thiocyanate on the Performance of Dye-Sensitized Solar Cells Based on Ionic Liquid Electrolytes. The Journal of Physical Chemistry C, 114(50), 22330-22337. https://doi.org/10.1021/jp1073686
- Yue, G., Li, F., Yang, G., & Zhang, W. (2016). Efficient Nickel Sulfide and Graphene Counter Electrodes Decorated with Silver Nanoparticles and Application in Dye-Sensitized Solar Cells. Nanoscale Research Letters, 11(1). https://doi.org/10.1186/s11671-016-1456-z
- Yun, H., Hai, N., Min, C., Thogiti, S., Cheruku, R., & Kim, J. (2017). Influence of Diffusion Coefficient of Cobalt Redox Mediator Using Triphenylamine Dyes with Various Number of Anchoring Groups: Photovoltaic Performance of DSSCs. Electrocatalysis, 8(5), 414-421. https://doi.org/10.1007/s12678-017-0388-4
- Zaki, M., Fouad, N., Mekhemer, G., Jagadale, T., & Ogale, S. (2011). TiO2 nanoparticle size dependence of porosity, adsorption, and catalytic activity. Colloids and Surfaces A: Physicochemical and Engineering Aspects, 385(1-3), 195-200. https://doi.org/10.1016/j.colsurfa.2011.06.010
- Zanatta, A. R. (2019). Revisiting the optical bandgap of semiconductors and the proposal of a unified methodology to its determination. Scientific Reports, 9(1). https://doi.org/10.1038/s41598-019-47670-y
- Zapata, M., Ayala, A. M., Franco, J. M., & Garrido, J. L. (1987). Separation of chlorophylls and their degradation products in marine phytoplankton by reversed-phase high-performance liquid chromatography. Chromatographia, 23(1), 26–30. https://doi.org/10.1007/bf02310413

- Zapata, M., Rodríguez, F., & Garrido, J. (2000). Separation of chlorophylls and carotenoids from marine phytoplankton: a new HPLC method using a reversed phase C8 column and pyridine-containing mobile phases. Marine Ecology Progress Series, 195, 29–45. https://doi.org/10.3354/meps195029
- Zatirostami, A. (2020). Increasing the efficiency of TiO2-based DSSC by means of a double layer RF-sputtered thin film blocking layer. Optik, 207, 164419. https://doi.org/10.1016/j.ijleo.2020.164419
- Zhang, H., Chen, Z., & Tian, H. (2020). Molecular engineering of metal-free organic sensitizers with polycyclic benzenoid hydrocarbon donor for DSSC applications: The effect of the conjugate mode. Solar Energy, 198, 239-246. https://doi.org/10.1016/j.solener.2020.01.067
- Zhang, L., & Cole, J. (2015). Anchoring Groups for Dye-Sensitized Solar Cells. ACS Applied Materials & Interfaces, 7(6), 3427-3455. https://doi.org/10.1021/am507334m
- Zhang, L., & Cole, J. (2017). Dye aggregation in dye-sensitized solar cells. Journal of Materials Chemistry A, 5(37), 19541-19559. https://doi.org/10.1039/c7ta05632j
- Zhang, Q., & Cao, G. (2011). Nanostructured photoelectrodes for dye-sensitized solar cells. Nano Today, 6(1), 91-109. https://doi.org/10.1016/j.nantod.2010.12.007
- Zhang, X., & Laursen, R. (2009). Application of LC–MS to the analysis of dyes in objects of historical interest. International Journal of Mass Spectrometry, 284(1–3), 108–114. https://doi.org/10.1016/j.ijms.2008.07.014
- Zhao, D., Xing, X., Liu, Y., Yang, J., & Wang, L. (2010). The relation of chlorophyll-a concentration with the reflectance peak near 700 nm in algae-dominated waters and sensitivity of fluorescence algorithms for detecting algal bloom. International Journal of Remote Sensing, 31(1), 39–48. https://doi.org/10.1080/01431160902882512

- Zhong, M., Huang, S., Wang, H., Huang, Y., Xu, J., & Zhang, L. (2019). Optimization of ultrasonic-assisted extraction of pigment from dioscorea cirrhosa by response surface methodology and evaluation of its stability. RSC Advances, 9(3), 1576–1585. https://doi.org/10.1039/c8ra07455k
- Zhu, K., Jang, S., & Frank, A. (2012). Effects of water intrusion on the charge-carrier dynamics, performance, and stability of dye-sensitized solar cells. Energy & Environmental Science, 5(11), 9492. https://doi.org/10.1039/c2ee22178k
- Zscheile, F. P., White, J. W., Beadle, B. W., & Roach, J. R. (1942). The preparation and absorption spectra of five pure carotenoid pigments. Plant Physiology, 17(3), 331–346. https://doi.org/10.1104/pp.17.3.331